Synthesis and pharmacological investigation of allosteric and bitopic ligands for the M$_1$ muscarinic acetylcholine receptor

A thesis submitted for the degree of
Doctor of Philosophy

by
Briana Jay Davie
B. Med. Chem. (Hons Pharm. Sci.)

Supervisors: Prof. Peter Scammells, Prof. Arthur Christopoulos
and Dr Ben Capuano

Medicinal Chemistry & Drug Discovery Biology
Monash Institute of Pharmaceutical Sciences
Faculty of Pharmacy and Pharmaceutical Sciences
Monash University
2014

MONASH University

Addendum

p 52 Conclusion: Comment: Whilst the synthesis of analogues of the isothiocyanate **11**, including one containing a flexible linker to allow for more conformational freedom in the allosteric site, was certainly considered, these we consider to be 2nd generation compounds and beyond the scope of this thesis.

p 94 Figure 10: replace with
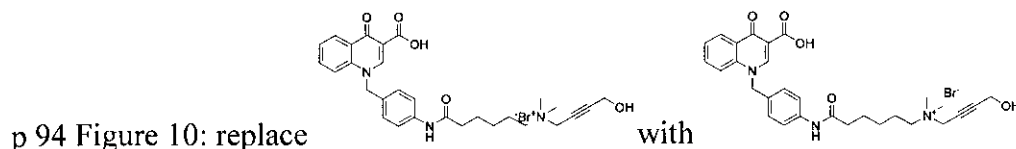
p 98 Para 1: Comment: More labile carboxyl protecting groups were considered as a method to resolve the difficulties experienced with the ethyl ester, however, as employing the amide in place of the acid proved successful it wasn't necessary to persist with alternative options.

General comment: The characterisation of more complex compounds, particularly those containing alkyl chains and multiple pharmacophores, was aided by COSY, HSQC and HMBC 2D NMR experiments.

Errata

p 106 line 9: replace "116.0223" with "117.0223"

p 146 line 1-2: replace "primary amine" with "aniline"

Copyright Notices

Notice 1

Notice 2

Table of Contents

Statement of Originality

I hereby declare that this thesis contains no material which has been accepted for the award of any other degree or diploma at any university or equivalent institution and that, to the best of my knowledge and belief, this thesis contains no material previously published or written by another person, except where due reference is made in the text of the thesis.

Briana Jay Davie

General Declaration

In accordance with Monash University Doctorate Regulation 17.2 Doctor of Philosophy and Research Master's regulations the following declarations are made:

I hereby declare that this thesis contains no material which has been accepted for the award of any other degree or diploma at any university or equivalent institution and that, to the best of my knowledge and belief, this thesis contains no material previously published or written by another person, except where due reference is made in the text of the thesis.

This thesis includes 3 original papers published in peer reviewed journals and 0 unpublished publications. The core theme of the thesis is the development of novel allosteric and bitopic ligands for the M_1 muscarinic acetylcholine receptor. The ideas, development and writing up of all the papers in the thesis were the principal responsibility of myself, the candidate, working within the Monash Institute of Pharmaceutical Sciences under the supervision of Prof. Peter J. Scammells, Prof. Arthur Christopoulos and Dr Ben Capuano.

The inclusion of co-authors reflects the fact that the work came from active collaboration between researchers and acknowledges input into team-based research.

In the case of chapters 1, 2 and 3 my contribution to the work involved the following:

Thesis chapter	Publication title	Publication status*	Nature and extent of candidate's contribution
1	Development of M_1 mAChR Allosteric and Bitopic Ligands: Prospective Therapeutics for the	published	All literature research. Main author of the manuscript.

	Treatment of Cognitive Deficits		85%
2	Synthesis and Pharmacological Evaluation of Analogues of Benzyl Quinolone Carboxylic Acid (BQCA) Designed to Bind Irreversibly to an Allosteric Site of the M_1 Muscarinic Acetylcholine Receptor	published	Synthesis and chemical characterization of all compounds. Pharmacological testing and data analysis for all compounds. Main author of manuscript. 80%
3	Development of a Photoactivatable Allosteric Ligand for the M_1 Muscarinic Acetylcholine Receptor	In press	Synthesis and chemical characterization of MIPS1455. Pharmacological testing and data analysis for BQCA and MIPS1455. Main author of manuscript.80%

I have not renumbered sections of published papers within the thesis. Every chapter stands on its own and therefore the numbering of the chemical structures, figures, schemes, tables and references begins in each chapter from 1. The referencing style required for publication in *ACS Chemical Neuroscience* has been used consistently throughout the thesis, with the exception of Chapter 2 which is published in the *Journal of Medicinal Chemistry*.

Signed: …███████████………………………………………

Date: 25/02/15
    …………………………………

Acknowledgements

Firstly, I'd like to thank my supervisors Prof. Peter Scammells, Prof. Arthur Christopoulos and Dr Ben Capuano for affording me the opportunity to undertake a PhD under their guidance. I feel very fortunate to have worked with and learnt from three of the most intelligent, driven and dedicated people I've ever met. Thank you for the scientific training you've provided me with and the time you've invested in supporting me both professionally and personally.

For their generous assistance and valuable advice in the Medicinal Chemistry lab and the Drug Discovery Biology lab, respectively, I'd like to thank Dr Shailesh Mistry and Dr Celine Valant. Thank you for your kind, patient mentorship and for inspiring me to emulate your meticulous, highly motivated approach to laboratory work. I'd also like to thank my thesis panel members Dr Rob Lane and Prof. Jonathan Baell for their valuable guidance, and everyone in the Medicinal Chemistry and Drug Discovery Biology departments for their friendly camaraderie. Furthermore, I'm immensely grateful to three inspiring professional mentors who've generously taken the time to listen to, advise and encourage me: Dr Erica Sloan, Dr Elizabeth Yuriev and Prof. Nigel Bunnett.

Massive undertakings such as PhDs simply don't get completed without a vast number of people believing in you on the days when you're unable to, providing moral support, keeping you sane, and simply being there for the high highs, the low lows, and everything in-between. To Anitha Kopinathan, Monika Szabo, Chris Shreurs, Ashleigh Keith, Michelle Stewart, Julie Taylor, Peter Murnane, Amy Chen, Carmen Klein Herenbrink, Georgina Thompson, Chris Leach, Alaa Abdul Ridha, Manuela Jorg, Kira Verde, Pam Conway, James Murfet, Luke Schembri, Tim Kirby, Martina and Martin Kocan, Rodrigo Morales, Emmanuel Birru, Anna Cook and Igor Mitrovic – I deeply appreciate every conversation, every hug and every smile.

I am immeasurably indebted to Gen Kelsang Dornying, Michelle Terry and the entire Kadampa Meditation Centre Melbourne/Australia Sangha communities. I thank them for welcoming me into their spiritual family and for their unwavering compassion, wise guidance and generous support. I thank the Buddhas for their blessings and for illuminating that which was once shrouded in complete darkness. I would like to dedicate the merit collected throughout the course of my PhD, culminating in this thesis, to the enlightenment of all living beings.

To Mum, Dad and Riley, words cannot describe my love for you three. Your stoicism, positivity, determination, and joyfulness have been and will continue to be an inspiration. Thank you for supporting me throughout what has been the most challenging endeavour of my life with warm hugs, long, long phone calls, late night conversations, peaceful lazy days, delicious meals, and heated Scrabble games. Thank you for giving me this precious life and thank you for every moment we've spent together.

Abbreviations

5-HT, 5-hydroxytryptamine

AC, adenylate cyclase

AChM, acetylcholine mustard

ACN, acetonitrile

AD, Alzheimer's disease

ADME, absorption, distribution, metabolism, and excretion

APP, amyloid precursor protein

BBB, blood brain barrier

BQCA, benzyl quinolone carboxylic acid (1-(4-methoxybenzyl)-4-oxo-1,4-dihydroquinoline-3-carboxylic acid)

BRET, bioluminescence resonance energy transfer

cAMP, cyclic adenosine monophosphate

CFC, contextual fear conditioning

CHO, Chinese hamster ovary

CNS, central nervous system;

COMU, (1-cyano-2-ethoxy-2-oxoethylidenaminoxy)dimethylamino-morpholino-carbenium hexafluorophosphate

COSY, correlation spectroscopy

CRC, concentration response curve

CSF, cerebrospinal fluid

DCM, dichloromethane

DIPEA, N,N-diisopropylethylamine

DMAP, 4-dimethylaminopyridine

DMEM, Dulbecco's Modified Eagle Medium

DMF, dimethylformamide

DMR, dynamic mass redistribution

DMSO, dimethyl sulfoxide

DNA, deoxyribonucleic acid

EC, extracellular or effective concentration

EPS, extrapyramidal side effects

ERK, extracellular-regulated kinase

ESI, electrospray ionization

FBS, foetal bovine serum

FF, free fraction

FLIPR, fluorometric imaging plate reader

GPCR, G protein-coupled receptor

HCTU, O-(6-chlorobenzotriazol-1-yl)-N, N, N, N, tetramethyluronium hexafluorophosphate

HEPES, 2-[4-(2-hydroxyethyl)-1-piperazinyl]ethanesulfonic acid

HMBC, heteronuclear multiple-bond correlation

HPLC, high performance liquid chromatography

HRMS, high resolution mass spectrometry

HSQC, heteronuclear single quantum coherence

IC, intracellular or inhibitory concentration

IP$_3$, inositol trisphosphate

KO, knockout

LCMS, liquid chromatography-mass spectrometry

LRMS, low resolution mass spectrometry

mAChR, muscarinic acetylcholine receptor

MAP, mitogen-activated protein

MD, molecular dynamics

MP, melting point

MWC, Monod-Wyman-Changeux

NAM, negative allosteric modulator

NBS, *N*-bromosuccinimide

NMDA, *N*-methyl-D-aspartate

NMPB, *N*-methyl-4-piperidyl *p*-azidobenzilate

NMR, nuclear magnetic resonance

NMS, *N*-methylscopolamine

PAM, positive allosteric modulator

PBS, phosphate-buffered saline

PET, positron emission tomography

PFC, prefrontal cortex

P-gp, P-glycoprotein

PKC, protein kinase C

PLC, phospholipase C

QNB, quinuclidinyl benzilate

RBF, round-bottomed flask

RT, room temperature

SAR, structure-activity relationship

SEM, standard error of the mean

sEPSCs, spontaneous excitatory postsynaptic currents

TBPB, [1-(1'-(2-tolyl)-1,4'-bipiperidin-4-yl)-1H benzo[*d*]imidazol-2(3H)-one]

TCDI, thiocarbonyldiimidazole

TEA, triethylamine

TFA, trifluoroacetic acid

THF, tetrahydrofuran

TLC, thin layer chromatography

TM, transmembrane

TOF, time of flight

UV, ultraviolet

Thesis Abstract

This thesis describes the development of allosteric and bitopic molecular tools for the M_1 muscarinic acetylcholine receptor (M_1 mAChR), a potential therapeutic target for the treatment of cognitive deficits experienced in central nervous system (CNS) disorders.

Chapter 1 presents a comprehensive review article that provides a rationale for targeting the M_1 mAChR and an account of the M_1 mAChR-selective allosteric and bitopic ligands that have emerged to date. The perspective at the end of Chapter 1 highlights the ongoing complexities encountered in the advancement of allosteric and bitopic ligand drug discovery. This perspective serves as a basis for the research undertaken in this thesis, as we contend that the development of molecular tools that are able to serve as structural and functional probes may contribute to the resolution of these complexities.

Chapters 2 and 3 describe the synthesis and pharmacological evaluation of a panel of putative irreversible allosteric ligands based on the structure of benzyl quinolone carboxylic acid (BQCA), the first reported orally-bioavailable M_1 mAChR allosteric ligand exhibiting absolute subtype selectivity. From this research, an electrophilic irreversible allosteric ligand MIPS1262 (**11**, Chapter 2) and a photoactivatable irreversible allosteric ligand MIPS1455 (**4**, Chapter 3), were developed, affording novel molecular tools for further probing allosteric interactions at the M_1 mAChR.

Chapter 4 details the development of novel putative bitopic ligands for the M_1 mAChR, including the selection of the constituent ligands (iperoxo and BQCA), the design and synthetic incorporation of linkers into their respective structures, and the synthesis and preliminary pharmacology of two putative bitopic ligands (**33a** and **44**, Chapter 4). Such ligands may prove useful in investigating specific structural and functional hypotheses at the

M_1 mAChR, in addition to presenting as a prospective therapeutic approach for the treatment of cognitive deficits.

In Chapter 5, known BQCA analogues exhibiting improved properties compared to the parent molecule were synthesized and subjected to more detailed pharmacological techniques and analysis than have been previously reported. Briefly, we demonstrate that it may be possible to introduce structural modifications into allosteric ligands to specifically 'fine-tune' individual pharmacological properties and use such molecules as *in vitro and in vivo* tools to delineate the requirements for optimal therapeutic effect without side effects.

A diverse toolbox of ligands were synthesized and pharmacologically validated for use in future studies of the M_1 mAChR. A discussion of potential directions for future research is provided in Chapter 6.

Thesis Overview and Aims

G protein-coupled receptors (GPCRs), as facilitators of intercellular chemical communication and major mediators of biological function, have been of significant therapeutic interest for decades, and account for the largest proportion of all pharmaceutical targets. One of the many breakthroughs to result from the extensive study of GPCR structure and function is the wide recognition that, in addition to the orthosteric site traditionally targeted by drug discovery programs, potentially all GPCRs contain topographically-distinct allosteric binding sites that can be targeted by novel therapeutic agents. Purely allosteric ligands and bitopic ligands (ligands capable of interacting with both the orthosteric and allosteric site simultaneously) have the potential to elicit a more fine-tuned, highly selective response than their purely orthosteric counterparts, and are hence avidly pursued by drug discovery programs.

One of the prototypical Family A GPCRs for which allosteric and bitopic ligands have been identified is the M_1 muscarinic acetylcholine receptor (mAChR); a target of therapeutic interest for the treatment of the cognitive deficits associated with neurodegenerative disorders such as Alzheimer's disease and schizophrenia. The prospective therapeutic utility of M_1 mAChR activation for enhanced cognitive function has been extensively validated in a vast number of *in vitro* and *in vivo* studies utilising orthosteric, allosteric and bitopic ligands (reviewed in Chapter 1). Despite this, our understanding of the precise mechanisms by which allosteric and bitopic ligands interact with the M_1 mAChR and elicit their unique binding and functional profiles remains limited; a factor that is likely slowing their development into clinically-viable drug candidates. The aim of the research described in this thesis is to synthesize and pharmacologically evaluate a range of molecular tools that may be employed to advance our understanding of allosteric and bitopic interactions with the M_1 mAChR.

Chapter 1

Chapter 1 contains a published review article (Davie *et al.* (2013), *ACS Chemical Neurosci.*, 4 (7), 1026-1048). The aim of Chapter 1 is to provide background and context to the research undertaken in this thesis. This review contains a detailed summary of the cholinergic hypothesis of memory dysfunction, the role of the M_1 mAChR in cognition, the prospective utility of targeting the M_1 mAChR for the treatment of Alzheimer's disease and schizophrenia, and the progress made in the development of allosteric and bitopic ligands for the M_1 mAChR. This review also affords a rationale for the research undertaken in this thesis by highlighting the endemic challenges hampering researchers in this field; complexities associated with screening, optimizing and classifying allosteric and bitopic ligands that the development of novel pharmacological tools may aid in resolving. Specifically, Chapters 2 and 3 describe novel affinity labels that may be employed in structural studies of the M_1 mAChR, potentially leading to more informed optimization of putative clinical candidates. Such tools may also aid classification of mAChR ligands for which the binding mode is unknown. Chapter 4 details the development of putative bitopic M_1 mAChR ligands; outlining an experimental method for rational design, optimization, and classification that may be applied to the engineering of putative bitopic molecules for any GPCR with established orthosteric and allosteric ligands. Finally, Chapter 5 demonstrates how applying a more in-depth screening approach to known ligands can uncover novel ligand properties that may be leveraged to further probe and understand GPCR activation.

Chapters 2 and 3

Chapters 2 and 3 detail the development of affinity labels designed to bind irreversibly to an M_1 mAChR allosteric site. Since their initial introduction in the 1960s, affinity labeling

techniques have found extensive utility in the study of protein structure, function, localization, dynamics and interaction with ligands both *in vitro* and *in vivo*. Affinity labeling at mAChRs has largely involved singly-labeled orthosteric ligands containing either mustard functionalities that cyclise at 37 °C to form a reactive aziridinium ion, or azide functionalities that require photoactivation to form a reactive nitrene, before covalently interacting with the receptor. Such ligands have been useful for elucidating the functional role of individual mAChR subtypes,[1] determining the structural basis of ligand binding,[2-4] investigating the effects of prolonged mAChR activation/desensitization *in vitro* and *in vivo*,[5-7] confirming the binding site of other, reversible ligands,[8] and aiding GPCR crystallization.[9]

The overall aim of Chapters 2 and 3 was to develop the first irreversible *allosteric* ligands for a mAChR with the potential to open up novel investigative opportunities for the study of the M_1 mAChR and to provide proof-of-concept for applying this approach at other GPCRs. Chapter 2 contains a published article (Davie *et al.* (2014), *J. Med. Chem.*, *57* (12), 5405-5418) describing the synthesis and pharmacological evaluation of four putative electrophilic irreversible allosteric M_1 mAChR ligands, based on the structure of BQCA. Utilising *in vitro* radioligand binding and ERK1/2 phosphorylation assays, we found that the allosteric binding and functional properties of BQCA were preserved to varying extents in all four analogues and that one analogue, MIPS1262 (**11**), is binding irreversibly to the M_1 mAChR. Appendix 2 contains a selectivity study demonstrating that MIPS1262 binds to all five mAChR subtypes, losing the high subtype selectivity of the parent molecule BQCA. Chapter 3 contains a published article (Davie *et al.* (2014), *ACS Chem. Neurosci.*, in press) detailing the synthesis and pharmacological evaluation of a photoactivatable irreversible allosteric M_1 mAChR ligand, MIPS1455 (**4**); also based on the structure of BQCA. Similar experiments to that performed in Chapter 2 indicate that this ligand is interacting irreversibly with the receptor.

Furthermore, a mAChR selectivity study performed with MIPS1455 reveals that, unlike the inherently reactive MIPS1262, MIPS1455 appears to retain the high subtype selectivity of the parent molecule BQCA (Appendix 3); thereby informing the nature of the studies in which these ligands may be applied. Such ligands may be utilized in a range of experiments including (photo)affinity-labeling, proteolytic peptide mapping, and crystallographic studies, which may enable us to elucidate the binding site and critical pharmacophoric features of BQCA's allosteric interaction with the M_1 mAChR, as well as examine the binding and functional impact of prolonged M_1 mAChR allosteric site occupation and of conformationally -constraining a GPCR with an irreversible allosteric ligand.

Chapter 4

Whilst Chapters 2 and 3 describe the development of irreversible affinity labels capable of binding covalently to the M_1 mAChR, Chapter 4 will illustrate how established *reversible* ligands may be covalently linked together, resulting in the generation of novel bitopic molecules that may serve as structural and pharmacological probes to advance our investigation of GPCRs. To date, bitopic ligands for the M_1 mAChR have been uncovered as a result of more detailed pharmacological analyses of ligands previously classified as either purely orthosteric or purely allosteric. However, the process of rationally designing bitopic ligands by the covalent linkage of known orthosteric and allosteric 'building blocks' has been successfully applied at the M_2 mAChR.

The aim of Chapter 4 was to apply a rational design approach to the development of putative bitopic ligands for the M_1 mAChR. Following selection of the constituent ligands, the highly potent, non-selective mAChR orthosteric agonist iperoxo and positive allosteric modulator BQCA, we confirmed a high degree of positive cooperativity between these two

ligands and demonstrate the feasibility of introducing linkers of varying lengths into select positions using novel analogues of both ligands. Synthesis and preliminary pharmacological evaluation of two putative bitopic molecules was completed, though a bitopic mechanism of action is yet to be confirmed. Pending future work, these compounds may be used to probe receptor subtype selectivity, investigate G protein-coupling specificity, manipulate conformational transitions and achieve graded receptor activation, as well as serving as templates for putative therapeutic leads.

Chapter 5

In Chapters 2, 3 and 4 we describe how known orthosteric and allosteric ligands of a GPCR can be synthetically modified in order to generate molecules that may afford novel advances in our understanding of the structural and functional interaction of ligands with their receptors. Chapter 5 briefly investigates how higher potency analogues of the positive allosteric modulator BQCA that are none-the-less suboptimal clinical candidates may still prove to be effective pharmacological tools if more detailed experiments are performed to unmask this potential. We reveal that the higher potency of some of these analogues can be accounted for by the enhancement of a single pharmacological parameter, but that, between analogues, this pharmacological parameter can vary. This offers the opportunity to examine the effect of selectively "dialing up" individual properties of allosteric ligands in both an *in vitro* and *in vivo* setting, potentially providing insight into the optimal balance of properties required to achieve a therapeutic effect without toxicity.

Chapter 6

Chapter 6 aims to conclude and provide a discussion of potential future directions for the research undertaken in this thesis.

References

(1) Ehlert, F. J. (1996) The Interaction of 4-DAMP Mustard with Subtypes of the Muscarinic Receptor. *Life Sci.*, *58*, 1971-1978.

(2) Spalding, T. A., Birdsall, N. J. M., Curtis, C. A. M. and Hulme, E. C. (1994) Acetylcholine Mustard Labels the Binding Site Aspartate in Muscarinic Acetylcholine Receptors. *J. Biol. Chem.*, *269*, 4092-4097.

(3) Ilien, B., Mejean, A. and Hirth, C. (1989) New Photoaffinity Labels for Rat Brain Muscarinic Acetylcholine Receptors. *Biochem. Pharmacol.*, *38*, 2879-2887.

(4) Karton, Y., Baumgold, J., Handen, J. S. and Jacobson, K. A. (1992) Molecular Probes for Muscarinic Receptors: Derivatives of the M_1-Antagonist Telenzepine. *Bioconjugate Chem.*, *3*, 234-240.

(5) Crocker, A. D. and Russell, R. W. (1990) Pretreatment With an Irreversible Muscarinic Agonist Affects Responses to Apomorphine. *Pharmacol. Biochem. Behav.*, *35*, 511-516.

(6) Ehlert, F. J., Jenden, D. J. and Ringdahl, B. (1984) An Alkylating Derivative of Oxotremorine Interacts Irreversibly with the Muscarinic Receptor. *Life Sci.*, *34*, 985-991.

(7) Overstreet, D. H., Booth, R. A. and Jenden, D. J. (1988) Effects of an Irreversible Muscarinic Agonist (BM123) on Avoidance and Spontaneous Alternation Performance. *Pharmacol. Biochem. Behav.*, *31*, 337-343.

(8) Suga, H., Figueroa, K. W. and Ehlert, F. J. (2008) Use of Acetylcholine Mustard to Study Allosteric Interactions at the M_2 Muscarinic Receptor. *J. Pharmacol. Exp. Ther.*, *327*, 518-528.

(9) Kruse, A. C., Ring, A. M., Manglik, A., Hu, J., Hu, K., Eitel, K., Hubner, H., Pardon, E., Valant, C., Sexton, P. M., Christopoulos, A., Felder, C. C., Gmeiner, P., Steyaert, J., Weis, W. I., Garcia, K. C., Wess, J. and Kobilka, B. K. (2013) Activation and Allosteric Modulation of a Muscarinic Acetylcholine Receptor. *Nature*, *504*, 101-106.

Chapter One

Declaration for Thesis Chapter 1

The introduction presented in Chapter 1 is published as the following the paper:

Davie, B.J., Christopoulos, A., Scammells, P.J. (2013), Development of M_1 mAChR Allosteric and Bitopic Ligands: Prospective Therapeutics for the Treatment of Cognitive Deficits, *ACS Chemical Neuroscience*, *4* (7), 1026-1048. Permission to reprint this publication for the purpose of this thesis was granted by ACS Publications.

Declaration by candidate

In the case of Chapter 1, the nature and extent of my contribution to the work was the following:
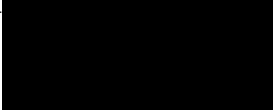
Nature of contribution	Extent of contribution (%)
All literature research. Main author of the manuscript.	85%

The following co-authors contributed to the work. If co-authors are students at Monash University, the extent of their contribution in percentage terms must be stated:

Name	Nature of contribution	Extent of contribution (%) for student co-authors only
Arthur Christopoulos	Co-author of manuscript.	
Peter J. Scammells	Co-author of manuscript.	

The undersigned hereby certify that the above declaration correctly reflects the nature and extent of the candidate's and co-authors' contributions to this work.

Candidate's Signature		**Date** 25/02/15

|		
Main Supervisor's Signature	███████	**Date** 25/02/15

Development of M$_1$ mAChR Allosteric and Bitopic Ligands: Prospective Therapeutics for the Treatment of Cognitive Deficits

Briana J. Davie,[‡,†] Arthur Christopoulos,*[‡] and Peter J. Scammells*[†]

[†]Medicinal Chemistry and [‡]Drug Discovery Biology, Monash Institute of Pharmaceutical Sciences, Monash University, 381 Royal Parade, Parkville VIC 3052, Australia

ABSTRACT: Since the cholinergic hypothesis of memory dysfunction was first reported, extensive research efforts have focused on elucidating the mechanisms by which this intricate system contributes to the regulation of processes such as learning, memory, and higher executive function. Several cholinergic therapeutic targets for the treatment of cognitive deficits, psychotic symptoms, and the underlying pathophysiology of neurodegenerative disorders, such as Alzheimer's disease and schizophrenia, have since emerged. Clinically approved drugs now exist for some of these targets; however, they all may be considered suboptimal therapeutics in that they produce undesirable off-target activity leading to side effects, fail to address the wide variety of symptoms and underlying pathophysiology that characterize these disorders, and/or afford little to no therapeutic effect in subsets of patient populations. A promising target for which there are presently no approved therapies is the M$_1$ muscarinic acetylcholine receptor (M$_1$ mAChR). Despite avid investigation, development of agents that selectively activate this receptor via the orthosteric site has been hampered by the high sequence homology of the binding site between the five muscarinic receptor subtypes and the wide distribution of this receptor family in both the central nervous system (CNS) and the periphery. Hence, a plethora of ligands targeting less structurally conserved allosteric sites of the M$_1$ mAChR have been investigated. This Review aims to explain the rationale behind allosterically targeting the M$_1$ mAChR, comprehensively summarize and critically evaluate the M$_1$ mAChR allosteric ligand literature to date, highlight the challenges inherent in allosteric ligand investigation that are impeding their clinical advancement, and discuss potential methods for resolving these issues.

KEYWORDS: M$_1$ mAChR, allosteric ligands, Alzheimer's disease, schizophrenia, cognitive deficits, memory
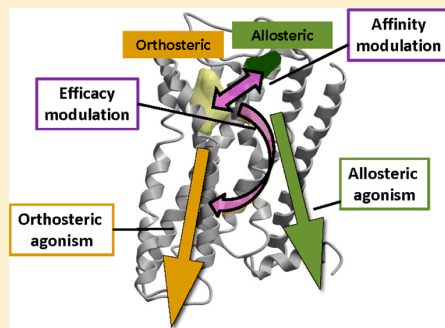
The muscarinic acetylcholine receptor (mAChR) family is a group of rhodopsin-like (Family A) G protein-coupled receptors (GPCRs) consisting of five distinct subtypes M$_1$–M$_5$. Activation of the M$_1$, M$_3$, and M$_5$ receptor subtypes primarily results in coupling to the G$_{q/11}$ family of G proteins, activation of phospholipase C (PLC), release of inositol-1,4,5-trisphosphate (IP$_3$), and subsequent mobilization of intracellular calcium Ca^{2+}. Activation of the M$_2$ and M$_4$ receptor subtypes primarily results in coupling to the G$_{i/o}$ family of G proteins, inhibition of adenylate cyclase (AC), reduction in cyclic AMP (cAMP), and a decrease in neurotransmitter release via the blockage of voltage-gated calcium channels (Figure 1). These pathways represent a generalized view of each receptor's coupling capacity, as all five subtypes couple to a broader range of G protein- and non-G protein-mediated signaling and regulatory pathways,[1] ultimately leading to the regulation of enzymes and neurotransmitters critical for intercellular chemical communication and biological function. In a broader molecular sense, this diversity is largely facilitated by the ability of GPCRs to adopt a range of conformational states that can lead to distinct functional outcomes.[2]

The relative distribution of the five mAChR subtypes in both the CNS and peripheral tissues was elucidated by mRNA hybridization and immunocytochemical methods.[3,4] The M$_1$
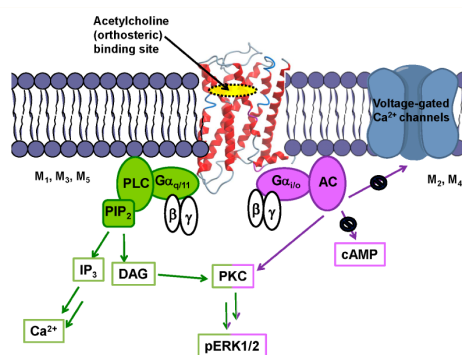

Figure 1. Common signal transduction pathways of the five muscarinic acetylcholine receptors.

mAChR is predominantly expressed postsynaptically in the CNS, particularly in regions of the hippocampus, prefrontal cortex, and striatum. The M$_2$ and M$_3$ mAChRs are expressed

both pre- and postsynaptically in different brain regions, most notably the basal forebrain, the thalamus, and the hippocampus. Furthermore, the peripheral tissues mostly express the M_2 and M_3 subtypes, particularly in cardiac and smooth muscle tissues. The M_4 and M_5 mAChRs are almost exclusively expressed in the CNS, the former presynaptically in the striatum and the hippocampus, and the latter in the substantia nigra.

This broad distribution is suggestive of muscarinic receptors mediating a diverse range of biological functions and hence playing potentially critical roles in a number of central and peripheral disease processes. This Review will henceforth focus on the role of the muscarinic system in the regulation of learning and memory in the CNS, specifically, the utility of targeting the M_1 mAChR for the treatment of neurodegenerative disorders, such as Alzheimer's disease (AD) and schizophrenia.

AD is a condition of the CNS with no definitive cause and no known cure. Four key "hallmarks" of this disease are cognitive decline in memory and learning, the dysfunction and eventual death of cholinergic neurons, the accumulation of β-amyloid plaques, and the formation of neurofibrillary tangles as a result of tau-protein hyperphosphorylation.[5] Schizophrenia is a debilitating disorder most likely caused by a combination of genetic and environmental factors, though the biological origin is unknown. The disease manifests as four "symptom domains":[6] positive (hallucinations, delusions), negative (social withdrawal, lack of initiative), cognitive (attention deficit and impaired memory), and affective (anxiety, depression, aggression, and suicidal tendencies).

A poorly treated symptom of both disorders is cognitive impairment, which manifests as dysfunctions in memory consolidation, learning, and higher-order processing. While disruption of multiple neurotransmitter systems may be implicated in these deficits,[7] considerable evidence suggests that impaired cortical-hippocampal cholinergic signaling plays an integral part in the manifestation of these conditions.[6] The advent of research tools such as receptor knockout (KO) mice and subtype-selective muscarinic ligands has afforded significant advances in our understanding of the role of the cholinergic system in the physiology and pathophysiology of cognition.[8,9] In particular, M_1 mAChR activation by subtype-selective allosteric enhancement has shown considerable promise as a means of ameliorating cognitive decline and treating disease state pathophysiology.[10] However, the lack of structural information about the M_1 mAChR allosteric binding sites and the complex behavior of allosteric ligands is such that rational drug design and preclinical pharmacological evaluation are fraught with challenges impeding the development of viable therapeutics. This Review will discuss essential considerations in the classification and pharmacological evaluation of allosteric ligands, summarize the M_1 mAChR allosteric ligands reported to date, and offer a perspective on the pharmacological methods employed in their development.

■ THE CHOLINERGIC HYPOTHESIS OF MEMORY DYSFUNCTION

The culmination of considerable biochemical, electrophysiological, and pharmacological evidence gained from studies in elderly patients gave rise to the cholinergic hypothesis of memory dysfunction some decades ago.[11] Four critical observations that unequivocally validated this hypothesis were as follows:

(i) the substantial loss of presynaptic cholinergic basal forebrain cortical projection neurons in human post-mortem Alzheimer's-diseased brains;[12]

(ii) the dysfunction of cholinergic markers, such as acetylcholine (ACh), choline (a precursor of ACh), and choline acetyl transferase (an enzyme for ACh production), observed in the human post-mortem brains of patients suffering from cognitive deficits;[13]

(iii) the behavioral cognitive impairments observed upon pharmacological disruption of cholinergic activity;[11] and

(iv) the improvement in cognition observed in elderly patients upon artificial enhancement of cholinergic activity[11]

Accordingly, cholinergic enhancement via inhibition of the enzyme responsible for ACh degradation, cholinesterase, was pursued, giving rise to the four anticholinesterase drugs currently approved for the treatment of the various stages of AD: tacrine, donepezil, rivastigmine, and galantamine. While widely used, these drugs have a propensity for nonselective activity, leading to a swathe of side effects associated with excessive cholinergic stimulation, such as diarrhea, hypersalivation, and bradycardia. The failing of the anticholinesterases is unsurprising considering that they target an enzyme present at the synapses of all cholinergic neurons, likely resulting in broad spectrum, abrupt muscarinic activation in whatever tissue compartment that these drugs are distributed. Furthermore, these therapies have been shown to elicit little to no therapeutic efficacy in up to 75% of the patient population,[14] which is possibly due to the progressive degeneration of presynaptic cholinergic nerve terminals as the disease state progresses.

■ XANOMELINE: AN IMPORTANT PROOF-OF-CONCEPT COMPOUND

An alternative method by which cholinergic enhancement may be achieved is to mimic the actions of ACh, namely, by selective mAChR activation (and nAChR activation, which is beyond the scope of this Review). Important proof-of-concept for selective mAChR activation as a potential therapy for the cognitive deficits associated with neurodegenerative conditions came with the discovery of the compound xanomeline (**1**, Figure 2),
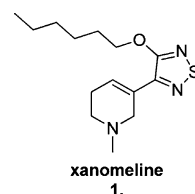

xanomeline
1.

Figure 2. Structure of the M_1/M_4 mAChR-preferring agonist xanomeline (**1**).

a M_1/M_4-preferring agonist (see Mirza et al.[15] for a comprehensive review). This compound produced increased brain ACh levels, demonstrated a reversal of antagonist-induced memory block following IP administration in mice, and attenuated cognitive decline in a 6 month clinical trial in human AD patients following oral administration.[16]

Studies in M_1–M_5 muscarinic receptor KO mice directly linking the absence of each receptor subtype to specific biochemical, physiological, and behavioral changes have enabled assignment of each receptor with likely biological

1027   dx.doi.org/10.1021/cn400086m | ACS Chem. Neurosci. 2013, 4, 1026–1048

22

functions.[8] M_1 mAChR KO mice exhibited deficits in tasks most likely involving neural communication between the cerebral cortex and the hippocampus. Moreover, activation of the M_1 mAChR was found to be the predominant mediator of the effects on cognition, attention, and learning that were observed following xanomeline administration;[17] these effects were attenuated in M_1 mAChR KO mice (but not M_4 mAChR KOs).

In addition to validating the therapeutic utility of M_1 mAChR targeting, xanomeline also validated M_4 mAChR activation as a potential treatment for psychosis, demonstrating in vivo efficacy in both animal[18] and human[19] clinical trials, and exhibiting a similar therapeutic profile to the atypical antipsychotics clozapine and olanzapine.[15] The attenuation of amphetamine-induced psychotic behaviors observed with administration of xanomeline was absent in M_4 mAChR KO mice (but remained present in M_1 mAChR KOs).[20] This antipsychotic action is postulated to occur via indirect modulation of dopamine levels; the M_4 mAChR is highly expressed within the mesolimbic dopaminergic system, commonly associated with positive symptoms of schizophrenia.[21]

Unfortunately, while xanomeline exhibits some degree of selectivity as a M_1/M_4 mAChR agonist, binding studies in cloned human muscarinic receptors revealed no preferential binding affinity for these two subtypes in relation to the others,[22] a factor that likely contributed to the peripheral cholinergic side effects that prompted the withdrawal of 52% of AD subjects in a phase III trial of xanomeline.[9] This, combined with its vastly different efficacy and selectivity profiles depending on the in vitro experimental paradigm utilized,[15] its off-target activity at dopaminergic and 5-HT receptor subtypes,[23] and the compound's metabolic instability and high hepatic first pass effect leading to <1% oral bioavailability in both animals and humans,[15] has rendered xanomeline an insufficient clinical candidate. Despite this clinical failure, the M_1 mAChR target validation afforded by xanomeline sparked considerable research interest into deconvoluting the mechanisms by which this receptor mediates cognitive processing.

■ THE ROLE OF THE M_1 mAChR IN COGNITION

M_1 mAChRs are most abundantly expressed postsynaptically in regions of the forebrain such as the hippocampus, striatum, and cerebral cortex.[3] Stimulation of M_1 mAChRs activates multiple signaling pathways leading to the production of numerous downstream effector molecules, each of which is likely to contribute to the overall physiological functioning of M_1 mAChRs, as well as the utility of targeting these receptors for the treatment of cognitive deficits. One such example is the protein kinase C (PKC) family, important signaling enzymes that are produced following $G\alpha_{q/11}$ pathway activation and are significantly reduced in the Alzheimer's diseased brain[24] (for a more detailed summary of the potential effects of PKC in cognition and Alzheimer's disease, see a recent publication by Fisher[25]). Additionally, it has been demonstrated that activation of M_1 mAChRs leads to potentiation of currents through the N-methyl-D-aspartate (NMDA) receptor in hippocampal pyramidal cells,[26] a receptor shown to play a critical role in synaptic plasticity and memory consolidation.[27]

Herein lies one of the key theoretical advantages of postsynaptic M_1 mAChR activation. Unlike the anticholinesterases, this mode of treatment does not rely on the presence of intact presynaptic cholinergic nerve terminals to be effective, neurons that are significantly compromised in neurodegener-

ative disorders.[28] Additionally, it has been shown that, in AD cortical tissue, postsynaptic M_1 mAChR density is unaltered[29] (and in a more recent study significantly increased[30]), establishing the availability of the target in the most critically affected brain region of patients, regardless of the extent of cognitive decline.

■ THE ROLE OF THE M_1 mAChR IN MODIFYING AD PATHOPHYSIOLOGY

A significant advantage of M_1 mAChR activation for the treatment of Alzheimer's disease is the potential for positive modification of the underlying pathophysiology of the condition that leads to cognitive symptoms in the first place, affording a prospective dual action treatment for AD unable to be accomplished by anticholinesterase therapies. Two widely acknowledged pathophysiological hallmarks of AD are the accumulation of β-amyloid plaques and the formation of neurofibrillary tangles as a result of tau-protein hyperphosphorylation,[5] "vicious cycles" that both lead to substantive CNS cholinergic neural death in the cortical and hippocampal regions of the basal forebrain (flowchart depicted in Figure 3).
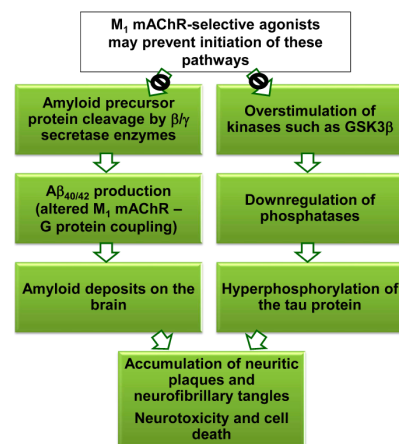

Figure 3. Two pathophysiological pathways underlying Alzheimer's disease.

Amyloid precursor protein (APP) has been linked to functions such as regulation of synaptic interactions and neuroplasticity.[31] APP can be differentially cleaved by secretase enzymes into amyloidogenic and nonamyloidogenic metabolites which forms the basis for the pathophysiology of Alzheimer's disease and the prospect of M_1 mAChR activation as a potential treatment. The amyloidogenic pathway is characterized by β/γ secretase cleavage of APP, resulting in peptides such as $A\beta_{40}$ and $A\beta_{42}$, the primary constituents of the aggregated amyloid neuritic plaques observed in the AD brain.[32] Accumulation of $A\beta$ peptides is also postulated to impair mAChR coupling to G proteins,[33] which is likely to further perpetuate the disease state. In contrast, the non-amyloidogenic pathway is stimulated by the action of the α-secretase enzyme, which cleaves APP within the $A\beta$ peptide sequence, leading to harmless metabolites. The question of which pathway predominates at any given time depends on the relative expression of the secretase enzymes, which is largely dictated by the actions of cellular second messenger systems downstream of GPCRs. Specifically, M_1 mAChR activation and

initiation of $G_{q/11}$-mediated activation of PKC has been linked to the increased expression of α-secretase,[34] and consequently promotion of the nonamyloidogenic pathway and a reduction in Aβ peptide levels, which could potentially slow or halt the formation of amyloid plaques and hence, the progression of AD.

Further validation of the critical role of the M_1 mAChR in modulating this process was obtained when the treatment of human AD patients with a selective M_1 mAChR agonist, talsaclidine (2, Figure 4), led to an observed reduction in Aβ_{42}
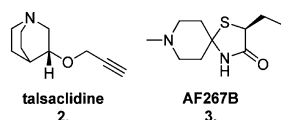

talsaclidine
2.

AF267B
3.

Figure 4. Structures of two M_1 mAChR selective agonists, talsaclidine (2) and AF267B (3).

levels in their cerebrospinal fluid (CSF).[32] Additionally, in vivo studies in 3xTg mice (injected with transgenes for β-amyloid and tau, and therefore a model for AD) reported increased CSF levels of α-secretase-producing enzyme, ADAM17, and a corresponding decrease in β-secretase formation following treatment with another M_1 mAChR-selective agonist, AF267B (3, Figure 4).[35]

The second "vicious cycle" referred to earlier is the formation of neurofibrillary tangles that occurs when the protein essential for the growth of microtubules in the neuronal cytoskeleton, tau, becomes hyperphosphorylated. Both in vitro and in vivo studies[33,35] have demonstrated that activation of the M_1 mAChR has the potential to decrease tau phosphorylation by PKC-mediated inhibition of kinases (particularly GSK3β) and upregulation of phosphatases, subsequently decreasing the likelihood of fibrous tangle formation.

A comparative analysis of M_1 mAChR expression and response in the post-mortem cortical tissue of humans observed to have no cognitive impairment, mild cognitive impairment, or Alzheimer's disease was conducted to further understand the link between activation of this receptor and AD pathophysiology.[30] [^{3}H]-Oxotremorine-M radioligand binding studies found M_1 mAChR expression to be elevated in the AD cortical tissue, indicative of compensatory upregulation in response to a reduction in ACh levels. It was also found that while there was no correlation between function of M_1 mAChRs and the degree of cognitive impairment, a negative correlation between M_1 mAChR functional activity and severity of neuropathology (based on post-mortem neurofibrillary tangle analysis) was observed, adding further weight to the argument for selective targeting of this receptor in the treatment of AD.

■ THE ROLE OF THE M_1 mAChR IN TREATING SCHIZOPHRENIA

Currently available pharmaceutical treatments for schizophrenia largely target dopamine (D) receptors or a combination of dopamine and serotonin (5-HT) receptors. First generation antipsychotics, such as haloperidol and chlorpromazine, are predominantly D_2R antagonists, treating the positive symptoms of the disorder but also eliciting Parkinsonian-like motor dysfunction (extrapyramidal side effects (EPS)).[36] Second generation antipsychotics, such as clozapine and olanzapine, treat positive symptoms by acting as D_2R antagonists but also partially treat the negative symptoms and reduce EPS by acting

as cortical 5-HT$_{2A}$R antagonists. However, these therapies still demonstrate poor efficacy and a lack of selectivity, resulting in a range of potentially dangerous side effects, including prolongation of QT interval, agranulocytosis, and severe weight gain.[37] Aripiprazole is a third generation antipsychotic exhibiting a unique mechanism of action: D_2R partial agonism, 5-HT$_{1A}$R partial agonism, and 5-HT$_{2A}$R antagonism, the combination of which results in increased and decreased neurotransmission in hypodopaminergic and hyperdopaminergic areas, respectively.[38] Thus, it is considered to be the first dopamine–serotonin system stabilizer. Despite reports of an excellent safety and tolerability profile, aripiprazole still demonstrates the potential to cause the same side effects as its first- and second-generation predecessors.

A major deficit of these three classes is that none were designed to treat, nor show substantial efficacy against, the cognitive deficits experienced as part of schizophrenia. This is despite the observation that the degree of cognitive impairment is the strongest predictor of clinical outcome for sufferers of this debilitating mental disorder,[39] and that cognitive symptoms are often evident in patients before the onset of psychosis.

The notion of treating schizophrenia by targeting the cholinergic system predates the widely regarded dopamine hypothesis,[40] the latter having given rise to the majority of schizophrenia medications to date. Decades-old clinical observations of muscarinic agonists exhibiting modest antipsychotic properties and anticholinergic exacerbation of schizophrenic symptoms formed the foundation of this theory, and more recent studies have demonstrated decreases in muscarinic receptor binding in both the prefrontal cortex and the hippocampus in schizophrenic patients,[41,42] regions rich in the M_1 mAChR subtype. Taken together, this suggests that the M_1 mAChR may represent a therapeutically beneficial target for both positive and cognitive symptom domains. Furthermore, the direct and indirect interactions between the dopaminergic and cholinergic neurotransmitter systems in the brain implicate a role for the M_1 mAChR (and indeed other muscarinic receptor subtypes) in modulating the complex underlying pathophysiology of schizophrenia.[43] However, while a muscarinic hypothesis of schizophrenia certainly warrants further investigation, particularly the roles of the M_1 and M_4 mAChR subtypes, it must be acknowledged that schizophrenia is a collection of syndromes likely to be dictated by multiple neurotransmitter systems and ultimately requiring combination drug therapy if all symptoms are to be alleviated.

■ CAVEATS OF TARGETING THE M_1 mAChR

In principle, selective M_1 mAChR agonists are less likely to exhibit side effects than anticholinesterases as they possess a more specific cholinergic objective, a single mAChR subtype. Despite this, there are presently no M_1 mAChR agonists approved as neurodegenerative therapies. While several ligands have demonstrated sufficient M_1 mAChR selectivity in in vitro studies supporting target validation, these compounds either show poor pharmacokinetic profiles and limited in vivo efficacy or fail to exhibit sufficient receptor subtype selectivity to avoid peripheral muscarinic side effects, such as gastrointestinal disruption, nausea, bradycardia, and excessive exocrine gland secretion.[44] This latter issue arises from their targeting the endogenous agonist-binding (orthosteric) site of the receptor, for which a high degree of sequence homology and structural conservation exists across the five mAChRs. This selectivity problem commonly manifests in therapeutics targeting GPCRs

with multiple receptor subtypes such as the adenosine, dopamine, and serotonin GPCRs. Another notable caveat of M_1 mAChR activation is that it may not necessarily improve coupling between the receptor and the G protein, a critical event that is significantly compromised in the AD prefrontal cortex.[45]

■ THE UTILITY OF TARGETING M_1 mAChR ALLOSTERIC SITES

Allosteric ligands bind to a site topographically distinct from the orthosteric site of the receptor and are able to enhance or reduce the effect of the concomitantly bound orthosteric ligand.

The three mechanisms by which allosteric ligands exert their effects,[46] as depicted in Figure 5, are as follows:
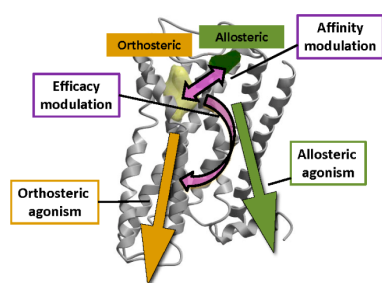

Figure 5. Three modes by which allosteric ligands exert their effects. (1) Orthosteric ligand affinity modulation; (2) orthosteric ligand efficacy modulation; and (3) direct allosteric agonism.

  (i) by modulating the binding affinity of the orthosterically bound ligand;
 (ii) by modulating the downstream efficacy of the orthosterically bound ligand; and
(iii) by activating the receptor in their own right, acting as allosteric agonists

Conformational changes in the receptor induced by allosteric ligand binding are the source of their modulatory activity. Localized alterations to the orthosteric site topography may either enhance or reduce the binding affinity of the orthosteric ligand, while a broader conformational shift in the GPCR may either enhance or reduce the overall signaling efficacy of the receptor. These modulatory effects, combined with any agonism conferred by the allosteric ligand alone, dictate the global change in receptor activity observed. For an elegant representation of the distinct allosteric ligand profiles that may arise from the combination of these three effects, see a recent review by Kenakin.[47] To gain an understanding of how the complex multidirectional interplay between an orthosteric ligand, allosteric ligand, and receptor (ternary) complex can be modeled and quantified, see the review by May et al.[48]

Recently marketed allosteric drugs afford practical validation for the development of allosteric ligands as therapeutic solutions. Cinacalcet[49] acts as an allosteric potentiator at the calcium-sensing receptor for the treatment of hyperparathyroidism, maraviroc[50] is an anti-HIV drug that acts as an allosteric inhibitor of the chemokine receptor CCR5, and the benzodiazepines,[51] used for the treatment of anxiety disorders, are allosteric modulators at $GABA_A$ receptors.

Allosteric ligands offer notable advantages over classic orthosteric drugs.[52] First, allosteric sites can have a less conserved amino acid sequence between receptor subclasses,[53]

potentially allowing for selective targeting and minimization of the side effects evident in the binding of pure orthosteric agonists, such as the undesirable peripheral muscarinic effects of xanomeline. Another advantage is the saturability of their effect. Drugs targeting the receptor orthosteric site frequently elicit an all-or-nothing response upon interaction, leading to complete activation or perturbation of downstream signaling and the associated biological function(s). The intensity of action of these ligands is directly proportional to their concentration in the receptor compartment;[54] so, depending on the dose that reaches the target receptor and the off-rate of the ligand from the receptor, the duration of effect of orthosteric drugs may carry the risks of side effects, overdose, or desensitization and tolerance.[55] In contrast, the effect of a positive or negative allosteric modulator is dictated by the degree of cooperativity they possess with the ligand occupying the orthosteric site,[56] such that the intensity of action reaches a limit once all allosteric binding sites are occupied; creating a "ceiling" for their biological effect and potentially avoiding the aforementioned risks.

A somewhat more contentious advantage is the precision of their effect. It is thought that "pure" allosteric modulators (that is, those devoid of agonist activity in their own right) afford the advantage of spatial and temporal specificity[52,56] in that they require the presence of the orthosteric ligand to exert their effect, confining their activity to the location and time in which physiological activity is occurring. However, it is now evident that an observed lack of allosteric agonism may also be a function of the ligand concentration, the degree of signal amplification of the pharmacological assay, and the coupling efficiency of the receptor for the signaling pathway being measured.[57,58] That is to say that if an allosteric ligand is assessed in an assay with minimal signal amplification that measures a pathway poorly coupled to the receptor of interest, any direct allosteric agonism of the ligand may go undetected. Indeed, it can be reasonably hypothesized that all positive allosteric modulators may display allosteric agonism and all negative allosteric modulators may display inverse agonism, under the right assay conditions.[2] Therefore, in order to more accurately predict the functional profile of an allosteric ligand in preclinical animal studies and subsequent clinical trials, in vitro cellular assays that follow initial hit detection ought to resemble the cellular background, native receptor expression levels, local neurotransmitter concentration, and biochemical outcomes of the human pathophysiological tissue of interest as closely as possible. This is likely to pose complex challenges, especially for CNS disorders in which multiple brain regions (with different receptor expression levels and neurotransmitter concentrations) are being targeted to achieve in vivo efficacy.

M_1 mAChR allosteric ligands may provide solutions to the problems hindering the development of an optimized cholinergic treatment for cognitive dysfunction. Their subtype selectivity will facilitate further investigation into the physiological and pathophysiological roles of this receptor in the brain, as well as offer the prospect of neurodegenerative disorder therapies devoid of side effects. Additionally, while their ability to modulate endogenous neurotransmitter activity affords the prospect of improved cholinergic tone, the potential for allosteric activation of the M_1 mAChR in their own right becomes all the more critical as functional ACh levels decrease in tandem with neurodegeneration and disease state progression. Moreover, the ability of such ligands to stabilize distinct receptor conformations may lead to the discovery of

1030

dx.doi.org/10.1021/cn400086m | *ACS Chem. Neurosci.* 2013, 4, 1026−1048

functional profiles that bias the receptor toward neurotrophic and pro-cognitive pathways while disfavoring pathophysiological and neurotoxic pathways.

STRUCTURAL STUDIES OF M_1 mAChR ORTHOSTERIC AND ALLOSTERIC SITES

Until recently, modeling of the muscarinic GPCR family has been largely based on the rhodopsin,[59] β-adrenergic,[60] and A_{2A} adenosine[61] GPCR crystal structures, other Family A GPCRs with which they share common structural motifs.[62] However, recent publication of the inactive human M_2 and the rat M_3 mAChR crystal structures[63,64] will undoubtedly provide unparalleled insight into the structures of the other muscarinic receptor subtypes going forward.

Studies of the cloned M_1–M_5 mAChRs have revealed a high degree of sequence homology between the subtypes, particularly in transmembrane (TM) units 2–7, a region containing a highly structurally conserved hydrophilic cavity.[65] Within this cavity projects a TM3 negatively charged aspartate residue common to all subtypes, which has been shown by binding and point-mutation studies to be critical for orthosteric ligand binding,[66] forming an ionic interaction with the polar, positively charged (or ionizable) headgroup of both agonists, such as acetylcholine, and antagonists, such as atropine (**4** and **5**, Figure 6). A combination of computational and molecular
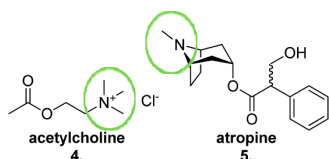
Figure 6. Structures of the muscarinic orthosteric agonist acetylcholine (**4**) and the muscarinic orthosteric antagonist atropine (**5**), highlighting the positively charged and ionizable head groups, respectively.

biological techniques have identified additional residues extending into this pocket as having key roles in orthosteric ligand binding, kinetics, and receptor activation.[67]

Similar approaches have been adopted to identify the key residues involved in the interaction of allosteric ligands with the M_1 mAChR. To date, two M_1 mAChR allosteric binding sites have been pharmacologically characterized. Early binding and site-directed mutagenesis studies using the allosteric muscarinic ligands gallamine (**6**) and alcuronium (**7**) provided evidence for the first site, an extracellular (EC) allosteric binding domain involving residues from EC loops 2 and 3 adjoining TMs 5, 6, and 7.[68] This site is often referred to as the "common" allosteric binding site[69] for mAChRs as its topographical location is preserved across the subtypes, while the nonconserved residues in this region confer allosteric ligand mAChR subtype selectivity. More specifically at the M_1 mAChR, the positive charges present on both gallamine and alcuronium (Figure 7) are thought to be important for interaction with negatively charged EC3 residues (S388, D393, and E397) extending into the hydrophilic EC space, while the hydrophobic portions of these molecules are thought to form interactions with tryptophan residues (W101 and W400) within upper TM units.[70]

The existence of a second allosteric site was proposed when the ability of the indolocarbazole KT5720 (**8**, Figure 8) to allosterically enhance the binding of both the agonist ACh and
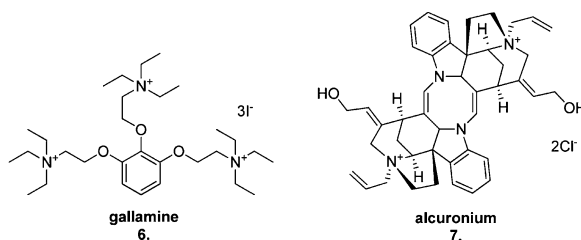
Figure 7. Structures of the two "common" muscarinic allosteric site binders, gallamine (**6**) and alcuronium (**7**).
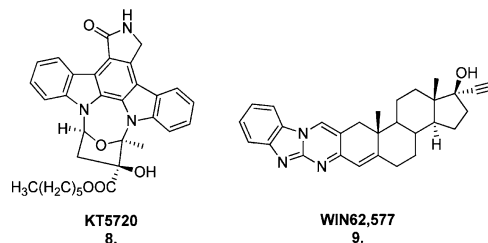
Figure 8. Structures of the second muscarinic allosteric site binders, KT5720 (**8**) and WIN62,577 (**9**).

the antagonist *N*-methylscopolamine (NMS) at the M_1–M_4 mAChRs was unchanged in the presence of the allosteric ligand gallamine.[71] This is indicative of two separate allosteric binding sites and, as neither allosteric ligand altered the potency or relative effectiveness of the other when co-bound, they exhibit neutral cooperativity with one another.[72] Additional muscarinic allosteric ligands reported to bind to this second site are WIN62,577 (**9**) and its analogues (Figure 8).[73]

Using a rhodopsin-based homology model of the M_1 mAChR, this second allosteric site was later postulated to be located on the intracellular (IC) face of the receptor close to the G protein-coupling domain, involving residues within TMs 2, 3, and 7, the C-terminal helix 8 and IC loop 3, a proposition that is yet to be experimentally validated.[74]

The future elucidation of the M_1 mAChR structure by X-ray crystallography (and eventual cocrystallization with proposed allosteric ligands) will hopefully further validate the homology model-based structural studies undertaken so far and greatly enhance our understanding of ligand–receptor interactions. Regardless, the existence of multiple allosteric sites on the M_1 mAChR adds another layer of complexity to the already complicated field of subtype-selective allosteric ligand design.

IMPORTANT CONSIDERATIONS IN ALLOSTERIC LIGAND CLASSIFICATION AND EVALUATION

Positive Allosteric Modulators (PAMs) Possessing Intrinsic Agonism. As alluded to earlier, it may be the case that all positive allosteric modulators may display allosteric agonism in their own right if evaluated in a sufficiently amplified pharmacological assay. Therefore, classifying a ligand as a "pure" allosteric modulator should be done tentatively and with due consideration to the context in which the ligand has been tested.

Estimating Ligand Potency. The M_1 mAChR PAM literature regularly reports ligand potency by determining an EC_{50} value. This value is determined by first generating a concentration response curve (CRC) for an orthosteric agonist of the M_1 mAChR (e.g., ACh) using the cellular background

and functional assay of choice (e.g., calcium mobilization in CHO cells). From this curve, a single concentration is selected depending on the type of allosteric modulation expected to be observed. If positive modulation is expected, as is the case with the M_1 mAChR PAM studies described here, an EC_{20} of ACh may be selected (Figure 9a), the concentration at which 20% of the maximal system response to the ligand is elicited, affording a suitable "window" in which to detect the anticipated modulatory activity.
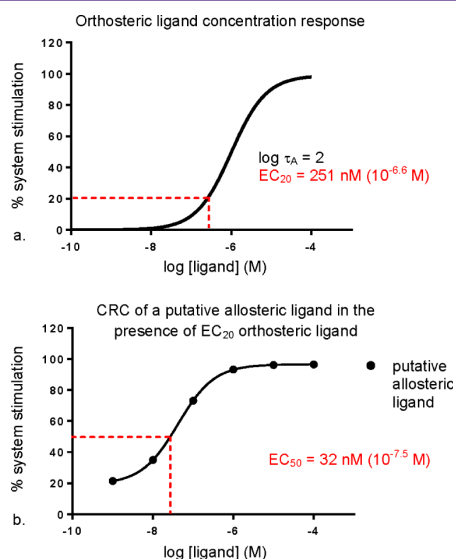

Figure 9. Simulated example of a common screening method for putative allosteric ligands. (a) A concentration−response curve of a known orthosteric ligand (e.g., ACh) used to derive an EC_{20} concentration value; $\log \tau_A$ is the operational efficacy parameter of the orthosteric ligand (the higher the value, the greater the efficacy). (b) How a concentration response curve of a putative allosteric ligand might look in the presence of the derived EC_{20} concentration of orthosteric ligand.

This predetermined concentration of orthosteric ligand is then coadded with increasing concentrations of the test allosteric ligand in the same cellular background and functional assay, and, assuming the predicted modulation is observed, the potency of the allosteric modulator is equated to the EC_{50} value, the concentration at which 50% of the maximal system response to the allosteric ligand in the presence of a fixed concentration of orthosteric ligand is elicited (the point of inflection of the titration curve, see Figure 9b).

This is a typical and efficient method for screening for activity of putative ligands, and can provide preliminary information about the mode of action of the ligand. However, by virtue of screening against a single concentration of orthosteric ligand, this method examines a one-dimensional cross section of the putative ligand's pharmacological profile, a cross section that may not necessarily capture the true behavior of the ligand. An interaction study in which the full CRC of the orthosteric ligand is assessed against increasing concentrations of the putative allosteric ligand is necessary to confidently classify the mode of action of the ligand. As demonstrated in Figure 10, a PAM, an allosteric agonist, and a competitive orthosteric agonist would all appear the same when coadded with a single orthosteric ligand concentration (note that Figure

9b and Figure 10d are indistinguishable). It is not until interaction studies over a range of orthosteric ligand concentrations are performed that the mode of action of the test ligands can begin to be deduced (Figure 10a−c).

A combination of functional and radioligand binding assays is necessary to determine whether the allosteric ligand's modulatory activity is elicited primarily through modulation of binding affinity, signaling efficacy, or a combination of the two. These experiments will also delineate its modulatory effects on the orthosteric ligand from any agonist response in its own right. These parameters can be estimated via application of the allosteric ternary complex model for binding experiments and the operational model of allosterism for functional experiments.[48] It is important to note that, even if this more detailed pharmacological characterization of the allosteric ligand is performed, the estimates of affinity, efficacy, and cooperativity obtained are only applicable in the context of the orthosteric probe utilized, the functional assays performed, and the cellular background under investigation.

Acknowledging Unique Allosteric Properties. Allosteric ligands possess a number of inherent properties that necessitate broader pharmacological evaluation than their orthosteric counterparts. Two fundamental pharmacological properties that can be engendered by GPCR allosteric ligands are stimulus bias[75] and probe dependence.[76] These terms refer to the differing allosteric modulatory effects observed depending on the cellular signaling pathway being assessed by the assay, and the orthosteric ligand cobound to the receptor, respectively.

The foundation of stimulus bias is the stabilization of distinct receptor conformations. In the same way that different orthosteric agonists and antagonists stabilize multiple active and inactive receptor states, respectively, allosteric ligands may stabilize diverse conformations that result in differential activation of receptor signaling pathways, or collateral efficacy.[54] Such molecular tools may afford a greater understanding of the complex relationship between receptor conformations, discrete signaling profiles, and particular physiological and pathophysiological outcomes.

Probe dependence is an important property to consider during the processes of hit identification and lead optimization of allosteric ligands. If the orthosteric probe used to screen and elucidate the structure−activity relationships of novel allosteric chemical scaffolds is not the pathophysiologically relevant endogenous neurotransmitter, the risk is that the novel ligand may exhibit a different, potentially undesirable functional profile (or no function at all) in an in vivo setting.

An excellent mAChR exemplar of these two properties is the M_4 mAChR allosteric ligand LY2033298 (**10**, Figure 11).[77] Leach et al.[57] performed radioligand binding, [^{35}S]GTPγS, calcium mobilization, ERK1/2 phosphorylation, GSK-3β phosphorylation, and receptor internalization assays to fully assess the allosteric capabilities of LY2033298. They found that the degree of allosteric potentiation conferred by LY2033298 varied widely depending on the signaling pathway being examined, ranging from modest positive modulation of ACh activity in [^{35}S]GTPγS assays to robust enhancement of ACh activity in receptor internalization studies. Estimates of the degree of allosteric agonist activity also varied, further illustrating the property of stimulus bias. This also disproved the original classification of the ligand as a positive allosteric modulator with no agonist activity in its own right.[77] Radioligand binding assays were used to highlight the probe
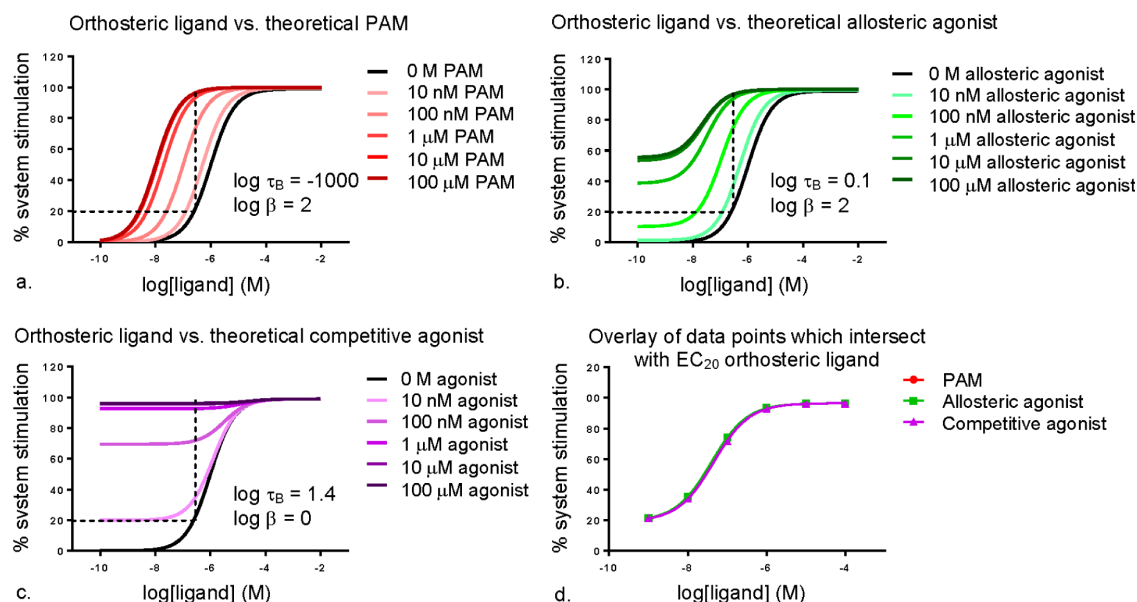
Figure 10. Simulated example of interaction studies between an orthosteric agonist and (a) a positive allosteric modulator (PAM), (b) an allosteric agonist, and (c) a competitive agonist, with broken lines indicating the intersection of the concentrations of test ligand with the EC_{20} of the orthosteric ligand. (d) An overlay of the data points from graphs (a)−(c) which intersect with the EC_{20} of the orthosteric ligand; log τ_B is the operational efficacy parameter of the allosteric ligand (the higher the value, the greater the efficacy; the high negative value represents a complete absence of allosteric ligand efficacy); log β is the functional cooperativity factor between the orthosteric and allosteric ligands (log $\beta > 0$ = positive cooperativity, log $\beta = 0$ = neutral cooperativity or, in this instance, direct competition between two orthosteric ligands).
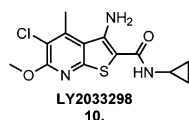

Figure 11. Structure of the M_4 mAChR allosteric ligand LY2033298 (**10**).

dependence of LY2033298; its allosteric agonism and modulatory effects were only detected when cobound with an orthosteric agonist, not an antagonist.

LY2033298 also revealed the ability of allosteric ligands to exhibit species-dependent differences in cooperativity.[78] This later led to the hypothesis that the proposed subtype selectivity of the modulator may arise from differential cooperativity, rather than variability of the allosteric pockets between receptor subtypes.[76] Despite LY2033298 exhibiting selective ACh potentiation at the M_4 mAChR, extensive evaluation of LY2033298 at wild-type and mutant M_2 mAChRs revealed marked degrees of probe dependence with a range of agonists and antagonists in radioligand binding assays, as well as both positive and negative cooperativity in two functional assays, [^{35}S]GTPγS binding and pERK1/2.

These findings highlight the highly contextual nature of allosteric effects and the importance of assessing binding, multiple functional pathways, different receptor subtypes, and a broad range of probes to fully characterize allosteric ligands.

Identifying a Purely Allosteric Mode of Action. For a ligand to be classified as an allosteric agonist at a particular receptor, it must possess intrinsic efficacy in its own right, regardless of whether an orthosteric ligand is co-bound to the receptor.[46] Its agonist effect must be elicited solely via an

allosteric mechanism, and the absence of direct activation via orthosteric site binding must be established.

Comprehensive radioligand binding and functional assays unequivocally demonstrated that the agonistic and modulatory behavior of LY2033298 at the M_4 mAChR was elicited via a purely allosteric mechanism;[57] with four key observations confirming this hypothesis.

In radioligand binding assays:

(a) LY2033298 exhibited a lack of significant affinity modulation of the muscarinic orthosteric antagonists NMS and QNB (3-quinuclidinyl benzilate), indicating no overlap with the orthosteric binding site

In [^{35}S]GTPγS binding assays:

(b) coaddition of the mAChR antagonist atropine caused a substantial reduction in the maximal effect of LY2033298 with a minimal change in potency, characteristic of noncompetitive negative cooperativity

(c) LY2033298 demonstrated a competitive interaction with the mAChR negative allosteric modulator $C_7/3$-phth, known to bind the "common" muscarinic allosteric site[79]

(d) LY2033298 exhibited neutral cooperativity upon coaddition with WIN51708, a known "second allosteric site" mAChR ligand,[73] confirming the allosteric agonist's site of action to be the "common" allosteric site on the M_4 mAChR

The Prospect of Bitopic Interactions. While the M_1 mAChR-selective ligand literature reviewed herein provides substantial evidence to suggest purely allosteric modes of action, there exist several examples where this evidence is inconclusive. Such ligands have hence been termed "putative bitopic M_1 mAChR agonists" in this Review. It has been noted that these ligands exhibit unique binding modes and divergent

functionality when compared to M_1 mAChR PAMs.[80,81] Depending on the experimental paradigm, many of these molecules have exhibited degrees of antagonistic interaction with different orthosteric mAChR ligands. While they may be acting as pure allosteric agonists possessing very high negative cooperativity with orthosterically bound ligands, it is equally if not more likely that they are interacting with the orthosteric site and an allosteric site simultaneously, behaving as "bitopic" ligands (also termed "dualsteric" or "multivalent") (Figure 12).
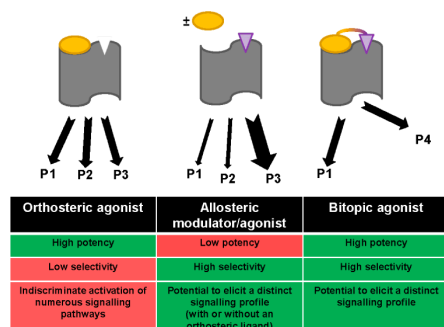
Figure 12. Advantages and disadvantages of orthosteric and allosteric ligands, and the theoretical fusion of their respective advantages by bitopic ligands: high potency, high subtype selectivity, and the potential to elicit distinct signaling profiles (Ps) that may be of therapeutic value.

This unique mode of ligand–receptor interaction has been validated[82] by a number of proof-of-concept studies (see Valant et al.[83] for a review). Notably, the conclusive classification of McN-A-343 (**11**, Figure 13) as a bitopic ligand,[84] initially
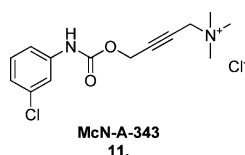

Figure 13. Structure of the M_2 mAChR bitopic ligand McN-A-343 (**11**).

thought to be an M_2 mAChR allosteric partial agonist,[85] highlights the detailed level of synthetic manipulation and pharmacological characterization necessary to appropriately classify the mode of action of a bitopic ligand. Just as McN-A-343 was truncated to form small molecular derivatives that were used to identify the orthosteric and allosteric portions of the molecule, similar methods will need to be employed to confirm the true nature of the putative bitopic M_1 mAChR agonists described within.

■ M_1 mAChR-SELECTIVE LIGANDS

Over the past two decades, a structurally diverse array of M_1 mAChR-selective ligands have been identified and characterized. Two distinct groups of these ligands will be reviewed herein: M_1 mAChR PAMs and putative bitopic M_1 mAChR agonists. Orthosteric M_1 mAChR ligands are beyond the scope of this Review. The methods used and the implications for the detection, optimization, and development of novel treatments for cognitive deficits of neurodegenerative conditions, and

indeed any allosterically derived treatment, will also be discussed.

M_1 mAChR PAMs. *Brucine.* In 1995, Lazareno and Birdsall[86] identified the naturally occurring alkaloid strychnine as an M_1-, M_2-, M_4-preferring allosteric ligand shown to possess low negative cooperativity with ACh, prompting the researchers to investigate a modified series of analogues with the intent of identifying ligands that possessed positive cooperativity with ACh as well as greater subtype selectivity.

The result was the discovery that the structurally related natural product brucine, 10,11-dimethoxy strychnine (**12**, Figure 14), exhibits modest positive cooperativity with ACh
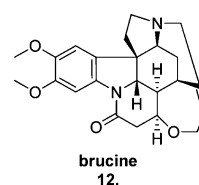

Figure 14. Structure of the M_1-preferring allosteric ligand brucine (**12**).

in both equilibrium binding experiments and functional assays (such as the [^{35}S]-GTPγS assay and the calcium mobilization assay) at the M_1 mAChR.[87] Unfortunately, brucine exhibited low affinity (0.1 mmol for the ACh-occupied receptor), minimal cooperativity (1.5–2-fold enhancement of ACh activity) and required high micromolar concentrations to produce any detectable activity. This, combined with its poor pharmacological profile, rendered the compound insufficient for use in native tissue and animal studies, and off-target activity suggested that the scaffold was unfavorable for further M_1 mAChR PAM analogue development. However, brucine provided important validation for selective allosteric modulation of M_1 mAChR activity as a viable field of therapeutic research.

Benzyl Quinolone Carboxylic Acid, BQCA. An exciting development in the pursuit of selective M_1 mAChR allosteric potentiators was Merck's discovery of BQCA (**13**, Figure 15),[88]
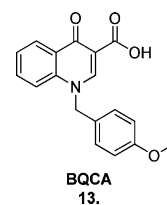

Figure 15. Structure of the breakthrough M_1-selective mAChR PAM BQCA (**13**).

by far the most actively investigated scaffold in this field to date. BQCA is the first reported orally bioavailable M_1 mAChR allosteric ligand exhibiting absolute subtype selectivity; no activity was detected at the other four muscarinic receptor subtypes in calcium mobilization assays (concentrations up to 100 μM). A notable feature of BQCA is its high degree of cooperativity; 100 μM of BQCA induced a robust 129-fold leftward shift in the ACh CRC (estimated from fluorometric imaging plate reader (FLIPR) calcium mobilization assays). Furthermore, BQCA produced an inflection point value of 845 nM in the presence of 3 nM ACh. A combination of molecular

modeling, site-directed mutagenesis, and radioligand binding studies revealed the residues Y179 and W400 to be important to the BQCA—receptor interaction, which is suggestive, but not conclusive, of the modulator exerting its effects via the "common" allosteric site.

Interestingly, it was recently reported that BQCA is the first allosteric GPCR ligand proven to abide by a strict two-state Monod-Wyman-Changeux (MWC) model of receptor activation,[2] in that its degree of modulation tracks with both the intrinsic efficacy of the cobound orthosteric ligand and the coupling efficiency of the receptor for a given intracellular signaling pathway.[58] Therefore, BQCA displays no stimulus bias, but still shows probe dependence by stabilizing the active receptor state favored by orthosteric agonists. As a result, it exhibits positive modulation when co-bound with orthosteric agonists and negative modulation when co-bound with orthosteric antagonists. It has been postulated that the inability of BQCA to stabilize a discrete receptor conformation arises from the ligand possessing few chemical functionalities capable of forming strong receptor interactions. Furthermore, the same study demonstrated that BQCA behaves as both a positive allosteric modulator and an allosteric agonist.[58]

BQCA possesses a sufficient pharmacological profile for analysis in both native tissue assays and in vivo animal studies. BQCA potentiated phosphorylated ERK production and RNA expression of the neuronal activation markers *c-fos* and *arc* in critical forebrain regions of the mouse brain where cholinergic degeneration in human AD patients is most pronounced.

Importantly, BQCA displayed efficacy in a contextual fear conditioning (CFC) mouse model of cognitive dysfunction. Mice dosed with 15−20 mg/kg BQCA exhibited behaviors suggesting a reversal of the scopolamine-induced block of memory formation.[88] As BQCA was shown to have no effect on [^{3}H]NMS affinity in radioligand binding assays (at concentrations up to 30 μM), this reversal of induced memory deficits was proposed to be solely due to BQCA's allosteric enhancement of endogenous ACh activity, decreasing the concentration of agonist required to displace the antagonist.

The short-term memory of acquired fear (as observed in the CFC model) is linked to the hippocampus, in which the M_1 mAChR is expressed in abundance. However, M_1 mAChR KO mice have shown intact cognitive processes associated with hippocampal-dependent learning[89] and no impairment in mAChR-mediated hippocampal pyramidal cell excitation.[90]

Shirey et al.[91] reported evidence indicating the M_1 mAChR is more likely to have a role in prefrontal cortex (PFC)-dependent learning, so the ability of BQCA to potentiate the carbachol (muscarinic agonist)-induced inward current (excitability) of medial (m)PFC pyramidal cells in rat brain slices was examined. BQCA increased the intensity and frequency of carbachol-induced spontaneous excitatory postsynaptic currents (sEPSCs), effects that were not observed in brain slices of M_1 mAChR KO mice. In support of these observations, another electrophysiology study demonstrated that coapplication of BQCA enhanced synaptic stimulation by carbachol in mPFC pyramidal cells, subsequently producing long-term depression (LTD), a critical process that, in conjunction with long-term potentiation (LTP), mediates synaptic plasticity.[92] These findings translated well to in vivo electrophysiology studies in which BQCA induced an elevation in the spontaneous firing rate of mPFC neurons in rats.[91]

In complement to these findings, further in vivo analysis using a mouse model of Alzheimer's disease (Tg2576 mice;

genetically modified to overexpress an amyloidogenic familial AD mutant form of APP) indicated that BQCA improved the performance of these mice in a discrimination reversal learning test, a PFC-dependent learning task.[91] The propensity for error was almost 7 times lower in BQCA-treated Tg2576 mice compared to controls. BQCA was found to be taken up into the brain between 30 min and 1 h after dosing, and maintained a constant level for 4 h; however, concentrations in the brain were found to be substantially lower than that in systemic circulation. Furthermore, BQCA (in the presence of carbachol) promoted the nonamyloidogenic pathway of APP cleavage in PC12 cells overexpressing human APP and M_1 mAChRs, as measured by increased levels of the protein fragments released by α-secretase cleavage of APP.

Overall, these studies validate the hypothesis that selective enhancement of M_1 mAChR activity in the PFC may lead to improved cognitive function in human patients, whether by directly enhancing PFC function and/or by modulating hippocampal function via cortical projection neurons. BQCA has shown efficacy in additional animal models of cognition that lend support to this hypothesis. A 10 mg/kg dose of BQCA attenuated scopolamine-induced memory deficit in a spontaneous alternation task[93] and prevented natural forgetting[94] in rats, suggestive of enhancement of both hippocampal- and PFC-dependent memory processes. Taken together, these studies endorse the investigation of M_1 mAChR PAMs as therapeutics for the symptoms and pathophysiology of AD.

Despite its many advantageous properties, critical deficits of BQCA include its low affinity (105 μM as estimated by Canals et al.[58]) and low free fraction (FF) of 1−4% (percentage of compound unbound by blood plasma proteins). However, the BQCA structure is highly amenable to optimization, affording the same benefits to medicinal chemists as conventional fragment hits do: a promising core scaffold with affinity for the target of interest, multiple points for diversification facilitating thorough structure—activity relationship (SAR) studies, and the ability to add functionalities for physicochemical optimization without exceeding a MW of 500 Da. This latter consideration is especially important for compounds like BQCA which require blood-brain barrier (BBB) permeability to reach their therapeutic target; a modified version of the Rule of Five suggests a MW < 450 Da for BBB passage.[95]

The multiple points for diversification on the BQCA scaffold have since resulted in a plethora of SAR studies that have generated a wide variety of analogues, some of which display substantial improvement on the characteristics of the parent compound. It is important to note however that all subsequent BQCA analogues described here were evaluated in only one functional assay against a single orthosteric ligand concentration, equating compound potencies to the EC_{50} (point of inflection) of the compound's CRC in the presence of an EC_{20} of ACh at human M_1 mAChR-expressing CHO cells using FLIPR calcium mobilization assays. Hence, the allosteric properties of stimulus bias and probe dependence remain untested.

After examining substituents with differing properties such as size, lipophilicity, and polarity, Yang et al.[96] derived some fundamental features they found to be critical to the scaffold's M_1 mAChR potency, summarized in Figure 17. Note that A-, B-, C-, and D-ring labeling will be used for ease of communication from this point onward.

Of the ∼100 analogues synthesized and tested, the compound possessing the best balance of potency and FF

was compound **14** (Figure 16); EC_{50} = 61 nM, hFF = 5.5%, rFF = 5.1%. However, subsequent evaluation of compound
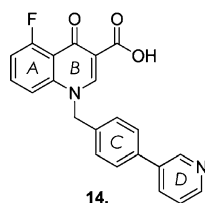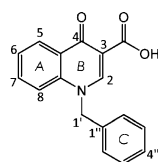

Figure 16. Structure of compound **14**.

A-ring - 5-fluoro, 8-fluoro and 5,8-difluoro substitutions preferred for potency
B/C-ring - longer linker or branching at 1' position not tolerated
C-ring - halogens and lipophilic moieties better tolerated than polar groups
          - *para*-substitution (4") preferred

Figure 17. Summary of the pharmacophoric features reported by Yang et al.[96]

concentration in CSF after oral dosing in rats (a surrogate measure for CNS exposure) yielded poor results, and was most likely the result of compound **14** being later confirmed as a P-glycoprotein (P-gp) substrate, one of the efflux transporters present in the BBB.

The most extensive BQCA analogue studies to date have been reported by Kuduk and co-workers.[97−105] Table 1 provides a summary of the most notable compounds from each series of structural modification; including their potency, favorable pharmacological properties and notable caveats.

Figure 18 provides a summary of the key SAR findings of these same publications. Challenging issues faced during these studies included the often confounding SAR, and difficulties in obtaining an optimal combination of pharmacological and pharmacokinetic properties. Additional patented structures discovered by this group not included in this Review are summarized in a recent publication.[106]

Vanderbilt University Compounds. Using high-throughput screening, researchers at Vanderbilt University investigated a broad range of chemical space to identify novel, structurally distinct chemical scaffolds that produce substantial allosteric modulatory activity at the M_1 mAChR.[107]

At a concentration of 10 μM, 1634 compounds significantly increased the muscarinic agonist carbachol's EC_{20} response above control levels in CHO cells expressing the rat M_1 mAChR. Subsequent screens of the more potent ligands confirmed 105 compounds (at 30 μM concentration) as positively modulating an EC_{20} concentration of ACh by measurement of intracellular calcium mobilization in the same cellular background. Four structurally diverse hits were selected for further analysis (**22−25**, Figure 19).

An allosteric mode of action was confirmed using [³H]NMS binding experiments; none of the test compounds demonstrated a competitive interaction with the orthosteric site-bound radio-labeled ligand. Using M_1 mAChR calcium mobilization assays as described previously, all four compounds demonstrated positive allosteric modulation of the ACh-induced receptor response and no observed allosteric agonism in their

own right. The most substantial enhancements of ACh potency were reported for VU0029767 (**25**) (15-fold) and VU0119498 (**22**) (14-fold). Unfortunately, none of the test compounds showed absolute subtype selectivity for the M_1 mAChR. As VU0029767 exhibited minimal modulation at the other four receptor subtypes and VU0090157 (**24**) showed only weak modulation at the M_4 mAChR, these two M_1 mAChR-preferring PAMs were further analyzed and found to exert their effects at the M_1 mAChR primarily through enhancement of ACh affinity for the orthosteric site (as indicated by shifts in the ACh/[³H]NMS competition binding assay curve). The two compounds were tested at both wild-type M_1 mAChRs and M_1 mAChRs containing the single point mutation Y381A, which replaces a tyrosine residue critical for orthosteric ACh binding with an alanine residue, thereby reducing ACh affinity and potency.
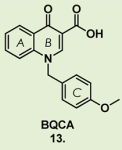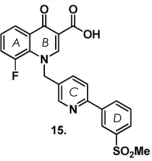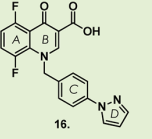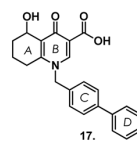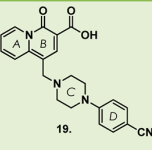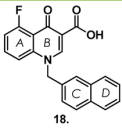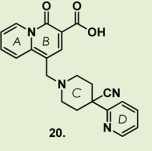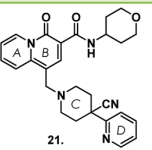
Interestingly, they found that the two ligands exhibited markedly different profiles. The potentiating ability of VU0029767 was preserved between wild-type and mutated receptors, while VU0090157 exhibited no potentiation of the ACh response at the mutated receptor. This suggests that these structurally diverse ligands may possess different degrees of cooperativity with ACh or two distinct binding modes at the M_1 mAChR. A shared characteristic, however, is that both ligands appear to stabilize a receptor conformation that renders ACh uncharacteristically tolerant of the Y381A mutation, as evidenced by the preserved 20% basal ACh activity between wild type and mutated receptors. The actual binding modes and sites of both allosteric compounds are thus far unconfirmed.

Additionally, the two ligands were found to induce different functional profiles in the ACh-mediated response of the wild-type receptor; the modulatory function of VU0090157 was preserved across three downstream signaling pathways linked to intracellular calcium release, phosphoinositide hydrolysis and phospholipase D activation respectively, while the degrees of potentiation of VU0029767 across these same pathways varied substantially. This finding highlights the importance of screening putative allosteric ligands across a broad range of functional assays to obtain thorough pharmacological characterization.

VU0119498 (**22**) was not pursued in earlier studies[107] as it potentiated ACh activity at all three $G_{q/11}$-coupled mAChRs, M_1, M_3, and M_5. However, following publication of BQCA,[88] to which it bears a resemblance, this compound was pursued as a candidate for further optimization to improve subtype selectivity.[108] Previous optimization of this structure to develop an M_5-selective PAM demonstrated that modifications to the aromatic left side of the isatin scaffold tended to yield ligands of highly variable activation, potentiation, and selectivity profiles.[109] Hence, modifications to the right side, such as chain length alterations, additional benzyl substituents, and introduction of a diverse range of substituted biaryl moieties, were explored.

The result was VU0366369 (**26**, Figure 20), the second highly selective and potent M_1 mAChR PAM reported.[108] BQCA and VU0366369 are reported to possess similar M_1 mAChR potencies in the same cellular background (EC_{50} = 845 and 830 nM respectively); however, the latter compound exhibited a markedly low degree of cooperativity (3-fold left shift of ACh CRC at 30 μM) compared to the former (129-fold left shift of ACh CRC at 100 μM). Taking into consideration the known promiscuity of isatin motifs in high-throughput screens, replacement with alternative structures was under-

Table 1. Summary of the BQCA Analogues Possessing the Best Balance of Properties, and Any Notable Caveats (as reported by Kuduk et al.)

Reference	Structural modifications	Most promising compound	No. in paper	Potency (nM)	Favourable pharmacological properties	Notable caveats
Ma, L. et al. (2009), PNAS, 106, 15950 Shirey, J. et al. (2009), J. Neurosci, 29, 14271	N/A	BQCA 13.	N/A	845	- 129-fold potentiation of ACh activity in Ca^{2+} mobilisation assays (at 100 µM) - efficacy in a mouse contextual fear conditioning (CFC) study (15-20 mg/kg dose) and a discrimination reversal learning test in Tg2576 mice (30 mg/kg dose)	- low free fraction (1-4% - Yang et al. (2010), Bioorg. Med. Chem. Lett. 20, 531) - poor affinity (105 µM – Canals et al. (2012), JBC, 287, 650)
Kuduk, S. et al. (2010), Bioorg. Med. Chem. Lett., 20, 657	- Benzyllic C-ring replacement with pyridine or diazines - D-ring benzyl substituents and heterocycles - A-ring fluorine substitution	15.	7e	28	- free fraction 5-7% - not a P-gp substrate	poor CNS exposure in rats
Kuduk, S. et al. (2010), Bioorg. Med. Chem. Lett., 20, 1334	Introduction of N-linked D-rings	16.	7	171	- free fraction 4-5% - 46-fold potentiation of ACh activity in Ca^{2+} mobilisation assays (at 1 µM) - efficacy in a mouse CFC study (10 mg/kg dose)	some degree of rat P-gp susceptibility
Kuduk, S. et al. (2010), Bioorg. Med. Chem. Lett., 20, 2533 Kuduk, S. et al. (2010), Bioorg. Med. Chem. Lett., 20, 2538	Heterocyclic or cycloalkyl A-rings	17.	10e	440	- free fraction 5-7% - excellent permeability (Papp = 20) - not a P-gp substrate - efficacy in a mouse CFC study (3 mg/kg dose)	
Kuduk, S. et.al. (2010), ACS Med. Chem. Lett. 1, 263 Kuduk, S. et.al. (2011), Bioorg. Med. Chem. Lett. 21, 1710	Replacement of quinolone with a quinolizidinone core	19.	10i	520	- excellent permeability (Papp = 22) - not a P-gp substrate - minimal hERG channel affinity - CNS exposure in rats - acceptable pharmacokinetics in rats and dogs - efficacy in a mouse CFC study (30 mg/kg dose)	
Kuduk, S. et al. (2011) Bioorg. Med. Chem. Lett., 21, 2769	Fused bicyclic C/D rings	18.	9a	69	- excellent permeability (Papp = 23) - not a P-gp substrate - 100-fold potentiation of ACh activity in Ca^{2+} mobilisation assays (at 1 µM)	
Kuduk, S. D. et al. (2011), J. Med. Chem. 54, 4773 Uslaner, J.M. et al. (2013), Psychopharmacol. 225, 21	Introduction of cyano group to the C-ring para position	20.	4i	135	- free fraction 29-32% - not a P-gp substrate - 146-fold potentiation of ACh activity in Ca^{2+} mobilisation assays (at 1 µM) - increased cerebral blood flow in mice - significant CNS exposure in rats - acceptable pharmacokinetics in rats and dogs - improved cognitive performance in three different animal models of cognition	potential for substantial hepatic first-pass effect
Kuduk, S.D. et al. (2012), ACS Med. Chem. Lett. 3, 1070	-Investigation of carboxylic acid surrogates	21.	4o	338	- free fraction 27-49% - excellent permeability (Papp = 33) - 52-fold potentiation of ACh activity in Ca^{2+} mobilisation assays (at 34 µM) - significant CNS exposure in rats - efficacy in a mouse CFC study (10 mg/kg dose)	P-gp substrate

A-ring - Cycloalkyl and heterocyclic derivatives unsuccessful
   - 5-fluoro substitution tended to improve free fraction but
     decrease permeability
   - 8-fluoro substitution tended to improve permeability but
     decrease free fraction
A/B-ring - replacing the quinolone with a quinolizidinone was not
     detrimental to potency
C-ring - 6-membered aromatic or saturated *N*-heterocyclic rings gave
     optimum balance of properties
   - cyano group at the 4" position improved potency and free fraction
D-ring - *meta*- and *para*-substitution (3'", 4'" and 5'") with small
     non-electron withdrawing groups preferred
   - 5-membered aromatic heterocycles improved potency and
     free fraction
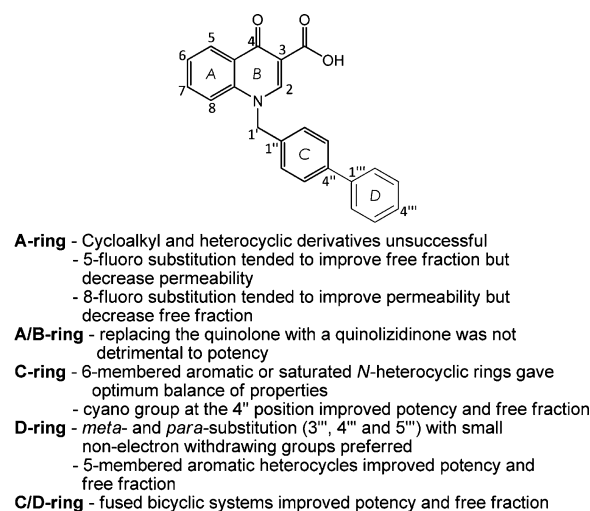C/D-ring - fused bicyclic systems improved potency and free fraction

Figure 18. Summary of the pharmacophoric features reported by Kuduk et al.
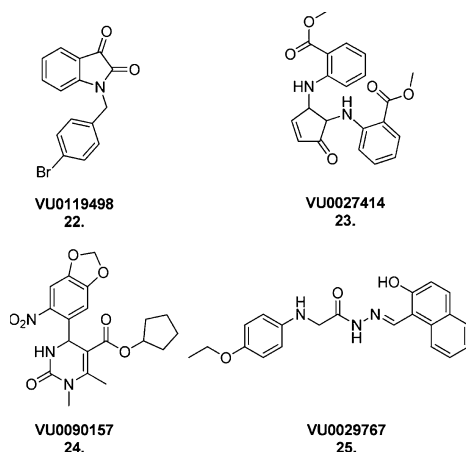

Figure 19. Structures of the structurally diverse muscarinic allosteric ligands VU0119498 (**22**), VU0027414 (**23**), VU0090157 (**24**), and VU0029767 (**25**).
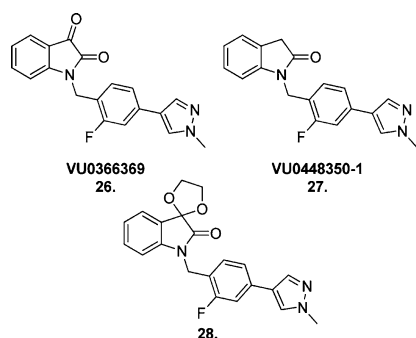

Figure 20. Structure of the BQCA-like PAMs VU0366369 (**26**), VU0448350-1 (**27**), and compound **28**.

taken.[110,111] Replacement with an indolinone (**27**, Figure 20) resulted in a marked reduction in M_1 mAChR potency compared to compound **26** (EC_{50} = 2.4 μM) but a 10-fold

improvement in ACh cooperativity (27-fold left shift of ACh CRC at 30 μM).[110] Similarly, spirocyclic replacements for the isatin core largely resulted in potency reductions but improvements in ACh cooperativity, as well as increased subtype selectivity. An exemplar compound from this series was compound **28** (Figure 20).

A novel chemical scaffold[112] derived from the same high-throughput screen as VU0366369 (**26**)[108] showing weak M_1 mAChR PAM activity but high M_1 mAChR selectivity was developed into a prospective lead, compound **29** (Figure 21).
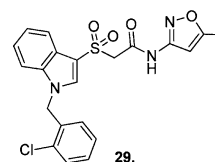

Figure 21. Structure of the novel scaffold compound **29**.

After modifications to the large northern portion of compound **29** proved detrimental to activity (evaluated in Ca^{2+} mobilization assays), synthetic efforts focused on introducing novel substituents to the southern benzyl moiety. 3-Chloro-, 3-bromo-, and 3-pyrazole-substitution gave the most potent analogues (EC_{50}s = 5.8, 3.8, and 2.2 μM, respectively) with highly basic and sterically bulky groups not tolerated at this or any other position.

Extensive SAR efforts around this scaffold afforded further pharmacological improvements, resulting in M_1 mAChR-selective compounds **30**[112] and **31**[113] (Figure 22). Compound
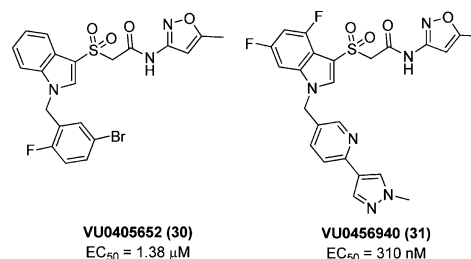

Figure 22. Structures of the novel scaffold analogues VU0405652 (**30**) and VU0456940 (**31**).

30 displayed relatively modest potency (when compared with BQCA and its optimized analogues) but promising positive modulation of ACh activity (at 30 μM). Compound **30** also displayed improved brain penetration compared to that of BQCA, minimal off-target activity and no orthosteric binding at any mAChR subtypes, and was observed to promote nonamyloidogenic processing of APP in conjunction with carbachol. Compound **31** displayed a substantial improvement in potency compared to BQCA and its predecessor compound **30**, and potentiated M_1 mAChR-mediated, carbachol-induced excitability of striatal medium spiny neurons as well as nonamyloidogenic APP processing.

Putative Bitopic M_1 mAChR Agonists. *ACADIA Pharmaceuticals Compounds.* AC-42 (**32**, Figure 23) selectively activates the M_1 mAChR subtype and was shown to bind to a novel combination of M_1 mAChR residues within the N-terminus/TM1 and EC3/TM7 regions.[114] This novel
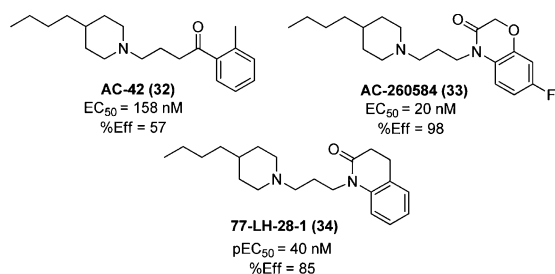
Figure 23. Structures of AC-42 (**32**), AC-260584 (**33**), and 77-LH-28-1 (**34**); R-SAT functional assays measuring β-galactosidase activity gave estimates of potency, EC_{50} (converted from pEC_{50}), and efficacy, %Eff (normalized to the maximum response to the muscarinic agonist carbachol).

binding epitope cannot, however, be used as conclusive evidence of a purely allosteric binding mode.

Extensive pharmacological studies have revealed that AC-42 exhibits characteristics suggestive of both orthosteric and allosteric modes of action.[114−118] IP accumulation assays in CHO cells expressing the hM_1 mAChR revealed the orthosteric antagonist atropine to decrease the potency of AC-42 as evidenced by a concentration-dependent dextral shift in the AC-42 CRC, characteristic of a competitive interaction.[116] In equilibrium binding studies,[115] AC-42 almost completely inhibited binding of the radiolabeled [^{3}H]NMS (0.2 nM), indicative of either competitive antagonism via the orthosteric site or a high degree of negative cooperativity via the allosteric site, or perhaps a combination of the two. Further studies confirmed the ability of AC-42 to interact allosterically with the M_1 mAChR; the ligand significantly slowed the rate of [^{3}H]NMS dissociation from the M_1 mAChR.[115]

Notably, single point mutations of key orthosteric site residues Y381A and W101A,[114,115,117] while reducing the affinity of prototypical orthosteric muscarinic agonists ACh and pilocarpine, actually led to increases in the affinity of AC-42 from that recorded at the wild-type M_1 mAChR.[115] Furthermore, AC-42 exhibited a divergent signaling and regulatory profile to that of other orthosteric muscarinic agonists such as oxotremorine-M. AC-42 was unable to stimulate M_1 mAChR-$G\alpha_{i1/2}$ coupling[119] and did not result in M_1 mAChR internalization after prolonged (24 h) exposure. Rather, it actually upregulated total receptor expression.[120] Taken together, these observations support the hypothesis that AC-42 adopts a binding mode distinct from that of traditional nonselective agonists,[121] but one which places AC-42 in close proximity to the orthosteric site, implying that its agonistic properties may be derived from interactions with orthosteric residues (as well as allosteric residues); the definition of a bitopic ligand.

AC-42 was superseded by the more potent and efficacious structural analogue, AC-260584 (**33**, Figure 23), when it was found to exhibit the same high M_1 mAChR subtype selectivity as its predecessor but with the added advantages of oral bioavailability in rodents and the exhibition of antipsychotic and pro-cognitive effects in animal models of schizophrenia and AD.[122,123] While these results show great therapeutic promise, the ligand's classification as a purely allosteric agonist is likely premature. AC-260584 exhibited the same potential for binding orthosteric site residues as did AC-42.[117]

77-LH-28-1 (**34**, Figure 23), an M_1 mAChR-selective compound closely structurally related to the AC compounds,

demonstrated agonistic behavior at rat hippocampal M_1 mAChRs in vitro and CNS penetration leading to the stimulation of rat hippocampal cell firing in vivo.[124] Furthermore, activation of M1 mAChRs by 77-LH-28-1 enhanced NMDA receptor activation in vitro, facilitating long-term potentiation.[125] Consistent with the interactions of AC-42, the mAChR orthosteric antagonists pirenzepine and scopolamine both produced a dextral displacement of the 77-LH-28-1 CRC;[124] however, 77-LH-28-1 has also been shown to compete with the prototypical muscarinic negative allosteric modulator C_7/3-phth (at the NMS-occupied receptor),[115] adding weight to the theory that this scaffold interacts with portions of both orthosteric and allosteric sites on the M_1 mAChR.

The affinity of 77-LH-28-1, like AC-42, was improved at M_1 mAChRs containing the orthosteric mutations Y381A and W101A (pK_a = 7.16 and 8.64, respectively) from that recorded at the wild-type (pK_a = 6.74). Additionally, a novel M_1 mAChR receptor mutation F77I resulted in substantially reduced efficacy of both AC-42 and 77-LH-28-1, while having little effect on the efficacy of traditional orthosteric ligands,[115,118] highlighting the importance of this residue in facilitating receptor activation by this scaffold, and the potential utility of this mutated receptor as a detection tool for this novel binding mode. Ligand docking studies performed on an M_1 mAChR homology model further support a bitopic binding mode for 77-LH-28-1.[115]

N-Desmethylclozapine. Clozapine is a second-generation antipsychotic known for its unrivaled efficacy as a dual-action treatment for the positive and negative symptoms of schizophrenia,[126] and notorious for promiscuous off-target activity that has rendered it a risky therapeutic option. *N*-Desmethylclozapine (**35**, Figure 24) is a biologically active metabolite of clozapine thought to play a role in the parent drug's unique therapeutic profile.
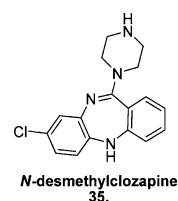

N-desmethylclozapine
35.

Figure 24. Structure of *N*-desmethylclozapine (**35**).

Following an evaluation of the metabolite's effects at human cloned mAChRs,[127] *N*-desmethylclozapine was described as an M_1 mAChR-preferring allosteric agonist, indirectly facilitating the potentiation of NMDA receptor activity, shown to be depleted in patients with psychotic disorders. In binding assays, *N*-desmethylclozapine demonstrated a competitive interaction with the known M_1 mAChR allosteric ligand brucine (**12**), suggesting an allosteric mode of action; however, the activity of *N*-desmethylclozapine in Ca^{2+} mobilization assays was completely blocked when coincubated with atropine, suggesting an interaction with the orthosteric site as well. These observations certainly indicate that the ligand may be behaving in a bitopic manner.

N-Desmethylclozapine has since been reported as a human native M_1 mAChR *antagonist*, despite its agonistic activity at human recombinant and rat native M_1 mAChRs,[128] rendering its therapeutic prospect as a treatment for cognitive deficits

1039

dx.doi.org/10.1021/cn400086m | ACS Chem. Neurosci. 2013, 4, 1026−1048

34

obsolete. Disappointing outcomes such as this serve as a lesson for future development, highlighting the importance of evaluating lead compounds not just on rat and human recombinant receptors to assess their viability for in vitro and early in vivo trials, but to examine their activity at human native receptors to ensure their viability as future therapeutics.

Vanderbilt University Compounds. Compared to the scaffolds of previously reported compounds, TBPB ([1-(1′-(2-**t**olyl)-1,4′-**bi**piperidin-4-yl)-1H **b**enzo[*d*]imidazol-2(3H)-one]) (**36**, Figure 25) represents a structurally unique

TBPB (36)
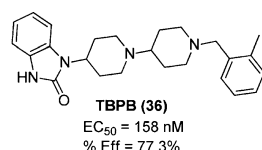EC_{50} = 158 nM
% Eff = 77.3%

Figure 25. Structure of TBPB (**36**). Calcium mobilization assays in rat M_1-transfected CHO-K1 cells gave an estimate of potency, EC_{50}, and efficacy, %Eff (normalized to the maximum response to the muscarinic agonist carbachol).

mAChR ligand that exhibits selectivity for the M_1 mAChR at the level of function. TBPB displayed agonistic behavior and potentiates NMDA receptor currents at rat hippocampal M_1 mAChRs in vitro and was also shown to promote non-amyloidogenic APP processing in PC12 cells as measured by a decrease in $A\beta42$ levels and an increase in α-secretase metabolites.[129] Furthermore, TBPB elicited antipsychotic-like behavior in rodent models of schizophrenia.

In calcium mobilization assays at the rM_1 mAChR, TBPB displayed an apparent noncompetitive interaction with the orthosteric antagonist atropine. However, as this assay does not assess the ligands in an equilibrated state, this is not conclusive of an allosteric mode of action. Indeed the TBPB-mediated modulation of APP processing in PC12 cells expressing the hM_1 mAChR was completely blocked by atropine which, as previously explained, could either be the result of a very high degree of negative cooperativity between the two ligands when concomitantly bound at the orthosteric site (atropine) and the allosteric site (TBPB), or evidence of a competitive interaction. Hence, the binding mode of TBPB is unclear and remains unresolved following the observed preservation of TBPB activity at M_1 mAChRs bearing a mutation at a residue critical to orthosteric ligand binding (Y381A). Despite confirming that this residue is not essential to the TBPB-M_1 mAChR interaction, binding to other orthosteric site residues remains a valid possibility (as in the case of AC-42 and related compounds).

Further evidence for the potential orthosteric site-interaction of TBPB is that the M_1 mAChR allosteric modulator VU0029767 (**25**) elicited a concentration-dependent potentiation of the cellular response to an EC_{20} concentration of TBPB "with a potency consistent with the potency of this compound for potentiating the response to ACh."[107] While this observation may be the result of positive cooperativity between two ligands binding to two distinct allosteric sites on the M_1 mAChR, the possibility that a portion of TBPB is in fact occupying the orthosteric site in this interaction cannot be ignored.

SAR studies on this scaffold to date have proven unfruitful,[130,131] with a range of substitutions at both the distal basic piperidine nitrogen and the fused benzyl ring mostly

yielding compounds displaying either decreases in M_1 mAChR potency, a loss of M_1 mAChR selectivity, or undesirable off-target activity. Interestingly, a recent study identified "molecular switches" within the structure of TBPB that convert the ligand from a selective allosteric agonist to a *pan*-mAChR orthosteric antagonist.[132] Surprisingly, addition of a single fluorine atom to the central piperidine ring was sufficient to disrupt an interaction critical for allosteric binding. This result, combined with the finding that TBPB behaves as an orthosteric antagonist at the other mAChR subtypes (in Ca^{2+} mobilization assays), led to the first definitive classification of TBPB as a bitopic ligand; though additional supportive pharmacological data will add further weight to this classification.

Following high-throughput screening and synthetic optimization, VU0184670 and VU0357017/ML071[133] (**37** and **38**, Figure 26) were identified as potent (EC_{50} = 152 and 198 nM,

VU0184670 (37) (R=H)
EC_{50} = 152 nM, % Eff = 85%
VU0357017 (38) (R=CH$_3$)
EC_{50} = 198 nM, % Eff = 81%

VU0364572 (39) (R=H)
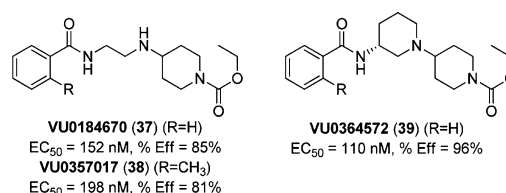EC_{50} = 110 nM, % Eff = 96%

Figure 26. Structures of VU0184670 (**37**), VU0357017 (**38**), and VU0364572 (**39**). Calcium mobilization assays in rat M_1-transfected CHO-K1 cells gave an estimate of potency, EC_{50}, and efficacy, %Eff (normalized to the maximum response to the muscarinic agonist ACh).

respectively) and selective M_1 mAChR agonists, producing maximum agonist effects of greater than 80% of the maximal response to ACh (as assessed by calcium mobilization assays). The activity of both VU0184670 and VU0357017 was preserved at receptors containing the mutated orthosteric site residue Y381A, and the ligands also demonstrated non-competitive interactions with the orthosteric antagonist atropine in calcium mobilization assays. In line with studies of TBPB, these findings suggest, but do not conclusively confirm, an allosteric mode of action for these compounds. While these compounds show minimal perturbation of [^{3}H]NMS binding at concentrations required for activity in calcium mobilization assays, concentrations greater than 1 μM displace radioligand binding, as evidenced by a clear reduction in the percentage of [^{3}H]NMS receptor occupancy, suggestive of an orthosteric site interaction. Hence, a bitopic mode of action for these compounds remains a valid possibility.

These compounds demonstrated selective M_1 mAChR-mediated potentiation of NMDA receptor currents in vitro and reversal of scopolamine-induced memory impairment in CFC in rats; however the need for improved potency and efficacy, as well as the elimination of functional D_2 antagonism, prompted additional synthetic modifications in the form of cyclic constraints to be pursued.[134] This study resulted in VU0364572 (**39**, Figure 26), a compound which produced enantioselective M_1 mAChR activation. This compound maintained the favorable in vitro characteristics observed previously but also displayed the desired improvements in activity and clean ancillary pharmacology. Moreover, VU0364572 possessed low plasma protein binding, increased oral bioavailability, and excellent CNS exposure. An alternative approach involving the introduction of a more diverse variety of

bicyclic constraints yielded some compounds with low nanomolar potency; however, a corresponding loss of muscarinic subtype selectivity was observed.[135] This led the authors to speculate that these compounds may possess a previously unappreciated bitopic mechanism of action, whereby lower potency analogues appear purely allosteric but higher potency analogues result in predominantly orthosteric interactions.

Interestingly, a recent publication demonstrated that VU0357017 and VU0364572 exhibit stimulus bias; both compounds behaved as agonists of M_1 mAChR-mediated Ca^{2+} mobilization and ERK1/2 phosphorylation while having no effect on β-arrestin recruitment.[136] Studies in native tissues of M_1 mAChR-mediated responses demonstrate that while both compounds potentiate NMDA receptor currents in hippocampal pyramidal cells and induce hippocampal LTP, they are devoid of electrophysiological activity in PFC pyramidal cells. These observations correlate well with the aforementioned study in which VU0357017 demonstrated efficacy in CFC, a hippocampal-dependent animal model of cognition.[133] As with TBPB, subtle "molecular switches" were also found within this scaffold,[132,137] where modifications such as inversion of chirality, reversed attachment, and benzyl ring replacement converted allosteric agonism to orthosteric antagonism. These observations prompted additional studies that ultimately led to the classification of VU0357017 and VU0364572 as bitopic ligands. Both ligands competitively displaced [³H]NMS binding at all five muscarinic receptor subtypes and behaved as orthosteric partial agonists at the M_1 mAChR, but they also exhibited a characteristic allosteric effect of slowing the rate of [³H]NMS dissociation at M_1 mAChR-expressing cell membranes.[137]

Lu AE51090. A more recent addition to the M_1 mAChR-selective ligand literature is Lundbeck's Lu AE51090[138] (**40**, Figure 27). The original hit compound was found to be highly
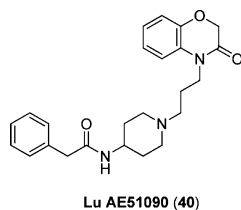

Lu AE51090 (40)

Figure 27. Structure of Lu AE51090 (**40**).

potent though not exclusively selective for the M_1 mAChR subtype, so a number of analogues were synthesized to attempt to remedy this. Structural modifications included fluoro- and methoxy-substitution of the tetrahydroquinolinone ring system, replacement of this system with benzoxazolone and benzothiazinone ring systems, and the introduction of a range of alkyl chains and saturated and unsaturated rings at the amide position. The panel of analogues was screened against all five muscarinic receptor subtypes in functional Ca^{2+} mobilization assays. From this, Lu AE51090 was selected as an ideal lead compound based on both M_1 mAChR activity preservation (the compound displayed a potency of 61 nM and a percentage efficacy of 83% compared to ACh) and M_1 mAChR selectivity (the compound showed no agonism and negligible binding at the M_2–M_5 subtypes). The compound demonstrated acceptable absorption, distribution, metabolism, and excretion

(ADME) properties for in vivo analysis, and subsequently showed a dose-dependent reversal in delay-induced memory decay evident in mice performing a PFC and hippocampal-dependent task.

In a functional interaction assay against the orthosteric antagonist atropine, Lu AE51090 exhibited a saturable, noncompetitive profile suggesting an allosteric mode of action. As with the aforementioned "allosteric agonists", Lu AE51090 activity was not compromised at Y381A mutated receptors. Once again, this evidence does not unequivocally rule out the possibility of a bitopic mechanism.

Interestingly, when screened against a broad range of 69 receptors, ion channels, transporters, and enzymes, Lu AE51090 exhibited only minor off-target activity. This is in contrast to AC-42 and TBPB, which displayed considerable affinity for other GPCRs including dopamine, serotonin, and adrenergic receptor subtypes, implying that Lu AE51090 may be a more useful molecular tool for exploring M_1 mAChR activation in disease-specific tissues and in vivo cognition models.

With a view to designing an antipsychotic drug with pro-cognitive potential, the same group recently reported the in silico screening, synthesis, and evaluation of compounds displaying combined D_2 R affinity and M_1 mAChR agonism,[139] giving rise to compound **41** (Figure 28). While the binding
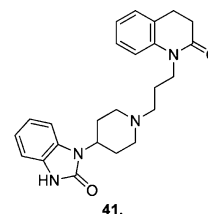

41.

Figure 28. Structure of compound **41**.

mode and activity profile of this compound at the D_2 R was unexamined, the M_1 mAChR activity of compound **41** was unaffected by the Y381A orthosteric mutation, consistent with an allosteric or possibly bitopic mode of action at this receptor. A similar mutagenesis approach, or functional interaction studies, would have elucidated a potential binding mode for the compound at the D_2 R, be it orthosteric, allosteric, or bitopic. The complete mode of action of this compound hence remains purely speculative. It may be an orthosteric D_2/allosteric M_1 ligand, a pure allosteric ligand at both receptors, or a bitopic ligand at one or both targets. This ambiguity remains unexplored as, unfortunately, the compound also displayed hERG channel inhibition and synthetic strategies to overcome this adverse property were unsuccessful, resulting in the hit-to-lead campaign being abandoned.

GlaxoSmithKline Compounds. GlaxoSmithKline have contributed a number of other subtype-selective M_1 mAChR agonists to this body of literature.[140−144] While these compounds are not purported specifically as either PAMs or allosteric agonists, their excellent subtype selectivity and striking similarities to some of the ligands previously described make them noteworthy.

Considerable SAR studies were performed around a 2′ biaryl amide scaffold,[140,141] ultimately yielding compounds **42** and **43** (Figure 29), which showed favorable pharmacokinetic characteristics in addition to their high potency, intrinsic activity and
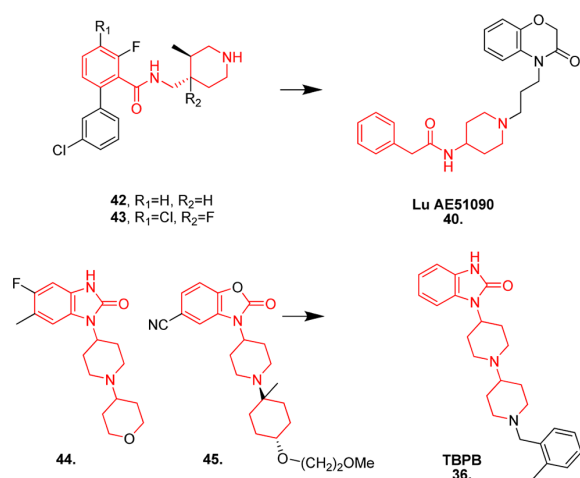
Figure 29. Structures of GSK compounds **42–45**, with the motifs common to other M$_1$ mAChR-selective ligands highlighted in red.

exceptional selectivity against a panel of targets (as assessed by FLIPR calcium mobilization assays). In other studies,[142,143] optimization of a novel N-substituted benzimidazolone hit structure gave the CNS-penetrant, orally active, and subtype-selective compounds **44** and **45** (Figure 29). Recently, the M$_1$ mAChR allosteric agonist GSK1034702, an isomer of compound **44**, has shown efficacy in improving episodic memory in humans in a nicotine abstinence model of cognitive dysfunction.[144] An 8 mg dose of GSK1034702 significantly improved immediate recall (but not delayed recall) following abstinence-induced impairment. Furthermore, in preclinical studies, the potency of GSK1034702 was sensitive to the M$_1$ mAChR F77I mutation, a mutation that also had a pronounced effect on the efficacy of AC-42 and 77-LH-28-1; suggesting a similar, potentially bitopic, binding mode.

More detailed pharmacological investigation would verify the binding mode and classification of these GSK ligands. However, simple visual comparison of these structures with both a putative bitopic ligand (Lu AE51090) and an acknowledged bitopic ligand (TBPB) reveals conspicuous similarities that support the notion of a shared mode of binding and activation at this receptor (Figure 29).

■ PERSPECTIVE

Our knowledge of the intricate behaviors and interactions of M$_1$ mAChR allosteric ligands is rapidly expanding; however, despite the increasing depth of our understanding, researchers are still hampered by a number of difficulties that largely arise from the complexities of *screening*, *optimizing*, and *classifying* allosteric ligands.

With regards to initial library *screening*, each analogue is typically evaluated in one pharmacological assay and tested in the presence of a single concentration of one orthosteric ligand to gain a measure of ligand potency and degree of allosteric effect. While this is a valid method for the detection of putative ligand activity, the properties of stimulus bias and probe dependence that may be engendered by allosteric ligands remain unassessed. This may potentially reveal only one aspect of the ligand's pharmacological capabilities, recognizing only one "string" in the putative allosteric ligand's "bow". If the test ligand selectively activates different downstream receptor

signaling pathways, but not the pathway being assessed by the assay, pharmacologically desirable molecules may go undetected.[54] Or, as outlined earlier in Figures 9 and 10, this may lead to misclassification of the ligand itself. Another consideration with regard to screening is the nature of the receptor, be it rat, human recombinant, or human native. As previously highlighted with LY2033298 (**10**)[76,78] and N-desmethylclozapine (**35**),[128] identification of species-dependent variability in both cooperativity and mode of action can lead to the discovery of altered selectivity and functional profiles that may have had deleterious results in a clinical setting if not identified earlier. Furthermore, the potential for allosteric ligands to elicit different physiological and toxicological outcomes in animal and human studies poses considerable challenges to the traditional drug discovery pipeline that will be difficult to resolve. In an ideal world, screening for novel allosteric drug candidates would involve a wide panel of orthosteric probes, assay outputs, and receptor targets. However, factoring in time, economic, and technological constraints, the best approach at present is to bear these considerations in mind and, following hit identification, apply this broader analysis in the hit-to-lead optimization process.

The potential issues surrounding the allosteric ligand screening process carry through into their *optimization*. While the evaluation of M$_1$ mAChR-selective allosteric ligands frequently encounters "flat" or "shallow" SAR as a challenge impeding the development of allosteric ligands,[98,102,103,108,112] it is possible that these observations are a consequence of too narrow a pharmacological analysis, given screening constraints. Broader evaluation of a limited cluster of novel scaffolds in radioligand binding and a variety of functional assays in the presence of multiple classes of orthosteric ligands at this stage of development may deconvolute the "confounding" SAR frequently observed in these studies and potentially reveal the capacity to differentially modulate discrete receptor signaling pathways and affect unique changes in the traditional behavior of orthosteric ligands. Additionally, quantification of properties such as binding cooperativity, functional cooperativity, and allosteric agonism would reduce the dependence on titration curve EC$_{50}$ values as the key determinant for future structural modifications. This would likely generate more detailed, "textured" SARs, advance our understanding of the relationship between allosteric ligand, orthosteric ligand, and receptor, and more accurately direct drug candidate optimization. Furthermore, as subtle changes in allosteric ligand structure have been shown to dramatically modify receptor subtype selectivity,[87] all promising analogues to emerge from the optimization process ought to be rescreened to ensure preservation of the desired selectivity profile.

Finally, the highly contextual (and sometimes premature) *classification* of allosteric ligands as PAMs, NAMs, and agonists further complicates this field of research. Misclassification typically results from incomplete investigation of the binding mode and functional profile of these ligands. Notable examples already described include the potential over-reliance on specific receptor mutants (e.g., orthosteric site Y381A mutation) as a means of discriminating orthosteric and allosteric binding modes, and the difficulty in distinguishing competitive and noncompetitive interactions, particularly when recording functional response data at a time point prior to the ligands reaching a state of equilibrium (e.g., the calcium mobilization assay). The prospect of bitopic modes of action further confounds this issue.

There is no simple means to overcoming this classification challenge. Confirming a purely allosteric mode of action and further investigating the exact nature of the putative bitopic M_1 mAChR agonists already described cannot be achieved using one experimental technique alone, such as a mutagenesis study or a single functional assay. More comprehensive synthetic and pharmacological studies need to be undertaken.[57,84] Knowledge of each ligand's true binding mode with the M_1 mAChR will facilitate rational drug design and will likely result in the more productive synthesis of potent, efficacious therapeutic leads. Additionally, adopting a global, more detailed lexicon to describe allosteric ligand activity[56] may aid communication between researchers.

■ CONCLUSION

The unique properties of allosteric ligands require more thorough pharmacological evaluation if we are to advance our understanding of their interactions and comprehend the complete therapeutic potential of these molecules. Their complex behavior also demands a more detailed classification system that is globally recognized. The sooner these necessities are acknowledged and embraced, the more fruitful our labors will be.

In the field of selective M_1 mAChRs specifically, this would translate to an improved ability to map the key binding residues of the multiple allosteric sites present on the receptor, more informed design of putative allosteric ligands, and a greater understanding of the intricate role of this muscarinic receptor subtype in the normal functioning of the CNS and the pathophysiology of CNS diseases. As a consequence, it will be possible to fully appreciate the scope of M_1 mAChR activation as a potential neurodegenerative disorder therapy.

■ AUTHOR INFORMATION

Corresponding Author

*████████████████ (P.J.S.); ███████████
(A.C.). ████████████████████ (P.J.S.); ███
██████████████ (A.C.).

Author Contributions

All authors have given approval to the final version of the manuscript.

Notes

The authors declare no competing financial interest.

■ ABBREVIATIONS

mAChR, muscarinic acetylcholine receptor; CNS, central nervous system; GPCR, G protein-coupled receptor; PLC, phospholipase C; IP_3, inositol trisphosphate; AC, adenylate cyclase; cAMP, cyclic adenosine monophosphate; AD, Alzheimer's disease; ACh, acetylcholine; KO, knockout; PKC, protein kinase C; NMDA, N-methyl-D-aspartate; APP, amyloid precursor protein; CSF, cerebrospinal fluid; EPS, extrapyramidal side effects; TM, transmembrane; EC, extracellular; NMS, N-methylscopolamine; IC, intracellular; PAM, positive allosteric modulator; CRC, concentration response curve; QNB, 3-quinuclidinyl benzilate; BQCA, benzyl quinolone carboxylic acid; FLIPR, fluorometric imaging plate reader; MWC, Monod-Wyman-Changeux; CFC, contextual fear conditioning; PFC, prefrontal cortex; sEPSCs, spontaneous excitatory postsynaptic currents; FF, free fraction; SAR, structure−activity relationship; BBB, blood-brain barrier; P-gp, P-glycoprotein; TBPB, [1-(1′-(2-tolyl)-1,4′-bipiperidin-4-yl)-1H benzo[d]imidazol-2(3H)-one]; ADME, absorption, distribution, metabolism, and excretion

■ REFERENCES

(1) van Koppen, C. J., and Kaiser, B. (2003) Regulation of muscarinic acetylcholine receptor signaling. Pharmacol. Ther. 98, 197−220.

(2) Canals, M., Sexton, P. M., and Christopoulos, A. (2011) Allostery in GPCRs: "MWC" revisited. Trends Biochem. Sci. 36, 663−672.

(3) Caulfield, M. P. (1993) Muscarinic Receptors-Characterization, Coupling and Function. Pharmacol. Ther. 58, 319−379.

(4) Nathanson, N. M. (2008) Synthesis, trafficking and localization of muscarinic acetylcholine receptors. Pharmacol. Ther. 119, 33−43.

(5) Fisher, A. (2008) M_1 Muscarinic Agonists Target Major Hallmarks of Alzheimer's Disease - The Pivotal Role of Brain M1 Receptors. Neurodegener. Dis. 5, 237−240.

(6) Langmead, C. J., Watson, J., and Reavill, C. (2008) Muscarinic acetylcholine receptors as CNS drug targets. Pharmacol. Ther. 117, 232−243.

(7) Xu, Y., Yan, J., Zhou, P., Li, J., Gao, H., Xia, Y., and Wang, Q. (2012) Neurotransmitter receptors and cognitive dysfunction in Alzheimer's disease and Parkinson's disease. Prog. Neurobiol. 97, 1−13.

(8) Wess, J. (2004) Muscarinic Acetylcholine Receptor Knockout Mice: Novel Phenotypes and Clinical Implications. Annu. Rev. Pharmacol. Toxicol. 44, 423−450.

(9) Bodick, N. C., Offen, W. W., Levey, A. I., Cutler, N. R., Gauthier, S. G., Satlin, A., Shannon, H. E., Tollefson, G. D., Rasmussen, K., Bymaster, F. P., Hurley, D. J., Potter, W. Z., and Paul, S. M. (1997) Effects of Xanomeline, a Selective Muscarinic Receptor Agonist, on Cognitive Function and Behavioral Symptoms in Alzheimer Disease. Arch. Neurol. 54, 465−473.

(10) Digby, G. J., Shirey, J. K., and Conn, P. J. (2010) Allosteric activators of muscarinic receptors as novel approaches for treatment of CNS disorders. Mol. BioSyst. 6, 1345−1354.

(11) Bartus, R. T., Dean, R. L., Beer, B., and Lippa, A. S. (1982) The Cholinergic Hypothesis of Geriatric Memory Dysfunction. Science 217, 408−417.

(12) Whitehouse, P. J., Price, D. L., Struble, R. G., Clark, A. W., Coyle, J. T., and Delon, M. R. (1982) Alzheimer's disease and senile dementia: loss of neurons in the basal forebrain. Science 215, 1237−1239.

(13) Francis, P. T., Palmer, A. M., Snape, M., and Wilcock, G. K. (1999) The cholinergic hypothesis of Alzheimer's disease: a review of progress. J. Neurol. Neurosurg. Psychiatry 66, 137−147.

(14) Giacobini, E. (2000) Cholinesterase Inhibitors Stabilize Alzheimer's Disease. Ann. N.Y. Acad. Sci. 920, 321−327.

(15) Mirza, N. R., Peters, D., and Sparks, R. G. (2003) Xanomeline and the Antipsychotic Potential of Muscarinic Receptor Subtype Selective Agonists. CNS Drug Rev. 9, 159−186.

(16) Bymaster, F. P., Whitesitt, C. A., Shannon, H. E., DeLapp, N., Ward, J. S., Calligaro, D. O., Shipley, L. A., Buelke-Sam, J. L., Bodick, N. C., Farde, L., Sheardown, M. J., Olesen, P. H., Hansen, K. T., Suzdak, P. D., Swedberg, M. D. B., Sauerberg, P., and Mitch, C. H. (1997) Xanomeline: A Selective Muscarinic Agonist for the Treatment of Alzheimer's Disease. Drug Dev. Res. 40, 158−170.

(17) Bymaster, F. P., McKinzie, D. L., Felder, C. C., and Wess, J. (2003) Use of M_1-M_5 Muscarinic Receptor Knockout Mice as Novel Tools to Delineate the Physiological Roles of the Muscarinic Cholinergic System. Neurochem. Res. 28, 437−442.

(18) Shannon, H. E., Rasmussen, K., Bymaster, F. P., Hart, J. C., Peters, S. C., Swedberg, M. D. B., Jeppeson, L., Sheardown, M. J., Sauerberg, P., and Fink-Jensen, A. (2000) Xanomeline, an M_1/M_4

preferring muscarinic cholinergic receptor agonist, produces anti-psychotic-like activity in rats and mice. *Schizophr. Res. 42*, 249−259.

(19) Shekhar, A., Potter, W. Z., Lightfoot, J., Lienemann, J., Dube, S., Mallinckrodt, C., Bymaster, F. P., McKinzie, D. L., and Felder, C. C. (2008) Selective Muscarinic Receptor Agonist Xanomeline as a Novel Treatment Approach for Schizophrenia. *Am. J. Psychiatry 165*, 1033−1039.

(20) Woolley, M. L., Carter, H. J., Gartlon, J. E., Watson, J. M., and Dawson, L. A. (2009) Attenuation of amphetamine-induced activity by the non-selective muscarinic receptor agonist, xanomeline, is absent in muscarinic M₄ receptor knockout mice and attenuated in muscarinic M₁ receptor knockout mice. *Eur. J. Pharmacol. 603*, 147−149.

(21) Tzavara, E. T., Bymaster, F. P., Davis, R. J., Wade, M. R., Perry, K. W., Wess, J., McKinzie, D. L., Felder, C., and Nomikos, G. G. (2004) M₄ muscarinic receptors regulate the dynamics of cholinergic and dopaminergic neurotransmission: relevance to the pathophysiology and treatment of related central nervous system pathologies. *FASEB J. 18*, 1410−1427.

(22) Wood, M. D., Murkitt, K. L., Ho, M., Watson, J. M., Brown, F., Hunter, A. J., and Middlemiss, D. N. (1999) Functional comparison of muscarinic partial agonists at muscarinic receptor subtypes hM₁, hM₂, hM₃, hM₄ and hM₅ using microphysiometry. *Br. J. Pharmacol. 126*, 1620−1624.

(23) Farrell, M., and Roth, B. L. (2010) Allosteric Antipsychotics: M4Muscarinic Potentiatiors as Novel Treatments for Schizophrenia. *Neuropsychopharmacology 35*, 851−852.

(24) Tsang, S. W. Y., Pomakian, J., Marshall, G. A., Vinters, H. V., Cummings, J. L., Chen, C. P. L.-H., Wong, P. T.-H., and Lai, M. K. P. (2007) Disrupted muscarinic M₁ receptor signaling correlates with loss of protein kinase C activity and glutamatergic deficit in Alzheimer's disease. *Neurobiol. Aging 28*, 1381−1387.

(25) Fisher, A. (2012) Cholinergic modulation of amyloid precursor protein processing with emphasis on M1 muscarinic receptor: perspectives and challenges in treatment of Alzheimer's disease. *J. Neurochem. 120*, 22−33.

(26) Marino, M. J., Rouse, S. T., Levey, A. I., Potter, L. T., and Conn, P. J. (1998) Activation of the genetically defined m1 muscarinic receptor potentiates *N*-methyl-D-aspartate (NMDA) receptor currents in hippocampal pyramidal cells. *Proc. Natl. Acad. Sci. U.S.A. 95*, 11465−11470.

(27) Collingridge, G. L., Volianskis, A., Bannister, N., France, G., Hanna, L., Mercier, M., Tidball, P., Fang, G., Irvine, M. W., Costa, B. M., Monaghan, D. T., Bortolotto, Z. A., Molnar, E., Lodge, D., and Jane, D. E. (2013) The NMDA receptor as a target for cognitive enhancement. *Neuropharmacology 64*, 13−26.

(28) Davies, P., and Maloney, A. J. F. (1976) Selective Loss of Central Cholinergic Neurons in Alzheimer's Disease. *Lancet 2*, 1403.

(29) Flynn, D. D., Ferrari-DiLeo, G., Mash, D. C., and Levey, A. I. (1995) Differential Regulation of Molecular Subtypes of Muscarinic Receptors in Alzheimer's Disease. *J. Neurochem. 64*, 1888−1891.

(30) Overk, C. R., Felder, C. C., Tu, Y., Schober, D. A., Bales, K. R., Wuu, J., and Mufson, E. J. (2010) Cortical M₁ receptor concentration increases without a concomitant change in function in Alzheimer's disease. *J. Chem. Neuroanat. 40*, 63−70.

(31) Turner, P. R., O'Connor, K., Tate, W. P., and Abraham, W. C. (2003) Roles of amyloid precursor protein and its fragments in regulating neural activity, plasticity and memory. *Prog. Neurobiol. 70*, 1−32.

(32) Hock, C., Maddalena, A., Raschig, A., Muller-Spahn, F., Eschweiler, G., Hager, K., Heuser, I., Hampel, H., Muller-Thomsen, T., Oertel, W., Wienrich, M., Signorell, A., Gonzalez-Agosti, C., and Nitsch, R. M. (2003) Treatment with the selective muscarinic m1 agonist talsaclidine decreases cerebrospinal fluid levels of Aβ₄₂ in patients with Alzheimer's disease. *Amyloid 10*, 1−6.

(33) Fisher, A., Michaelson, D. M., Brandeis, R., Haring, R., Chapman, S., and Pittel, Z. (2000) M1Muscarinic Agonists as Potential Disease-Modifying Agents in Alzheimer's Disease: Rationale and Perspectives. *Ann. N.Y. Acad. Sci. 920*, 315−320.

(34) Buxbaum, J. D., Gandy, S. E., Cicchetti, P., Ehrlich, M. E., Czernik, A. J., Fracasso, R. P., Ramabhadran, T. V., Unterbeck, A. J., and Greengard, P. (1990) Processing of Alzheimer beta/A4 amyloid precursor protein: Modulation by agents that regulate protein phosphorylation. *Proc. Natl. Acad. Sci. U.S.A. 87*, 6003−6006.

(35) Caccamo, A., Oddo, S., Billings, L. M., Green, K. N., Martinez-Coria, H., Fisher, A., and LaFerla, F. M. (2006) M₁ Receptors Play a Central Role in Modulating AD-like Pathology in Transgenic Mice. *Neuron 49*, 671−682.

(36) Farde, L., Nordstrom, A.-L., Wiesel, F.-A., Pauli, S., Halldin, C., and Sedvall, G. (1992) Positron Emission Tomographic Analysis of Central D₁ and D₂ Dopamine Receptor Occupancy in Patients Treated With Classical Neuroleptics and Clozapine. *Arch. Gen. Psychiatry 49*, 538−544.

(37) Serretti, A., De Ronchi, D., Lorenzi, C., and Berardi, D. (2004) New Antipsychotics and Schizophrenia: A Review on Efficacy and Side Effects. *Curr. Med. Chem. 11*, 343−358.

(38) DeLeon, A., Patel, N. C., and Crismon, M. L. (2004) Aripiprazole: A Comprehensive Review of Its Pharmacology, Clinical Efficacy, and Tolerability. *Clin. Ther. 26*, 649−666.

(39) Minzenberg, M. J., and Carter, C. S. (2012) Developing treatments for impaired cognition in schizophrenia. *Trends Cognit. Sci. 16*, 35−42.

(40) Felder, C. C., Bymaster, F. P., and DeLapp, N. (2000) Therapeutic Opportunities for Muscarinic Receptors in the Central Nervous System. *J. Med. Chem. 43*, 4333−4353.

(41) Crook, J. M., Tomaskovic-Crook, E., Copolov, D. L., and Dean, B. (2000) Decreased Muscarinic Receptor Binding in Subjects with Schizophrenia: A Study of the Human Hippocampal Formation. *Biol. Psychiatry 48*, 381−388.

(42) Crook, J. M., Tomaskovic-Crook, E., Copolov, D. L., and Dean, B. (2001) Low Muscarinic Receptor Binding in Prefrontal Cortex From Subjects With Schizophrenia: A Study of Brodmann's Areas 8, 9, 10 and 46 and the Effects of Neuroleptic Drug Treatment. *Am. J. Psychiatry 158*, 918−925.

(43) Raedler, T. J., Bymaster, F. P., Tandon, R., Copolov, D., and Dean, B. (2007) Towards a muscarinic hypothesis of schizophrenia. *Mol. Psychiatry 12*, 232−246.

(44) Korczyn, A. D. (2000) Muscarinic M₁ agonists in the treament of Alzheimer's disease. *Expert Opin. Invest. Drug 9*, 2259−2267.

(45) Flynn, D. D., Weinstein, D. A., and Mash, D. C. (1991) Loss of High-Affinity Agonist Binding to M1Muscarinic Receptors in Alzheimer's Disease: Implications for the Failure of Cholinergic Replacement Therapies. *Ann. Neurol. 29*, 256−262.

(46) Langmead, C. J., and Christopoulos, A. (2006) Allosteric agonists of 7TM receptors: expanding the pharmacological toolbox. *Trends Pharmacol. Sci. 27*, 475−481.

(47) Kenakin, T. P. (2012) Biased signalling and allosteric machines: new vistas and challenges for drug discovery. *Br. J. Pharmacol. 165*, 1659−1669.

(48) May, L. T., Leach, K., Sexton, P. M., and Christopoulos, A. (2007) Allosteric Modulation of G Protein-Coupled Receptors. *Annu. Rev. Pharmacol. Toxicol. 47*, 1−51.

(49) Dong, B. J. (2005) Cinacalcet: An Oral Calcimimetic Agent for the Management of Hyperparathyroidism. *Clin. Ther. 27*, 1725−1751.

(50) Garcia-Perez, J., Rueda, P., Staropoli, I., Kellenberger, E., Alcami, J., Arenzana-Seisdedos, F., and Lagane, B. (2011) New Insights into the Mechanisms whereby Low Molecular Weight CCR5 Ligands Inhibit HIV-1 Infection. *J. Biol. Chem. 286*, 4978−4990.

(51) Ehlert, F. J., Roeske, W. R., Gee, K. W., and Yamamura, H. I. (1983) An Allosteric Model For Benzodiazepine Receptor Function. *Biochem. Pharmacol. 32*, 2375−2383.

(52) Christopoulos, A. (2002) Allosteric Binding Sites On Cell-Surface Receptors: Novel Targets For Drug Discovery. *Nat. Rev. Drug Discovery 1*, 198−210.

(53) Conn, P. J., Jones, C. K., and Lindsley, C. W. (2009) Subtype-selective allosteric modulators of muscarinic receptors for the treatment of CNS disorders. *Trends Pharmacol. Sci. 30*, 148−155.

1044　　　　　　　　dx.doi.org/10.1021/cn400086m | *ACS Chem. Neurosci.* 2013, 4, 1026−1048

39

(54) Kenakin, T. (2005) New Concepts In Drug Discovery: Collateral Efficacy And Permissive Antagonism. *Nat. Rev. Drug Discovery 4*, 919–927.

(55) Kenakin, T. (2003) Ligand-selective receptor conformations revisited: the promise and the problem. *Trends Pharmacol. Sci. 24*, 346–354.

(56) Keov, P., Sexton, P. M., and Christopoulos, A. (2011) Allosteric modulation of G protein-coupled receptors: A pharmacological perspective. *Neuropharmacology 60*, 24–35.

(57) Leach, K., Loiacono, R. E., Felder, C. C., McKinzie, D. L., Mogg, A., Shaw, D. B., Sexton, P. M., and Christopoulos, A. (2010) Molecular Mechanisms of Action and *In Vivo* Validation of an M_4 Muscarinic Acetylcholine Receptor Allosteric Modulator with Potential Antipsychotic Properties. *Neuropsychopharmacology 35*, 855–869.

(58) Canals, M., Lane, J. R., Wen, A., Scammells, P. J., Sexton, P. M., and Christopoulos, A. (2012) A Monod-Wyman-Changeux Mechanism Can Explain G Protein-coupled Receptor (GPCR) Allosteric Modulation. *J. Biol. Chem. 287*, 650–659.

(59) Palczewski, K., Kumasaka, T., Hori, T., Behnke, C. A., Motoshima, H., Fox, B. A., Le Trong, I., Teller, D. C., Okada, T., Stenkamp, R. E., Yamamoto, M., and Miyano, M. (2000) Crystal Structure of Rhodopsin: A G Protein-Coupled Receptor. *Science 289*, 739–745.

(60) Rasmussen, S. G. F., Choi, H.-J., Rosenbaum, D. M., Kobilka, T. S., Thian, F. S., Edwards, P. C., Burghammer, M., Ratnala, V. R. P., Sanishvili, R., Fischetti, R. F., Schertler, G. F. X., Weis, W. I., and Kobilka, B. K. (2007) Crystal structure of the human b_2 adrenergic G-protein coupled receptor. *Nature 450*, 383–388.

(61) Jaakola, V.-P., Griffith, M. T., Hanson, M. A., Cherezov, V., Chien, E. Y. T., Lane, J. R., Ijzerman, A. P., and Stevens, R. C. (2008) The 2.6 Angstrom Crystal Structure of a Human A_{2A} Adenosine Receptor Bound to an Antagonist. *Science 322*, 1211–1217.

(62) Strotmann, R., Schrock, K., Boselt, I., Staubert, C., Russ, A., and Schoneberg, T. (2011) Evolution of GPCR: Change and continuity. *Mol. Cell. Endocrinol. 331*, 170–178.

(63) Haga, K., Kruse, A. C., Asada, H., Yurugi-Kobayashi, T., Shiroishi, M., Zhang, C., Weis, W. I., Okada, T., Kobilka, B. K., Haga, T., and Kobayashi, T. (2012) Structure of the human M2 muscarinic acetylcholine receptor bound to an antagonist. *Nature 482*, 547–552.

(64) Kruse, A. C., Hu, J., Pan, A. C., Arlow, D. H., Rosenbaum, D. M., Rosemond, E., Green, H. F., Liu, T., Chae, P. S., Dror, R. O., Shaw, D. E., Weis, W. I., Wess, J., and Kobilka, B. K. (2012) Structure and dynamics of the M3 muscarinic acetylcholine receptor. *Nature 482*, 552–559.

(65) Hulme, E. C., Birdsall, N. J. M., and Buckley, N. J. (1990) Muscarinic Receptor Subtypes. *Annu. Rev. Pharmacol. Toxicol. 30*, 633–673.

(66) Spalding, T. A., Birdsall, N. J. M., Curtis, C. A. M., and Hulme, E. C. (1994) Acetylcholine Mustard Labels the Binding Site Aspartate in Muscarinic Acetylcholine Receptors. *J. Biol. Chem. 269*, 4092–4097.

(67) Goodwin, J. A., Hulme, E. C., Langmead, C. J., and Tehan, B. G. (2007) Roof and Floor of the Muscarinic Binding Pocket: Variations in the Binding Modes of Orthosteric Ligands. *Mol. Pharmacol. 72*, 1484–1496.

(68) Ellis, J. (1997) Allosteric Binding Sites on Muscarinic Receptors. *Drug Dev. Res. 40*, 193–204.

(69) Wess, J. (2005) Allosteric Binding Sites on Muscarinic Acetylcholine Receptors. *Mol. Pharmacol. 68*, 1506–1509.

(70) Gnagey, A. L., Seidenberg, M., and Ellis, J. (1999) Site-Directed Mutagenesis Reveals Two Epitopes Involved in the Subtype Selectivity of the Allosteric Interactions of Gallamine at Muscarinic Acetylcholine Receptors. *Mol. Pharmacol. 56*, 1245–1253.

(71) Lazareno, S., Popham, A., and Birdsall, N. J. M. (2000) Allosteric Interactions of Staurosporine and Other Indolocarbazoles with N-[methyl-^{3}H]Scopolamine and Acetylcholine at Muscarinic Receptor Subtypes: Identification of a Second Allosteric Site. *Mol. Pharmacol. 58*, 194–207.

(72) Birdsall, N. J. M., Lazareno, S., Popham, A., and Saldanha, J. (2001) Multiple allosteric sites on muscarinic receptors. *Life Sci. 68*, 2517–2524.

(73) Lazareno, S., Popham, A., and Birdsall, N. J. M. (2002) Analogs of WIN 62,577 Define a Second Allosteric Site on Muscarinic Receptors. *Mol. Pharmacol. 62*, 1492–1505.

(74) Espinoza-Fonseca, L. M., and Trujillo-Ferrara, J. G. (2006) The existence of a second allosteric site on the M_1 muscarinic acetylcholine receptor and its implications for drug design. *Bioorg. Med. Chem. Lett. 16*, 1217–1220.

(75) Kenakin, T., and Christopoulos, A. (2013) Signalling bias in new drug discovery: detection, quantification and therapeutic impact. *Nat. Rev. Drug Discovery 12*, 205–216.

(76) Valant, C., Felder, C. C., Sexton, P. M., and Christopoulos, A. (2012) Probe Dependence in the Allosteric Modulation of a G Protein-Coupled Receptor: Implications for Detection and Validation of Allosteric Ligand Effects. *Mol. Pharmacol. 81*, 41–52.

(77) Chan, W. Y., McKinzie, D. L., Bose, S., Mitchell, S. N., Witkin, J. M., Thompson, R. C., Christopoulos, A., Lazareno, S., Birdsall, N. J. M., Bymaster, F. P., and Felder, C. C. (2008) Allosteric modulation of the muscarinic M_4 receptor as an approach to treating schizophrenia. *Proc. Natl. Acad. Sci. U.S.A. 105*, 10978–10983.

(78) Suratman, S., Leach, K., Sexton, P. M., Felder, C. C., Loiacono, R. E., and Christopoulos, A. (2011) Impact of species variability and 'probe dependence' on the detection and in vivo validation of allosteric modulation at the M_4 muscarinic acetylcholine receptor. *Br. J. Pharmacol. 162*, 1659–1670.

(79) Lanzafame, A., Christopoulos, A., and Mitchelson, F. (1997) Three Allosteric Modulators Act at a Common Site, Distinct from that of Competitive Antagonists, at Muscarinic Acetylcholine M_2 Receptors. *J. Pharmacol. Exp. Ther. 282*, 278–285.

(80) May, L. T., Avlani, V. A., Langmead, C. J., Herdon, H. J., Wood, M. D., Sexton, P. M., and Christopoulos, A. (2007) Structure-Function Studies of Allosteric Agonism at M_2 Muscarinic Acetylcholine Receptors. *Mol. Pharmacol. 72*, 463–476.

(81) Antony, J., Kellershohn, K., Mohr-Andra, M., Kebig, A., Prilla, S., Muth, M., Heller, E., Disingrini, T., Dallanoce, C., Bertoni, S., Schrobang, J., Trankle, C., Kostenis, E., Christopoulos, A., Holtje, H.-D., Barocelli, E., De Amici, M., Holzgrabe, U., and Mohr, K. (2009) Dualsteric GPCR targeting: a novel route to binding and signaling pathway selectivity. *FASEB J. 23*, 442–450.

(82) Lane, J. R., Sexton, P. M., and Christopoulos, A. (2013) Bridging the gap: bitopic ligands of G-protein-coupled receptors. *Trends Pharmacol. Sci. 34*, 59–66.

(83) Valant, C., Sexton, P. M., and Christopoulos, A. (2009) Orthosteric/Allosteric Bitopic Ligands - Going Hybrid at GPCRs. *Mol. Interventions 9*, 125–135.

(84) Valant, C., Gregory, K. J., Hall, N. E., Scammells, P. J., Lew, M. J., Sexton, P. M., and Christopoulos, A. (2008) A Novel Mechanism of G Protein-coupled Receptor Functional Selectivity - Muscarinic Partial Agonist McN-A-343 As A Bitopic Orthosteric/Allosteric Ligand. *J. Biol. Chem. 283*, 29312–29321.

(85) Birdsall, N. J. M., Burgen, A. S. V., Hulme, E. C., Stockton, J. M., and Zigmond, M. J. (1983) The effect of McN-A-343 on muscarinic receptors in the cerebral cortex and heart. *Br. J. Pharmacol. 78*, 257–259.

(86) Lazareno, S., and Birdsall, N. J. M. (1995) Detection, Quantitation, and Verification of Allosteric Interactions of Agents with Labeled and Unlabeled Ligands at G Protein-Coupled Receptors: Interactions of Strychnine and Acetylcholine at Muscarinic Receptors. *Mol. Pharmacol. 48*, 362–378.

(87) Birdsall, N. J. M., Farries, T., Gharagozloo, P., Kobayashi, S., Kuonen, D., Lazareno, S., Popham, A., and Sugimoto, M. (1997) Selective Allosteric Enhancement of the Binding and Actions of Acetylcholine at Muscarinic Receptor Subtypes. *Life Sci. 60*, 1047–1052.

(88) Ma, L., Seager, M. A., Wittman, M., Jacobson, M., Bickel, D., Burno, M., Jones, K., Graufelds, V. K., Xu, G., Pearson, M., McCampbell, A., Gaspar, R., Shughrue, P., Danziger, A., Regan, C.,

1045   dx.doi.org/10.1021/cn400086m | *ACS Chem. Neurosci.* 2013, 4, 1026–1048

40

Flick, R., Pascarella, D., Garson, S., Doran, S., Kreatsoulas, C., Veng, L., Lindsley, C. W., Shipe, W., Kuduk, S., Sur, C., Kinney, G., Seabrook, G. R., and Ray, W. J. (2009) Selective activation of the M₁ muscarinic acetylcholine receptor achieved by allosteric potentiation. *Proc. Natl. Acad. Sci. U.S.A. 106*, 15950−15955.

(89) Miyakawa, T., Yamada, M., Duttaroy, A., and Wess, J. (2001) Hyperactivity and Intact Hippocampus-Dependent Learning in Mice Lacking the M₁ Muscarinic Acetylcholine Receptor. *J. Neurosci. 21*, 5239−5250.

(90) Rouse, S. T., Hamilton, S. E., Potter, L. T., Nathanson, N. M., and Conn, P. J. (2000) Muscarinic-induced modulation of potassium conductances is unchanged in mouse hippocampal pyramidal cells that lack functional M₁ receptors. *Neurosci. Lett. 278*, 61−64.

(91) Shirey, J. K., Brady, A. E., Jones, P. J., Davis, A. A., Bridges, T. M., Kennedy, J. P., Jadhav, S. B., Menon, U. N., Xiang, Z., Watson, M. L., Christian, E. P., Doherty, J. J., Quirk, M. C., Snyder, D. H., Lah, J. J., Levey, A. I., Nicolle, M. M., Lindsley, C. W., and Conn, P. J. (2009) A Selective Allosteric Potentiator of the M₁ Muscarinic Acetylcholine Receptor Increases Activity of Medial Prefrontal Cortical Neurons and Restores Impairments in Reversal Learning. *J. Neurosci. 29*, 14271−14286.

(92) Caruana, D. A., Warburton, E. C., and Bashir, Z. I. (2011) Induction of Activity-Dependent LTD Requires Muscarinic Receptor Activation in Medial Prefrontal Cortex. *J. Neurosci. 31*, 18464−18478.

(93) Chambon, C., Jatzke, C., Wegener, N., Gravius, A., and Danysz, W. (2012) Using cholinergic M₁ receptor positive allosteric modulators to improve memory via enhancement of brain cholinergic communication. *Eur. J. Pharmacol. 697*, 73−80.

(94) Chambon, C., Wegener, N., Gravius, A., and Danysz, W. (2011) A new automated method to assess the rat recognition memory: Validation of the method. *Behav. Brain Res. 222*, 151−157.

(95) Reichel, A. (2006) The Role of Blood-Brain Barrier Studies in the Pharmaceutical Industry. *Curr. Drug Metab. 7*, 183−203.

(96) Yang, F. V., Shipe, W. D., Bunda, J. L., Nolt, M. B., Wisnoski, D. D., Zhao, Z., Barrow, J. C., Ray, W. J., Ma, L., Wittman, M., Seager, M. A., Koeplinger, K. A., Hartman, G. D., and Lindsley, C. W. (2010) Parallel synthesis of N-biaryl quinolone carboxylic acids as selective M₁ positive allosteric modulators. *Bioorg. Med. Chem. Lett. 20*, 531−536.

(97) Kuduk, S. D., Chang, R. K., Di Marco, C. N., Ray, W. J., Ma, L., Wittman, M., Seager, M. A., Koeplinger, K. A., Thompson, C. D., Hartman, G. D., and Bilodeau, M. T. (2010) Quinolizidinone Carboxylic Acids as CNS Penetrant, Selective M₁ Allosteric Muscarinic Receptor Modulators. *ACS Med. Chem. Lett. 1*, 263−267.

(98) Kuduk, S. D., Chang, R. K., Di Marco, C. N., Ray, W. J., Ma, L., Wittman, M., Seager, M. A., Koeplinger, K. A., Thompson, C. D., Hartman, G. D., and Bilodeau, M. T. (2011) Quinolizidinone carboxylic acid selective M1 allosteric modulators: SAR in the piperidine series. *Bioorg. Med. Chem. Lett. 21*, 1710−1715.

(99) Kuduk, S. D., Di Marco, C. N., Chang, R. K., Ray, W. J., Ma, L., Wittman, M., Seager, M. A., Koeplinger, K. A., Thompson, C. D., Hartman, G. D., and Bilodeau, M. T. (2010) Heterocyclic fused pyridone carboxylic acid M₁ positive allosteric modulators. *Bioorg. Med. Chem. Lett. 20*, 2533−2537.

(100) Kuduk, S. D., Di Marco, C. N., Cofre, V., Pitts, D. R., Ray, W. J., Ma, L., Wittman, M., Seager, M., Koeplinger, K., Thompson, C. D., Hartman, G. D., and Bilodeau, M. T. (2010) Pyridine containing M₁ positive allosteric modulators with reduced plasma protein binding. *Bioorg. Med. Chem. Lett. 20*, 657−661.

(101) Kuduk, S. D., Di Marco, C. N., Cofre, V., Pitts, D. R., Ray, W. J., Ma, L., Wittman, M., Veng, L., Seager, M. A., Koeplinger, K., Thompson, C. D., Hartman, G. D., and Bilodeau, M. T. (2010) N-Heterocyclic derived M₁ positive allosteric modulators. *Bioorg. Med. Chem. Lett. 20*, 1334−1337.

(102) Kuduk, S. D., Di Marco, C. N., Cofre, V., Ray, W. J., Ma, L., Wittman, M., Seager, M. A., Koeplinger, K. A., Thompson, C. D., Hartman, G. D., and Bilodeau, M. T. (2011) Fused heterocyclic M₁ positive allosteric modulators. *Bioorg. Med. Chem. Lett. 21*, 2769−2772.

(103) Kuduk, S. D., DiPardo, R. M., Beshore, D. C., Ray, W. J., Ma, L., Wittman, M., Seager, M. A., Koeplinger, K. A., Thompson, C. D., Hartman, G. D., and Bilodeau, M. T. (2010) Hydroxy cycloalkyl fused pyridone carboxylic acid M₁ positive allosteric modulators. *Bioorg. Med. Chem. Lett. 20*, 2538−2541.

(104) Kuduk, S. D., Chang, R. K., Greshock, T. J., Ray, W. J., Ma, L., Wittmann, M., Koeplinger, K. A., Seager, M. A., Thompson, C. D., Hartman, G., and Bilodeau, M. T. (2012) Identification of Amides as Carboxylic Acid Surrogates for Quinolizidinone-Based M₁ Positive Allosteric Modulators. *ACS Med. Chem. Lett. 3*, 1070−1074.

(105) Uslaner, J. M., Eddins, D., Puri, V., Cannon, C. E., Sutcliffe, J., Chew, C. S., Pearson, M., Vivian, J. A., Chang, R. K., Ray, W. J., Kuduk, S. D., and Wittmann, M. (2013) The muscarinic M1 receptor positive allosteric modulator PQCA improves cognitive measures in rat, cynomolgus macaque, and rhesus macaque. *Psychopharmacology 225*, 21−30.

(106) Kuduk, S. D., and Beshore, D. C. (2012) Novel M₁ allosteric ligands: a patent review. *Expert Opin. Ther. Pat. 22*, 1385−1398.

(107) Marlo, J. E., Niswender, C. M., Days, E. L., Bridges, T. M., Xiang, Y., Rodriguez, A. L., Shirey, J. K., Brady, A. E., Nalywajko, T., Luo, Q., Austin, C. A., Baxter Williams, M., Kim, K., Williams, R., Orton, D., Brown, H. A., Lindsley, C. W., Weaver, C. D., and Conn, P. J. (2009) Discovery and Characterization of Novel Allosteric Potentiators of M₁ Muscarinic Receptors Reveals Multiple Modes of Activity. *Mol. Pharmacol. 75*, 577−588.

(108) Bridges, T. M., Kennedy, J. P., Noetzel, M. J., Breininger, M. L., Gentry, P. R., Conn, P. J., and Lindsley, C. W. (2010) Chemical lead optimization of a pan G_q mAChR M₁, M₃, M₅ positive allosteric modulator (PAM) lead. Part II: Development of a potent and highly selective M₁ PAM. *Bioorg. Med. Chem. Lett. 20*, 1972−1975.

(109) Bridges, T. M., Kennedy, J. P., Cho, H. P., Breininger, M. L., Gentry, P. R., Hopkins, C. R., Conn, P. J., and Lindsley, C. W. (2010) Chemical lead optimization of a pan G_q mAChR M₁, M₃, M₅ positive allosteric modulator (PAM) lead. Part I: Development of the first highly selective M₅ PAM. *Bioorg. Med. Chem. Lett. 20*, 558−562.

(110) Melancon, B. J., Poslusney, M. S., Gentry, P. R., Tarr, J. C., Sheffler, D. J., Mattmann, M. E., Bridges, T. M., Utley, T. J., Daniels, J. S., Niswender, C. M., Conn, P. J., Lindsley, C. W., and Wood, M. R. (2013) Isatin replacements applied to the highly selective, muscarinic M₁ PAM ML137: Continued optimization of an MLPCN probe molecule. *Bioorg. Med. Chem. Lett. 23*, 412−416.

(111) Poslusney, M. S., Melancon, B. J., Gentry, P. R., Sheffler, D. J., Bridges, T. M., Utley, T. J., Daniels, J. S., Niswender, C. M., Conn, P. J., Lindsley, C. W., and Wood, M. R. (2013) Spirocyclic replacements for the isatin in the highly selective, muscarinic M₁ PAM ML137: the continued optimization of an MLPCN probe molecule. *Bioorg. Med. Chem. Lett. 23*, 1860−1864.

(112) Reid, P. R., Bridges, T. M., Sheffler, D. J., Cho, H. P., Lewis, L. M., Days, E., Daniels, J. S., Jones, C. K., Niswender, C. M., Weaver, C. D., Conn, P. J., Lindsley, C. W., and Wood, M. R. (2011) Discovery and optimization of a novel, selective and brain penetrant M₁ positive allosteric modulator (PAM): The development of ML169, an MLPCN probe. *Bioorg. Med. Chem. Lett. 21*, 2697−2701.

(113) Tarr, J. C., Turlington, M. L., Reid, P. R., Utley, T. J., Sheffler, D. J., Cho, H. P., Klar, R., Pancani, T., Klein, M. T., Bridges, T. M., Morrison, R. D., Blobaum, A. L., Xiang, Z., Daniels, J. S., Niswender, C. M., Conn, P. J., Wood, M. R., and Lindsley, C. W. (2012) Targeting Selective Activation of M₁ for the Treatment of Alzheimer's Disease: Further Chemical Optimization and Pharmacological Characterization of the M₁ Positive Allosteric Modulator ML169. *ACS Chem. Neurosci. 3*, 884−895.

(114) Spalding, T. A., Trotter, C., Skjaerbaek, N., Messier, T. L., Currier, E. A., Burstein, E. S., Li, D., Hacksell, U., and Brann, M. R. (2002) Discovery of an Ectopic Activation Site on the M1 Muscarinic Receptor. *Mol. Pharmacol. 61*, 1297−1302.

(115) Avlani, V. A., Langmead, C. J., Guida, E., Wood, M. D., Tehan, B. G., Herdon, H. J., Watson, J. M., Sexton, P. M., and Christopoulos, A. (2010) Orthosteric and Allosteric Modes of Interaction of Novel Selective Agonists of the M₁ Muscarinic Acetylcholine Receptor. *Mol. Pharmacol. 78*, 94−104.

41

(116) Langmead, C. J., Fry, V. A. H., Forbes, I. T., Branch, C. L., Christopoulos, A., Wood, M. D., and Herdon, H. J. (2006) Probing the Molecular Mechanism of Interaction between 4-n-Butyl-1-[4-(2-methylphenyl)-4-oxo-1-butyl]-piperidine (AC-42) and the Muscarinic M$_1$ Receptor: Direct Pharmacological Evidence That AC-42 Is an Allosteric Agonist. Mol. Pharmacol. 69, 236−246.

(117) Spalding, T. A., Ma, J.-N., Ott, T. R., Friberg, M., Bajpai, A., Bradley, S. R., Davis, R. E., Brann, M. R., and Burstein, E. S. (2006) Structural Requirements of Transmembrane Domain 3 for Activation by the M$_1$ Muscarinic Receptor Agonists AC-42, AC-260584, Clozapine, and N-Desmethylclozapine: Evidence for Three Distinct Modes of Receptor Activation. Mol. Pharmacol. 70, 1974−1983.

(118) Jacobson, M. A., O'Brien, J. A., Pascarella, D., Mallorga, P. J., Scolnick, E. M., and Sur, C. (2004) Mapping the interaction site of M$_1$ muscarinic receptor allosteric agonists. Soc. Neurosci. Abstr. 30, 846.16.

(119) Thomas, R. L., Mistry, R., Langmead, C. J., Wood, M. D., and Challiss, R. A. J. (2008) G Protein Coupling and Signaling Pathway Activation by M$_1$ Muscarinic Acetylcholine Receptor Orthosteric and Allosteric Agonists. J. Pharmacol. Exp. Ther. 327, 365−374.

(120) Thomas, R. L., Langmead, C. J., Wood, M. D., and Challiss, R. A. J. (2009) Contrasting Effects of Allosteric and Orthosteric Agonists on M$_1$ Muscarinic Acetylcholine Receptor Internalization and Down-regulation. J. Pharmacol. Exp. Ther. 331, 1086−1095.

(121) Lebon, G., Langmead, C. J., Tehan, B. G., and Hulme, E. C. (2009) Mutagenic Mapping Suggests a Novel Binding Mode for Selective Agonists of M$_1$ Muscarinic Acetylcholine Receptors. Mol. Pharmacol. 75, 331−341.

(122) Bradley, S. R., Lameh, J., Ohrmund, L., Son, T., Bajpai, A., Nguyen, D., Friberg, M., Burstein, E. S., Spalding, T. A., Ott, T. R., Schiffer, H. H., Tabatabaei, A., McFarland, K., Davis, R. E., and Bonhaus, D. W. (2010) AC-260584, an orally bioavailable M$_1$ muscarinic receptor allosteric agonist, improves cognitive performance in an animal model. Neuropharmacology 58, 365−373.

(123) Vanover, K. E., Veinbergs, I., and Davis, R. E. (2008) Antipsychotic-Like Behavioural Effects and Cognitive Enhancement by a Potent and Selective Muscarinic M$_1$ Receptor Agonist AC-260584. Behav. Neurosci. 122, 570−575.

(124) Langmead, C. J., Austin, N. E., Branch, C. L., Brown, J. T., Buchanan, K. A., Davies, C. H., Forbes, I. T., Fry, V. A. H., Hagan, J. J., Herdon, H. J., Jones, G. A., Jeggo, R., Kew, J. N. C., Mazzali, A., Melarange, R., Patel, N., Pardoe, J., Randall, A. D., Roberts, C., Roopun, A., Starr, K. R., Teriakidis, A., Wood, M. D., Whittington, M., Wu, Z., and Watson, J. (2008) Characterization of a CNS penetrant, selective M$_1$ muscarinic receptor agonist, 77-LH-28-1. Br. J. Pharmacol. 154, 1104−1115.

(125) Buchanan, K. A., Petrovic, M. M., Chamberlain, S. E. L., Marrion, N. V., and Mellor, J. R. (2010) Facilitation of Long-Term Potentiation by Muscarinic M$_1$ Receptors Is Mediated by Inhibition of SK Channels. Neuron 68, 948−963.

(126) Kuroki, T., Nagao, N., and Nakahara, T. (2008) Neuro-pharmacology of second-generation antipsychotic drugs: a validity of the serotonin-dopamine hypothesis. Prog. Brain Res. 172, 199−212.

(127) Sur, C., Mallorga, P. J., Wittmann, M., Jacobson, M. A., Pascarella, D., Williams, J. B., Brandish, P. E., Pettibone, D. J., Scolnick, E. M., and Conn, P. J. (2003) N-Desmethylclozapine, an allosteric agonist at muscarinic 1 receptor, potentiates N-methyl-D-aspartate receptor activity. Proc. Natl. Acad. Sci. U.S.A. 100, 13674−13679.

(128) Thomas, D. R., Dada, A., Jones, G. A., Deisz, R. A., Gigout, S., Langmead, C. J., Werry, T. D., Hendry, N., Hagan, J. J., Davies, C. H., and Watson, J. M. (2010) N-Desmethylclozapine (NDMC) is an antagonist at the human native muscarinic M$_1$ receptor. Neuro-pharmacology 58, 1206−1214.

(129) Jones, C. K., Brady, A. E., Davis, A. A., Xiang, Z., Bubser, M., Noor Tantawy, M., Kane, A. S., Bridges, T. M., Kennedy, J. P., Bradley, S. R., Peterson, T. E., Ansari, M. S., Baldwin, R. M., Kessler, R. M., Deutch, A. Y., Lah, J. J., Levey, A. I., Lindsley, C. W., and Conn, P. J. (2008) Novel Selective Allosteric Activator of the M$_1$ Muscarinic Acetylcholine Receptor Regulates Amyloid Processing and Produces Antipsychotic-Like Activity in Rats. J. Neurosci. 28, 10422−10433.

(130) Bridges, T. M., Brady, A. E., Kennedy, J. P., Daniels, R. N., Miller, N. R., Kim, K., Breininger, M. L., Gentry, P. R., Brogan, J. T., Jones, C. K., Conn, P. J., and Lindsley, C. W. (2008) Synthesis and SAR of analogues of the M$_1$ allosteric agonist TBPB. Part I: Exploration of alternative benzyl and privileged structure moieties. Bioorg. Med. Chem. Lett. 18, 5439−5442.

(131) Miller, N. R., Daniels, R. N., Bridges, T. M., Brady, A. E., Conn, P. J., and Lindsley, C. W. (2008) Synthesis and SAR of analogs of the M1 allosteric agonist TBPB. Part II: Amides, sulfonamides and ureas-The effect of capping the distal basic piperidine nitrogen. Bioorg. Med. Chem. Lett. 18, 5443−5447.

(132) Sheffler, D. J., Sevel, C., Le, U., Lovett, K. M., Tarr, J. C., Carrington, S. J. S., Cho, H. P., Digby, G. J., Niswender, C. M., Conn, P. J., Hopkins, C. R., Wood, M. R., and Lindsley, C. W. (2013) Further exploration of M$_1$ allosteric agonists: Subtle structural changes abolish M$_1$ allosteric agonism and result in pan-mAChR orthosteric antagonism. Bioorg. Med. Chem. Lett. 23, 223−227.

(133) Lebois, E. P., Bridges, T. M., Lewis, L. M., Dawson, E. S., Kane, A. S., Xiang, Z., Jadhav, S. B., Yin, H., Kennedy, J. P., Meiler, J., Niswender, C. M., Jones, C. K., Conn, P. J., Weaver, C. D., and Lindsley, C. W. (2010) Discovery and Characterization of Novel Subtype-Selective Allosteric Agonists for the Investigation of M$_1$ Receptor Function in the Central Nervous System. ACS Chem. Neurosci. 1, 104−121.

(134) Lebois, E. P., Digby, G. J., Sheffler, D. J., Melancon, B. J., Tarr, J. C., Cho, H. P., Miller, N. R., Morrison, R., Bridges, T. M., Xiang, Z., Daniels, J. S., Wood, M. R., Conn, P. J., and Lindsley, C. W. (2011) Development of a highly selective, orally bioavailable and CNS penetrant M$_1$ agonist derived from the MLPCN probe ML071. Bioorg. Med. Chem. Lett. 21, 6451−6455.

(135) Melancon, B. J., Gogliotti, R. D., Tarr, J. C., Saleh, S. A., Chauder, B. A., Lebois, E. P., Cho, H. P., Utley, T. J., Sheffler, D. J., Bridges, T. M., Morrison, R. D., Daniels, J. S., Niswender, C. M., Conn, P. J., Lindsley, C. W., and Wood, M. R. (2012) Continued optimization of the MLPCN probe ML071 into highly potent agonists of the hM$_1$ muscarinic acetylcholine receptor. Bioorg. Med. Chem. Lett. 22, 3467−3472.

(136) Digby, G. J., Noetzel, M. J., Bubser, M., Utley, T. J., Walker, A. G., Byun, N. E., Lebois, E. P., Xiang, Z., Sheffler, D. J., Cho, H. P., Davis, A. A., Nemirovsky, N. E., Mennenga, S. E., Camp, B. W., Bimonte-Nelson, H. A., Bode, J., Italiano, K., Morrison, R., Daniels, J. S., Niswender, C. M., Olive, M. F., Lindsley, C. W., Jones, C. K., and Conn, P. J. (2012) Novel Allosteric Agonists of M$_1$ Muscarinic Acetylcholine Receptors Induce Brain Region-Specific Responses That Correspond with Behavioural Effects in Animal Models. J. Neurosci. 32, 8532−8544.

(137) Digby, G. J., Utley, T. J., Lamsal, A., Sevel, C., Sheffler, D. J., Lebois, E. P., Bridges, T. M., Wood, M. R., Niswender, C. M., Lindsley, C. W., and Conn, P. J. (2012) Chemical Modification of the M$_1$ Agonist VU0364572 Reveals Molecular Switches in Pharmacology and a Bitopic Binding Mode. ACS Chem. Neurosci. 3, 1025−1036.

(138) Sams, A. G., Hentzer, M., Mikkelsen, G. K., Larsen, K., Bundgaard, C., Plath, N., Christoffersen, C. T., and Bang-Andersen, B. (2010) Discovery of N-{1-[3-(3-Oxo-2,3-dihydrobenzo[1,4]oxazin-4-yl)propyl]piperidin-4-yl}-2-phenylacetamide (Lu AE51090): An Allos-teric Muscarinic M$_1$ Receptor Agonist with Unprecedented Selectivity and Procognitive Potential. J. Med. Chem. 53, 6386−6397.

(139) Sams, A. G., Larsen, K., Mikkelsen, G. K., Hentzer, M., Christoffersen, C. T., Jensen, K. G., Frederiksen, K., and Bang-Andersen, B. (2012) Hit-to-lead investigation of a series of novel combined dopamine D$_2$ and muscarinic M$_1$ receptor ligands with putative antipsychotic and pro-cognitive potential. Bioorg. Med. Chem. Lett. 22, 5134−5140.

(140) Budzik, B., Garzya, V., Shi, D., Foley, J. J., Rivero, R. A., Langmead, C. J., Watson, J., Wu, Z., Forbes, I. T., and Jin, J. (2010) 2′ Biaryl amides as novel and subtype selective M$_1$ agonists. Part I: Identification, synthesis, and initial SAR. Bioorg. Med. Chem. Lett. 20, 3540−3544.

(141) Budzik, B., Garzya, V., Shi, D., Walker, G., Lauchart, Y., Lucas, A. J., Rivero, R. A., Langmead, C. J., Watson, J., Wu, Z., Forbes, I. T., and Jin, J. (2010) 2′ Biaryl amides as novel and subtype selective M_1 agonists. Part II: Further optimization and profiling. *Bioorg. Med. Chem. Lett. 20*, 3545−3549.

(142) Budzik, B., Garzya, V., Shi, D., Walker, G., Woolley-Roberts, M., Pardoe, J., Lucas, A., Tehan, B., Rivero, R. A., Langmead, C. J., Watson, J., Wu, Z., Forbes, I. T., and Jin, J. (2010) Novel *N*-Substituted Benzimidazolones as Potent, Selective, CNS-Penetrant, and Orally Active M_1 mAChR Agonists. *ACS Med. Chem. Lett. 1*, 244−248.

(143) Johnson, D. J., Forbes, I. T., Watson, S. P., Garzya, V., Stevenson, G. I., Walker, G. R., Mudhar, H. S., Flynn, S. T., Wyman, P. A., Smith, P. W., Murkitt, G. S., Lucas, A. J., Mookherjee, C. R., Watson, J. M., Gartlon, J. E., Bradford, A. M., and Brown, F. (2010) The discovery of a series of *N*-substituted 3-(4-piperidinyl)-1,3-benzoxazolinones and oxindoles as highly brain penetrant, selective muscarinic M_1 agonists. *Bioorg. Med. Chem. Lett. 20*, 5434−5438.

(144) Nathan, P. J., Watson, J., Lund, J., Davies, C. H., Peters, G., Dodds, C. M., Swirski, B., Lawrence, P., Bentley, G. D., O'Neill, B. V., Robertson, J., Watson, S., Jones, G. A., Maruff, P., Croft, R. J., Laruelle, M., and Bullmore, E. T. (2013) The potent M_1 receptor allosteric agonist GSK1034702 improves episodic memory in humans in the nicotine abstinence model of cognitive dysfunction. *Int. J. Neuropsychopharmacol. 16*, 721−731.

43

Chapter Two

Declaration for Thesis Chapter 2

The original research article presented in Chapter 2 is published as the following the paper:

Davie, B.J., Valant, C., White, J.M., Sexton, P.M., Capuano, B., Christopoulos, A., Scammells, P.J. (2014), Synthesis and Pharmacological Evaluation of Analogues of Benzyl Quinolone Carboxylic Acid (BQCA) Designed to Bind Irreversibly to an Allosteric Site of the M_1 Muscarinic Acetylcholine Receptor, *Journal of Medicinal Chemistry*, *57* (12), 5405-5418. Permission to reprint this publication for the purpose of this thesis was granted by ACS Publications.

Declaration by candidate

In the case of Chapter 2, the nature and extent of my contribution to the work was the following:

Nature of contribution	Extent of contribution (%)
Synthesis and chemical characterization of all compounds. Pharmacological testing and data analysis for all compounds. Main author of manuscript.	80%

The following co-authors contributed to the work. If co-authors are students at Monash University, the extent of their contribution in percentage terms must be stated:

Name	Nature of contribution	Extent of contribution (%) for student co-authors only
Celine Valant	Contributed to optimization of pharmacological testing and data analysis.	
Jonathan M. White	Generated crystal structure of compound **4a**	
Patrick M. Sexton	Co-author of manuscript	
Ben Capuano	Co-author of manuscript	
Arthur Christopoulos	Co-author of manuscript	

Peter J. Scammells	Co-author of manuscript	

The undersigned hereby certify that the above declaration correctly reflects the nature and extent of the candidate's and co-authors' contributions to this work.

Candidate's Signature		**Date**	25/02/15
Main Supervisor's Signature		**Date**	25/02/15

Synthesis and Pharmacological Evaluation of Analogues of Benzyl Quinolone Carboxylic Acid (BQCA) Designed to Bind Irreversibly to an Allosteric Site of the M₁ Muscarinic Acetylcholine Receptor

Briana J. Davie,[†,‡] Celine Valant,[‡] Jonathan M. White,[§] Patrick M. Sexton,[‡] Ben Capuano,[†] Arthur Christopoulos,*[,‡] and Peter J. Scammells*[,†]

[†]Medicinal Chemistry and [‡]Drug Discovery Biology, Monash Institute of Pharmaceutical Sciences, Monash University, 381 Royal Parade, Parkville, Victoria 3052, Australia

[§]School of Chemistry and the Bio21 Molecular Science and Biotechnology Institute, The University of Melbourne, Parkville, Victoria 3010, Australia

S *Supporting Information*

ABSTRACT: Activation of the M₁ muscarinic acetylcholine receptor (mAChR) is a prospective treatment for alleviating cognitive decline experienced in central nervous system (CNS) disorders. Current therapeutics indiscriminately enhance the activity of the endogenous neurotransmitter ACh, leading to side effects. BQCA is a positive allosteric modulator and allosteric agonist at the M₁ mAChR that has high subtype selectivity and is a promising template from which to generate higher affinity, more pharmacokinetically viable drug candidates. However, to efficiently guide rational drug design, the binding site of BQCA needs to be conclusively elucidated. We report the synthesis and pharmacological validation of BQCA analogues designed to bind irreversibly to the M₁ mAChR. One analogue in particular, **11**, can serve as a useful structural probe to confirm the location of the BQCA binding site; ideally, by co-crystallization with the M₁ mAChR. Furthermore, this ligand may also be used as a pharmacological tool with a range of applications.
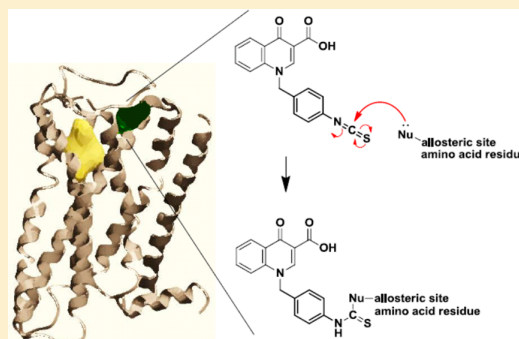
■ INTRODUCTION

The M₁ mAChR is a Family A G protein-coupled receptor (GPCR) that is well-established as a target of therapeutic interest for the treatment of cognitive deficits associated with Alzheimer's disease and schizophrenia.[1] This receptor is primarily expressed in regions of the hippocampus, striatum, and prefrontal cortex,[2] and the prospective therapeutic utility of M₁ mAChR activation for enhanced cognitive function has been extensively validated in vitro and in vivo.[1,3] The primary challenge impeding the development of clinically viable M₁ mAChR drug candidates is achieving high receptor subtype selectivity so as to avoid side effects associated with indiscriminate activity at other mAChRs. Achieving such selectivity with ligands that target the orthosteric (endogenous ligand binding) site has been difficult due to the high sequence conservation across the orthosteric sites of the M₁–M₅ mAChR family. Allosteric ligands are attractive alternatives to orthosteric drugs that have the potential to elicit more fine-tuned, highly selective responses than their orthosteric counterparts.[4] Allosteric ligands are capable of binding to topographically distinct sites and can elicit their effects by three different mechanisms: (1) by modulating the affinity of the cobound orthosteric ligand, (2) by modulating the efficacy of the cobound orthosteric ligand as well as (3) activating the receptor in their own right.[5]

An array of M₁ mAChR-selective allosteric ligands has been characterized to date.[6] An exemplar molecule is 1-(4-methoxybenzyl)-4-oxo-1,4-dihydroquinoline-3-carboxylic acid (more commonly abbreviated to "benzyl quinolone carboxylic acid" or BQCA), a subtype-selective, orally bioavailable M₁ mAChR positive allosteric modulator (PAM) and allosteric agonist with an extraordinary degree of positive cooperativity with orthosteric agonists, including the endogenous neurotransmitter acetylcholine (ACh).[7] BQCA has undergone the most extensive pharmacological evaluation and synthetic derivatization of all M₁ mAChR allosteric ligands reported to date.[7−12] While this campaign has led to the discovery of several higher potency, more pharmacokinetically viable analogues of BQCA, the structure–activity relationships (SAR) reported to date have been frequently described as "flat" or "shallow",[13−17] which is not an uncommon observation in the broader field of allosteric ligand development.[18] Performing more detailed pharmacological analyses that deconstruct the binding and functional profile of allosteric

ligands has proven fruitful in obtaining more detailed, "enriched" SAR[12,19] and in further understanding their functional capabilities.[20] However, to more efficiently guide rational drug design, identification and characterization of the BQCA allosteric binding site by co-crystallization with the M_1 mAChR would offer unequivocal insight into the critical interactions that dictate its unique mode of action, the geometry of the binding pocket with which it interacts, and its global influence on receptor conformation. The recent publication of the M_2 mAChR co-crystallized with both an orthosteric and an allosteric ligand[21] demonstrates that this approach is achievable, however, being a low-affinity ligand ($pK_B \sim 4$),[9,12] BQCA itself may not be an optimal candidate for a similar study at the M_1 mAChR.

An alternative approach to elucidating the BQCA binding site has recently been published.[22] Comprehensive mutagenesis in conjunction with molecular dynamics simulations and ligand docking revealed the BQCA binding site to likely reside in the extracellular (EC) vestibule common to all mAChRs, overlapping with what is often dubbed the "common" allosteric binding site.[23] The BQCA binding site itself appears to involve residues within transmembrane (TM) 2, TM 7, and EC loop 2, building on observations made in the original BQCA publication where the positive modulation of ACh-mediated calcium mobilization by BQCA was absent at the Y179A (EC loop 2) and W400A (TM 7) mutants.[7] Furthermore, subtype-specific transmission of cooperativity was proposed as the potential mechanism underlying BQCA's exquisite selectivity.

To further advance our understanding of the interaction between BQCA and the M_1 mAChR, and to aid interrogation of such new insights, the current study sought to design novel analogues of BQCA that bind irreversibly to the M_1 mAChR and form a covalently modified receptor complex. Such ligands may be utilized as pharmacological tools in a range of preclinical applications, including co-crystallization.

Irreversible ligands (also known as covalent modifiers) are molecules that contain a reactive functionality rendering them capable of binding to a site on a protein target of interest (such as an enzyme or GPCR) and forming a covalent bond with one or more of the protein's amino acid residues. More relevant to our experimental rationale, irreversible ligands have also been developed as biological investigative tools for a range of protein targets including adrenergic, histaminergic, imidazoline, muscarinic, opioid, and adenosine receptors.[24−30] As with the BQCA analogues published herein, such ligands most commonly comprise a reactive moiety incorporated into a known reversible ligand for which the target selectivity and pharmacological profile is well established. In the past, these modified ligands have enabled researchers to identify and map ligand binding sites,[29,31] characterize ligand binding modes,[30] determine functional roles,[32] and investigate cell surface expression, receptor occupancy, and cellular processing of different receptor families, and specific subtypes within those families.[25,33] The advent of fluorescently labeled irreversible ligands has facilitated imaging of membrane-bound and intracellular proteins in vitro.[34,35] Ultimately, valuable structural and functional insight into the role of biological targets in physiological and pathophysiological processes is gained, potentially informing the selection of novel points of therapeutic intervention and directing subsequent rational drug design. Adding further support to our rationale, co-crystallization of an irreversible agonist-β2 adrenergic GPCR complex was achieved,[31] validating this strategy as a means for

obtaining structural knowledge about ligand binding mode and receptor conformation.

While irreversible *orthosteric* mAChR ligands have been previously developed,[27−30] this is the first time that development of an irreversible purely *allosteric* mAChR ligand has been achieved. We began our investigation with the synthesis of four BQCA analogues, each containing a different electrophilic functionality capable of reacting covalently with a nucleophilic amino acid residue. The 4-benzylic position of BQCA was selected as an ideal starting point for introducing our reactive functionalities as this region of the molecule is highly tolerant of a range of synthetic modifications[10] and appears to be an important determinant of analogue affinity.[12] Furthermore, molecular dynamics simulations suggest that this moiety lies in close proximity to EC loops 2 and 3 as well as upper segments of TMs 6 and 7.[22] Using competition radioligand binding and ERK1/2 phosphorylation assays, pharmacological evaluation of these BQCA analogues confirmed the preservation of allosteric binding and functional activation at hM_1 mAChR-expressing Chinese hamster ovary (CHO) cells. Utilizing saturation radioligand binding assays to evaluate potential irreversible interaction, we found that **11** binds irreversibly to the M_1 mAChR and is therefore the first known alkylating PAM of a GPCR.

■ RESULTS AND DISCUSSION

Chemistry. The 4-oxo-1,4-dihydroquinoline core of BQCA was synthesized in two steps (Scheme 1) by employing well-

Scheme 1. Synthesis of BQCA (4b) and Analogues 4a, 4c, and 4d[a]
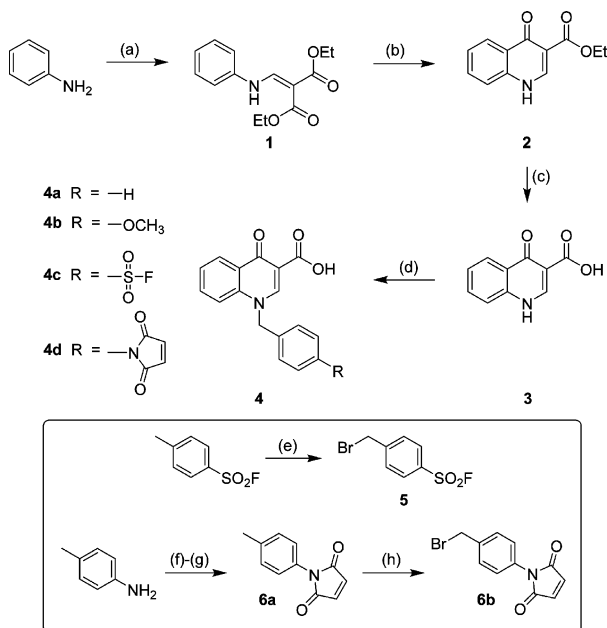
[a]Reagents and conditions: (a) diethylethoxymethylene malonate, 120 °C, 83%; (b) diphenyl ether, 240 °C, 48% or Eaton's reagent, 100 °C, quantitative; (c) 1 M LiOH(aq), THF, 80 °C, 75%; (d) benzyl halide ± KI, DIPEA, ACN, 80 °C, 87% (**4a**), 97% (**4b**), 21% (**4c**), 53% (**4d**); (e) NBS, benzoyl peroxide, EtOAc, microwave 100 °C, 81%; (f) maleic anhydride, DMF, 110 °C, 100%; (g) sodium acetate, acetic anhydride, 120 °C, 51%; (h) NBS, benzoyl peroxide, EtOAc, microwave 100 °C, 45%.

established reaction conditions reported previously.[12,36,37] In line with observations noted in a recent publication by Mistry et al.,[12] while the neat reaction between aniline and diethylethoxymethylene malonate afforded an easily isolatable, crystalline **1** in good yield, cyclization with diphenyl ether to form **2** required unfavorably high temperatures and typically resulted in widely variable yields and purity. Eaton's reagent (1:10 w/w P_2O_5 in methanesulfonic acid) was found to be an ideal alternative, requiring milder conditions and resulting in quantitative yields. In the earliest reported synthesis of BQCA, Yang et al.[36] follow this cyclization step with N-benzylation followed by ester saponification to yield the target compound. In our case, subsequent syntheses introducing irreversible functionalities in place of the 4-methoxy group of BQCA necessitate incorporation of the *N*-benzyl moiety as the final synthetic step so as to avoid any unwanted reactivity in subsequent synthetic steps. Hence, for pre-emptive optimization purposes, the order of the third and final steps of the BQCA synthesis was reversed from that of the initial publication.[36] Based on a procedure reported by Juli et al.,[38] ester saponification to form **3** was achieved in good yield.

It was noted that, as a result of the need to perform the N-benzylation step last, O-benzylation of the free carboxylic acid moiety was also a possibility. The position of alkylation was confirmed through a model study involving the alkylation of **3** with benzyl bromide where an X-ray crystal structure of the product **4a** was obtained (Figure 1) and confirmed the
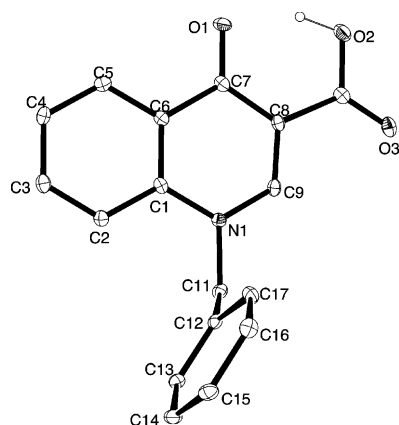
Figure 1. Thermal ellipsoid plot for **4a** (ellipsoids are at the 20% probability level).

regioselectivity of the reaction. The N-alkylation with 4-methoxybenzyl chloride proceeded in excellent yield, with the pure product **4b** precipitating from the reaction mixture unaided. A HMBC 2D NMR experiment confirmed formation of the N-benzylated product; the spectrum showed a cross peak between H2 of the quinolinone ring system at δ 9.32 ppm and the methylene carbon of the benzyl group at δ 55.5 ppm that would not be apparent had O-benzylation occurred.

The fluorosulfonyl (**4c**) and maleimide (**4d**) analogues of BQCA both required preparation of the requisite substituted benzyl bromide precursors (Scheme 1). Radical bromination of *p*-toluenesulfonyl fluoride gave a mixture of mono- and dibrominated species, with the former (**5**) easily isolated by column chromatography prior to N-benzylation with **3** to yield the target fluorosulfonyl analogue **4c**. Synthesis of 1-(*p*-tolyl)-1*H*-pyrrole-2,5-dione (**6a**) required a two-step methodology

after the reaction of *p*-toluidine and maleic anhydride resulted in the uncyclized intermediate 4-oxo-4-(*p*-tolylamino)but-2-enoic acid (structure not shown). Stirring with sodium acetate in acetic anhydride rapidly recyclized the molecule to reform the maleimide functionality, then radical bromination was performed as previously described to yield the precursor **6b**, following column chromatography. Finally, N-benzylation with **3** gave the target maleimide analogue **4d** in low but sufficient yield for chemical and pharmacological characterization.

The bromoacetamide (**10**) and isothiocyanate (**11**) analogues of BQCA were both accessed via the intermediate **9**. This compound was synthesized from the 4-oxo-1,4-dihydroquinoline core in three steps (Scheme 2). N-Benzylation with 4-nitrobenzyl bromide (**7**) was achieved in good yield by employing reaction conditions established in Scheme 1. Reduction of the nitro functionality to the amine with 10% Pd/C under a hydrogen atmosphere gave **8** in quantitative yield. The ester saponification conditions outlined in Scheme 1 (1 M $LiOH_{(aq)}$, THF) were insufficient for ester bond cleavage of **8**, however, 1 M $KOH_{(aq)}$ in 3:1 $MeOH:H_2O$ afforded conversion to the target carboxylic acid **9** in excellent yield.

Cooling of **9**, triethylamine (TEA), and acetonitrile (ACN) in a dry ice/acetone bath (approximately −80 °C) was required prior to addition of bromoacetyl bromide. Allowing the reaction mixture to warm to room temperature (RT) naturally was critical for obtaining clean conversion to the target bromoacetamide analogue **10**, which precipitated from the reaction mixture and required no further purification (Scheme 2).

The isothiocyanate analogue **11** was isolated following reaction of **9** with 1,1′-thiocarbonyldiimidazole (TCDI) and catalytic 4-dimethylaminopyridine (DMAP), requiring only a simple organic extraction to attain >95% purity (Scheme 2).

Pharmacology. To assess the binding activity, [3H]*N*-methylscopolamine (NMS) equilibrium whole cell binding interactions between ACh and each of our test allosteric ligands (BQCA, **4c**, **4d**, **10**, and **11**) were conducted in CHO cells stably expressing the hM$_1$ mAChR (Figure 2). Application of an allosteric ternary complex model to these data allowed us to estimate each ligand's affinity for the free receptor (pK_B), binding cooperativity with [3H]NMS (log $\alpha_{[NMS]}$), and binding cooperativity with ACh (log $\alpha_{[ACh]}$) (Table 1).

To assess functional activity, ERK1/2 phosphorylation assays were performed in CHO cells stably expressing the hM1 mAChR. Time course assays were first performed to establish the length of incubation time required to measure the peak phosphorylated ERK1/2 response for each test compound (data not shown). Concentration−response curves (CRCs) were subsequently constructed using this peak time point to estimate the pEC$_{50}$ of each compound and to select a suitable concentration range for interaction studies with ACh (Figure 3, Table 1). Interaction studies were conducted between ACh and each of our test allosteric ligands (BQCA, **4c**, **4d**, **10**, and **11**) (Figure 3). Application of an operational model of allosterism to these data allowed us to estimate each ligand's signaling efficacy (τ_B) and the combined binding/activation cooperativity ($\alpha\beta$) (Table 1).

As expected, BQCA exhibited a modest micromolar affinity (K_B = 36 μM), a moderate potency (EC$_{50}$ = 170 nM), and agonism in its own right (τ_B = 162) in this system. BQCA demonstrated a very high degree of positive cooperativity with ACh found to be driven predominantly by binding (α = 759), rather than functional (β = 7) cooperativity. Importantly, the

Scheme 2. Synthesis of BQCA Analogues 10 and 11[a]
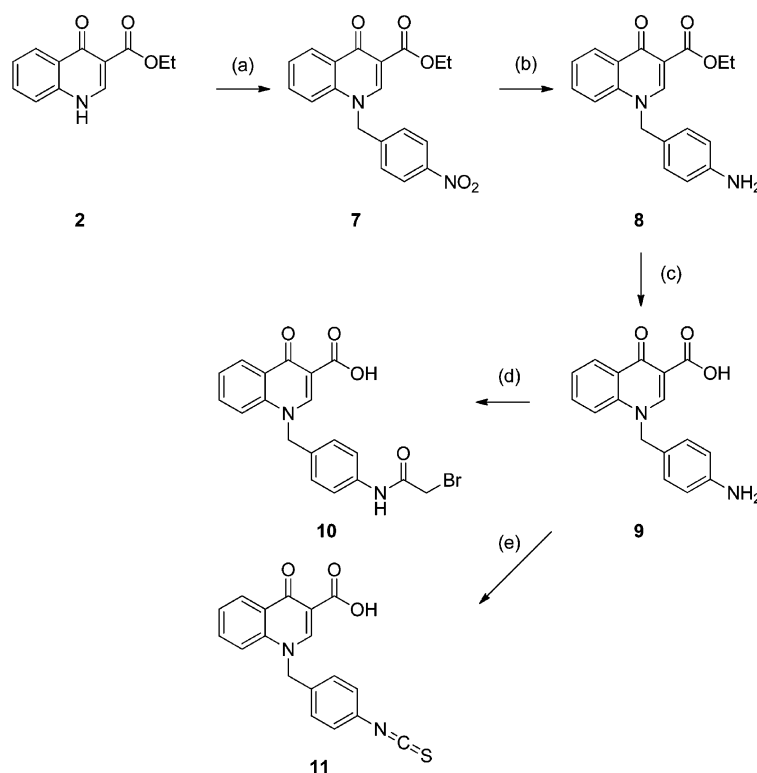
[a]Reagents and conditions: (a) 4-nitrobenzyl bromide, DIPEA, ACN, 80 °C, 78%; (b) H$_2$, 10% Pd/C, DMF, RT, 93%; (c) 1 M KOH$_{(aq)}$, 3:1 MeOH:water, 80 °C, 82%; (d) bromoacetyl bromide, TEA, ACN, −80 °C−RT, 74%; (e) 1,1′-thiocarbonyldiimidazole, DMAP, dry DCM, RT, 96%.

results of these binding and functional experiments confirmed the preservation of allosteric activity in each of our four BQCA analogues, although the impact on individual parameters varied across the set. Our results suggest that interaction of the 4-methoxy group of BQCA with the receptor is an important factor in the ligand's high degree of positive binding cooperativity with ACh as well as its signaling efficacy. Introduction of the fluorosulfonyl moiety (**4c**) appears to preserve this critical interaction; log $\alpha_{[ACh]}$ and log τ_B values were not significantly different from BQCA. However, this interaction is clearly less-favored by the maleimide (**4d**), bromoacetamide (**10**), and isothiocyanate (**11**) moieties, as evidenced by the significant reduction in the log $\alpha_{[ACh]}$ values ($p < 0.0001$) as well as the log τ_B values ($p < 0.01$). In contrast, the affinity (pK_B) values for the maleimide and isothiocyanate analogues were significantly improved relative to BQCA ($p < 0.001$) while the potency values were unaffected.

Prior to assessing the ability of our BQCA analogues to bind irreversibly, we conducted [³H]NMS saturation whole cell binding assays in CHO cells stably expressing the hM$_1$ mAChR following preincubation with buffer, the reversible endogenous agonist, ACh, or the known irreversible ligand, acetylcholine mustard (AChM), a nonselective muscarinic orthosteric agonist, for which protocols are well-established.[30,39]

Time course experiments were performed to determine the preincubation time at 37 °C necessary to observe at least 50% receptor alkylation (irreversible binding) by AChM but without observing significant internalization by ACh (Table 2, Figure 4). Both receptor internalization and receptor alkylation would be expected to manifest as a decrease in B_{max} (total receptor

density), due to a reduction in cell-surface receptor expression or by competition between [³H]NMS and AChM at the orthosteric site, respectively. A key assumption in this experiment is that, if a given incubation time does not induce receptor internalization by ACh, any effect observed following the same incubation time with AChM is likely the result of receptor alkylation. No internalization was observed following 30 min preincubation with ACh, and 60% receptor alkylation was observed following 30 min preincubation with AChM. Hence, this time was selected as a suitable starting point for probing the irreversibility of our BQCA analogues. In applying this protocol to our experiments with allosteric ligands, it should be noted that, rather than direct blockade of the radioligand binding site, we hypothesized that irreversible binding of our allosteric ligands would stabilize a conformation of the receptor that would be unfavorable for [³H]NMS binding. Hence, we would expect to see a reduction in B_{max} as a result of high irreversible negative cooperativity (Table 1), rather than direct competition.

No change in B_{max} was observed following 30 min preincubation with BQCA and subsequent washout (Table 3, Figure 5A,C), indicating that the ligand does not cause receptor internalization during this time period. Preincubation with BQCA in the presence of ACh gave a small, nonsignificant reduction in B_{max}, suggesting that the positive cooperativity between the two molecules potentially induced a small amount of receptor internalization not observed with either compound alone. This modest effect allowed us to hypothesize that any substantial reduction in B_{max} observed with our putative irreversible ligands would be most likely due to receptor
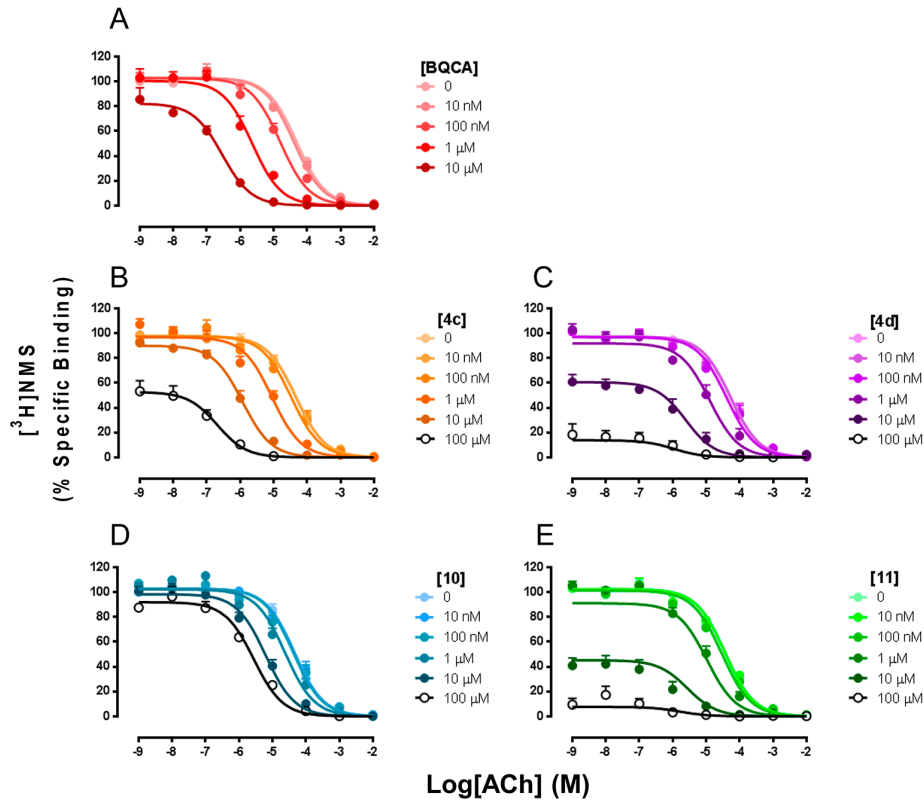
Figure 2. Pharmacological characterization of BQCA and the putative irreversible analogues in radioligand competition whole cell binding assays. (A−E) Radioligand competition binding experiments performed in hM$_1$ mAChR-expressing CHO cells in the presence of a K_D concentration of radiolabeled orthosteric antagonist [^{3}H]NMS (0.1 nM), increasing concentrations of ACh with or without increasing concentrations of BQCA (A), **4c** (B), **4d** (C), **10** (D), or **11** (E). Values represent the mean ± SEM from at least three to four experiments performed in duplicate.

Table 1. Ternary Complex Model Parameters for the Binding Interaction between [^{3}H]NMS, ACh, and Each Allosteric Ligand, and the Operational Model of Allosterism Functional Parameters for the Activity of Each Allosteric Ligand Alone and in the Presence of Acetylcholine (ACh)^a

	BQCA	4c	4d	10	11
pK_B^{b}	4.44 ± 0.07	3.97 ± 0.05	5.09 ± 0.04	4.72 ± 0.14	5.22 ± 0.04
log $\alpha_{[NMS]}$^{c}	−3.00*	−3.00*	−3.00*	−0.06 ± 0.01	−3.00*
log $\alpha_{[ACh]}$^{d}	2.88 ± 0.11	2.66 ± 0.09	1.46 ± 0.11	1.29 ± 0.09	1.26 ± 0.13
$\alpha_{[ACh]}$	759	457	29	19	18
pEC$_{50}$^{e}	6.77 ± 0.07	6.50 ± 0.09	6.38 ± 0.12	5.80 ± 0.10	6.41 ± 0.11
log τ_B^{f}	2.21 ± 0.08	1.79 ± 0.35	1.10 ± 0.06	1.04 ± 0.07	0.83 ± 0.04
τ_B	162	62	13	11	7
log $\alpha\beta$^{g}	3.71 ± 0.18	3.62 ± 0.21	1.91 ± 0.17	2.15 ± 0.18	1.33 ± 0.26
log β (β)^h	0.83 (7)	0.96 (9)	0.45 (3)	0.87 (7)	0.07 (1)

^{a}Estimated parameter values represent the mean ± SEM from at least three to four experiments performed in duplicate. ^{b}Negative logarithm of the equilibrium dissociation constant of the allosteric ligand. ^{c}Logarithm of the binding cooperativity factor between [^{3}H]NMS and the allosteric ligand; * denotes when the parameter was constrained to an arbitrary low value consistent with very high negative cooperativity between the allosteric ligand and the radioligand. ^{d}Logarithm of the binding cooperativity factor between ACh and the allosteric ligand. pK_B value was fixed to that estimated for each ligand in whole cell binding experiments. ^{e}Negative logarithm of the ligand concentration that produces half the maximal response. ^{f}Logarithm of the operational efficacy parameter of the ligand. ^{g}Logarithm of the product of the binding and activation cooperativity factors between ACh and the allosteric ligand. ^{h}Logarithm (and antilogarithm) of the activation cooperativity factor between ACh and the allosteric ligand (derived by fixing the binding cooperativity value to that estimated for each ligand in whole cell binding experiments (log $\alpha_{[ACh]}$)).

alkylation and not receptor internalization. No significant reductions in B_{max} were observed following preincubation with **4c**, **4d**, and **10** (data not shown), however, we observed a significant reduction in B_{max} following preincubation with the isothiocyanate analogue **11** (Table 3, Figure 5B,D). Thirty minutes preincubation of **11** in the presence of ACh resulted in

a further reduction in B_{max}. This is most likely due to the positive cooperativity between the two molecules facilitating additional binding and receptor alkylation by **11** than when preincubated alone. However, given our observations with BQCA and ACh, it is also possible that receptor internalization may be contributing to this reduction in B_{max} to some extent.
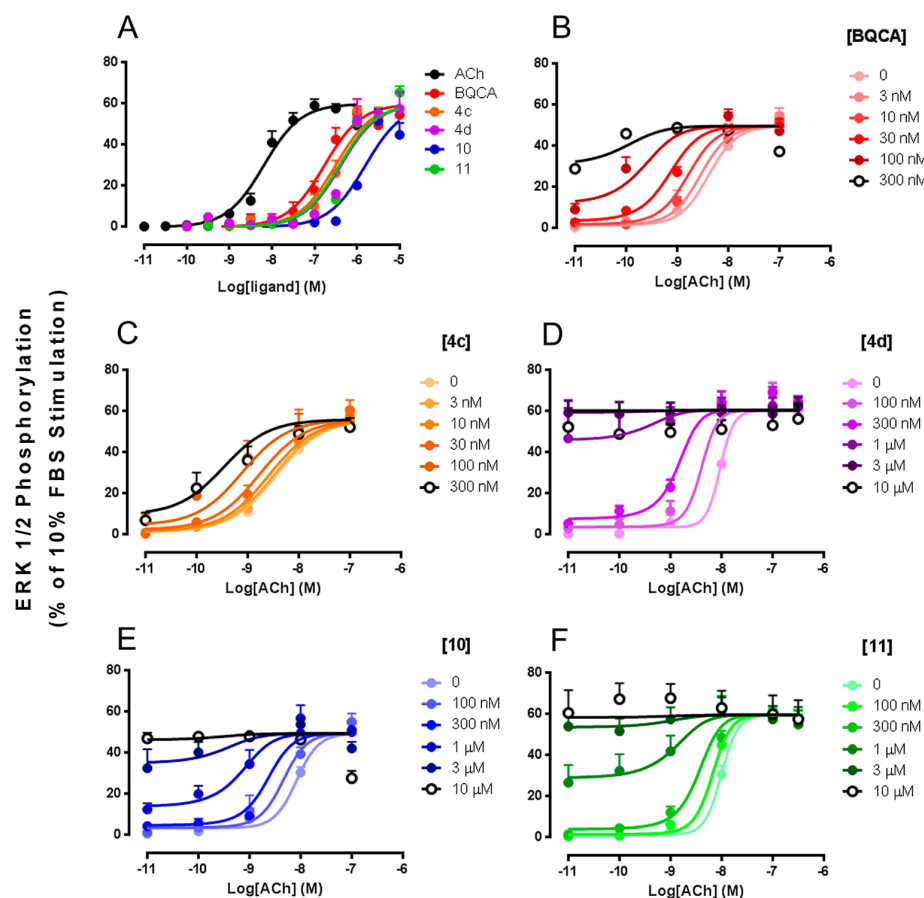
E

Figure 3. Pharmacological characterization of BQCA and the putative irreversible analogues in ERK1/2 phosphorylation assays. (A−F) ERK1/2 phosphorylation experiments performed in hM1 mAChR-expressing CHO cells. (A) Increasing concentrations of ACh, BQCA, **4c**, **4d**, **10**, and **11** alone. (B−F) Increasing concentrations of ACh with or without increasing concentrations of BQCA (B), **4c** (C), **4d** (D), **10** (E), or **11** (F). Values represent the mean $\pm$ SEM from at least three to four experiments performed in duplicate.

Table 2. B_{max} (% Vehicle) Values (Total Receptor Density) Following Different Pre-incubation Times of M_1 mAChR-Expressing Cells with Vehicle, ACh, or AChM

	5 min	10 min	15 min	20 min	30 min
vehicle	99.87	99.87	99.87	99.87	99.87
ACh	98.61	100.43	98.30	88.35	95.43
AChM	84.81	79.20	58.49	50.32	38.25

[³H]NMS saturation radioligand binding experiments with 30 min preincubation of ACh, AChM, BQCA ($\pm$ACh) and **11** ($\pm$ACh) were repeated in CHO cell membranes stably expressing the hM$_1$ mAChR to eliminate the possibility of observing receptor internalization and, hence, ascertain whether the reduction in B_{max} observed in the whole cell binding experiments was indeed the result of receptor alkylation. Encouragingly, we still observed no change in B_{max} following preincubation with BQCA but a significant reduction in B_{max} following preincubation with **11** ($\pm$ACh), conclusively confirming that **11** is binding irreversibly to the M_1 mAChR (Table 3, Figure 6).

■ CONCLUSIONS

Herein we report the development of an irreversible allosteric ligand for a GPCR, the M_1 mAChR. Four analogues of the

highly selective positive allosteric modulator BQCA were synthesized, incorporating different reactive functionalities capable of forming a covalent bond with the receptor: fluorosulfonyl (**4c**), maleimide (**4d**), bromoacetamide (**10**) and isothiocyanate (**11**). The pharmacological profile of BQCA was preserved, though to varying extents, in all four analogues; they were able to bind to (pK_B) and activate (τ_B) the M_1 mAChR and showed positive binding (α) and functional (β) cooperativity with the endogenous neurotransmitter and orthosteric agonist ACh in CHO cells stably expressing the receptor of interest.

Saturation radioligand binding experiments demonstrated that 30 min incubation of **11** with M_1 mAChR-expressing cell membranes resulted in a 50% reduction in the total detectable receptor density (B_{max}). This is indicative of irreversible noncompetitive blockade of previously available binding sites by high negative cooperativity between **11** and the radioligand [³H]NMS.

Taken together, we confirm that **11** is likely binding irreversibly to an allosteric site of the M_1 mAChR, suggesting the presence of a nucleophilic amino acid residue within this allosteric domain. This ligand may be employed in crystallo-graphic studies to gain further structural insight into the BQCA binding site. Alternatively, this ligand may also be used as a chemical probe in proteomics studies to identify the interacting
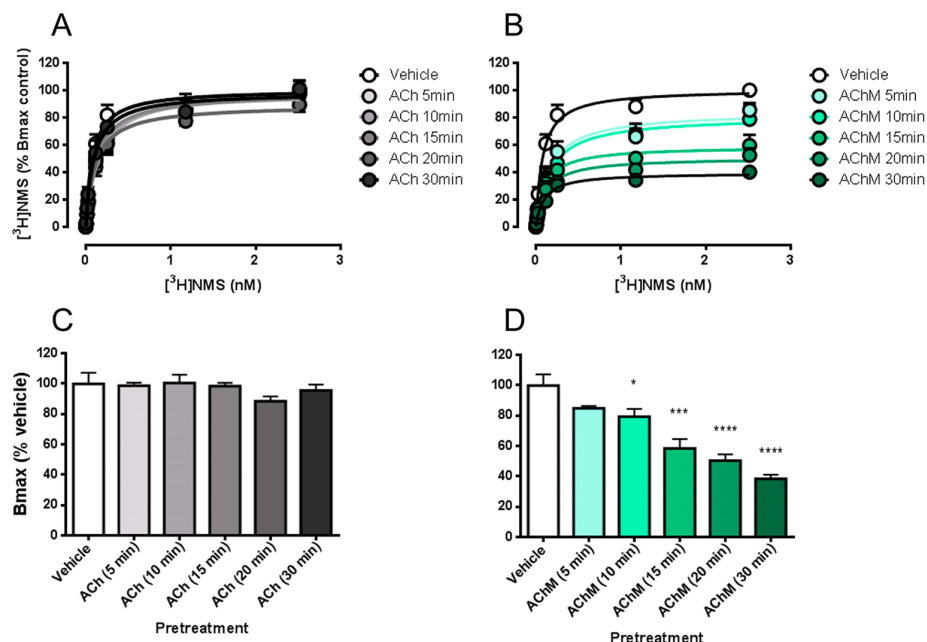
Figure 4. Pharmacological characterization of ACh and AChM in radioligand saturation whole cell binding assays. (A–D) Radioligand saturation binding experiments performed in hM_1 mAChR-expressing CHO cells in the presence of increasing concentrations of radiolabeled orthosteric antagonist [^{3}H]NMS. (A) Preincubation with vehicle or ACh for increasing lengths of time. (B). Preincubation with vehicle or AChM for increasing lengths of time. (C–D) B_{max} (% vehicle) bar graphs where values significantly different from Vehicle are indicated by an * (where * = p <0.05, ** = p <0.01, *** = p <0.001, and **** = p <0.0001). Values represent the mean ± SEM from three experiments performed in duplicate.

Table 3. B_{max} (% Vehicle) Values (Total Receptor Density) Following 30 min Pre-incubation of Either M_1 mAChR-Expressing Whole Cells or M_1 mAChR-Expressing Cell Membranes with Vehicle, BQCA (±ACh), or 11 (±ACh)

	vehicle	BQCA	BQCA + ACh	11	11 + ACh
whole cells	99.22	107.06	88.49	64.67	36.75
membranes	100.00	90.79	91.42	49.96	33.71

amino acid residue[29] which may subsequently inform molecular modeling of the binding site. This ligand may also serve as a template for the design of novel fluorescent irreversible allosteric ligands for the M_1 mAChR. Furthermore, **11** may aid classification of forthcoming orthosteric and allosteric ligands at the M_1 mAChR[30] and may prove useful in examining the effects of prolonged M_1 mAChR allosteric site occupation. Finally, we postulate that **11** may "lock" the M_1 mAChR in a distinct conformation, thereby allowing us to build a pharmacological fingerprint or "allosteric phenotype" using different classes of orthosteric ligand and different functional assay pathways, pursuing conformation-specific pharmacology.

■ EXPERIMENTAL SECTION

Chemistry. All materials were reagent grade and purchased commercially from Sigma-Aldrich or Matrix Scientific. Anhydrous solvents were obtained from a MBraun MB SPS-800 solvent purification system. Analytical thin layer chromatography (TLC) was performed on Silica Gel 60 F_{254} precoated plates (0.25 mm, Merck ART 5554) and visualized by ultraviolet light, iodine or ninhydrin as necessary. Silica gel 60 (Fluka) was used for silica gel flash chromatography.

Melting points (mp) were determined on a Mettler Toledo MP50 melting point system.

^{1}H NMR spectra were routinely recorded at 400 MHz using a Brüker Avancell Ultrashield Plus spectrometer equipped with a Silicon

Graphics workstation. Chemical shifts (δ_H) for all ^{1}H NMR spectra are reported in parts per million (ppm) using the center peak of the deuterated solvent chemical shift as the reference: $CDCl_3$ (7.26) and DMSO-d_6 (2.50).[40] Each resonance was assigned according to the following convention: chemical shift (δ) (multiplicity, coupling constant(s) in Hz, and number of protons). Coupling constants (J) are reported to the nearest 0.5 Hz. In reporting spectral data, the following abbreviations have been used: s, singlet; d, doublet; t, triplet; q, quartet; p, pentet; m, multiplet; app, apparent; as well as combinations of these where appropriate.

^{13}C NMR spectra were routinely recorded at 100 MHz using a Brüker Avance 400 Ultra Shield Plus spectrometer equipped with a Silicon Graphics workstation. Chemical shifts (δ_C) for all ^{13}C NMR spectra are reported in parts per million (ppm), using the center peak of the deuterated solvent chemical shift as the reference: $CDCl_3$ (77.16) and DMSO-d_6 (39.52).[40] Coupling to fluorine (^{19}F) is reported as $^1J_{CF}$, $^2J_{CF}$, $^3J_{CF}$, and $^4J_{CF}$ to the nearest Hz.[41]

HSQC, HMBC, and COSY spectra were obtained using the standard Brüker pulse sequence to assist with structural assignment of the compounds.

Low resolution mass spectrometry (LRMS) analyses were recorded in the specified ion mode using a Micromass Platform II single quadropole mass spectrometer in acetonitrile:water (1:1) at a cone voltage of 20 V. The principle ions (m/z) are reported. High resolution mass spectrometry (HRMS) analyses were recorded in the specified ion mode using a LCT Premier XE TOF mass spectrometer coupled to 2795 Alliance separations module at cone voltages of 45 V (ESI+) and 60 V (ESI−).

Analytical reverse-phase high performance liquid chromatography (HPLC) was performed on a Waters HPLC system using a Phenomenex Luna C8 (2) 100 Å column (150 mm × 4.6 mm, 5 μm) and a binary solvent system; solvent A, 0.1% TFA/H_2O; solvent B, 0.1% TFA/80% MeOH/H_2O. Isocratic elution was carried out using the following protocol (time, % solvent A, % solvent B): 0 min, 100, 0; 10 min, 20, 80; 11 min, 20, 80; 12 min, 100, 0; 20 min, 100, 0; at a flow rate of 1.0 mL/min monitored at 254 nm using a Waters 996 photodiode array detector.
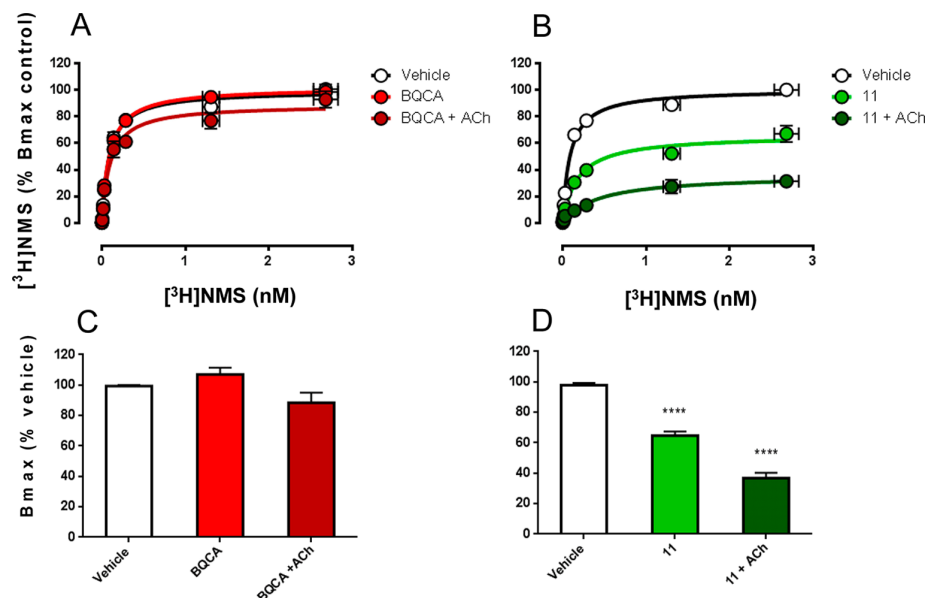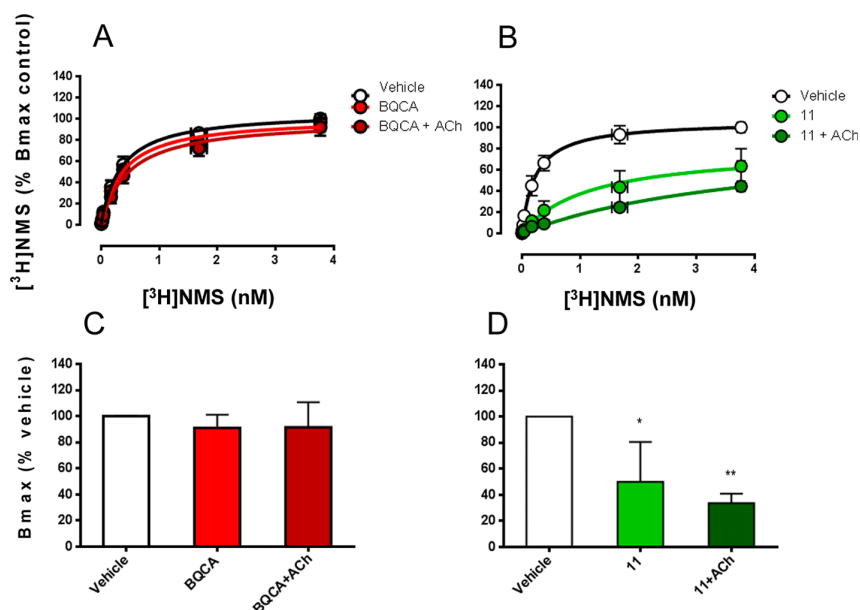
Figure 5. Pharmacological characterization of BQCA and **11** in radioligand saturation whole cell binding assays. (A−D) Radioligand saturation binding experiments performed in hM$_1$ mAChR-expressing CHO cells in the presence of increasing concentrations of radiolabeled orthosteric antagonist [^{3}H]NMS. (A) 30 min preincubation with vehicle, BQCA, or BQCA + ACh. (B) 30 min preincubation with vehicle, **11**, or **11** + ACh. (C−D) B_{max} (% vehicle) bar graphs where values significantly different from Vehicle are indicated by an * (where * = p <0.05, ** = p <0.01, *** = p <0.001 and **** = p <0.0001). Values represent the mean ± SEM from at least three to four experiments performed in duplicate.

Figure 6. Pharmacological characterization of BQCA and **11** in radioligand saturation membrane binding assays. (A−D) Radioligand saturation binding experiments performed in hM$_1$ mAChR-expressing CHO cell membranes in the presence of increasing concentrations of radiolabeled orthosteric antagonist [^{3}H]NMS. (A) 30 min preincubation with vehicle, BQCA, or BQCA + ACh. (B) 30 min preincubation with vehicle, **11**, or **11** + ACh. (C−D) B_{max} (% vehicle) bar graphs where values significantly different from vehicle are indicated by an * (where * = p <0.05, ** = p <0.01, *** = p <0.001, and **** = p <0.0001). Values represent the mean ± SEM from three experiments performed in duplicate.

Liquid chromatography−mass spectrometry (LCMS) was performed on an Agilent 1200 series coupled to the 6120 quadrupole mass spectrometer. Elution was also monitored at 254 nm.

Characterization requirements for intermediate compounds were set as mp, ^{1}H NMR, ^{13}C NMR, LRMS (or LCMS if unattainable), and HPLC (254 nm) or LCMS purity.

Characterization requirements for final compounds were set as mp, ^{1}H NMR, ^{13}C NMR, LRMS, HRMS, and HPLC (254 and 214 nm) purity >95%.

Diethyl 2-((Phenylamino)methylene)malonate (1). Aniline (9.80 mL, 107 mmol) and diethylethoxymethylene malonate (21.70 mL, 107 mmol) were syringed into an RBF and heated at 120 °C for 4 h. The reaction mixture was removed from the heat, 20 mL of cold petroleum

spirits added and the flask cooled on an ice bath for 30 min. The yellow crystals that formed were transferred to a conical flask and sonicated (in small batches) in cold petroleum spirits for 2−3 min. The target compound was obtained as pale yellow−white crystals following vacuum filtration and additional washes with petroleum spirits (23.5 g, 83%); mp 43−44 °C. δ_H (CDCl$_3$) 11.02 (br d, J = 13.5 Hz, 1H), 8.55 (d, J = 13.5 Hz, 1H), 7.39 (app t, J = 8.0 Hz, 2H), 7.21−7.12 (m, 3H), 4.33 (q, J = 7.0 Hz, 2H), 4.27 (q, J = 7.0 Hz, 2H), 1.40 (t, J = 7.0 Hz, 3H), 1.35 (t, J = 7.0 Hz, 3H); δ_C (CDCl$_3$) 169.2, 165.7, 151.9, 139.4, 129.8, 125.0, 117.2, 93.6, 60.4, 60.1, 14.4, 14.3. m/z LRMS (TOF ES$^+$) [MH]$^+$ 264.3. HPLC: t_R = 10.67 min, purity = 97.3%

Ethyl 4-Oxo-1,4-dihydroquinoline-3-carboxylate (2). Procedure 1 (diphenyl ether): Diphenyl ether (8 mL) was heated to 220 °C in a small beaker directly placed on the hot plate. Diethyl 2-((phenylamino)methylene)malonate (**1**) (1.00 g, 3.80 mmol) was added and the reaction mixture heated, uncovered, for 20 min. The beaker was removed from the heat and allowed to cool to RT, resulting in product formation and almost total solidification of the reaction mixture. The target compound was isolated as a gray−white powder by vacuum filtration and copious washing with cold petroleum spirits (395 mg, 48%). Procedure 2 (Eaton's reagent): Diethyl 2-((phenylamino)methylene)malonate (**1**) (23.5 g, 89.1 mmol) and Eaton's reagent (1:10 w/w phosphorus pentoxide solution in methanesulfonic acid, 80 mL) were stirred at 100 °C for 3.5 h. The reaction mixture was cooled to RT before being slowly pouring into saturated sodium bicarbonate. The precipitated product was collected as an orange−yellow powder by vacuum filtration and washed copiously with cold petroleum spirits (19.0 g, quantitative); mp 271−273 °C. δ_H (DMSO-d_6) 8.63 (s, 1H), 8.25 (dd, J = 8.0, 1.5 Hz, 1H), 7.79 (ddd, J = 8.5, 7.0, 1.5 Hz, 1H), 7.71 (dd, J = 8.5, 1.0 Hz, 1H), 7.50 (ddd, J = 8.0, 7.0, 1.0 Hz, 1H), 4.31 (q, J = 7.0 Hz, 2H), 1.37 (t, J = 7.0 Hz, 3H). δ_C (DMSO-d_6) 173.4, 164.9, 144.8, 139.0, 132.3, 127.3, 125.6, 124.6, 118.7, 110.0, 59.5, 14.4. m/z LRMS (TOF ES$^+$) [MH]$^+$ 218.2. HPLC: t_R = 6.61 min, purity = 98.8%

4-Oxo-1,4-dihydro-quinoline-3-carboxylic Acid (3). Ethyl 4-oxo-1,4-dihydroquinoline-3-carboxylate (**2**) (500 mg, 2.30 mmol) and THF (10 mL) were brought to 0 °C in an ice bath. A solution of aqueous 1 M LiOH$_{(aq)}$ (4.60 mL, 4.60 mmol) was added dropwise while stirring, and then the reaction mixture was heated at 80 °C for 24 h. Following addition of excess aqueous 1 M HCl$_{(aq)}$, the target molecule precipitated out and was isolated as an off-white powder by vacuum filtration, washed with distilled water to remove the residual acid, and then dried under vacuum overnight (327 mg, 75%); mp 273−275 °C. δ_H (DMSO-d_6) 15.48 (br s, 1H), 8.88 (s, 1H), 8.29 (dd, J = 8.0, 1.5 Hz, 1H), 7.89 (ddd, J = 8.5, 7.0, 1.5 Hz, 1H), 7.82 (dd, J = 8.0, 1.5 Hz, 1H), 7.60 (ddd, J = 8.0, 7.0, 1.5 Hz, 1H). δ_C (DMSO-d_6) 178.3, 166.5, 145.1, 139.4, 133.9, 126.3, 125.0, 124.4, 119.6, 107.7. m/z LRMS (TOF ES$^+$) [MH]$^+$ 190.2. HPLC: t_R = 6.44 min, purity = >99.0%

General Procedure for N-B of Either Ethyl 4-Oxo-1,4-dihydroquinoline-3-carboxylate (2) or 4-Oxo-1,4-dihydro-quinoline-3-carboxylic Acid (3). The ethyl carboxylate (**2**) or carboxylic acid (**3**) (30−500 mg) and acetonitrile (7−15 mL) were placed in an RBF and cooled to 0 °C in an ice bath. The appropriately substituted benzyl halide (2 equiv) and *N,N*-diisopropylethylamine (DIPEA) (4 equiv) were added and the reaction stirred at 80 °C for between 2 and 22 h. Note: 1.1 equiv of potassium iodide was added at the beginning of the reaction if a substituted benzyl chloride was being used. If the product was observed to precipitate from the reaction mixture, the resulting solid was isolated by vacuum filtration and washed with diethyl ether or hot ethanol. If no precipitate was observed, the reaction mixture was partitioned between chloroform (10 mL) and 1 M HCl$_{(aq)}$ (10 mL) and the aqueous layer extracted with chloroform (3 × 10 mL). The combined organic fractions were dried over anhydrous MgSO$_4$, filtered, and the solvent evaporated in vacuo to yield solid product.

1-(4-Methoxybenzyl)-4-oxo-1,4-dihydroquinoline-3-carboxylic Acid (4b). Fine white crystals; 3 h; 790 mg, 97%; mp 250−251 °C. δ_H (DMSO-d_6) 15.17 (s, 1H), 9.26 (s, 1H), 8.39 (dd, J = 8.0, 1.5 Hz, 1H), 7.96 (d, J = 8.5 Hz, 1H), 7.88 (ddd, J = 8.5, 7.0, 1.5 Hz, 1H), 7.63 (ddd, J = 8.0, 7.0, 1.0 Hz, 1H), 7.28 (d, J = 9.0 Hz, 2H), 6.92 (d, J = 9.0 Hz, 2H), 5.80 (s, 2H), 3.78 (s, 3H, CH$_3$). δ_C (DMSO-d_6) 177.9, 166.0, 159.0, 149.8, 139.4, 134.1, 128.4, 127.0, 126.3, 125.9, 125.7, 118.7, 114.3, 107.8, 55.9, 55.1. m/z LRMS (TOF ES$^+$) [MH]$^+$ 310.4. m/z HRMS (TOF ES$^+$) C$_{18}$H$_{16}$NO$_4$ [MH]$^+$ calcd 310.1074; found 310.1086. HPLC: t_R = 9.13 min, purity (254 nm) = 98.3%, purity (214 nm) = 99.0%

1-(4-(Fluorosulfonyl)benzyl)-4-oxo-1,4-dihydroquinoline-3-carboxylic Acid (4c). Clear glassy crystals; 22 h; 12.1 mg, 21%; mp 289−290 °C. δ_H (DMSO-d_6) 15.12 (br s, 1H), 9.35 (s, 1H), 8.42 (dd, J = 8.0, 1.5 Hz, 1H), 8.12 (dd, J = 8.0, 6.5 Hz, 2H), 7.86 (ddd, J = 8.5, 7.0, 1.5 Hz, 1H), 7.75 (d, J = 8.5 Hz, 1H), 7.68−7.59 (m, 3H), 6.08 (s, 2H). δ_C (DMSO-d_6) 178.1, 165.9, 150.7, 144.8, 139.3, 134.4, 130.8, 129.0, 128.2, 126.5, 126.1, 125.7, 118.3, 108.2, 55.8. m/z LRMS (TOF ES$^+$) [MH]$^+$ 362.3. m/z HRMS (TOF ES$^+$) C$_{17}$H$_{13}$FNO$_5$S [MH]$^+$ calcd 362.0493; found 362.0485. HPLC: t_R = 9.56 min, purity (254) = 98.8%, purity (214) = 98.9%

1-(4-(2,5-Dioxo-2,5-dihydro-1H-pyrrol-1-yl)benzyl)-4-oxo-1,4-dihydroquinoline-3-carboxylic Acid (4d). Pale purple-tinged white solid; 2 h; 42 mg, 53%; mp 292−293 °C. δ_H (DMSO-d_6) 15.18 (br s, 1H), 9.35 (s, 1H), 8.42 (d, J = 7.5 Hz, 1H), 7.95−7.84 (m, 2H), 7.64 (ddd, J = 8.0, 5.5, 2.5 Hz, 1H), 7.40 (d, J = 8.5 Hz, 2H), 7.32 (d, J = 8.5 Hz, 2H), 7.17 (s, 2H), 5.94 (s, 2H). δ_C (DMSO-d_6) 178.0, 169.8, 166.0, 150.4, 139.4, 134.9, 134.7, 134.3, 131.2, 127.14, 127.07, 126.4, 126.0, 125.7, 118.6, 108.0, 56.0. m/z LCMS [MH]$^+$ 375.0. m/z HRMS (TOF ES$^+$) C$_{21}$H$_{15}$N$_2$O$_5$ [MH]$^+$ calcd 375.0981, found 375.0966. HPLC: t_R = 8.32 min, purity (254) = 97.8%, purity (214) = 97.9%

Ethyl 1-(4-Nitrobenzyl)-4-oxo-1,4-dihydroquinoline-3-carboxylate (7). White crystals; 22 h; 253 mg, 78%; mp 282−283 °C. δ_H (DMSO-d_6) 8.98 (s, 1H), 8.27 (dd, J = 8.0, 1.5 Hz, 1H), 8.22 (d, J = 9.0 Hz, 2H), 7.67 (ddd, J = 8.5, 7.0, 1.5 Hz, 1H), 7.59−7.39 (m, 4H), 5.86 (s, 2H), 4.26 (q, J = 7.0 Hz, 2H), 1.31 (t, J = 7.0 Hz, 3H). δ_C (DMSO-d_6) 172.9, 164.6, 150.3, 147.0, 143.9, 138.9, 132.7, 128.4, 127.6, 126.5, 125.0, 124.0, 117.5, 110.6, 59.8, 54.9, 14.3. m/z LRMS (TOF ES$^+$) [MH]$^+$ 353.4. HPLC: t_R = 9.19 min, purity = 99.1%

General Procedure for Radical Bromination of Either p-Toluenesulfonyl Fluoride or 1-(p-Tolyl)-1H-pyrrole-2,5-dione. *p*-Toluenesulfonyl fluoride or 1-(*p*-tolyl)-1H-pyrrole-2,5-dione (50−250 mg), *N*-bromosuccinimide (NBS) (1.1−1.8 equiv), and benzoyl peroxide (0.05 equiv) were placed in a microwave vial with ethyl acetate (4 mL), and the reaction mixture was stirred briefly to dissolve. The vessel was sealed and reacted in the microwave for 30 min at 100 °C. The reaction mixture was filtered to remove any precipitated NBS, then the solvent evaporated in vacuo. The target molecule was isolated by column chromatography (stationary phase, silica; mobile phase,\ 5:2 hexane:DCM or 2:1 chloroform:hexane). Percentage purity was observed to be low due to difficulty in separating the desired monobrominated product from the dibrominated side product.

p-Sulfonylfluorobenzyl Bromide (5). White crystalline powder; 293 mg, 81%; mp 65−66 °C. δ_H (DMSO-d_6) 7.92 (d, J = 8.5 Hz, 2H), 7.58 (d, J = 8.0 Hz, 2H), 4.44 (s, 2H). δ_C (DMSO-d_6) 145.9, 130.2, 129.0, 128.2 ($^2J_{CF}$ = 48 Hz), 30.7. m/z LRMS (TOF ES$^-$) [MBr]$^-$: 331.2. LCMS: t_R = 6.04 min, purity = 87.4%.

1-(p-Tolyl)-1H-pyrrole-2,5-dione (6a). Step A: *p*-Toluidine (1.00 g, 9.33 mmol) was dissolved in DMF (15 mL) and maleic anhydride added (1.1 g, 10.27 mmol). The reaction mixture was stirred at 110 °C for 5 h, after which time the solvent evaporated in vacuo to yield the intermediate (*Z*)-4-oxo-4-(*p*-tolylamino)but-2-enoic acid as a yellow solid (1.92 g, 100%); mp 180−181 °C. δ_H (DMSO-d_6) 10.37 (br s, 1H), 7.96 (s, 1H), 7.52 (d, J = 8.5 Hz, 2H), 7.14 (d, J = 8.0 Hz, 2H), 6.47 (d, J = 12.0 Hz, 1H), 6.30 (d, J = 12.0 Hz, 1H), 2.27 (s, 3H). δ_C (DMSO-d_6) 166.7, 163.0, 135.9, 133.0, 131.6, 130.7, 129.2, 119.6, 20.5. m/z LCMS [M − H]$^-$ 204.1. HPLC: t_R = 7.45 min, purity = 97.3%. Step B: (*Z*)-4-Oxo-4-(*p*-tolylamino)but-2-enoic acid (2 g, 9.75 mmol) and sodium acetate (400 mg, 4.87 mmol) were refluxed in 10 mL of acetic anhydride at 120 °C for 2.5 h. The reaction mixture was then cooled to RT and the solvent evaporated in vacuo. Addition of methanol (30 mL) resulted in precipitation of the target compound as yellow needle-like crystals that were collected by vacuum filtration. The crude filtrate was concentrated and purified by column

chromatography (stationary phase, silica; mobile phase, 3:1 chloroform:hexane) to isolate additional product (925 mg, 51%); mp 151–153 °C. δ_H (DMSO-d_6) 7.29 (d, J = 8.0 Hz, 2H), 7.20 (d, 2H, J = 8.5 Hz), 7.17 (s, 2H), 2.35 (s, 3H). δ_C (DMSO-d_6) 170.0, 137.2, 134.6, 129.3, 128.9, 126.7, 20.7. m/z LCMS [MH]$^+$ 188.1. HPLC: t_R = 7.36 min, purity = 96.5%

1-(4-(Bromomethyl)phenyl)-1H-pyrrole-2,5-dione (6b). Yellow solid; 32 mg, 45%; mp 113–114 °C. δ_H (CDCl$_3$) 7.43 (d, J = 8.5 Hz, 2H), 7.28 (d, 2H, J = 8.5 Hz), 6.79 (s, 2H), 4.44 (s, 2H); δ_C (CDCl$_3$) 169.3, 137.4, 134.3, 131.2, 129.9, 126.1, 32.5. m/z LCMS [MH]$^+$ 267.9. HPLC: t_R = 8.52 min, purity = 81.9%.

Ethyl 1-(4-Aminobenzyl)-4-oxo-1,4-dihydroquinoline-3-carboxylate (8). Ethyl 1-(4-nitrobenzyl)-4-oxo-1,4-dihydroquinoline-3-carboxylate (7) (700 mg, 2 mmol) was dissolved in dimethylformamide (DMF) (25 mL). Then 10% Pd/C (20 mg) was added under a nitrogen atmosphere, following evacuation of nitrogen, the reaction mixture was stirred at RT for 5 h under a hydrogen atmosphere. The reaction mixture was then filtered through Celite, washed with methanol, and the solvents evaporated in vacuo to yield a yellow solid that required no further purification (594 mg, 93%); mp 186–187 °C. δ_H (DMSO-d_6) 8.88 (s, 1H), 8.29 (dd, J = 8.0, 1.0 Hz, 1H), 7.80 (d, J = 8.5 Hz, 1H), 7.78–7.70 (m, 1H), 7.49 (app t, J = 7.0 Hz, 1H), 7.03 (d, J = 8.5 Hz, 2H), 6.58 (d, J = 8.5 Hz, 2H), 5.49 (s, 2H), 5.19 (s, 2H), 4.29 (q, J = 7.0 Hz, 2H), 1.34 (t, J = 7.0 Hz, 3H). δ_C (DMSO-d_6) 172.9, 164.7, 149.5, 148.5, 139.0, 132.4, 128.4, 127.9, 126.3, 124.8, 121.90, 117.9, 113.9, 109.8, 59.7, 55.6, 14.3. m/z LRMS (TOF ES$^+$) [M + H]$^+$ 323.5. HPLC: t_R = 6.01 min, purity = 95.1%

1-(4-Aminobenzyl)-4-oxo-1,4-dihydroquinoline-3-carboxylic Acid (9). Ethyl 1-(4-aminobenzyl)-4-oxo-1,4-dihydroquinoline-3-carboxylate (8) (700 mg, 2.17 mmol) was stirred in 3:1 methanol:distilled H$_2$O (12 mL). A solution of aqueous 1 M KOH$_{(aq)}$ (6.51 mL, 6.51 mmol) was added and the reaction stirred for at 80 °C for 6.5 h, at which point the reaction was allowed to cool to room temperature. Following addition of 1 M HCl$_{(aq)}$ (7.60 mL, 7.60 mmol), the target molecule precipitated out and was isolated as a yellow powder by vacuum filtration and dried under vacuum overnight. (524 mg, 82%); mp 215–216 °C. δ_H (DMSO-d_6) 15.24 (br s, 1H), 9.16 (s, 1H), 8.39 (dd, J = 8.0, 1.5 Hz, 1H), 8.02 (d, J = 8.5 Hz, 1H), 7.90 (ddd, J = 8.5, 7.0, 1.5 Hz, 1H), 7.64 (app t, J = 7.5 Hz, 1H), 7.02 (d, J = 8.5 Hz, 2H), 6.52 (d, J = 8.5 Hz, 2H), 5.63 (s, 2H), 5.19 (s, 2H). δ_C (DMSO-d_6) 178.0, 166.0, 150.2, 139.4, 134.2, 133.8, 133.5, 128.0, 126.4, 125.9, 125.7, 122.7, 118.6, 107.9, 55.9. m/z LRMS (TOF ES$^+$) [M + H]$^+$ 295.4. LCMS: t_R = 4.55 min, purity = >99.0%

1-(4-(2-Bromoacetamido)benzyl)-4-oxo-1,4-dihydroquinoline-3-carboxylic Acid (10). 1-(4-Aminobenzyl)-4-oxo-1,4-dihydroquinoline-3-carboxylic acid (9) (200 mg, 680 μmol) was stirred in acetonitrile (8 mL) in a dry ice/acetone bath. TEA (231.7 μL, 1.70 mmol) and bromoacetyl bromide (65.6 μL, 748 μmol) were added dropwise and the reaction mixture allowed to slowly return to RT as the dry ice evaporated. After 20 h stirring at RT, the precipitated target molecule was isolated by vacuum filtration as a beige powder and washed with 0.1 M HCl$_{(aq)}$ to remove the residual base, followed by distilled water to remove the residual acid, then dried under vacuum overnight (208 mg, 74%); mp 239–240 °C. δ_H (DMSO-d_6) 15.23 (br s, 1H), 10.48 (s, 1H), 9.32 (s, 1H), 8.44 (d, J = 8.0 Hz, 1H), 7.96–7.88 (m, 2H), 7.67 (ddd, J = 8.0, 5.0, 3.0 Hz, 1H), 7.61 (d, J = 8.5 Hz, 2H), 7.33 (d, J = 8.5 Hz, 2H), 5.88 (s, 2H), 4.07 (s, 2H). δ_C (DMSO-d_6) 178.0, 171.0, 165.4, 150.1, 138.9, 134.1, 130.5, 130.0, 127.3, 126.4, 125.9, 125.7, 119.8, 118.7, 107.8, 61.8, 56.1. m/z LRMS (TOF ES$^+$) [M − Br]$^+$ 335.4. m/z HRMS (TOF ES$^-$) C$_{19}$H$_{14}$BrN$_2$O$_4$ [M − H]$^-$ calcd 413.0142, found 413.0141. HPLC: t_R = 8.60 min, purity (254) = 99.1%, purity (214) = 97.9%

1-(4-Isothiocyanatobenzyl)-4-oxo-1,4-dihydroquinoline-3-carboxylic Acid (11). 1-(4-Aminobenzyl)-4-oxo-1,4-dihydroquinoline-3-carboxylic acid (9) (50 mg, 170 μmol) was stirred in dry DCM (4 mL) under a N$_2$ atmosphere. 1,1′-Thiocarbonyl diimidazole (41.5 mg, 233 μL) and DMAP (1.89 mg, 15.5 μmol) were added and the reaction mixture stirred at RT for 5 h. The reaction mixture was partitioned between chloroform (20 mL) and 1 M HCl$_{(aq)}$ (20 mL) and the aqueous layer extracted with chloroform (3 × 20 mL). The combined

organic fractions were dried over anhydrous MgSO$_4$, filtered, and the solvent evaporated in vacuo to yield the target molecule as a fine pearly white powder (54.7 mg, 96%); mp 237–238 °C. δ_H (DMSO-d_6) 15.14 (s, 1H), 9.30 (s, 1H), 8.41 (dd, J = 8.0, 1.5 Hz, 1H), 7.87 (ddd, J = 8.5, 7.0, 1.5 Hz, 1H), 7.81 (d, J = 8.5 Hz, 1H), 7.64 (ddd, J = 8.0, 7.0, 1.0 Hz, 1H), 7.42 (d, J = 8.5 Hz, 2H), 7.36 (d, J = 8.5 Hz, 2H), 5.90 (s, 2H). δ_C (DMSO-d_6) 178.0, 165.9, 150.4, 139.3, 135.3, 134.2, 133.7, 129.6, 128.1, 126.45, 126.41, 126.0, 125.7, 118.5, 108.0, 55.8. m/z LCMS [MH]$^+$ 337.1. m/z HRMS (TOF ES$^+$) C$_{18}$H$_{12}$N$_2$O$_3$ [M + H]$^+$ calcd 337.0569, found 337.0639. HPLC: t_R = 10.76 min, purity (254) = 97.7%, purity (214) = 97.4%

Crystallography. Intensity data were collected with an Oxford Diffraction SuperNova CCD diffractometer using Cu Kα radiation, and the temperature during data collection was maintained at 100.0(1) using an Oxford Cryosystems cooling device. The structure of compound **4a** was solved by direct methods and difference Fourier synthesis.[42] Thermal ellipsoid plots were generated using the program ORTEP-3[43] integrated within the WINGX[44] suite of programs.

Crystal Data for 4a. C$_{17}$H$_{13}$NO$_3$, M = 279.28, T = 100.0 K, λ = 1.54180, orthorhombic, space group $Pna2_1$, a = 16.2869(6) b = 15.6800(6), c = 5.0797(2) Å, V 1297.25(9) Å^3, Z = 4, D_c = 1.430 mg M^{-3} μ(Cu Kα) 0.808 mm^{-1}, $F(000)$ = 584, crystal size 0.67 × 0.04 × 0.02 mm^3, 3118 reflections measured, 1714 independent reflections [R(int) = 0.0367]; the final R was 0.0578, [$I > 2\sigma(I)$] and $wR(F^2)$ was 0.1601 (all data).

Pharmacology. *Radioligand Competition Whole Cell Binding Assays.* Plate preparation: FlpIn-CHO cells stably expressing human muscarinic M$_1$ receptors (hM$_1$ mAChR FlpIn-CHO) were cultured at 37 °C in 5% CO$_2$ in Dulbecco's Modified Eagle Medium (DMEM) supplemented with 5% (v/v) fetal bovine serum (FBS) and 16 mM HEPES. Cells were seeded into white opaque Isoplates at 8.0 × 10^3 cells per well and then grown at 37 °C for 20–24 h. Cells were then washed twice with cold HEPES-buffered saline, 140 μL per well, cold HEPES-buffered saline was added, and the plates kept on ice. Assay protocol: A stock solution of ACh (10^{-2} M) was made up in cold HEPES-buffered saline. Stock solutions of the interacting allosteric ligands of choice (10^{-2} M) were made up in DMSO. Dilutions of all ligands were made up in cold HEPES-buffered saline at 10× the required concentration and added to stock plates on ice. Cells were equilibrated at 4 °C for 4 h with 20 μL of ACh, 20 μL of a single interacting allosteric ligand, and 20 μL of 0.1 nM [^{3}H]NMS (total volume 200 μL per well). Assay termination and data collection: Assays were terminated by media removal, 2 × 200 μL per well washes with 0.9% NaCl solution and addition of 100 μL per well Microscint-20 scintillation liquid. The levels of remaining bound radioligand, and therefore the degree of radioligand displacement, was measured in disintegrations per minute (dpm) on the Microbeta2 LumiJET 2460 microplate counter (PerkinElmer).

AlphaScreen ERK1/2 Phosphorylation Assays. Plate preparation: FlpIn-CHO cells stably expressing human muscarinic M$_1$ receptors (hM$_1$ mAChR FlpIn-CHO) were cultured at 37 °C in 5% CO$_2$ in DMEM supplemented with 5% (v/v) FBS and 16 mM HEPES. Cells were seeded into transparent 96-well plates at 5 × 10^4 cells per well and grown for 6 h. Cells were then washed once with phosphate-buffered saline (PBS) and incubated in serum-free DMEM (180 μL per well) at 37 °C overnight (16–18 h) to allow FBS-stimulated phosphorylated ERK1/2 levels to subside. Time course assays: A stock solution of ACh (10^{-2} M) was made up in Milli-Q water. Stock solutions of the test ligands (10^{-2} M) were made up in DMSO. All ligands were diluted to 10^{-5} M in serum-free DMEM. Ligand additions (20 μL) were made at predetermined time points over a 30 min period (30, 25, 20, 15, 10, 8, 6, 5, 3, and 1 min) with the cells being incubated at 37 °C following each addition. FBS, which triggers ERK1/2 phosphorylation via a tyrosine kinase receptor, was added at 6 min as a measure of the maximal levels of pERK1/2 production. Concentration–response curves (CRCs): A stock solution of ACh (10^{-2} M) was made up in Milli-Q water. Stock solutions of the test ligands (10^{-2} M) were made up in DMSO. Dilutions of all ligands were made up in FBS-free media at 10× the required concentration and added to stock plates. Cells were incubated at 37 °C with 20 μL per well of each

concentration of all compounds at 5 min (as determined by time course assays). Interaction studies: A stock solution of ACh (10^{-2} M) was made up in Milli-Q water. Stock solutions of the allosteric test ligands and atropine (10^{-2} M) were made up in DMSO. In the case of the allosteric ligand interactions, dilutions of ACh and the interacting ligand were made up in FBS-free media at 20× the ideal concentration range (as determined by CRC assays). Equal volumes of each concentration of ACh and each concentration of the interacting ligand of choice were premixed in stock plates. Cells were incubated at 37 °C with 20 μL per well of each ligand mixture at 5 min (as determined by time course assays). In the case of atropine, dilutions of ACh and atropine were made up in FBS-free media at 10× the ideal concentration range as determined by laboratory colleagues. Atropine was equilibrated with the receptor at 30 min before the addition of ACh at 5 min. Assay termination and data collection: Agonist-stimulated ERK1/2 phosphorylation was terminated by the removal of drugs and the addition of 100 μL p/well of SureFire lysis buffer. The cell lysates were agitated for 5−10 min. Following agitation, 5 μL of cell lysates were transferred into a 384-well white opaque Optiplate, followed by addition of 8.5 μL of a solution of reaction buffer/activation buffer/acceptor beads/donor beads in a ratio of 6/1/0.3/0.3 (v/v/v/v) under green light conditions. The plates were then incubated at 37 °C in the dark for 1 h, and fluorescence was measured on a Fusion-α plate reader (PerkinElmer) using standard AlphaScreen settings.

Radioligand Saturation Whole Cell Binding Assays. Plate preparation: FlpIn-CHO cells stably expressing human muscarinic M_1 receptors (hM_1 mAChR FlpIn-CHO) were cultured at 37 °C in 5% CO_2 in DMEM supplemented with 5% (v/v) FBS and 16 mM HEPES. Cells were seeded into white opaque Isoplates at 7.0×10^3 cells per well and then grown at 37 °C for 6 h. Cells were then washed once with PBS and incubated in serum-free DMEM (160 μL per well) at 37 °C overnight (16−18 h). Preincubation with controls and test ligands: A stock solution of ACh (10^{-2} M) was made up in Milli-Q water. A stock solution of AChM was made up in ethanol. Stock solutions of other test ligands (10^{-2} M) were made up in DMSO. All ligands were diluted to 10^{-3} M in HEPES-buffered saline, except AChM, which was diluted to 10^{-3} M in 50 mM phosphate buffer and incubated at 37 °C for 20 min to form the reactive aziridinium ion and then stored on ice and used as quickly as possible. Buffer controls (10% DMSO/HEPES-buffered saline and 10% ethanol/50 mM phosphate buffer) were also made up. Ligand additions (20 and 20 μL buffer for single ligand additions), for a final volume of 200 μL, were made at 30 min (or at 5, 10, 15, or 20 min during experimental optimization) and the cells incubated at 37 °C, during which time any irreversible binding of the test ligands would be expected to take place. Cells were then washed twice with cold PBS and 160 μL per well of cold HEPES-buffered saline was added and the plates kept on ice. Assay protocol: Stock solutions of [^{3}H]NMS ($10^{-7.5}$ and 10^{-8} M) were made up in HEPES-buffered saline. Dilutions of [^{3}H]NMS were made up in HEPES-buffered saline at 10× the required concentration and added to a stock plate. A stock solution of atropine (10^{-4} M) was made up at 10× the required concentration. Cells were equilibrated at 4 °C for 4 h with 20 μL of HEPES-buffered saline (specific wells) or 20 μL of atropine (nonspecific wells) and 20 μL per well of each concentration of [^{3}H]NMS (total volume 200 μL per well). Assay termination and data collection: Assays were terminated by media removal, 2 × 200 μL per well washes with 0.9% NaCl solution, and addition of 100 μL per well of Microscint-20 scintillation liquid. The levels of remaining bound radioligand, and therefore the degree of radioligand displacement was measured in disintegrations per minute (dpm) on the Microbeta2 LumiJET 2460 microplate counter (PerkinElmer).

Radioligand Saturation Membrane Binding Assays. Membrane preparation: Prepreprared FlpIn-CHO cell membranes stably expressing human muscarinic M_1 receptors (hM_1 mAChR FlpIn-CHO) were thawed, diluted to a concentration of 1250 μg/mL, and resuspended using the hand-held homogenizer (at slow speed to minimize frothing). Ultracentrifuge tubes (one per buffer/ligand treatment) were labeled, 500 μg of membrane pipetted into each, the volume

made up to 8 mL with cold HEPES-buffered saline, and the tubes kept on ice. Preincubation with controls and test ligands: A stock solution of ACh (10^{-2} M) was made up in Milli-Q water. A stock solution of AChM was made up in ethanol. Stock solutions of other test ligands (10^{-2} M) were made up in DMSO. All ligands were diluted to 10^{-3} M in HEPES-buffered saline, except AChM which was diluted to 10^{-3} M in 50 mM phosphate buffer and incubated at 37 °C for 20 min to form the reactive aziridinium ion and then stored on ice and used as quickly as possible. Buffer controls (10% DMSO/HEPES-buffered saline and 10% ethanol/50 mM phosphate buffer) were also made up. Then 1 mL ligand additions (and 1 mL buffer for single ligand additions), for a final volume of 10 mL, were made at 30 min and the membrane tubes incubated in a water bath at 37 °C, during which time any irreversible binding of the test ligands would be expected to take place. Then 10 mL of ice-cold HEPES-buffered saline was added, and then additional ice cold buffer was added to bring all tubes to equal mass. Tubes were centrifuged on the Sorval Ultracentrifuge at 4 °C for 20 min at 40000 rpm. The supernatant was discarded, the membranes were resuspended thoroughly in 1 mL of ice-cold HEPES-buffered saline, and an additional 19 mL of ice-cold buffer added, and the tubes brought to equal mass again. Tubes were centrifuged again on the Sorval ultracentrifuge at 4 °C for 20 min at 40000 rpm. Two centrifugation steps were used in place of the PBS washes in the whole cell binding experiment described previously. The supernatant was discarded and the membranes resuspended in 400 μL of cold HEPES-buffered saline. A Bradford assay was performed to ascertain the concentration of membrane in each treatment tube, and then the required amount of cold HEPES-buffered saline was added to bring the concentration of each to 30 μg/mL. Assay protocol: Stock solutions of [^{3}H]NMS ($10^{-7.5}$ and 10^{-8} M) were made up in HEPES-buffered saline. Dilutions of [^{3}H]NMS were made up in HEPES-buffered saline at 10× the required concentration. A stock solution of atropine (10^{-4} M) was made up at 10× the required concentration. Membranes (100 μL per tube) were equilibrated at 37 °C for 1 h with 100 μL of HEPES-buffered saline (specific wells) or 100 μL of atropine (nonspecific wells) and 100 μL per well of each concentration of [^{3}H]NMS (in the required amount of HEPES-buffered saline to make a total volume of 1 mL per tube). Assay termination and data collection: Assays were terminated by harvesting the tubes in the Brandel harvester and rinsing tubes twice with 2 mL of ice-cold 0.9% NaCl solution. Membranes were dried under the heat lamp, picked, and placed into 6 mL scintillation tubes. Then 4 mL per tube of Ultima Gold scintillation liquid was added and the tubes capped, vortexed, and left on the bench for 1 h at RT. The levels of bound radioligand, and therefore the degree of radioligand blockade by any irreversibly bound test ligands, was measured in disintegrations per minute (dpm) on the TriCarb 2910 TR liquid scintillation analyzer (PerkinElmer).

Data Analysis. All data analysis was managed using Prism 6 software (GraphPad Software, San Diego, CA). Experiments measuring radioligand competition binding interactions were fitted to the allosteric ternary complex model 1:

$$Y = \frac{[A]}{[A] + \left(\frac{K_A K_B}{\alpha'[B] + K_B}\right)\left(1 + \frac{[I]}{K_I} + \frac{[B]}{K_B} + \frac{\alpha[I][B]}{K_I K_B}\right)} \quad (1)$$

where Y is the percentage (vehicle control) binding, [A], [B], and [I] are the concentrations of [^{3}H]NMS, the allosteric ligand, and ACh, respectively, K_A and K_B are the equilibrium dissociation constants of [^{3}H]NMS and the allosteric ligand, respectively, K_I is the equilibrium dissociation constant of ACh, and α and α' are the cooperativities between the allosteric ligand and [^{3}H]NMS or ACh, respectively. Values of α (or α') > 1 denote positive cooperativity, values <1 (but >0) denote negative cooperativity, and values = 1 denote neutral cooperativity. Functional orthosteric and allosteric agonist concentration−response curves were fitted via nonlinear regression to the three-parameter logistic function 2:

$$E = \text{basal} + \frac{(E_{\max} - \text{basal})}{1 + 10^{-pEC_{50} - \log[A])}} \tag{2}$$

where E is response, $E_{\max}$ and basal are the top and bottom asymptotes of the curve, respectively, log $[A]$ is the logarithm of the agonist concentration, and pEC_{50} is the negative logarithm of the agonist

concentration that gives a response halfway between $E_{\max}$ and basal. Functional experiments measuring the interactions between ACh and each allosteric ligand were fitted to the operational model of allosterism and agonism $3^{45,46}$ to derive functional estimates of modulator affinity, cooperativity, and efficacy.

$$E = \frac{E_m (\tau_A[A](K_B + \alpha\beta[B]) + \tau_B[B]K_A)^n}{([A]K_B + K_AK_B + [B]K_A + \alpha[A][B])^n + (\tau A[A](K_A + \alpha\beta[B]) + \tau B[B]K_A)^n} \tag{3}$$

where E_m is the maximum attainable system response for the pathway under investigation; $[A]$ and $[B]$ are the concentrations of orthosteric and allosteric ligands, respectively; K_A and K_B are the equilibrium dissociation constants of the orthosteric and allosteric ligands, respectively; τ_A and τ_B are the operational measures of orthosteric and allosteric ligand efficacy (which incorporate both signal efficiency and receptor density), respectively; n is a transducer slope factor linking occupancy to response; α is the binding cooperativity parameter between the orthosteric and allosteric ligand; and β denotes the magnitude of the allosteric effect of the modulator on the efficacy of the orthosteric agonist.[12,45] In all cases, the equilibrium dissociation constant of each allosteric ligand was fixed to that determined from the competition binding experiments.

Experiments measuring radioligand saturation binding were fitted to the one site-specific binding model 4:

$$Y = \frac{B_{\max}[A]}{K_d + [A]} + NS[A] \tag{4}$$

where Y is the specific binding + nonspecific binding, $B_{\max}$ is the maximum receptor binding (in the same units as Y), $[A]$ is the concentration of $[^3H]NMS$, and K_d is the equilibrium dissociation constant of $[^3H]NMS$ in the same units as $[A]$.

Statistical analyses were performed where appropriate using one-way analysis of variance with Dunnett's post test, and significance indicated as follows: * = $p < 0.05$, ** = $p < 0.01$, *** = $p < 0.001$ and **** = $p < 0.0001$.

■ ASSOCIATED CONTENT

Ⓢ Supporting Information

Assigned HMBC spectrum of BQCA, HPLC chromatograms (254 and 214 nm) for compounds **4b**, **4c**, **4d**, **10**, and **11**, and $B_{\max}$ (% vehicle) bar graphs for compounds **4c**, **4d**, and **10**. This material is available free of charge via the Internet at http://pubs.acs.org.

■ AUTHOR INFORMATION

Corresponding Authors
*For P.J.S.: ███████████████████████
████████████████████.
*For A.C.: ███████████████████████
████████████████████

Author Contributions

The manuscript was written through contributions of all authors. All authors have given approval to the final version of the manuscript.

Notes

The authors declare no competing financial interest.

■ ACKNOWLEDGMENTS

■ ABBREVIATIONS USED

AChM, acetylcholine mustard; ACN, acetonitrile; BQCA, benzyl quinolone carboxylic acid (1-(4-methoxybenzyl)-4-oxo-1,4-dihydroquinoline-3-carboxylic acid); CHO, Chinese hamster ovary; CNS, central nervous system; COSY, correlation spectroscopy; CRC, concentration−response curve; DCM, dichloromethane; DIPEA, N,N-diisopropylethylamine; DMAP, 4-dimethylaminopyridine; DMEM, Dulbecco's Modified Eagle Medium; DMF, dimethylformamide; DMSO, dimethyl sulfoxide; ERK, extracellular-regulated kinase; FBS, fetal bovine serum; GPCR, G protein-coupled receptor; HEPES, 2-[4-(2-hydroxyethyl)-1-piperazinyl]ethanesulfonic acid; HMBC, heteronuclear multiple-bond correlation; HPLC, high performance liquid chromatography; HRMS, high resolution mass spectrometry; HSQC, heteronuclear single quantum coherence; LCMS, liquid chromatography−mass spectrometry; LRMS, low resolution mass spectrometry; mAChR, muscarinic acetylcholine receptor; MP, melting point; NBS, N-bromosuccinimide; NMR, nuclear magnetic resonance; NMS, N-methylscopolamine; PAM, positive allosteric modulator; PBS, phosphate-buffered saline; RBF, round-bottomed flask; RT, room temperature; SAR, structure−activity relationship; TCDI, thiocarbonyldiimidazole; TEA, triethylamine; TFA, trifluoroacetic acid; THF, tetrahydrofuran; TLC, thin layer chromatography; TOF, time-of-flight; WBC, whole cell binding

■ REFERENCES

(1) Langmead, C. J.; Watson, J.; Reavill, C. Muscarinic Acetylcholine Receptors as CNS Drug Targets. *Pharmacol. Ther.* **2008**, *117*, 232−243.

(2) Caulfield, M. P. Muscarinic Receptors—Characterization, Coupling and Function. *Pharmacol. Ther.* **1993**, *58*, 319−379.

(3) Fisher, A. M₁ Muscarinic Agonists Target Major Hallmarks of Alzheimer's Disease—The Pivotal Role of Brain M₁ Receptors. *Neurodegener. Dis.* **2008**, *5*, 237−240.

(4) May, L. T.; Leach, K.; Sexton, P. M.; Christopoulos, A. Allosteric Modulation of G Protein-Coupled Receptors. *Annu. Rev. Pharmacol. Toxicol.* **2007**, *47*, 1−51.

(5) Langmead, C. J.; Christopoulos, A. Allosteric Agonists of 7TM Receptors: Expanding the Pharmacological Toolbox. *Trends Pharmacol. Sci.* **2006**, *27*, 475−481.

(6) Davie, B. J.; Christopoulos, A.; Scammells, P. J. Development of M₁ mAChR Allosteric and Bitopic Ligands: Prospective Therapeutics for the Treatment of Cognitive Deficits. *ACS Chem. Neurosci.* **2013**, *4*, 1026−1048.

(7) Ma, L.; Seager, M. A.; Wittman, M.; Jacobson, M.; Bickel, D.; Burno, M.; Jones, K.; Graufelds, V. K.; Xu, G.; Pearson, M.; McCampbell, A.; Gaspar, R.; Shughrue, P.; Danziger, A.; Regan, C.; Flick, R.; Pascarella, D.; Garson, S.; Doran, S.; Kreatsoulas, C.; Veng, L.; Lindsley, C. W.; Shipe, W.; Kuduk, S.; Sur, C.; Kinney, G.; Seabrook, G. R.; Ray, W. J. Selective Activation of the M₁ Muscarinic Acetylcholine Receptor Achieved by Allosteric Potentiation. *Proc. Natl. Acad. Sci. U. S. A.* **2009**, *106*, 15950−15955.

(8) Shirey, J. K.; Brady, A. E.; Jones, P. J.; Davis, A. A.; Bridges, T. M.; Kennedy, J. P.; Jadhav, S. B.; Menon, U. N.; Xiang, Z.; Watson, M. L.; Christian, E. P.; Doherty, J. J.; Quirk, M. C.; Snyder, D. H.; Lah, J. J.; Levey, A. I.; Nicolle, M. M.; Lindsley, C. W.; Conn, P. J. A Selective Allosteric Potentiator of the M$_1$ Muscarinic Acetylcholine Receptor Increases Activity of Medial Prefrontal Cortical Neurons and Restores Impairments in Reversal Learning. *J. Neurosci.* **2009**, *29*, 14271−14286.

(9) Canals, M.; Lane, J. R.; Wen, A.; Scammells, P. J.; Sexton, P. M.; Christopoulos, A. A Monod−Wyman−Changeux Mechanism Can Explain G Protein-Coupled Receptor (GPCR) Allosteric Modulation. *J. Biol. Chem.* **2012**, *287*, 650−659.

(10) Kuduk, S. D.; Beshore, D. C. Novel M$_1$ Allosteric Ligands: A Patent Review. *Expert Opin. Ther. Pat.* **2012**, *22*, 1385−1398.

(11) Chambon, C.; Jatzke, C.; Wegener, N.; Gravius, A.; Danysz, W. Using Cholinergic M$_1$ Receptor Positive Allosteric Modulators to Improve Memory via Enhancement of Brain Cholinergic Communication. *Eur. J. Pharmacol.* **2012**, *697*, 73−80.

(12) Mistry, S. N.; Valant, C.; Sexton, P. M.; Capuano, B.; Christopoulos, A.; Scammells, P. J. Synthesis and Pharmacological Profiling of Analogues of Benzyl Quinolone Carboxylic Acid (BQCA) as Allosteric Modulators of the M$_1$ Muscarinic Receptor. *J. Med. Chem.* **2013**, *56*, 5151−5172.

(13) Kuduk, S. D.; Chang, R. K.; Di Marco, C. N.; Ray, W. J.; Ma, L.; Wittman, M.; Seager, M. A.; Koeplinger, K. A.; Thompson, C. D.; Hartman, G. D.; Bilodeau, M. T. Quinolizidinone Carboxylic Acid Selective M$_1$ Allosteric Modulators: SAR in the Piperidine Series. *Bioorg. Med. Chem. Lett.* **2011**, *21*, 1710−1715.

(14) Kuduk, S. D.; Di Marco, C. N.; Cofre, V.; Ray, W. J.; Ma, L.; Wittman, M.; Seager, M. A.; Koeplinger, K. A.; Thompson, C. D.; Hartman, G. D.; Bilodeau, M. T. Fused Heterocyclic M$_1$ Positive Allosteric Modulators. *Bioorg. Med. Chem. Lett.* **2011**, *21*, 2769−2772.

(15) Kuduk, S. D.; DiPardo, R. M.; Beshore, D. C.; Ray, W. J.; Ma, L.; Wittman, M.; Seager, M. A.; Koeplinger, K. A.; Thompson, C. D.; Hartman, G. D.; Bilodeau, M. T. Hydroxy Cycloalkyl Fused Pyridone Carboxylic Acid M$_1$ Positive Allosteric Modulators. *Bioorg. Med. Chem. Lett.* **2010**, *20*, 2538−2541.

(16) Bridges, T. M.; Kennedy, J. P.; Noetzel, M. J.; Breininger, M. L.; Gentry, P. R.; Conn, P. J.; Lindsley, C. W. Chemical Lead Optimization of a Pan G$_q$ mAChR M$_1$, M$_3$, M$_5$ Positive Allosteric Modulator (PAM) Lead. Part II: Development of a Potent and Highly Selective M$_1$ PAM. *Bioorg. Med. Chem. Lett.* **2010**, *20*, 1972−1975.

(17) Reid, P. R.; Bridges, T. M.; Sheffler, D. J.; Cho, H. P.; Lewis, L. M.; Days, E.; Daniels, J. S.; Jones, C. K.; Niswender, C. M.; Weaver, C. D.; Conn, P. J.; Lindsley, C. W.; Wood, M. R. Discovery and Optimization of a Novel, Selective and Brain Penetrant M$_1$ Positive Allosteric Modulator (PAM): The Development of ML169, an MLPCN Probe. *Bioorg. Med. Chem. Lett.* **2011**, *21*, 2697−2701.

(18) Conn, P. J.; Kuduk, S. D.; Doller, D. Drug Design Strategies for GPCR Allosteric Modulators. *Annu. Rep. Med. Chem.* **2012**, *47*, 441−457.

(19) Huynh, T.; Valant, C.; Crosby, I. T.; Sexton, P. M.; Christopoulos, A.; Capuano, B. Probing Structural Requirements of Positive Allosteric Modulators of the M$_4$ Muscarinic Receptor. *J. Med. Chem.* **2013**, *56*, 8196−8200.

(20) Leach, K.; Loiacono, R. E.; Felder, C. C.; McKinzie, D. L.; Mogg, A.; Shaw, D. B.; Sexton, P. M.; Christopoulos, A. Molecular Mechanisms of Action and in Vivo Validation of an M$_4$ Muscarinic Acetylcholine Receptor Allosteric Modulator with Potential Antipsychotic Properties. *Neuropsychopharmacology* **2010**, *35*, 855−869.

(21) Kruse, A. C.; Ring, A. M.; Manglik, A.; Hu, J.; Hu, K.; Eitel, K.; Hubner, H.; Pardon, E.; Valant, C.; Sexton, P. M.; Christopoulos, A.; Felder, C. C.; Gmeiner, P.; Steyaert, J.; Weis, W. I.; Garcia, K. C.; Wess, J.; Kobilka, B. K. Activation and Allosteric Modulation of a Muscarinic Acetylcholine Receptor. *Nature* **2013**, *504*, 101−106.

(22) Abdul-Ridha, A.; Lopez, L.; Keov, P.; Thal, D. M.; Mistry, S. N.; Sexton, P. M.; Lane, J. R.; Canals, M.; Christopoulos, A. Molecular Determinants of Allosteric Modulation at the M$_1$ Muscarinic Acetylcholine Receptor. *J. Biol. Chem.* **2014**, *289*, 6067−6079.

(23) Wess, J. Allosteric Binding Sites on Muscarinic Acetylcholine Receptors. *Mol. Pharmacol.* **2005**, *68*, 1506−1509.

(24) Kenakin, T. P. The Classification of Drugs and Drug Receptors in Isolated Tissues. *Pharmacol. Rev.* **1984**, *36*, 165−222.

(25) Scammells, P. J.; Baker, S. P.; Belardinelli, L.; Olsson, R. A. Substituted 1,3-Dipropylxanthines as Irreversible Antagonists of A$_1$ Adenosine Receptors. *J. Med. Chem.* **1994**, *37*, 2704−2712.

(26) Coates, P. A.; Grundt, P.; Robinson, E. S. J.; Nutt, D. J.; Tyacke, R.; Hudson, A. L.; Lewis, J. W.; Husbands, S. M. Probes for Imidazoline Binding Sites: Synthesis and Evaluation of a Selective, Irreversible I$_2$ Ligand. *Bioorg. Med. Chem. Lett.* **2000**, *10*, 605−607.

(27) Ehlert, F. J. The Interaction of 4-DAMP Mustard with Subtypes of the Muscarinic Receptor. *Life Sci.* **1996**, *58*, 1971−1978.

(28) Crocker, A. D.; Russell, R. W. Pretreatment With an Irreversible Muscarinic Agonist Affects Responses to Apomorphine. *Pharmacol., Biochem. Behav.* **1990**, *35*, 511−516.

(29) Spalding, T. A.; Birdsall, N. J. M.; Curtis, C. A. M.; Hulme, E. C. Acetylcholine Mustard Labels the Binding Site Aspartate in Muscarinic Acetylcholine Receptors. *J. Biol. Chem.* **1994**, *269*, 4092−4097.

(30) Suga, H.; Figueroa, K. W.; Ehlert, F. J. Use of Acetylcholine Mustard to Study Allosteric Interactions at the M$_2$ Muscarinic Receptor. *J. Pharmacol. Exp. Ther.* **2008**, *327*, 518−528.

(31) Rosenbaum, D. M.; Zhang, C.; Lyons, J. A.; Holl, R.; Aragao, D.; Arlow, D. H.; Rasmussen, S. G. F.; Choi, H.-J.; DeVree, B. T.; Sunahara, R. K.; Seok Chae, P.; Gellman, S. H.; Dror, R. O.; Shaw, D. E.; Weis, W. I.; Caffrey, M.; Gmeiner, P.; Kobilka, B. K. Structure and Function of an Irreversible Agonist−β_2 Adrenoceptor Complex. *Nature* **2011**, *469*, 236−242.

(32) Ehlert, F. J.; Griffin, M. T. The Use of Irreversible Ligands to Inactivate Receptor Subtypes 4-DAMP Mustard and Muscarinic Receptors in Smooth Muscle. *Life Sci.* **1998**, *62*, 1659−1664.

(33) Max, S. I.; Liang, J.-S.; Potter, L. T. Purification and Properties of M$_1$-Toxin, a Specific Antagonist of M$_1$ Muscarinic Receptors. *J. Neurosci.* **1993**, *13*, 4293−4300.

(34) Fujishima, S.-H.; Yasui, R.; Miki, T.; Ojida, A.; Hamachi, I. Ligand-Directed Acyl Imidazole Chemistry for Labelling of Membrane-Bound Proteins on Live Cells. *J. Am. Chem. Soc.* **2012**, *134*, 3961−3964.

(35) Chen, Z.; Jing, C.; Gallagher, S. S.; Sheetz, M. P.; Cornish, V. W. Second-Generation Covalent TMP-Tag for Live Cell Imaging. *J. Am. Chem. Soc.* **2012**, *134*, 13692−13699.

(36) Yang, F. V.; Shipe, W. D.; Bunda, J. L.; Nolt, M. B.; Wisnoski, D. D.; Zhao, Z.; Barrow, J. C.; Ray, W. J.; Ma, L.; Wittman, M.; Seager, M. A.; Koeplinger, K. A.; Hartman, G. D.; Lindsley, C. W. Parallel Synthesis of *N*-Biaryl Quinolone Carboxylic Acids as Selective M$_1$ Positive Allosteric Modulators. *Bioorg. Med. Chem. Lett.* **2010**, *20*, 531−536.

(37) Kuduk, S. D.; Di Marco, C. N.; Cofre, V.; Pitts, D. R.; Ray, W. J.; Ma, L.; Wittman, M.; Seager, M.; Koeplinger, K.; Thompson, C. D.; Hartman, G. D.; Bilodeau, M. T. Pyridine Containing M$_1$ Positive Allosteric Modulators with Reduced Plasma Protein Binding. *Bioorg. Med. Chem. Lett.* **2010**, *20*, 657−661.

(38) Juli, C.; Snippel, M.; Jager, J.; Thiele, A.; Weiward, M.; Schweimer, K.; Rosch, P.; Steinert, M.; Sotriffer, C. A.; Holzgrabe, U. Pipecolic Acid Derivatives as Small-Molecule Inhibitors of the *Legionella* MIP Protein. *J. Med. Chem.* **2011**, *54*, 277−283.

(39) Ehlert, F. J.; Jenden, D. J.; Ringdahl, B. An Alkylating Derivative of Oxotremorine Interacts Irreversibly with the Muscarinic Receptor. *Life Sci.* **1984**, *34*, 985−991.

(40) Gottlieb, H. E.; Kotlyar, V.; Nudelman, A. NMR Chemical Shifts of Common Laboratory Solvents as Trace Impurities. *J. Org. Chem.* **1997**, *62*, 7512−7515.

(41) Furniss, B. S.; Hannaford, A. J.; Smith, P. W. G.; Tatchell, A. R. *Vogel's Textbook of Practical Organic Chemistry*. 5th ed.; Longman Scientific and Technical: London, 1989; p 1431.

(42) Sheldrick, G. M. A Short History of SHELX. *Acta Crystallogr. Sect. A: Found. Crystallogr.* **2008**, *A64*, 112−122.

(43) Farrugia, L. J. ORTEP-3 for Windows—A Version of ORTEP-III with a Graphical User Interface (GUI). *J. Appl. Crystallogr.* **1997**, *30*, 565.

(44) Farrugia, L. J. WinGX Suite for Small-Molecule Single-Crystal Crystallography. *J. Appl. Crystallogr.* **1999**, *32*, 837.

(45) Leach, K.; Sexton, P. M.; Christopoulos, A. Allosteric GPCR Modulators: Taking Advantage of Permissive Receptor Pharmacology. *Trends Pharmacol. Sci.* **2007**, *28*, 382−389.

(46) Valant, C.; Aurelio, L.; Urmaliya, V. B.; White, P.; Scammells, P. J.; Sexton, P. M.; Christopoulos, A. Delineating the Mode of Action of Adenosine A_1 Receptor Allosteric Modulators. *Mol. Pharmacol.* **2010**, *78*, 444−455.

Chapter Three

Declaration for Thesis Chapter 3

The original research article presented in Chapter 3 is published as the following the paper:

Davie, B.J., Sexton, P.M., Capuano, B., Christopoulos, A., Scammells, P.J. (2014), Development of a Photoactivatable Allosteric Ligand for the M_1 Muscarinic Acetylcholine Receptor, *ACS Chemical Neuroscience*, *in press,* DOI: 10.1021/cn500173x. Permission to reprint this publication for the purpose of this thesis was granted by ACS Publications.

Declaration by candidate

In the case of Chapter 3, the nature and extent of my contribution to the work was the following:

Nature of contribution	Extent of contribution (%)
Synthesis and chemical characterization of MIPS1455. Pharmacological testing and data analysis for BQCA and MIPS1455. Main author of manuscript.	80%

The following co-authors contributed to the work. If co-authors are students at Monash University, the extent of their contribution in percentage terms must be stated:

Name	Nature of contribution	Extent of contribution (%) for student co-authors only
Patrick M. Sexton	Co-author of manuscript	
Ben Capuano	Co-author of manuscript	
Arthur Christopoulos	Co-author of manuscript	
Peter J. Scammells	Co-author of manuscript	

The undersigned hereby certify that the above declaration correctly reflects the nature and extent of the candidate's and co-authors' contributions to this work.

Candidate's Signature		Date 25/02/15
Main Supervisor's Signature		Date 25/02/15

Development of a Photoactivatable Allosteric Ligand for the M1 Muscarinic Acetylcholine Receptor

Briana J. Davie,[†,‡] Patrick M. Sexton,[‡] Ben Capuano,[†] Arthur Christopoulos,*[,‡] and Peter J. Scammells*[,†]

[†]Medicinal Chemistry and [‡]Drug Discovery Biology, Monash Institute of Pharmaceutical Sciences, Monash University, Parkville, Victoria 3052, Australia

S Supporting Information

ABSTRACT: The field of G protein-coupled receptor drug discovery has benefited greatly from the structural and functional insights afforded by photoactivatable ligands. One G protein-coupled receptor subfamily for which photoactivatable ligands have been developed is the muscarinic acetylcholine receptor family, though, to date, all such ligands have been designed to target the orthosteric (endogenous ligand) binding site of these receptors. Herein we report the synthesis and pharmacological investigation of a novel photoaffinity label, MIPS1455 (**4**), designed to bind irreversibly to an allosteric site of the M1 muscarinic acetylcholine receptor; a target of therapeutic interest for the treatment of cognitive deficits. MIPS1455 may be a valuable molecular tool for further investigating allosteric interactions at this receptor.

KEYWORDS: Muscarinic, allosteric, photoactivatable, photoaffinity, BQCA, cognition
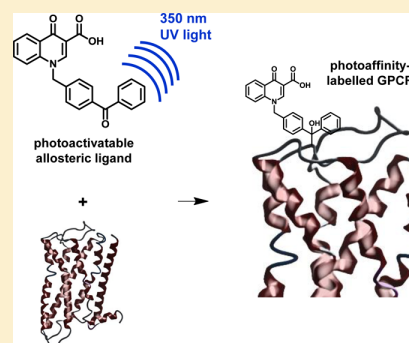
Photoaffinity labeling is a robust technique that is highly amenable to the study of ligand interactions with G protein-coupled receptors (GPCRs).[1] The utility of photo-affinity labeling arises from the range of photoactivatable functionalities available for incorporation into both ligands and receptors,[2] the potential for applying this technique to study any ligand−receptor[1] or, indeed, receptor−receptor complex,[3] and the ability to use the technique in tandem with more recently developed computational, genetic, and crystallographic technologies.

Photoaffinity labeling involves taking a known ligand or receptor and incorporating a photoactivatable moiety; a functional group capable of forming a reactive species (typically a carbene, nitrene, or diradical) upon electronic excitation at a specific wavelength of ultraviolet (UV) light. This species is then able to rapidly react or "cross-link" with a chemical bond of a neighboring entity in close proximity. Photoactivatable ligands offer the significant advantage of temporal control of reactivity, compared to affinity-labeled ligands containing, for example, inherently reactive electrophilic functionalities. The receptor may be pretreated with the "ground state" ligand prior to photoactivation, increasing the likelihood of "capturing" the ligand−receptor complex of interest. However, as with affinity-labeled ligands, reasonable affinity for the receptor and a similar pharmacological profile to the parent molecule are important to ensure selective labeling of the binding site of interest.[4]

Photoactivatable functionalities that are routinely incorporated into known ligands include benzophenones, diazirines and aryl azides (Figure 1).[5] Benzophenone-containing probes undergo photoactivation at 350−360 nm and have the notable advantages of higher chemical stability and higher cross-linking
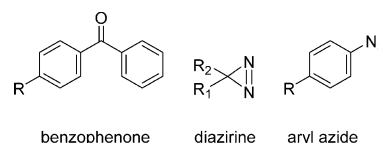
Figure 1. Three commonly used photoactivatable functionalities.

efficiency compared to diazirines and aryl azides. However, their bulk means that they may result in a less accurate representation of the parent ligand−receptor interaction. Diazirines and aryl azides are hence more prudent choices if incorporation of a benzophenone is likely to result in steric clashes with the binding pocket.

Diazirines, which photoactivate at 350−380 nm, may also prove to be an advantageous choice if considerable nonspecific cross-linking is anticipated; they display low cross-linking efficiency such that a covalent complex will only form if the ligand has very high affinity for the receptor.[5] A considerable drawback is that their synthesis can be complicated and time-consuming. Aryl azides, while more synthetically accessible that diazirines, require photoirradiation at <300 nm; wavelengths likely to cause nonspecific damage to the biological system under investigation.[6]

Photoaffinity labeling has considerably advanced our understanding of ligand−receptor and receptor−receptor interactions at Family A GPCRs. The technique has enabled the identification and structural characterization of ligand binding sites,[1,7] provided early evidence for receptor dimerization,[3] and

facilitated receptor purification that has subsequently aided GPCR crystallization.[8] Muscarinic acetylcholine receptors (mAChRs) are Family A GPCRs that, due to their widespread expression in the central nervous system,[9] have been extensively investigated as therapeutic targets for enhancing cognition and alleviating psychotic symptoms in conditions such as schizophrenia and Alzheimer's disease.[10] Examples of photo-activatable ligands for mAChRs include aryl azide derivatives of the potent orthosteric antagonists tropine,[11] 3-quinuclidinyl benzilate (3QNB),[12] and N-methyl-4-piperidyl benzilate (4NMPB).[12,13] In addition to the highly structurally conserved orthosteric ligand binding site, the existence of multiple, topographically distinct allosteric ligand binding sites at mAChRs has been extensively experimentally validated.[14] While an array of mAChR allosteric ligands have subsequently been developed,[15] our knowledge about the precise location and structure of their binding sites and the interactions of allosteric ligands within them is in its infancy. Hence, photoactivatable ligands for allosteric sites may be of significant worth to this field of research.

Herein we describe the development of a photoactivatable irreversible allosteric ligand, MIPS1455 (**4**, Figure 2), for the M_1 mAChR that may be useful in further probing the structural and functional mechanisms governing allosteric ligand-mAChR interactions.
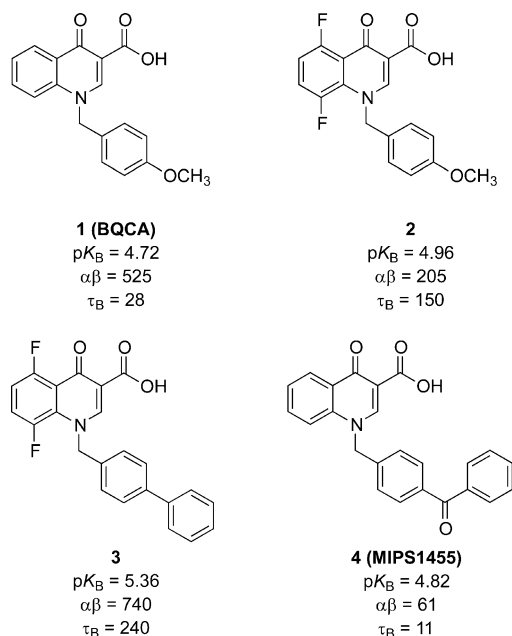
Figure 2. Structures of BQCA (**1**), two BQCA analogues (**2** and **3**), and the photoactivatable irreversible allosteric ligand MIPS1455 (**4**).

The extensive structure–activity relationship studies[16] performed on the parent molecule, the highly selective M_1 mAChR positive allosteric modulator benzyl quinolone carboxylic acid (BQCA, **1**, Figure 2),[17] guided our selection of the benzophenone group as our photoactivatable functionality. Many high potency BQCA analogues contain biaryl and fused aryl systems.[18−21] Specifically, replacement of the 4-methoxy group with a phenyl ring (**2** and **3**, Figure 2) resulted in improved affinity (pK_B), positive cooperativity ($\alpha\beta$), and allosteric agonism (τ_B).[22,23] This enabled us to confidently

incorporate the benzophenone group into our ligand design without concern about steric disruption of the ligand−receptor binding interaction or functional activation.

Using [^{3}H]N-methylscopolamine (NMS) competition radioligand binding and ERK1/2 phosphorylaton assays performed at human M_1 mAChR-expressing Chinese hamster ovary (CHO) cells, we confirm that the allosteric binding and functional profile of BQCA, as well as the parent molecule's high mAChR subtype selectivity, is preserved in MIPS1455. Importantly, saturation radioligand binding assays using hM_1 mAChR-expressing CHO cell membranes reveal the ability of MIPS1455 to irreversibly bind to the receptor following photoactivation.

The quinolone carboxylic acid **5** was prepared in three steps as previously described.[24] Radical bromination of 4-methyl-benzophenone gave a mixture of the desired monobrominated **6** and a small amount of dibrominated product. These compounds display a similar retention time and were unable to be separated by chromatographic methods. Fortunately, the crude mixture was successfully employed in the N-benzylation step to form the target molecule **4** in an acceptable yield (54%).

The allosteric binding and functional properties of BQCA (**1**) and MIPS1455 (**4**) were assessed, utilizing methods previously described,[24] by interacting the ligands with ACh in [^{3}H]NMS competition binding assays and ERK1/2 phosphorylation functional assays conducted in CHO cells stably expressing the hM_1 mAChR (Figure 3). MIPS1455 exhibited a similar affinity to BQCA (MIPS1455 K_B = 15 μM compared to BQCA K_B = 36 μM) and displayed positive binding (α = 61) and functional (β = 1.1) cooperativity with the agonist ACh and negative binding cooperativity with the antagonist [^{3}H]NMS (log $\alpha_{[NMS]}$ = −3.00) consistent with the two-state model of receptor activity reported for BQCA.[25] MIPS1455 also behaved as an allosteric agonist in its own right (MIPS1455 τ_B = 11 compared to BQCA τ_B = 28). [^{3}H]NMS competition binding curves and ERK1/2 phosphorylation concentration−response curves for BQCA and MIPS1455 in the absence of orthosteric agonist are available in Supporting Information Figure 1.

Next, we repeated the [^{3}H]NMS competition binding assays at the M_2-M_5 mAChR subtypes to evaluate the selectivity profiles of BQCA and MIPS1455. Neither significant positive cooperativity with ACh nor negative cooperativity with [^{3}H]NMS was observed with either ligand, suggesting that BQCA and MIPS1455 are unable to bind to, or else display neutral cooperativity with, the M_2-M_5 mAChRs (Supporting Information Figure 2).

Finally, we performed [^{3}H]NMS saturation membrane binding assays to ascertain whether MIPS1455 is capable of binding irreversibly to the M_1 mAChR. A protocol previously reported by our laboratory[24] was modified to incorporate a photoactivation step. Specifically, following a 1 h preincubation of M_1 mAChR-expressing CHO cell membranes with MIPS1455, the sample was exposed to 350 nm UV light for 30 min at 4 °C;[2] optimal conditions to affect photolysis, diradical formation, and covalent cross-linking by the benzophenone functionality (Figure 4).

[^{3}H]NMS saturation membrane binding assays revealed that MIPS1455 is binding irreversibly to the M_1 mAChR; a significant reduction in B_{max} (total receptor density) was observed following MIPS1455 preincubation and photo-activation compared to vehicle (B_{max} (% vehicle) = 50.2%; Figure 5A,D). This is indicative of reduced [^{3}H]NMS binding

B

dx.doi.org/10.1021/cn500173x | ACS Chem. Neurosci. XXXX, XXX, XXX−XXX

65
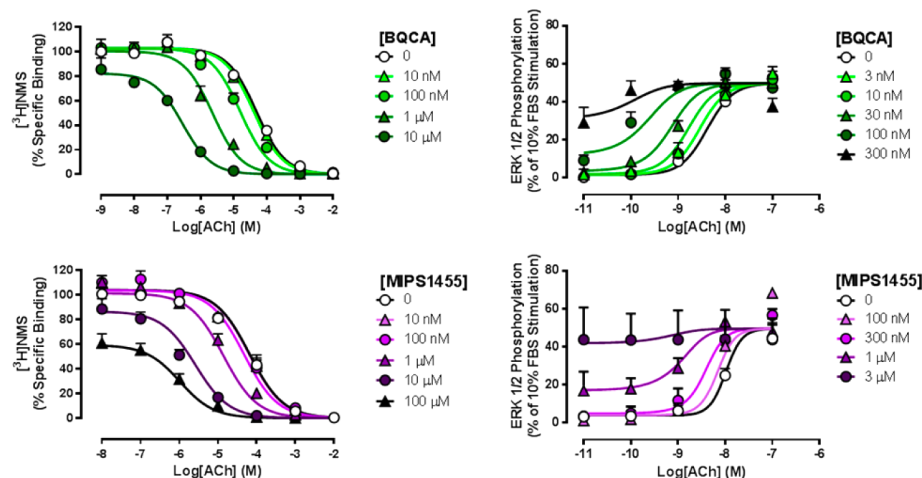
Figure 3. Pharmacological characterization of BQCA (**1**) and MIPS1455 (**4**) in a [³H]NMS-ACh competition binding assay (left) and an ERK1/2 phosphorylation functional assay (right). Experiments performed in hM$_1$ mAChR-expressing CHO cells in the presence of increasing concentrations of ACh with or without increasing concentrations of BQCA (**1**) or MIPS1455 (**4**) (and, in the case of the binding assay, in the presence of a K_D concentration of radiolabeled orthosteric antagonist [³H]NMS (0.1 nM)). The binding cooperativity factor between [³H]NMS and each allosteric ligand was constrained to an arbitrary low value (log $\alpha_{[NMS]}$ = −3.00) consistent with very high negative cooperativity. Values represent the mean ± SEM from at least three experiments performed in duplicate.
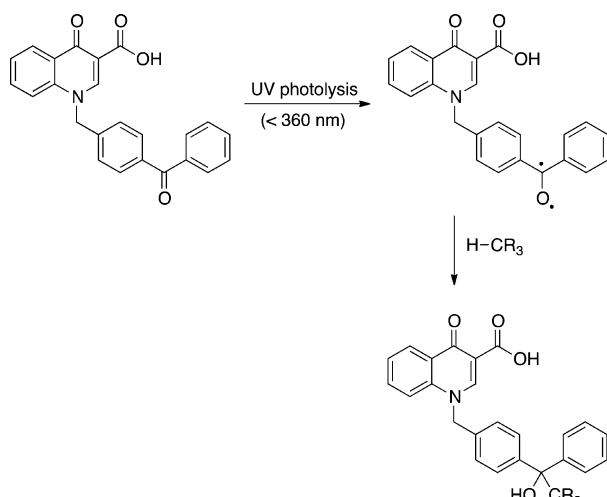
Figure 4. Scheme depicting UV photolysis, generation of a diradical intermediate, and covalent bond formation by a benzophenone functionality.

as a result of irreversible allosteric site occupation by MIPS1455, with which the radioligand has high negative cooperativity. No significant difference in B_{max} was observed following UV exposure of membranes preincubated with BQCA (B_{max} (% vehicle) = 88.6%, Figure 5B,D). Importantly, no change in B_{max} was observed following preincubation with MIPS1455 if the UV exposure step was omitted (B_{max} (% vehicle) = 90.3%, Figure 5C,D).

Herein we report the development of MIPS1455, a photoactivatable allosteric ligand for the M$_1$ mAChR. The synthesis of the ligand was completed following previously established methods (Scheme 1). In vitro [³H]NMS competition binding assays and ERK1/2 phosphorylation functional assays confirmed that MIPS1455, like the parent molecule BQCA, acts as an M$_1$ mAChR positive allosteric modulator (Figure 3). Importantly, we demonstrate that MIPS1455 is

capable of binding irreversibly to the M$_1$ mAChR following photoactivation with 350 nm UV light (Figure 5).

We postulate that this ligand may possess advantageous properties compared to our previously reported irreversible allosteric ligand MIPS1262 (see the Supporting Information Figure 3 for structure),[2] which contains an electrophilic isothiocyanate moiety.[24] MIPS1262 is limited to reacting with nucleophilic amino acid residues such as cysteine, serine and lysine. Such a requirement may result in the ligand adopting a distinct binding pose from that of BQCA in the allosteric binding site in order to orient itself around such residues (which may in turn lead to stabilization of a different receptor conformation), making it difficult to extrapolate any structural or functional findings to BQCA. Furthermore, the isothiocyanate moiety of MIPS1262 is inherently reactive, increasing the likelihood that the ligand binds nonselectively to multiple sites on the M$_1$ mAChR, in addition to the BQCA allosteric binding site. In a more complex in vitro setting, this reactivity is also likely to result in considerable off-target binding. In contrast, the benzophenone MIPS1455 affords the advantages of temporal control of reactivity, the ability to rapidly cross-link with any neighboring methylene unit (within 3.1 Å[4]) once activated, and more closely mimicking the structure of higher potency BQCA analogues than does MIPS1262. Furthermore, we demonstrate that the high mAChR subtype selectivity of BQCA is preserved with MIPS1455 (Supporting Information Figure 2). While these experiments were performed with the "ground state", nonphotoactivated MIPS1455, the results suggest that this ligand has little to no affinity for the other mAChRs and the likelihood of it cross-linking with these receptors following photoactivation is greatly reduced. Taken together, while MIPS1262 may serve as a useful ligand for investigating allosteric interactions in a recombinant in vitro setting, MIPS1455 may likely be a more favorable pharmacological tool for selectively probing structural and functional allosteric interactions at the M$_1$ mAChR in both a recombinant and native in vitro setting.
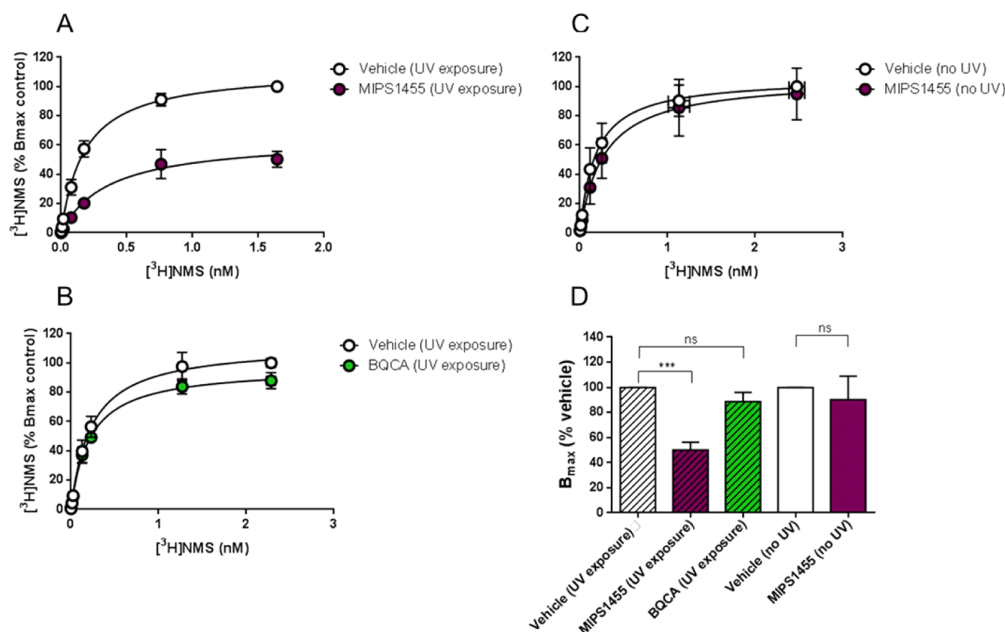
Figure 5. Pharmacological characterization of MIPS1455 (**4**) and BQCA (**1**) in [^{3}H]NMS saturation binding assays performed in hM$_1$ mAChR-expressing CHO cell membranes in the presence of increasing concentrations of radiolabeled orthosteric antagonist [^{3}H]NMS. (A) 1 h preincubation with vehicle or MIPS1455, followed by 30 min exposure to 350 nm UV light. (B) 1 h preincubation with vehicle or BQCA, followed by 30 min exposure to 350 nm UV light. (C) 1 h preincubation with vehicle or MIPS1455, without 30 min exposure to 350 nm UV light. (D) B_{max} (% vehicle) bar graphs where values significantly different from vehicle are indicated by asterisk(s) (*) (where * = $p < 0.05$, ** = $p < 0.01$, *** = $p < 0.001$, **** = $p < 0.0001$, and ns = not significant). Values represent the mean ± SEM from three experiments performed in duplicate.

Scheme 1. Synthesis of MIPS1455 (**4**)[a]
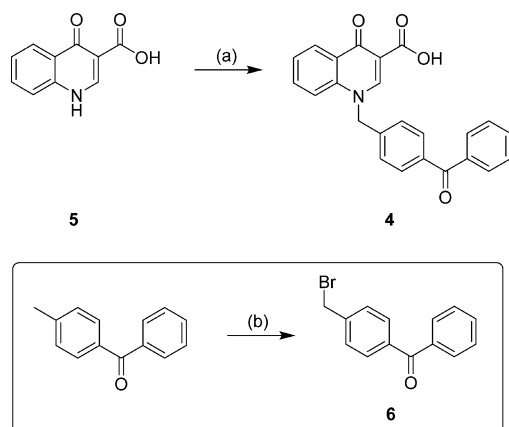
[a]Reagents and conditions: (a) **6**, DIPEA, ACN, 80 °C, 54%; (b) NBS, benzoyl peroxide, EtOAc, microwave 120 °C.

■ METHODS

Chemistry. *General.* All materials were reagent grade and purchased commercially from Sigma-Aldrich or Matrix Scientific. Anhydrous solvents were obtained from a MBraun MB SPS-800 Solvent Purification System. Analytical thin layer chromatography (TLC) was performed on silica gel 60 F$_{254}$ precoated plates (0.25 mm, Merck ART 5554) and visualized by ultraviolet light, iodine, or ninhydrin as necessary. Silica gel 60 (Fluka) was used for silica gel flash chromatography. Microwave reactions were performed in a CEM Discover microwave reactor. Melting points (mp) were determined on a Mettler Toledo MP50 Melting Point System.

^{1}H NMR spectra were routinely recorded at 400 MHz using a Brüker Avancell Ultrashield Plus spectrometer equipped with a Silicon Graphics workstation. Chemical shifts (δ_H) for all ^{1}H NMR spectra are reported in parts per million (ppm) using the center peak of the deuterated solvent chemical shift as the reference: CDCl$_3$ (7.26) and d_6-DMSO (2.50).[26] Each resonance was assigned according to the following convention: chemical shift (δ) (multiplicity, coupling constant(s) in Hz, and number of protons). Coupling constants (J) are reported to the nearest 0.5 Hz. In reporting spectral data, the following abbreviations have been used: s, singlet; d, doublet; t, triplet; q, quartet; p, pentet; m, multiplet; br, broad; app, apparent; as well as combinations of these where appropriate.

^{13}C NMR spectra were routinely recorded at 100 MHz using a Brüker Avance 400 Ultra Shield Plus spectrometer equipped with a Silicon Graphics workstation. Chemical shifts (δ_C) for all ^{13}C NMR spectra are reported in parts per million (ppm), using the center peak of the deuterated solvent chemical shift as the reference: CDCl$_3$ (77.16) and d_6-DMSO (39.52).[26]

HSQC, HMBC, and COSY spectra were obtained using the standard Brüker pulse sequence to assist with structural assignment of the compounds.

Liquid chromatography–mass spectrometry (LCMS) was performed on an Agilent 1200 Series coupled to the 6120 quadrupole mass spectrometer. Elution was also monitored at 254 nm. High resolution mass spectrometry (HRMS) analyses were recorded in the specified ion mode using a LCT Premier XE TOF mass spectrometer coupled to a 2795 Alliance Separations Module at cone voltages of 45 V (ESI+) and 60 V (ESI−).

Analytical reverse-phase high performance liquid chromatography (HPLC) was performed on a Waters HPLC system using a Phenomenex Luna C8 (2) 100 Å column (150 × 4.6 mm, 5 μm) and a binary solvent system; solvent A, 0.1% TFA/H$_2$O; solvent B, 0.1% TFA/80% MeOH/H$_2$O. Isocratic elution was carried out using the following protocol (time, % solvent A, % solvent B): 0 min, 100, 0; 10 min, 20, 80; 11 min, 20, 80; 12 min, 100, 0; 20 min, 100, 0; at a flow rate of 1.0 mL/min monitored at 254 nm using a Waters 996 Photodiode Array detector.

D   dx.doi.org/10.1021/cn500173x | *ACS Chem. Neurosci.* XXXX, XXX, XXX–XXX

67

Characterization requirements for intermediate compounds were set as mp, ^{1}H NMR, ^{13}C NMR, LCMS and HPLC (254 nm) or LCMS purity. Characterization requirements for final compounds were set as mp, ^{1}H NMR, ^{13}C NMR, LRMS, HRMS, and HPLC (254 and 214 nm) purity >95%.

1-(4-Benzoylbenzyl)-4-oxo-1,4-dihydroquinoline-3-carboxylic Acid (4). 4-Oxo-1,4-dihydroquinoline-3-carboxylic acid (180 mg, 952 μmol), crude 4-(bromomethyl)benzophenone (6) (393 mg, 1.43 mmol), and acetonitrile (8 mL) were placed in an RBF and cooled to 0 °C in an ice bath. *N,N*-Diisopropylethylamine (DIPEA) (4 equiv) was added, and the reaction stirred at 80 °C for 22 h. The reaction mixture was cooled to room temperature, and the precipitated product isolated as a white solid by vacuum filtration and washed with diethyl ether (197 mg, 54%); mp 235−236 °C. δ_H (d_6-DMSO) 15.15 (s, 1H), 9.36 (s, 1H), 8.43 (dd, *J* = 8.0, 1.0 Hz, 1H), 7.93−7.82 (m, 2H), 7.75−7.62 (m, 6H), 7.58−7.51 (m, 2H), 7.45 (d, *J*= 8.5 Hz, 2H), 6.02 (s, 2H). δ_C (d_6-DMSO) 195.1, 178.1, 165.9, 150.5, 140.2, 139.5, 136.8, 136.6, 134.3, 132.8, 130.2, 129.6, 128.6, 126.6, 126.5, 126.0, 125.7, 118.5, 108.1, 56.1. LCMS *m/z* [M + H]⁺: 384.1. *m/z* HRMS (TOF ES⁺) $C_{24}H_{17}NO_4$ [M + H]⁺ calcd 384.1230, found 384.1226. HPLC: t_R = 9.88 min, purity (254) = 97.0%, purity (214) = 96.3%

4-(Bromomethyl)benzophenone (6). 4-Methylbenzophenone (200 mg, 1.02 mmol), *N*-bromosuccinimide (NBS) (218 mg, 1.22 mmol), and benzoyl peroxide (12.3 mg, 51 μmol) were placed in a microwave vial with ethyl acetate (4 mL), and the reaction mixture was stirred briefly to dissolve the reagents. The vessel was sealed and reacted in the microwave for 15 min at 120 °C. The reaction mixture was filtered to remove any precipitated NBS, and then the solvent evaporated in vacuo. The target molecule was reacted on without any further purification (crude mass: 577 mg); δ_H (CDCl₃) 7.76−7.69 (m, 4H), 7.46−7.39 (m, 5H), 4.47 (s, 2H). δ_C (CDCl₃) 178.4, 142.2, 137.4, 137.3, 132.7, 130.6, 130.4, 130.1, 129.0, 128.4, 126.6, 32.4. LCMS *m/z* [M(^{81}Br) + H]⁺: 277.0. LCMS: t_R = 6.78 min, purity = 85.0% monobrominated product, 15.0% dibrominated byproduct.

Pharmacology. [3]HNMS competition whole cell binding assays, ERK1/2 phosphorylation assays, and data analysis were performed as previously described.[24] [3]HNMS saturation membrane binding assays were performed as follows.

Membrane Preparation. Preprepared FlpIn-CHO cell membranes stably expressing human muscarinic M₁ receptors (hM₁ mAChR FlpIn-CHO) were thawed, diluted to a concentration of 1250 μg/mL, and resuspended using a hand-held homogenizer (at slow speed to minimize frothing). Ultracentrifuge tubes (one per buffer/ligand treatment) were labeled, 500 μg of membrane pipetted into each, the volume made up to 9 mL with cold HEPES-buffered saline, and the tubes kept on ice.

Preincubation with Controls and Test Ligands. Stock solutions of MIPS1455 and BQCA (10^{-2} M) were made up in DMSO. Ligands were diluted to 10^{-3} M in HEPES-buffered saline. A buffer control (10% DMSO/HEPES-buffered saline) was also made up. One milliliter buffer or ligand additions, for a final volume of 10 mL, were made, and the membrane tubes incubated in a water bath at 37 °C for 1 h. Membrane tubes were placed immediately on ice for 3 min and then exposed to 350 nm UV light at 4 °C for 30 min. Next, 10 mL of ice cold HEPES-buffered saline was added, and then additional ice cold buffer was added to bring all tubes to equal mass. Tubes were centrifuged on the Sorval ultracentrifuge at 4 °C for 20 min at 40 000 rpm. The supernatant was discarded, the membranes were washed and resuspended thoroughly in 1 mL of ice cold HEPES-buffered saline (to ensure the removal of any noncovalently bound ligand), an additional 19 mL of ice-cold buffer added, and the tubes brought to equal mass again. Tubes were centrifuged again on the Sorval ultracentrifuge at 4 °C for 20 min at 40 000 rpm. The supernatant was discarded, and the membranes resuspended in 400 μL of cold HEPES-buffered saline. A Bradford assay was performed to ascertain the concentration of membrane in each treatment tube, and then the required amount of cold HEPES-buffered saline was added to bring the concentration of each to 30 μg/mL.

Assay Protocol. Stock solutions of [3]HNMS ($10^{-7.5}$ and 10^{-8} M) were made up in HEPES-buffered saline. Dilutions of [3]HNMS were

made up in HEPES-buffered saline at 10× the required concentration. A stock solution of atropine (10^{-4} M) was made up at 10× the required concentration. Membranes (100 μL per tube) were equilibrated at 37 °C for 1 h with 100 μL of HEPES-buffered saline (specific wells) or 100 μL of atropine (nonspecific wells) and 100 μL per well of each concentration of [3]HNMS, in the required amount of HEPES-buffered saline to make a total volume of 1 mL per tube.

Assay Termination and Data Collection. Assays were terminated by harvesting the tubes in the Brandel harvester and rinsing tubes twice with 2 mL of ice-cold 0.9% NaCl solution. Membranes were dried under the heat lamp, picked, and placed into 6 mL scintillation tubes. Then 4 mL per tube of Ultima Gold scintillation liquid was added, and the tubes capped, vortexed, and left on the bench for 1 h at RT. The levels of bound radioligand, and therefore the degree of radioligand blockade by any irreversibly bound test ligands, was measured in disintegrations per minute (dpm) on the TriCarb 2910 TR liquid scintillation analyzer (PerkinElmer).

■ ASSOCIATED CONTENT

ⓢ Supporting Information

(1) [3]HNMS competition binding curves and ERK1/2 phosphorylation concentration−response curves for BQCA (1) and MIPS1455 (4) alone, (2) [3]HNMS competition binding selectivity study of BQCA (1) and MIPS1455 (4) in hM₂−hM₅ mAChR-expressing CHO cells, "(3) structure of MIPS1262, and (4) HPLC chromatograms (254 and 214 nm) for compound 4. This material is available free of charge via the Internet at http://pubs.acs.org.

■ AUTHOR INFORMATION

Corresponding Authors

*For P.J.S.: ██████████████████
██████████████.

*For A.C.: ██████████████████
████████████████████

Author Contributions

The manuscript was written through contributions of all authors. All authors have given approval to the final version of the manuscript.

Author Contributions

B.J.D. conducted all of the experimentation, all authors contributed to experimental design and the production of the manuscript.

Notes

The authors declare no competing financial interest.

■ ACKNOWLEDGMENTS

■ ABBREVIATIONS

ACN, acetonitrile; BQCA, benzyl quinolone carboxylic acid (1-(4-methoxybenzyl)-4-oxo-1,4-dihydroquinoline-3-carboxylic acid); CHO, Chinese hamster ovary; COSY, correlation spectroscopy; DIPEA, *N,N*-diisopropylethylamine; DMSO, dimethyl sulfoxide; ERK, extracellular-regulated kinase; ESI,

electrospray ionization; GPCR, G protein-coupled receptor; HMBC, heteronuclear multiple-bond correlation; HPLC, high performance liquid chromatography; HRMS, high resolution mass spectrometry; HSQC, heteronuclear single quantum coherence; LCMS, liquid chromatography–mass spectrometry; LRMS, low resolution mass spectrometry; mAChR, muscarinic acetylcholine receptor; MP, melting point; NBS, N-bromosuccinimide; NMPB, N-methyl-4-piperidyl p-azidobenzilate; NMR, nuclear magnetic resonance; NMS, N-methylscopolamine; QNB, quinuclidinyl benzilate; RBF, round-bottomed flask; SEM, standard error of the mean; TFA, trifluoroacetic acid; TLC, thin layer chromatography; TOF, time-of-flight; UV, ultraviolet

■ REFERENCES

(1) Grunbeck, A., and Sakmar, T. P. (2013) Probing G Protein-Coupled Receptor–Ligand Interactions with Targeted Photoactivatable Cross-Linkers. *Biochemistry 52*, 8625–8632.

(2) Vodovozova, E. L. (2007) Photoaffinity Labeling and Its Application in Structural Biology. *Biochemistry 72*, 1–20.

(3) Gomes, I., Jordan, B. A., Gupta, A., Rios, C., Trapaidze, N., and Devi, L. A. (2001) G Protein Coupled Receptor Dimerization: Implications in Modulating Receptor Function. *J. Mol. Med. 79*, 226–242.

(4) Dorman, G., and Prestwich, G. D. (2000) Using photolabile ligands in drug discovery and development. *Trends Biotechnol. 18*, 64–77.

(5) Bin, X. U., and Ling, W. U. (2014) Analysis of Receptor-Ligand Binding by Photoaffinity Cross-Linking. *Sci. China Chem. 57*, 232–242.

(6) Lapinsky, D. J. (2012) Tandem Photoaffinity Labeling-Bioorthogonal Conjugation in Medicinal Chemistry. *Biorg. Med. Chem. 20*, 6237–6247.

(7) Brune, S., Pricl, S., and Wunsch, B. (2013) Structure of the σ_1 Receptor and Its Ligand Binding Site. *J. Med. Chem. 56*, 9809–9819.

(8) Benovic, J. L. (2012) G-Protein-Coupled Receptors Signal Victory. *Cell 151*, 1148–1150.

(9) Caulfield, M. P. (1993) Muscarinic Receptors- Characterization, Coupling and Function. *Pharmacol. Ther. 58*, 319–379.

(10) Langmead, C. J., Watson, J., and Reavill, C. (2008) Muscarinic Acetylcholine Receptors as CNS Drug Targets. *Pharmacol. Ther. 117*, 232–243.

(11) Moreno-Yanes, J. A., and Mahler, H. R. (1980) Photoaffinity Labeling of Specific Muscarinic Antagonist Binding Sites of Brain: I. Preliminary Studies Using Two p-Azidophenylacetate Esters of Tropine. *Biochem. Biophys. Res. Commun. 92*, 610–617.

(12) Amitai, G., Avissar, S., Balderman, D., and Sokolovsky, M. (1982) Affinity Labeling of Muscarinic Receptors in Rat Cerebral Cortex with a Photolabile Antagonist. *Proc. Natl. Acad. Sci. U.S.A. 79*, 243–247.

(13) Avissar, S., Amitai, G., and Sokolovsky, M. (1983) Oligomeric Structure of Muscarinic Receptors Is Shown by Photoaffinity Labeling: Subunit Assembly May Explain High- And Low-Affinity Agonist States. *Proc. Natl. Acad. Sci. U.S.A. 80*, 156–159.

(14) Gregory, K. J., Sexton, P. M., and Christopoulos, A. (2007) Allosteric Modulation of Muscarinic Acetylcholine Receptors. *Curr. Neuropharmacol. 5*, 157–167.

(15) Kruse, A. C., Kobilka, B. K., Gautam, D., Sexton, P. M., Christopoulos, A., and Wess, J. (2014) Muscarinic Acetylcholine Receptors: Novel Opportunities for Drug Development. *Nat. Rev. Drug Discovery 13*, 549–560.

(16) Davie, B. J., Christopoulos, A., and Scammells, P. J. (2013) Development of M_1 mAChR Allosteric and Bitopic Ligands: Prospective Therapeutics for the Treatment of Cognitive Deficits. *ACS Chem. Neurosci. 4*, 1026–1048.

(17) Ma, L., Seager, M. A., Wittman, M., Jacobson, M., Bickel, D., Burno, M., Jones, K., Graufelds, V. K., Xu, G., Pearson, M.,

McCampbell, A., Gaspar, R., Shughrue, P., Danziger, A., Regan, C., Flick, R., Pascarella, D., Garson, S., Doran, S., Kreatsoulas, C., Veng, L., Lindsley, C. W., Shipe, W., Kuduk, S., Sur, C., Kinney, G., Seabrook, G. R., and Ray, W. J. (2009) Selective Activation of the M_1 Muscarinic Acetylcholine Receptor Achieved by Allosteric Potentiation. *Proc. Natl. Acad. Sci. U.S.A. 106*, 15950–15955.

(18) Kuduk, S. D., Di Marco, C. N., Chang, R. K., Ray, W. J., Ma, L., Wittman, M., Seager, M. A., Koeplinger, K. A., Thompson, C. D., Hartman, G. D., and Bilodeau, M. T. (2010) Heterocyclic Fused Pyridone Carboxylic Acid M_1 Positive Allosteric Modulators. *Bioorg. Med. Chem. Lett. 20*, 2533–2537.

(19) Kuduk, S. D., DiPardo, R. M., Beshore, D. C., Ray, W. J., Ma, L., Wittman, M., Seager, M. A., Koeplinger, K. A., Thompson, C. D., Hartman, G. D., and Bilodeau, M. T. (2010) Hydroxy Cycloalkyl Fused Pyridone Carboxylic Acid M_1 Positive Allosteric Modulators. *Bioorg. Med. Chem. Lett. 20*, 2538–2541.

(20) Kuduk, S. D., Di Marco, C. N., Cofre, V., Pitts, D. R., Ray, W. J., Ma, L., Wittman, M., Veng, L., Seager, M. A., Koeplinger, K., Thompson, C. D., Hartman, G. D., and Bilodeau, M. T. (2010) N-Heterocyclic Derived M_1 Positive Allosteric Modulators. *Bioorg. Med. Chem. Lett. 20*, 1334–1337.

(21) Kuduk, S. D., Di Marco, C. N., Cofre, V., Ray, W. J., Ma, L., Wittman, M., Seager, M. A., Koeplinger, K. A., Thompson, C. D., Hartman, G. D., and Bilodeau, M. T. (2011) Fused Heterocyclic M_1 Positive Allosteric Modulators. *Bioorg. Med. Chem. Lett. 21*, 2769–2772.

(22) Yang, F. V., Shipe, W. D., Bunda, J. L., Nolt, M. B., Wisnoski, D. D., Zhao, Z., Barrow, J. C., Ray, W. J., Ma, L., Wittman, M., Seager, M. A., Koeplinger, K. A., Hartman, G. D., and Lindsley, C. W. (2010) Parallel Synthesis of N-Biaryl Quinolone Carboxylic Acids as Selective M_1 Positive Allosteric Modulators. *Bioorg. Med. Chem. Lett. 20*, 531–536.

(23) Mistry, S. N., Valant, C., Sexton, P. M., Capuano, B., Christopoulos, A., and Scammells, P. J. (2013) Synthesis and Pharmacological Profiling of Analogues of Benzyl Quinolone Carboxylic Acid (BQCA) as Allosteric Modulators of the M_1 Muscarinic Receptor. *J. Med. Chem. 56*, 5151–5172.

(24) Davie, B. J., Valant, C., White, J. M., Sexton, P. M., Capuano, B., Christopoulos, A., and Scammells, P. J. (2014) Synthesis and Pharmacological Evaluation of Analogues of Benzyl Quinolone Carboxylic Acid (BQCA) Designed to Bind Irreversibly to an Allosteric Site of the M_1 Muscarinic Acetylcholine Receptor. *J. Med. Chem. 57*, 5405–5418.

(25) Canals, M., Lane, J. R., Wen, A., Scammells, P. J., Sexton, P. M., and Christopoulos, A. (2012) A Monod-Wyman-Changeux Mechanism Can Explain G Protein-coupled Receptor (GPCR) Allosteric Modulation. *J. Biol. Chem. 287*, 650–659.

(26) Gottlieb, H. E., Kotlyar, V., and Nudelman, A. (1997) NMR Chemical Shifts of Common Laboratory Solvents as Trace Impurities. *J. Org. Chem. 62*, 7512–7515.

F

dx.doi.org/10.1021/cn500173x | *ACS Chem. Neurosci.* XXXX, XXX, XXX–XXX

69

Chapter Four

Towards the Development of Rationally-Designed Bitopic Ligands for the M$_1$ Muscarinic Acetylcholine Receptor

Introduction

Following the lead of the message-address concept first published in the 1970s,[1] as well as the pioneering work on bivalent ligands brought into prominence by Portoghese,[2] the development of bitopic ligands has gained momentum over the past several years as a fruitful method for targeting G protein-coupled receptors (GPCRs).[3,4] A bitopic ligand, by definition, is able to simultaneously engage an orthosteric site and an allosteric site of the same receptor. Covalently linking the pharmacophores of known ligands for the orthosteric site and the allosteric site to form a single chemical entity may result in the fusion of the desirable features of the individual pharmacophores.[5] Such rationally-designed hybrid ligands may exhibit:

- improved affinity and potency compared to their orthosteric and allosteric constituents alone

- improved subtype selectivity, as the allosteric moiety may form interactions with less conserved amino acid residues of the receptor thereby localizing the non-selective orthosteric moiety at the receptor subtype of interest

- improved pathway selectivity (or the promotion of stimulus bias) through stabilization of a distinct receptor conformation from that engendered by the orthosteric and allosteric constituents alone

Hence, such molecules present as potentially useful pharmacological tools to study GPCRs that may pave the way towards novel, improved therapeutics. This was exemplified recently by an important proof-of-concept study at the adenosine A$_1$ GPCR, where it was demonstrated that bitopic ligands may be designed to activate signaling pathways that give

rise to a therapeutic effect without activating pathways that give rise to on-target adverse effects.[6]

Bitopic ligands at muscarinic acetylcholine receptors

The muscarinic acetylcholine receptors (mAChRs) represent an ideal subfamily of GPCRs at which to probe bitopic interactions. Both orthosteric and allosteric interactions have been extensively characterized at these receptors,[7] and their prospective therapeutic utility as novel targets for the treatment of a range of central and peripheral disorders is well-established.[8,9] Furthermore, the discoveries made at these receptors may be reasonably hypothesized to be a general feature of other structurally-similar Family A GPCRs.[8] There are numerous examples of both previously-unappreciated and rationally-designed bitopic ligands at mAChRs; largely at the M_2 subtype.

Previously-unappreciated bitopic ligands at mAChRs

By generating and pharmacologically evaluating a series of truncated derivatives of the M_2 mAChR partial agonist McN-A-343 (**1**, **Figure 1**), Valant *et al.*[10] were able to confirm that this molecule in fact behaves in a bitopic manner; engendering stimulus bias (i.e. divergent G protein-coupling specificity compared to classic mAChR agonists) and receptor subtype functional selectivity. This seminal publication raised the possibility of uncovering hitherto unappreciated bitopic mechanisms of action for other GPCR ligands, prompting the in-depth study of another mAChR ligand, TBPB ([1-(1'-(2-**t**olyl)-1,4'-**bip**iperidin-4-yl)-1H **b**enzo[*d*]imidazol-2(3*H*)-one]) (**2**, **Figure 1**). TBPB was originally purported as an M_1 mAChR allosteric agonist following the observation that the molecule elicited an apparent non-competitive interaction with the orthosteric antagonist atropine.[11] However, this molecule was re-classified as a bitopic ligand following the identification of "molecular switches" within the structure of TBPB that convert the ligand from a M_1 mAChR-selective

agonist to a *pan*-mAChR orthosteric antagonist, and the observation that TBPB acts as an orthosteric antagonist at the other mAChR subtypes.[12] This classification was further confirmed by a "reverse engineering" study that employed truncated derivatives of TBPB to identify the orthosteric and allosteric pharmacophores within the ligand.[13] Other "allosteric agonists" that are likely to be behaving bitopically are GSK1034702 (**3**, **Figure 1**), which shows some structural similarity to TBPB, as well as AC-42, 77-LH-28-1, and AC260584 (**4-6**, **Figure 1**), another distinct structural class of M$_1$ mAChR ligand.[14,15]
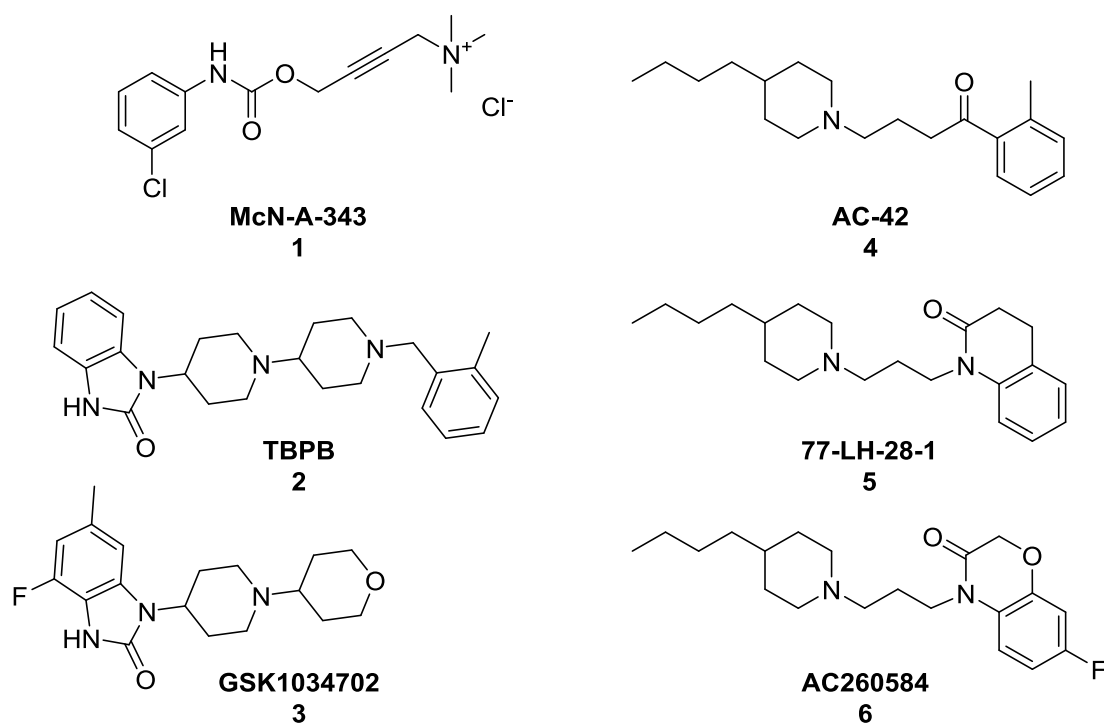
Figure 1. Structures of McN-A-343 (1), TBPB (2), GSK1034702 (3), AC-42 (4), 77-LH-28-1 (5) and AC260584 (6).

Rationally-designed bitopic ligands at mAChRs

Fusion of the highly potent non-selective muscarinic orthosteric ligand iperoxo (**7**, **Figure 3**) with two different M_2 mAChR-selective allosteric fragments via a six-carbon linker resulted in bitopic ligands H1 and H2 (**8a** and **8b**, **Figure 2**) that engendered a degree of selectivity at the level of the receptor and at the level of signalling in hM_2 mAChR-transfected COS7 cells, though a reduction in affinity was observed compared to that of iperoxo.[16,17] Another rationally-designed bitopic ligand, THRX-160209 (**9**, **Figure 2**), demonstrated an apparent affinity several orders of magnitude higher than its monovalent constituents, in addition to exhibiting subtype specificity for the M_2 mAChR.[18] A recent *Nature Communications* publication[19] described the potential utility of bitopic ligands as tools for 'controlled' manipulation of GPCR conformational transitions. A series of elegant experiments, including dynamic mass redistribution (DMR) and bioluminescence resonance energy transfer (BRET), demonstrated that bitopic ligands can be used to affect conformational changes in the allosteric vestibule of the M_2 mAChR in a systematic manner. Using four bitopic ligands (including H1 and H2[16]) to probe specific structural hypotheses, the authors were able to link the degree of spatial freedom/conformational flexibility in the allosteric vestibule with the extent of receptor activation and the promiscuity of G protein-coupling. Specifically, they found that receptor activation could be impaired or restored depending on the positioning of the bulky allosteric component of the bitopic ligands and that G_s signalling was more substantially impaired by conformational restriction of the vestibule than G_i signalling. Furthermore, in a recent Nature Chemical Biology communication, H2 was proposed to adopt two different orientations at the M_2 mAChR, giving rise to two functionally-divergent receptor populations.[20] Whilst the ligand preferentially bound in a bitopic manner and stabilized an active receptor conformation, it also bound in a purely

allosteric manner, stabilizing an inactive receptor conformation; highlighting a novel mechanism by which partial agonism at a GPCR may be achieved.

Taken together, both retrospective investigation of existing ligands and the rational design of novel bitopic ligands have yielded fascinating results that have enhanced our understanding of ligand-GPCR interactions and broadened our view of the capabilities of this class of ligands as both investigative tools and innovative prospective therapeutics.
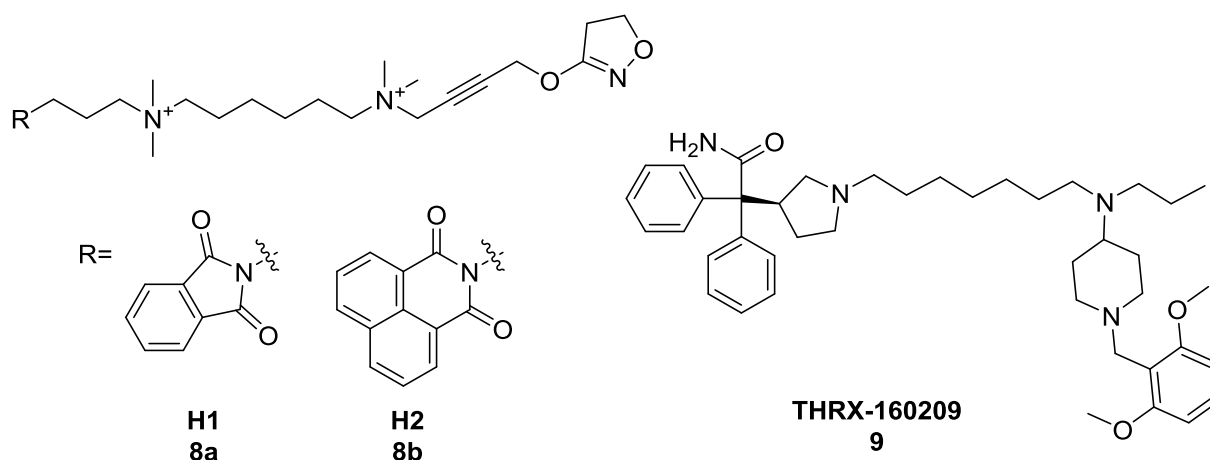
Figure 2. Structures of H1 (8a) and H2 (8b), and THRX-160209 (9)

Project Aim and Design

Inspired by the research previously described at the M_2 mAChR,[8] the aim of the present study was to rationally-design, synthesize and pharmacologically characterize novel putative bitopic ligands for the M_1 mAChR that may provide similarly valuable mechanistic insights into the function of this receptor. We were guided in our ligand design by the important structural considerations highlighted by Lane *et al.*;[21] namely, selection of appropriate constituent molecules, the linkage point and the nature, length and flexibility of the linker.

Bitopic ligand design

Given the unparalleled potency of iperoxo (**7**, **Figure 3**) at the orthosteric site of mAChRs[22] and its successful incorporation into the hybrid molecules already discussed,[16,19] we selected this compound as the orthosteric pharmacophore for our putative M_1 mAChR bitopic ligands. For the allosteric pharmacophore we selected 1-(4-methoxy**b**enzyl)-4-oxo-1,4-dihydro**q**uinoline-3-**c**arboxylic **a**cid (BQCA, **10**, **Figure 3**), a highly selective, though low affinity, M_1 mAChR positive allosteric modulator (PAM) and allosteric agonist.[23,24]
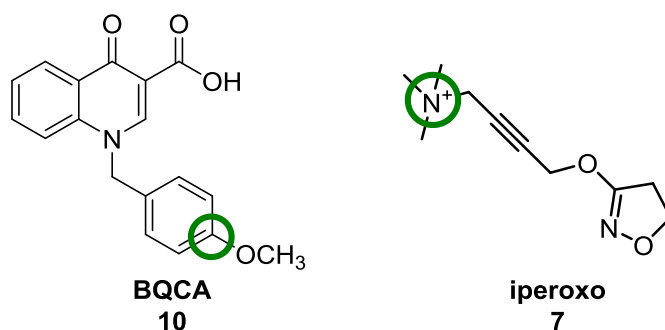
BQCA
10

iperoxo
7

Figure 3. Structures of the non-selective orthosteric muscarinic agonist iperoxo (7) and the subtype selective M_1 mAChR allosteric ligand BQCA (10) with our selected linkage point circled in green

In selecting the appropriate constituent orthosteric and allosteric ligands to link together to form a putative bitopic molecule, it is critical to consider the receptor conformational preference of each ligand.[21] When orthosteric and allosteric ligands that preferentially stabilize an active conformation of the same receptor are co-bound, it is probable that they will exhibit positive cooperativity; in that they enhance the binding affinity and/or functional efficacy of one another.[24-26] Such ligand combinations, which should prefer the same receptor state, are likely to be more thermodynamically-favourable as building blocks in the construction of a putative bitopic ligand. Iperoxo, as a high potency agonist, prefers an active

receptor conformation; as does BQCA, which acts as a PAM of orthosteric agonists and a negative allosteric modulator (NAM) of orthosteric antagonists, in accordance with the Monod-Wyman-Changeux (MWC) two-state model.[24]

Linker design

The crystal structures of the antagonist-bound M_2 and M_3 mAChRs, as well as the recently published crystal structure of the nanobody-stabilized active state of the M_2 mAChR co-bound with iperoxo and the allosteric ligand LY2119620, have definitively established the nature of the muscarinic orthosteric site and the extracellular (EC) vestibule allosteric site.[25,27,28] The orthosteric site of mAChRs resides in the hydrophilic cavity embedded within transmembrane (TM) domains 2-7. The quaternary ammonium moiety of iperoxo forms an ionic interaction with a conserved aspartate residue in TM3, which is likely the case for other muscarinic orthosteric agonists.[29] Furthermore, the quaternary ammonium moiety also forms cation-π interactions with three tyrosine residues which in turn hydrogen bond with each other to form an "aromatic lid" that forms the key divide between the orthosteric site and the EC vestibule allosteric site. LY2119620 forms critical interactions with residues in TM7, EC loop 2 and EC loop 3; all previously purported to be involved in the "common" allosteric binding site of mAChRs.[30,31] Mutagenesis studies and molecular dynamics (MD) simulations suggest that BQCA also interacts with this allosteric site.[23,32] However, whilst some common structural features for allosteric ligand binding to the EC vestibule (at the M_2 mAChR) have been revealed through MD simulations and radioligand binding,[33] it remains difficult to extrapolate the binding pose from one ligand to another given their structural diversity and the flexibility of this receptor region.

Given the high structural conservation observed between mAChRs, we took into account the observations from these crystal structures, as well as the known muscarinic bitopic ligands described earlier, in informing the nature, length and flexibility of the linkers we selected for our putative M_1 mAChR bitopic ligands. The rationally-designed bitopic ligands H1, H2 and THRX-160209 all contain simple, flexible polymethylene linkers, so we felt confident in applying this to our own design. Furthermore, we hypothesized that such a linker may be likely to span the narrow divide between orthosteric and allosteric sites with minimal disruption to the cation-π interactions formed with the "aromatic lid", which appears to be a critical feature of mAChR activation;[34,35] where polyethylene glycol, polyamide or bulkier linkers might disrupt these interactions. In terms of linker length, we chose to synthesize three putative bitopic ligands with 1-, 5- and 9-methylene linkers. This decision was based on the observation that a linker of no more than a one carbon unit may be necessary to span the orthosteric and allosteric sites of mAChRs (given the pharmacophores of McN-A-343 and TBPB, and the nature of the "aromatic lid") but that a longer linker may indeed be favourable (as in the structures of H1, H2 and THRX-160209). Our limited knowledge about the exact location of the BQCA binding site, and therefore its proximity to the orthosteric site, reinforced this decision; though MD simulations of the BQCA-M_1 mAChR interaction suggest that a longer linker may be required.[32] We selected the quaternary nitrogen as the linkage point on iperoxo, in line with H1 and H2, and we selected the *para*-position of the benzylic pendant as the linkage point on BQCA, in line with previous SAR studies that demonstrate this region of the ligand as highly tolerant to a range of synthetic modifications, in terms of the preservation or improvement of potency (green circles, **Figure 3**).[36-39] Furthermore, the MD model of the BQCA-M_1 mAChR interaction suggests that, whilst in close proximity to TM7, this moiety extends into the space defining the entrance to the orthosteric binding pocket.[32] Past success in incorporating an amide into this region of BQCA

(Chapter 2[40]) encouraged us to select this as an appropriate and synthetically-accessible functionality to connect the BQCA scaffold to our methylene linkers.

Project design

Our experimental design was based on the flowchart reported by Lane *et al.* that we have adapted in **Figure 4**.
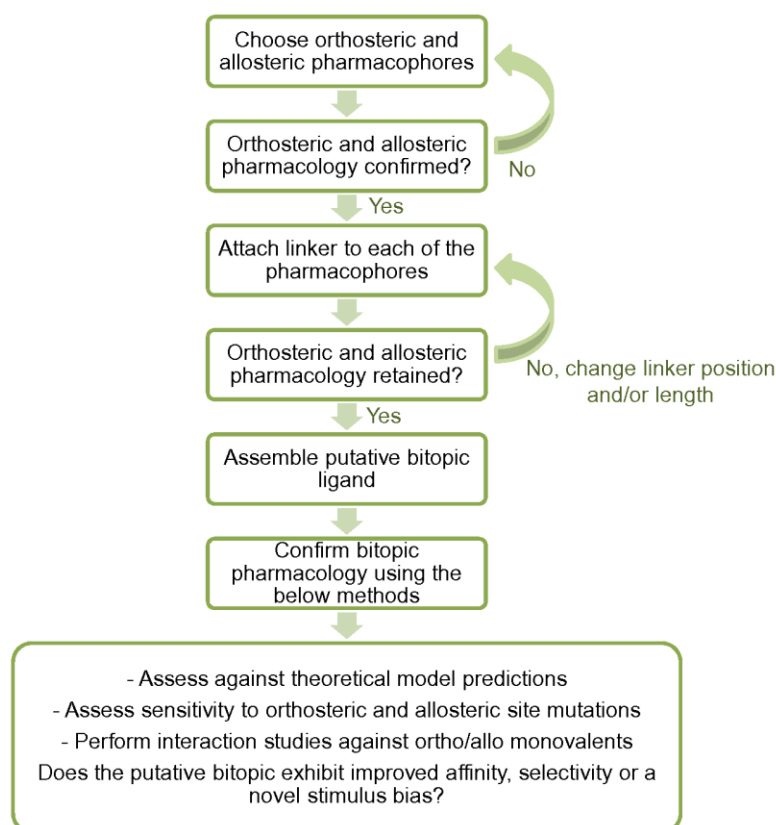
Figure 4. A flowchart describing a method by which bitopic ligands can be rationally designed and experimentally validated (adapted from Lane *et al.*[21])

Iperoxo and BQCA were synthesized and pharmacologically characterized to confirm that they exhibit positive binding and/or functional cooperativity at the M_1 mAChR. Then to assess the feasibility of introducing linkers into these molecules, iperoxo and BQCA

analogues containing 1-, 5- and 9-methylene linkers were synthesized and pharmacologically evaluated for the preservation of their respective orthosteric and allosteric binding and functional profiles (**11**-**15**, **Figure 5**).
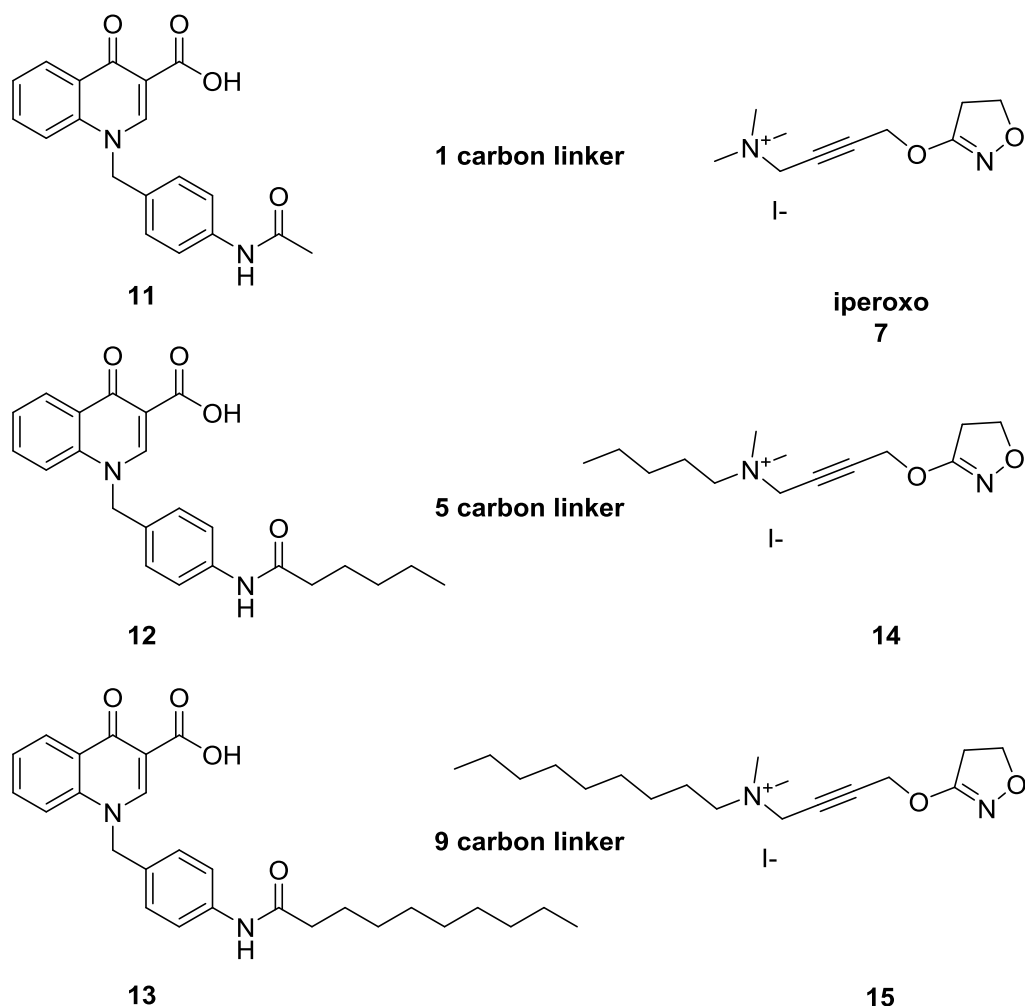
Figure 5. Structures of the BQCA analogues containing 1-, 5- and 9-methylene linkers (11, 12 and 13), iperoxo (7), and analogues containing 5- and 9-methylene linkers (14 and 15)

Finally, two putative bitopic molecules were synthesized and pharmacologically evaluated to estimate affinity and potency at the M_1 mAChR. A bitopic mode of action is yet to be confirmed. All pharmacological assessment was performed in Chinese hamster ovary (CHO)

cells expressing the M_1 mAChR of interest using both radioligand binding and ERK1/2 phosphorylation assays. Pending more detailed pharmacological investigation, these ligands may serve as useful molecular tools or as a starting point for M_1 mAChR-selective therapeutic lead compounds.

Results

Synthesis of iperoxo and BQCA

Iperoxo (**7**) was synthesized in accordance with the convergent procedure reported by Kloeckner *et al.*[41] (**Scheme 1**).
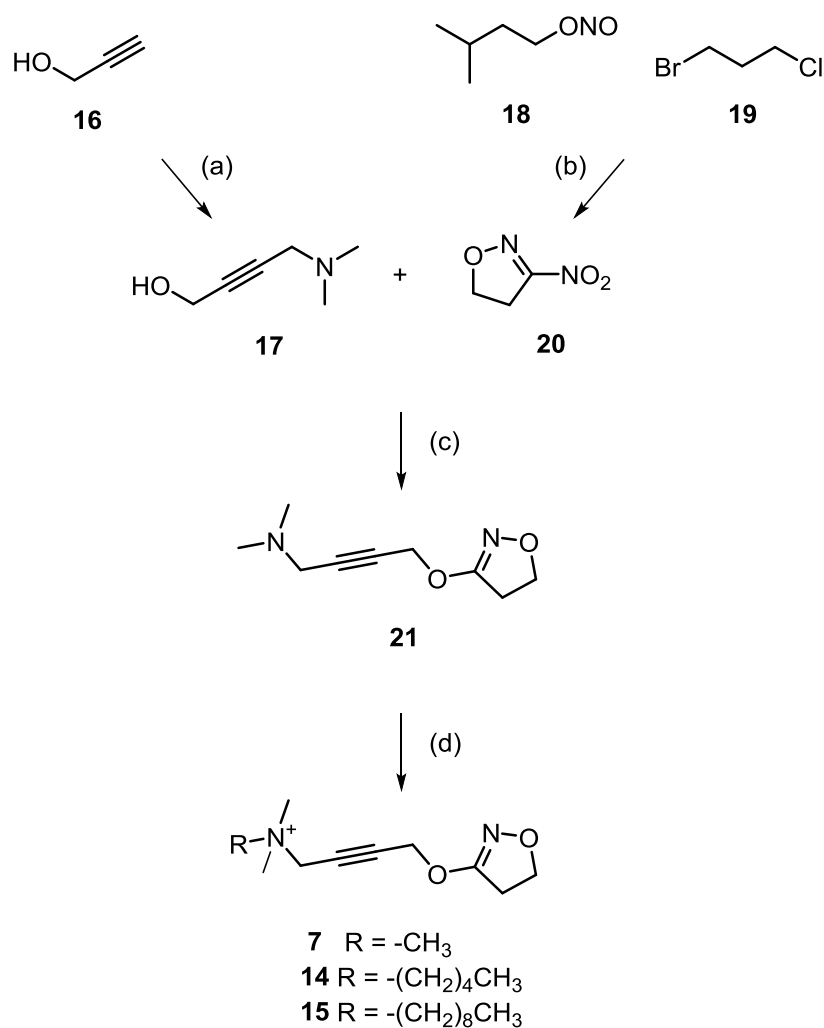
Scheme 1. The synthetic pathway[41] for iperoxo (7) and analogues 14 and 15. Reagents and conditions: (a) dimethylammonium hydrochloride, 40% formaldehyde$_{(aq)}$, CuSO$_4$.5H$_2$O, 2 M NaOH$_{(aq)}$, 80 °C, 20%; (b) sodium nitrite, DMSO, RT, 79%; (c) NaH, dry THF, N$_2$, 65 °C, 80%; (d) iodoalkane, chloroform, RT, 70% (**7**), 46% (**14**), 17% (**15**).

The reaction between isopentyl nitrite (**18**) and 1-bromo-3-chloropropane (**19**) was reproducibly high yielding, despite requiring distillation to isolate the target molecule **20**. Conversely, the yield of **17** was often considerably lower than the 80% quoted in the literature, which may be attributed to the difficulty in extracting the compound into an organic medium following reaction completion; reflecting the isolatable yield, rather than the actual yield. Reaction of **17** and **20** in the presence of sodium hydride under an inert atmosphere gave **21** in excellent yield. Finally, reaction of **21** with iodomethane in chloroform resulted in a white crystalline precipitate that was identified as pure iperoxo (**7**) by ^{1}H NMR with the correct mass obtained by high resolution mass spectrometry (HRMS).

Despite the clean ^{1}H NMR spectrum, the high performance liquid chromatography (HPLC) trace of iperoxo revealed at least two clear peaks suggestive of a substantial impurity (**Figure 6**). Recrystallization failed to resolve this issue, as did re-purifying the starting material **21** and repeating the reaction. We then hypothesized and subsequently confirmed that this effect was due to the presence of the iodide counter-ion, as a HPLC trace of potassium iodide alone produced a similar broad peak at a retention time of 2.4 min (**Figure 6**). The appearance of a second, overlapping peak at this retention time in the iperoxo HPLC trace is possibly the result of ion-exchange occurring in the HPLC column between the iodide ions of the molecule and the trifluoroacetate (TFA) ions routinely included in the HPLC solvent mixture.

BQCA (**10**) was synthesised as described in Chapter 2.
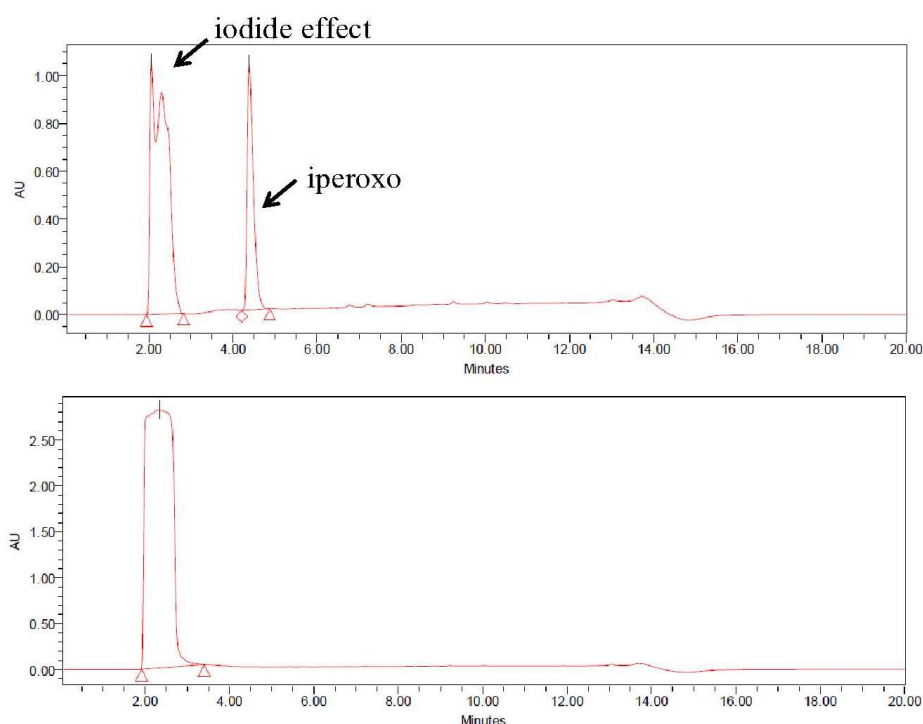
Figure 6. HPLC traces of iperoxo (top) and potassium iodide (bottom); the peak with a retention time of 2.4 min is an artefact resulting from the presence of the iodide ions, the peak with a retention time of 4.5 min is iperoxo

Confirming the positive cooperativity between iperoxo and BQCA

The degree of positive cooperativity between iperoxo and BQCA was assessed by conducting [^{3}H]NMS equilibrium whole cell binding interactions and ERK1/2 phosphorylation functional interactions between the two ligands in CHO cells stably expressing the hM$_1$ mAChR (**Figure 7**). Applying the ternary complex model and the operational model of allosterism to these data confirmed positive binding ($\alpha = 513$) and functional ($\beta = 10$) cooperativity between iperoxo and BQCA, supporting our rationale for linking them together into putative bitopic molecules.
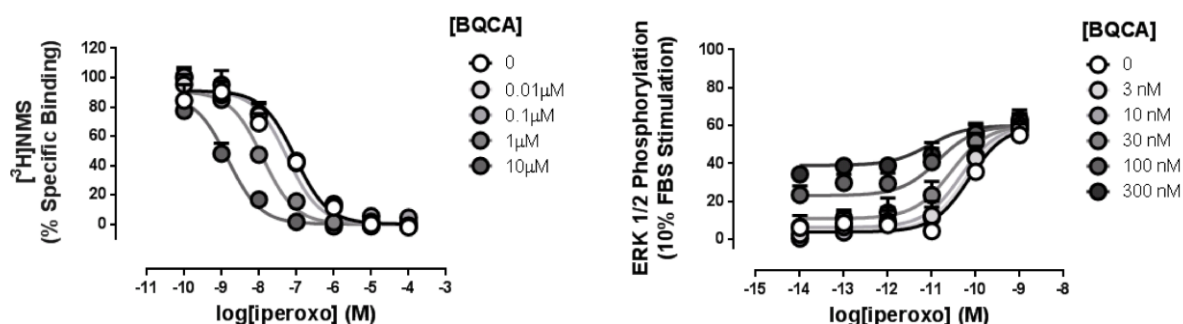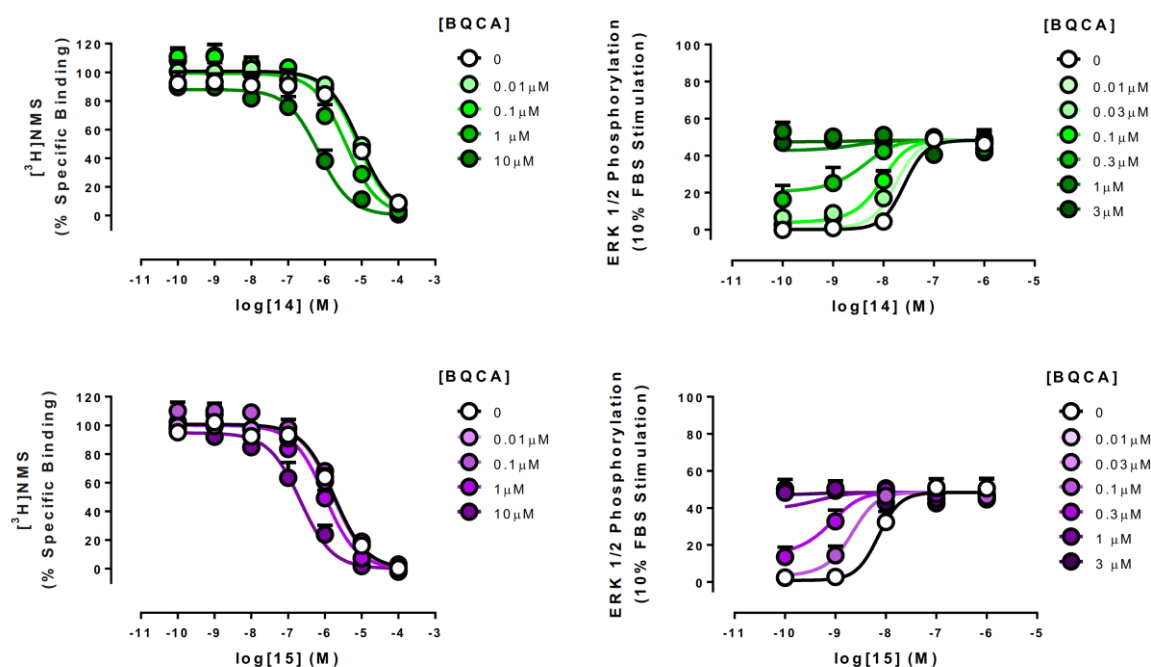
Figure 7. Equilibrium whole cell binding and ERK1/2 phosphorylation functional interaction studies between iperoxo and BQCA (in the presence of a K_D concentration of [³H]NMS in binding). Values represent the mean ± S.E.M. from three experiments performed in duplicate.

Synthesis of analogues of iperoxo and BQCA containing the 1-, 5- and 9-methylene linkers

Iperoxo served as the 1-methylene linker orthosteric ligand. The 5-methylene and 9-methylene iperoxo analogues **14** and **15** were synthesized in the same manner as iperoxo; utilizing 1-iodopentane and 1-iodononane, respectively (**Scheme 1**). The iodide effect was also observed in the HPLC traces of these molecules (see Appendix 5) so the ¹H NMR spectra were used to assess purity.

The *N*-benzylic pendants of the novel BQCA analogues **11** and **13** were synthesized in two steps prior to reaction with the BQCA core (**Scheme 2**). 4-Aminobenzylalcohol (**22**) was reacted with either acetic anhydride or decanoyl chloride to yield the corresponding acetamide **24a** or decanamide **24b**. Functional group interconversion from the alcohol to the bromide employing Appel conditions[42] gave **25a** and **25b** and subsequent *N*-benzylation with 4-oxo-1,4-dihydroquinoline-3-carboxylic acid (synthesized in Chapter 2) gave the target compounds **11** and **13**. Yields were consistently higher for the 1-methylene compounds

compared to the 9-methylene compounds. Surprisingly, this synthetic route was unable to be applied to the 5-methylene analogue **12**. The reaction between 4-aminobenzyl alcohol and hexanoyl chloride resulted in a diacylated product (not shown). Subsequent saponification of the unwanted ester was successful, but attempts to convert the resulting alcohol into the bromide gave an unstable product that degraded during attempted purification by column chromatography. Hence, an alternative 5-step procedure was employed (**Scheme 2**). 4-Aminobenzylamine (**23**) was Boc-protected using Boc-anhydride to form **26** in quantitative yield. Coupling with hexanoyl chloride gave the Boc-protected hexanamide **27** which was then deprotected using trifluoroacetic acid to give **28** in good yield. Reaction with ethyl 3-(dimethylamino)-2-(2-fluorobenzoyl)acrylate, followed by saponification with lithium hydroxide, gave the target 5-methylene analogue **12**.
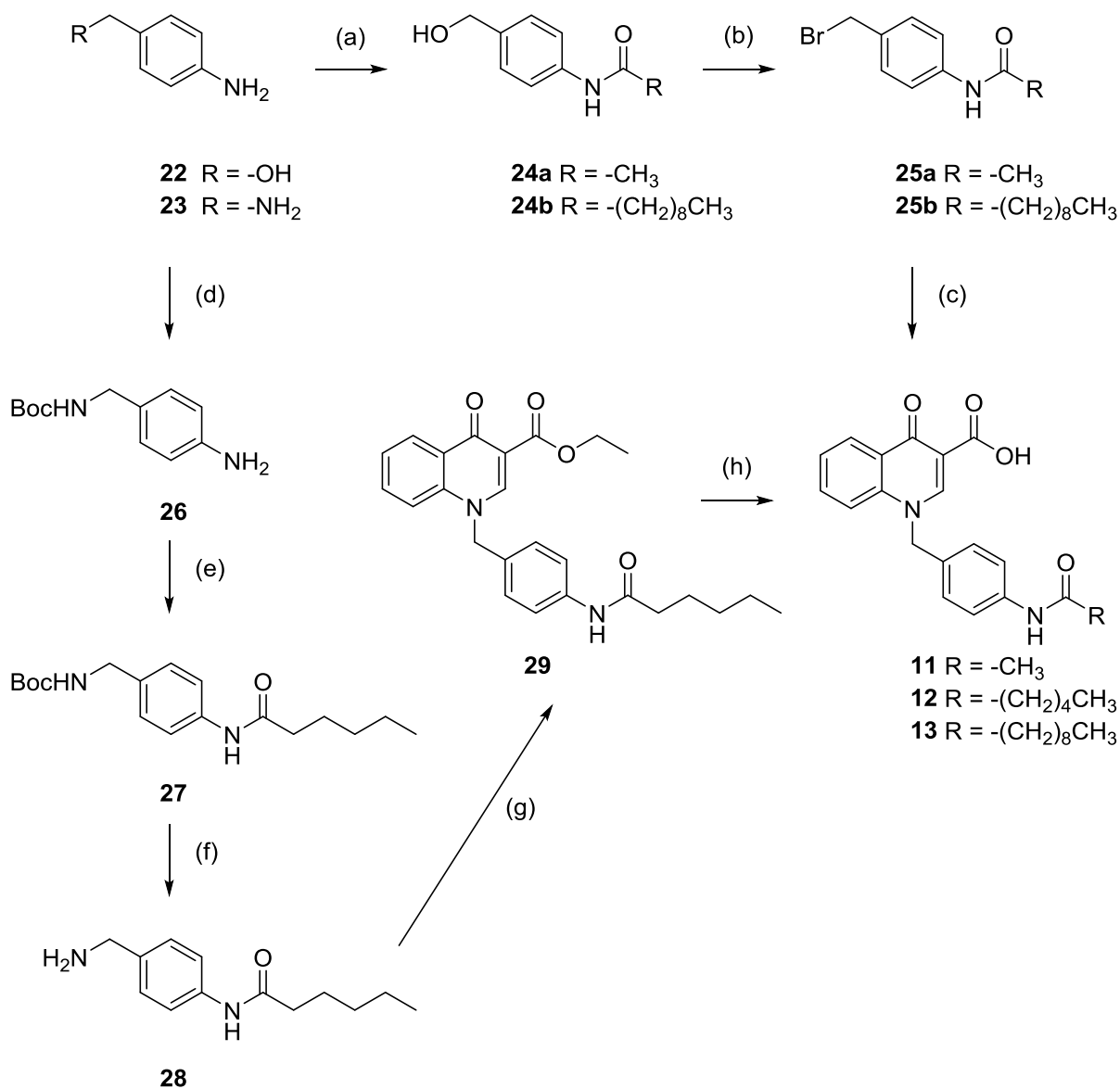
Scheme 2. The synthetic pathway for the BQCA analogues 11, 12 and 13. Reagents and conditions: (a) acetic anhydride or decanoyl chloride, ACN, 0 °C, 78% (**20a**), 55% (**20b**); (b) CBr$_4$, PPh$_3$, ACN, 0-80 °C, 89% (**21a**), 57% (**21b**); (c) 4-oxo-1,4-dihydroquinoline-3-carboxylic acid, DIPEA, ACN, 80 °C, 87% (**7**), 22% (**9**); (d) Di-*tert*-butyl carbamate (Boc anhydride), THF, 0 °C-RT, 100%; (e) hexanoyl chloride, TEA, DCM, 0 °C-RT, 72%; (f) TFA, DCM, 0 °C-RT, 63%; (g) ethyl 3-(dimethylamino)-2-(2-fluorobenzoyl)acrylate, dry DMF, N$_2$, 100 °C, 70%; (h) 1 M LiOH$_{(aq)}$, THF, 80 °C, 38%.

Pharmacological evaluation of analogues of iperoxo and BQCA containing the 1-, 5- and 9-methylene linkers

The same experimental protocols described for iperoxo and BQCA were utilized to investigate the pharmacological profiles of our linker-containing iperoxo and BQCA analogues (**11-15**). The BQCA analogues (**11**, **12**, and **13**) were interacted with iperoxo (**Figure 8, Table 1**) and the iperoxo analogues (**14** and **15**) were interacted with BQCA (**Figure 9, Table 1**). The BQCA analogue **11**, containing the 1-methylene linker, still behaved as a PAM of iperoxo though with a markedly reduced binding cooperativity (from $\alpha = 513$ to $\alpha = 4$). Replacement of the 4-methoxy group with a bulkier acetamide functionality may have disrupted the alignment of the benzylic pendant of BQCA with the W400 amino acid residue in TM7; this residue is postulated to form a $\pi-\pi$ interaction with the benzylic pendant and appears to be critical for BQCA binding and cooperativity transmission.[32] Interestingly, the 5-methylene linker BQCA analogue **12**, whilst maintaining a comparable degree of binding cooperativity to that of **11**, actually elicited an increase in functional cooperativity with iperoxo exceeding that of the parent molecule (from $\beta = 10$ to $\beta = 33$). This suggests that this linker is engaging additional interactions or that the molecule as a whole is adopting a subtly different pose to BQCA that may be facilitating the enhanced transmission of functional cooperativity. The 9-methylene linker BQCA analogue **13**, whilst clearly still binding to the M_1 mAChR, exhibited close to neutral cooperativity with iperoxo. Its pharmacological profile suggests that it may be behaving as either a neutral allosteric modulator or a competitive agonist. In the case of the former, introduction of the linker appears to have dramatically compromised the conformational compatibility, and hence positive cooperativity, observed between iperoxo and BQCA (from $\alpha\beta = 5012$ to $\alpha\beta = 0.89$); either by disrupting interactions that BQCA usually adopts with residues that propagate positive cooperativity, or by engaging additional interactions that do not favour co-binding

with iperoxo. In the case of the latter, **13** may be bridging both the orthosteric and allosteric sites, with the linker extending into the orthosteric pocket and giving rise to a competitive relationship with iperoxo.
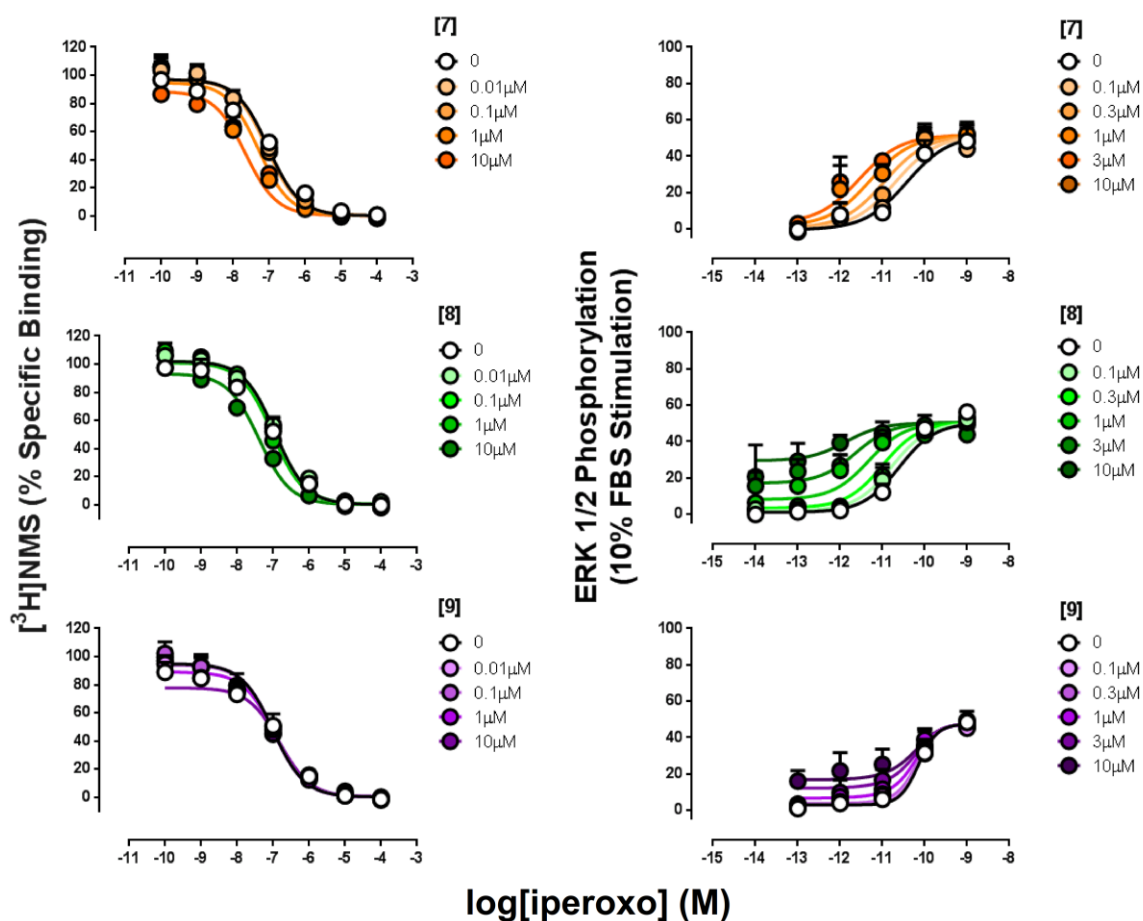
Figure 8. Equilibrium whole cell binding and ERK1/2 phosphorylation functional interaction studies between iperoxo and the BQCA analogues 11-13 (in the presence of a K_D concentration of [^{3}H]NMS in binding). Values represent the mean ± S.E.M. from three experiments performed in duplicate.

The equilibrium dissociation constants of both iperoxo analogues **14** and **15** were lower than that of iperoxo, however both were still able to fully displace [^{3}H]NMS binding.

Furthermore, both analogues retained high positive binding cooperativity with BQCA, though not as pronounced as that of iperoxo.

Figure 9. Equilibrium whole cell binding and ERK1/2 phosphorylation functional interaction studies between the iperoxo analogues 14-15 and BQCA (in the presence of a K_D concentration of [^{3}H]NMS in binding) Values represent the mean ± S.E.M. from three experiments performed in duplicate.

Taken together, we can conclude that the attachment of methylene linkers to the *para*-position of the benzylic pendant of BQCA and the tertiary amine of iperoxo does not abolish binding at the M$_1$ mAChR. Furthermore, these results demonstrate that the allosteric character of BQCA is preserved in analogues **11** and **12**, whereas **13** may be behaving in a neutral allosteric or competitive manner, and analogues **14** and **15** maintain the orthosteric profile of the parent molecule iperoxo. An undeniable caveat of this approach is that there is no guarantee that the individual interacting ligands are adopting the same binding poses as

they would if they were pharmacophores within a single bitopic molecule. None the less, these results provide us with a reasonable rationale for the synthesis of the commensurate putative bitopic molecules.

Table 1. Equilibrium dissociation constants in competition with [³H]NMS and binding and functional cooperativity parameters for BQCA, BQCA analogues 11-13, iperoxo and iperoxo analogues 14-15

	$pK_B{}^a$	$\log\alpha\beta_{[iperoxo]}\,(\alpha\beta)^b$	$\log\alpha_{[iperoxo]}\,(\alpha)^c$	$\beta_{[iperoxo]}{}^d$
BQCA	4.12	3.70 ± 0.24 (5012)	2.71 ± 0.09 (513)	10
11	5.47	1.47 ± 0.24 (30)	0.62 ± 0.11 (4)	7
12	4.49	2.22 ± 0.23 (166)	0.71 ± 0.15 (5)	33
13	5.75	-0.05 ± 0.22 (0.89)	-0.48 ± 0.19 (0.33)	3
	$pK_A{}^a$	$\log\alpha\beta_{[BQCA]}\,(\alpha\beta)^b$	$\log\alpha_{[BQCA]}\,(\alpha)^c$	$\beta_{[BQCA]}{}^d$
Iperoxo	7.38	3.70 ± 0.24 (5012)	2.71 ± 0.09 (510)	10
14	5.46	2.41 ± 0.27 (257)	1.35 ± 0.21 (22)	11
15	6.23	2.57 ± 0.18 (372)	1.80 ± 0.12 (63)	6

Estimated parameter values represent the mean ± S.E.M. from three to four experiments performed in duplicate

[a] Negative logarithm of the equilibrium dissociation constant of each ligand
[b] Logarithm (and antilogarithm) of the product of the binding and activation cooperativity factors between the orthosteric ligand and the allosteric ligand
[c] Logarithm (and antilogarithm) of the binding cooperativity factor between the orthosteric ligand and the allosteric ligand
[d] Logarithm (and antilogarithm) of the activation cooperativity factor between the orthosteric ligand and the allosteric ligand (derived by fixing the binding cooperativity value to that estimated for each ligand in whole cell binding experiments – Log α)

Synthesis of the 1-, 5- and 9-methylene linker putative bitopic molecules

Synthesis of the target putative bitopic molecules proved to be more challenging than expected, with three different synthetic approaches and some design modification undertaken before two of the three molecules were successfully synthesized.

Approach 1 (Scheme 3)

Compounds **30a** and **30b** were synthesized according to Chapter 2. Reaction between **30a** and bromoacetyl bromide gave **31a** in good yield. This compound was subsequently reacted with iperoxo analogue **21** in a nucleophilic substitution reaction to form the target 1-methylene putative bitopic molecule **33a**, which was easily isolated in good yield following precipitation from the reaction mixture and required no further purification. Reaction of either **30a** or **30b** with either 6-bromohexanoyl chloride or 10-bromodecanoyl chloride gave rise to complex mixtures that were difficult to separate by column chromatography. Hence, an alternative method was employed for the synthesis of **31b** and **31c**. Compound **30b** was reacted with either 6-bromohexanoic acid or 10-bromodecanoic acid using a peptide coupling reagent (either COMU or HCTU, respectively) and DIPEA in DMF to give **31b** and **31c** in modest yields. Compounds **31b** and **31c** were reacted in the same manner as **31a** to give the penultimate 5-methylene and 9-methylene putative bitopic esters **32b** and **32c**.
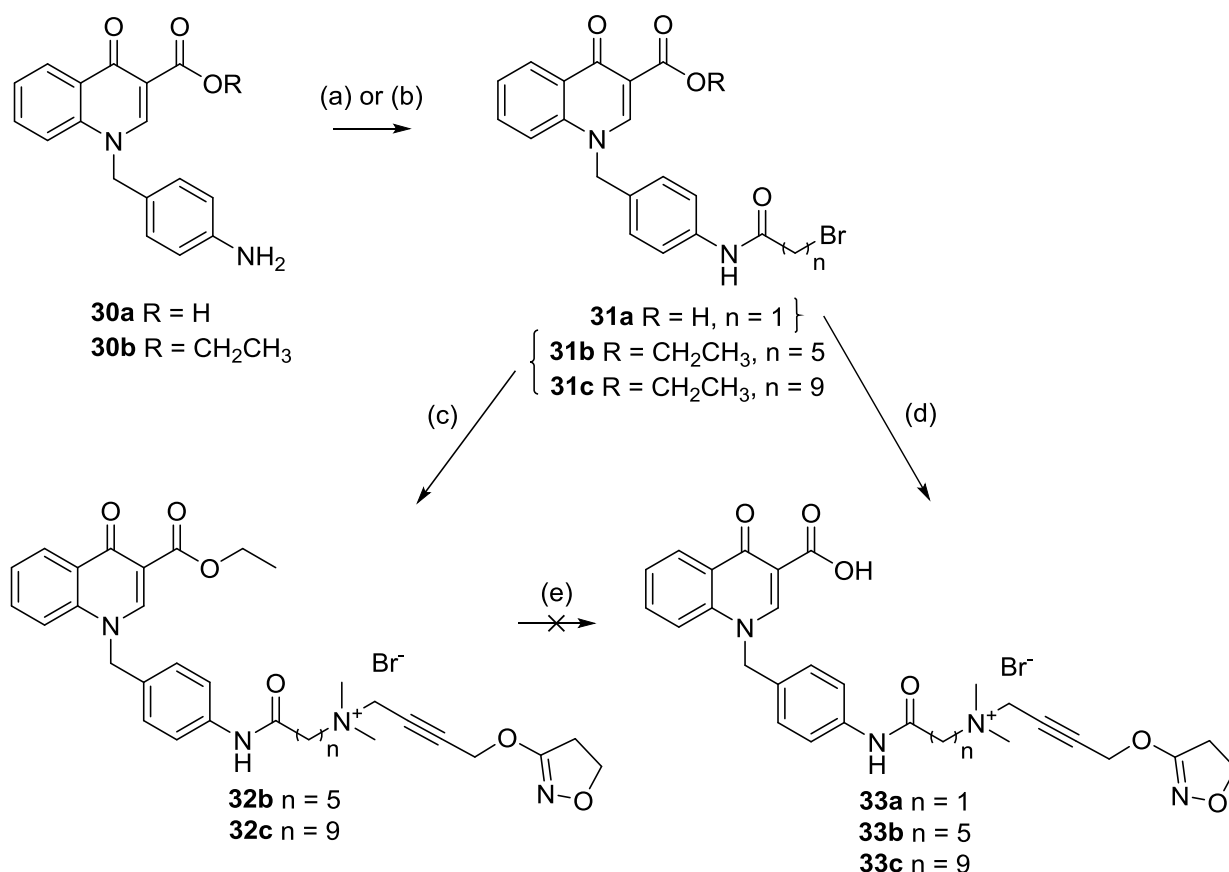
Scheme 3. The synthetic pathway for the putative bitopic iperoxo-BQCA hybrid molecules 33a, 33b and 33c. Reagents and conditions: (a) bromoacetyl bromide, TEA, ACN, -80 °C-RT, 74% (**27a**); (b) 6-bromohexanoic acid or 10-bromodecanoic acid, COMU or HCTU, DIPEA, DMF, 0 °C - RT, 34% (**27b**), 21% (**27c**); (c) 4-((4,5-dihydroisoxazol-3-yl)oxy)-N,N-dimethylbut-2-yn-1-amine (**21**), ACN, 80 °C, 83% (**28b**), 24% (**28c**); (d) 4-((4,5-dihydroisoxazol-3-yl)oxy)-N,N-dimethylbut-2-yn-1-amine (**21**), ACN, 80 °C, 78%; (e) LiOH.H₂O, distilled H₂O, 0 - 70 °C or HBr (33% w/w in acetic acid), distilled H₂O, 0 - 80 °C.

Attempts to cleave the ester via saponification appeared to result in nucleophilic attack of the C=N bond of the dihydrooxazole within the iperoxo moiety and hydrolysis to form the alcohol (**Figure 10**) as indicated by LCMS (Appendix 5); though this molecule was never

isolated from the complex mixture. Attempts to cleave the ester under acidic conditions resulted in hydrolysis of the amide to the ammonium bromide salt (**Figure 11**) as confirmed by ^{1}H NMR and LCMS (Appendix 5).
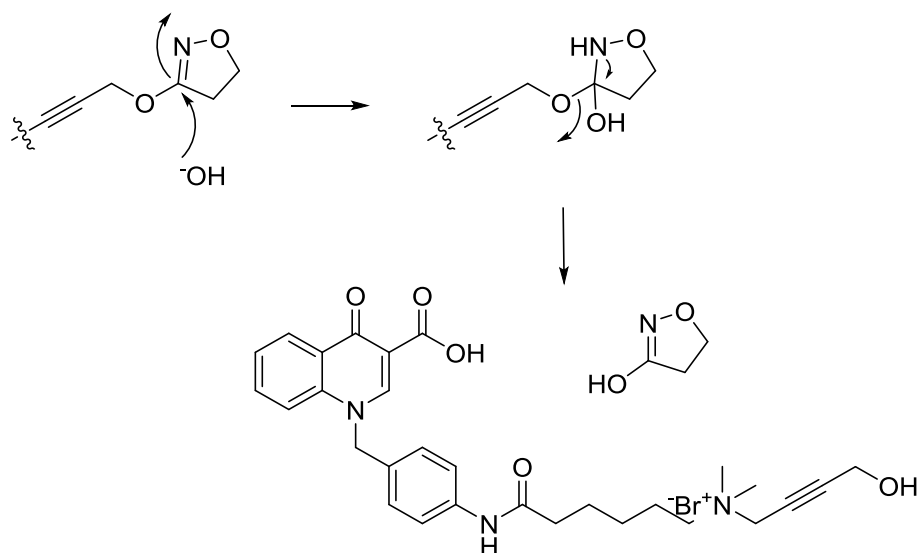
Figure 10. Proposed mechanism for the base-catalyzed side reaction of 32b
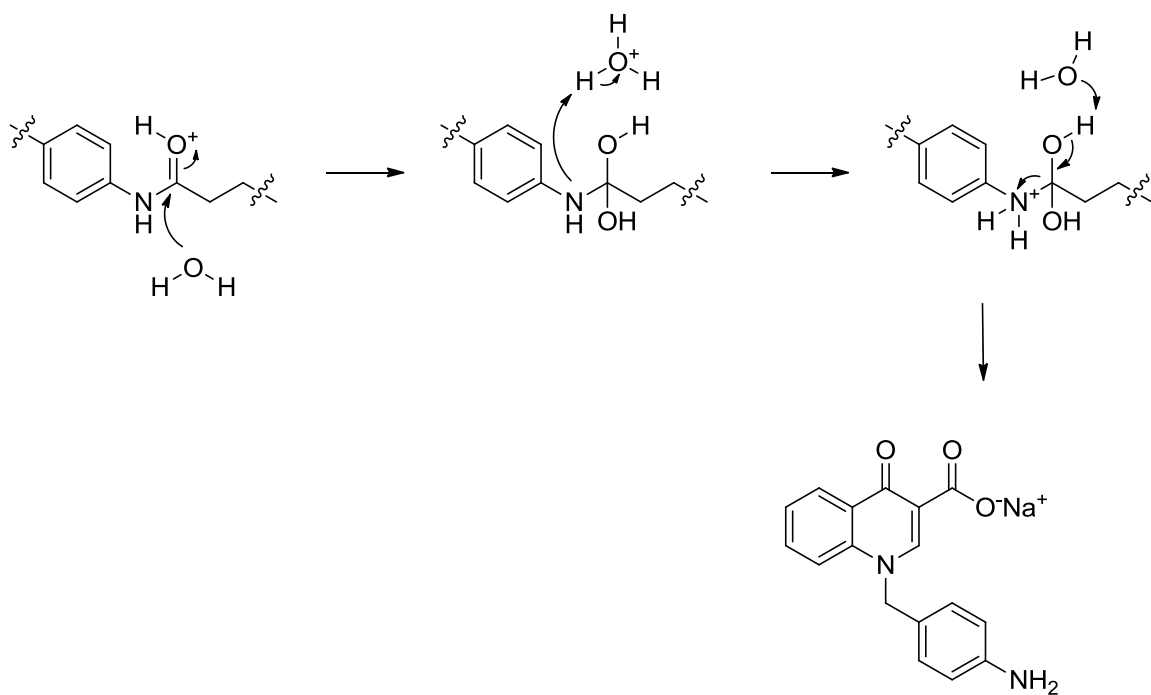
Figure 11. Proposed mechanism for the acid-catalyzed side reaction of 32b

Approach 2 (Scheme 4)

An alternative approach, focussing on the 5-methylene putative bitopic molecule, was undertaken whereby the ester was converted to the acid earlier in the synthesis to avoid the complications experienced in the final step in Approach 1. A coupling reaction between **30b** and 6-hydroxyhexanoic acid gave **34** in moderate yield, and subsequent ester saponification gave **35** in quantitative yield.
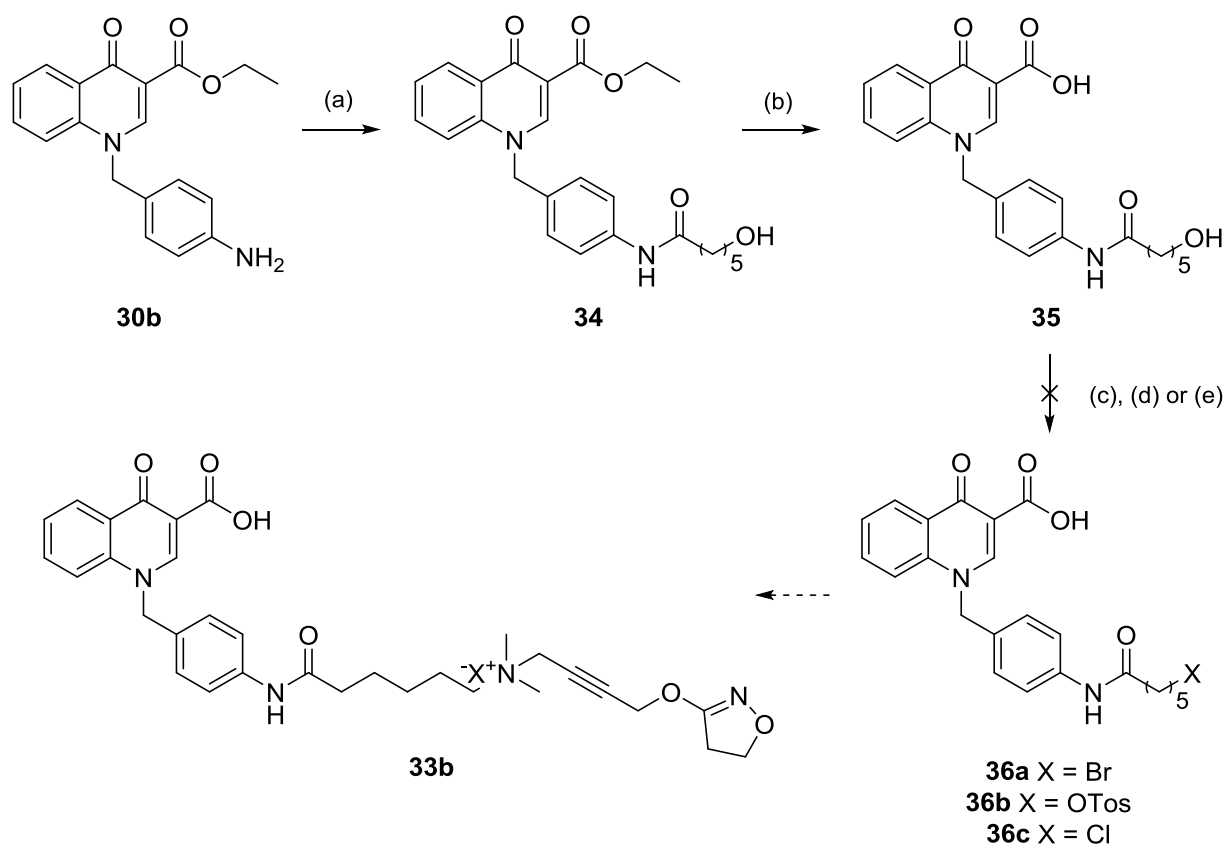
Scheme 4. The synthetic pathway for the putative bitopic iperoxo-BQCA hybrid molecule 33b. Reagents and conditions: (a) 6-hydroxyhexanoic acid, COMU, DIPEA, DMF, 0 °C - RT, 53%; (b) 1 M KOH$_{(aq)}$, 3:1 MeOH:water, 80 °C, quantitative; (c) CBr$_4$, PPh$_3$, ACN, 0-80 °C; (d) tosyl chloride, TEA, DCM, RT; (e) thionyl chloride (in ACN or neat), 0-80 °C.

Unfortunately, attempts to convert the alcohol of **35** into a suitable leaving group prior to quaternization were unsuccessful. No reaction was observed under Appel conditions, whereas tosylation and chlorination both resulted in complex mixtures, most likely due to the reactivity of the carboxylic acid.

Approach 3 (Scheme 5)

Given that the presence of the carboxylic acid moiety was clearly impeding the completion of the synthesis, it was decided to replace it with a functionality less likely to pose a synthetic liability. The (1*S*, 2*S*)-2-hydroxycyclohexyl amide was selected as it has previously been incorporated into the BQCA scaffold without affecting a loss of M_1 mAChR affinity and leading to a gain in positive cooperativity with ACh (**Figure 12**).[43] The approach involved installing the carboxamide moiety into the BQCA scaffold prior to linker attachment and reaction with iperoxo analogue **21**.

37
pK_B = 5.0
αβ = 205

38
pK_B = 5.0
αβ = 840
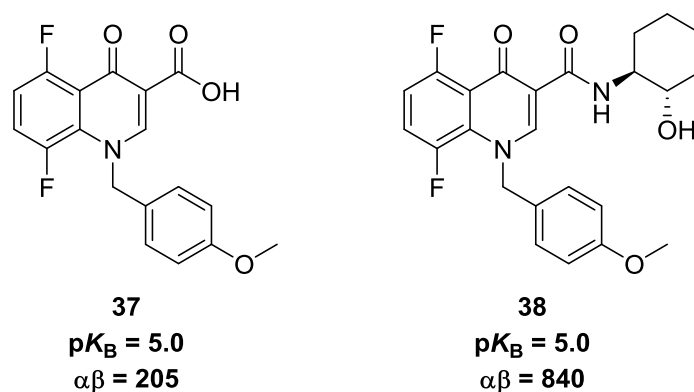
Figure 12. Structures of 37 and 38, fluorinated BQCA analogues that illustrate the preserved affinity and improved cooperativity observed upon replacement of the carboxylic acid with the (1*S*, 2*S*)-2-hydroxycyclohexyl amide
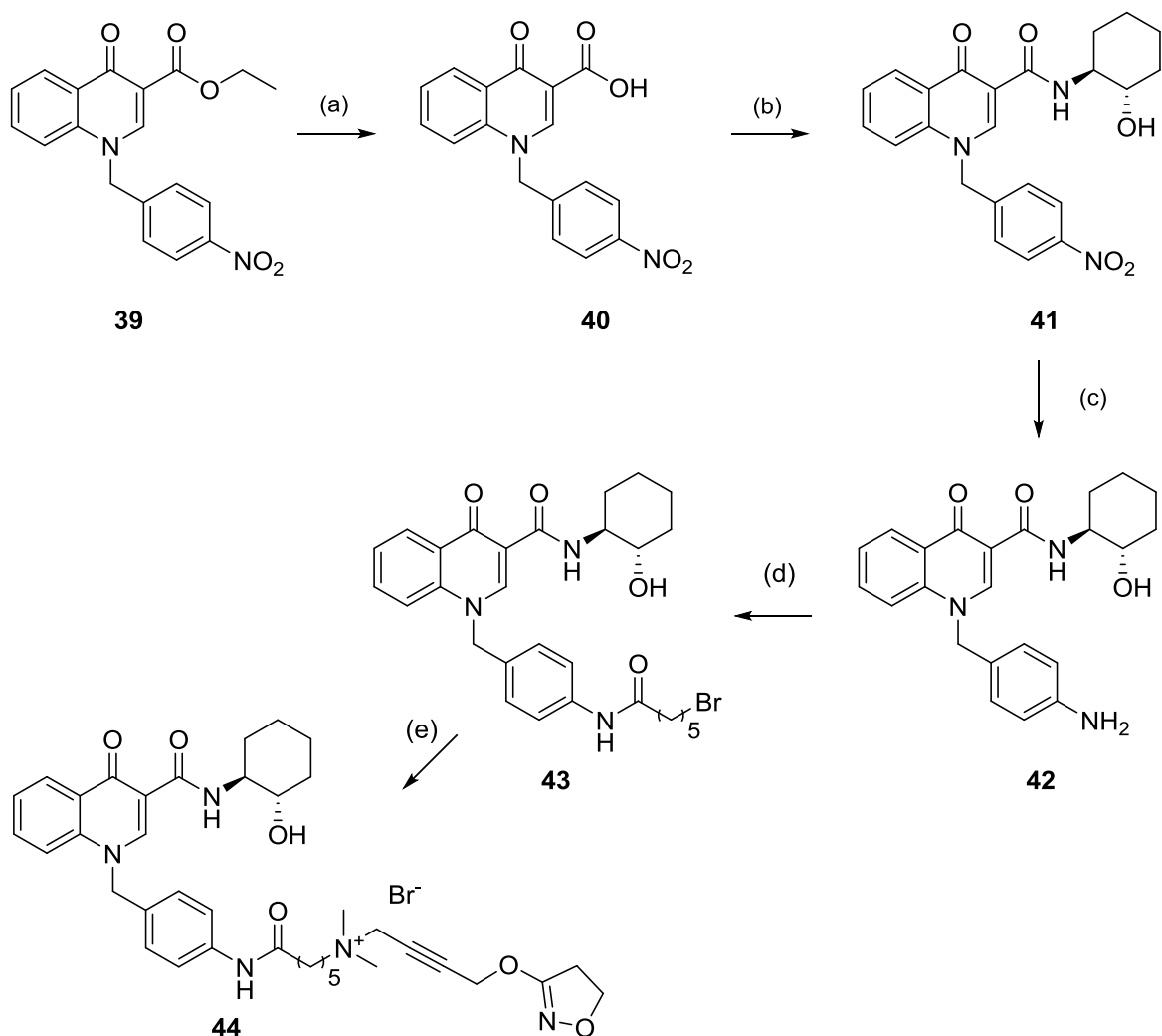
Scheme 5. The synthetic pathway for the putative bitopic iperoxo-BQCA hybrid molecule 44. Reagents and conditions: (a) LiOH.H$_2$O$_{(s)}$, 1:1 THF:water, RT, 57%; (b) (1*S*,2*S*)-2-aminocyclohexanol hydrochloride, HCTU, DIPEA (in DCM), DMF, RT, 97%; (c) H$_2$, 10% Pd/C, DMF, RT, 92%; (d) 6-bromohexanoic acid, HCTU, DIPEA (in DCM), DMF, RT, 75%; (e) 4-((4,5-dihydroisoxazol-3-yl)oxy)-*N*,*N*-dimethylbut-2-yn-1-amine (**21**), ACN, 80 °C, 36%.

Ester saponification of **39** using lithium hydroxide gave **40** in moderate yield. HCTU coupling of **40** and (1*S*,2*S*)-2-aminocyclohexanol hydrochloride gave **41**, which was then subjected to hydrogenation conditions to give **42** in excellent yield. A second HCTU coupling

between **42** and 6-bromohexanoic acid gave **43** with a yield of 85%, though a purity of only 70%. As **43** and the associated impurities were all organic-soluble, and the product of the next and final step was a salt expected to be aqueous-soluble, crude **43** was carried through without any further purification. Compound **44** was isolated as a clear, colourless oil following extraction into the aqueous layer with a yield of 25% (over two steps) and a purity >95%.

Pharmacological evaluation of the 1- and 5-methylene linker putative bitopic molecules

Equilibrium whole cell binding and ERK1/2 phosphorylation functional assays were performed to estimate an affinity and potency value, respectively, for BQCA, iperoxo and our putative bitopic molecules **33a** and **44** (**Figure 13**, **Table 2**). The BQCA and iperoxo affinity values estimated from the interaction studies detailed in **Figure 8**, **Figure 9** and **Table 1** are slightly though not significantly different to that obtained from the experiments depicted in **Figure 13** and **Table 2**.

Table 2. Estimates of affinity (pK_A) and potency (pEC$_{50}$) for ACh, BQCA, iperoxo and the putative bitopic molecules 33a and 44

	BQCA	Iperoxo	33a	44
pK_A	4.44 ± 0.07	7.02 ± 0.10	6.58 ± 0.06	6.65 ± 0.12
pEC$_{50}$	6.68 ± 0.13	10.27 ± 0.13	7.59 ± 0.12	8.13 ± 0.14
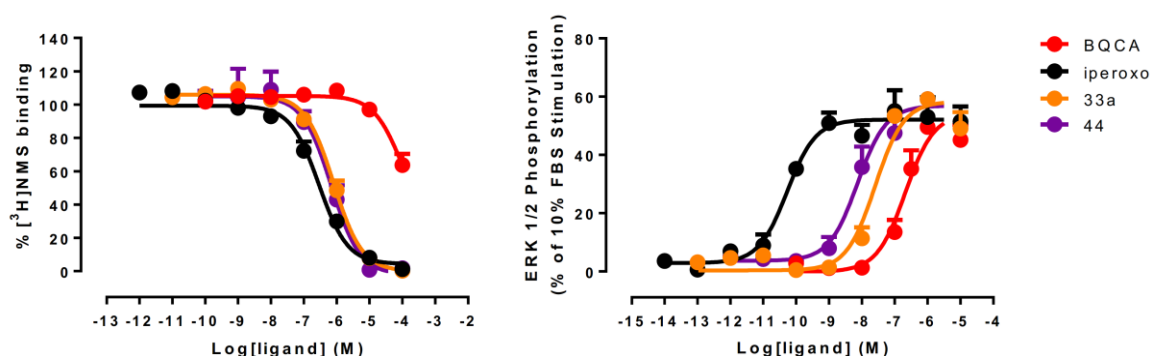
Figure 13. Equilibrium whole cell binding and ERK1/2 phosphorylation functional assays (n=3) for ACh, BQCA, iperoxo and the putative bitopic molecules 33a and 44 (in the presence of a fixed concentration of [³H]NMS in binding)

The high affinity of iperoxo was preserved in **33a** and **44**, and both ligands were able to completely inhibit [³H]NMS binding, however a 2-3 log unit reduction in potency was observed (**Figure 13**, **Table 2**). This suggests that the iperoxo pharmacophore of both ligands is binding to the receptor, but that the presence of the BQCA pharmacophore is detrimental to the potency of the ligands. This may be occurring through local alteration of the orthosteric binding domain such that the iperoxo pharmacophore is precluded from forming the necessary interactions that elicit its high potency, or through a global shift in the receptor conformation such that functional signalling via the MAP kinase pathway is impaired. The two pharmacophores are clearly not able to interact with the receptor in the same manner as the parent molecules, otherwise we would expect an improvement in both affinity and potency compared to iperoxo indicative of positive cooperativity between the two pharmacophores. This suggests that both the 1-methylene and the 5-methylene linker are of insufficient length for the ligand to successfully bridge the two parent ligand binding sites simultaneously. This does not necessarily mean that the ligands are not binding bitopically.

We speculate that, whilst the iperoxo pharmacophore is likely binding to the orthosteric site in a manner similar to the parent molecule, the BQCA pharmacophore is interacting with a region of the receptor above the orthosteric cavity which, though distinct from the BQCA binding site, is also distinct from the orthosteric site. We also propose that the interactions formed by the BQCA pharmacophore with this site are not entirely unfavourable; **44** shows improved affinity and potency compared to the values obtained for the 5-methylene iperoxo analogue **14**.

Discussion

This chapter describes the early stages of development of rationally-designed putative bitopic ligands for the M$_1$ mAChR. The constituent molecules BQCA and iperoxo were selected, synthesized and their positive binding and functional cooperativity was confirmed. Linker-containing analogues of BQCA and iperoxo were synthesized and pharmacological analysis suggested that the respective orthosteric or allosteric pharmacology of almost all analogues was preserved, with the exception of **13**. Finally, two putative bitopic ligands, **33a** and **44**, were synthesized, though this required some design modification in order to be achieved. Both ligands were still able to bind to and activate the M$_1$ mAChR. As alluded to in the flowchart in **Figure 4**, more detailed pharmacological analysis will be required to ascertain the binding mode of **33a** and **44** to the M$_1$ mAChR. One approach would be to determine the affinity and potency of these ligands at M$_1$ mAChRs containing point mutations shown to affect orthosteric and allosteric pharmacology. Tyr381 is thought to form a hydrogen bond and a cation-π interaction that are crucial for orthosteric ligand binding and stabilization of an active receptor state; the Tyr381Ala mutation diminishes both ACh binding and receptor activation at the M$_1$ mAChR.[44] Trp400 is thought to form a π–π stacking interaction with the benzyllic pendant of BQCA and has been shown to be critical for the modulatory behaviour of the ligand;[23,32] the Trp400Ala mutation completely abolishes the high degree of positive cooperativity observed between orthosteric agonists and BQCA. Examining the binding and functional profile of **33a** and **44** in the presence of either of these mutants may reveal whether they are engaging the receptor in a bitopic manner. Though, given our hypothesis that the allosteric pharmacophore of these ligands may be unable to interact with the binding site of the parent molecule BQCA, the Trp400Ala mutation may not be particularly informative. A more definitive approach for ascertaining

whether these ligands are engaging with an allosteric site is radioligand dissociation kinetics. The ability of allosteric/bitopic ligands to alter the dissociation kinetics of radio-labelled orthosteric ligands (where purely orthosteric ligands will not) is well-established at mAChRs[45] and was employed in validating a bitopic mechanism of action for TBPB at the M_1 mAChR.[13]

Regardless of the outcome of such experiments, further synthetic chemistry undertakings will be necessary to advance this project. Firstly, as the (1*S*, 2*S*)-2-hydroxycyclohexyl amide proved to be more synthetically tractable than the carboxylic acid of BQCA, it will be important to synthesize and pharmacologically evaluate linker-containing BQCA analogues and a 1-methylene putative bitopic ligand containing this functionality for the sake of comparison with **44**. It would also be valuable to attempt the synthesis of putative bitopic molecules containing longer linkers, such as 9- and 13-methylene units, to examine whether the parent BQCA binding mode can be accessed by the allosteric pharmacophore, what linker length is necessary to achieve this bridging of the two sites and if the high positive cooperativity between the two parent ligands can be recapitulated. Indeed, the ability of the allosteric pharmacophore to comfortably adopt a similar orientation to BQCA is likely to be essential if M_1 mAChR selectivity is to be preserved. This is due to BQCA's high degree of receptor subtype selectivity being proposed to arise via selective transmission of cooperativity via a distinct complement of residues at the M_1 mAChR, rather than by it interacting with a binding site unique to the receptor.[32] Substantial deviations from the binding mode of BQCA will likely result in abolishment of any selectivity we might expect the allosteric pharmacophore to confer.

Pending such experiments, these putative bitopic ligands may prove to be interesting tools for exploring structural and functional phenomena at the M_1 mAChR and may in time serve as templates for the design of novel lead drug candidates for this receptor.

Experimental

Chemistry

General

All materials were reagent grade and purchased commercially from Sigma-Aldrich or Matrix Scientific. Anhydrous solvents were obtained from a MBraun MB SPS-800 Solvent Purification System. Analytical thin layer chromatography (TLC) was performed on Silica Gel 60 F_{254} pre-coated plates (0.25 mm, Merck ART 5554) and visualized by ultraviolet light, iodine or ninhydrin as necessary. Silica gel 60 (Fluka) was used for silica gel flash chromatography. Microwave reactions were performed in a CEM Discover microwave reactor. Melting points (mp) were determined on a Mettler Toledo- MP50 Melting Point System.

^{1}H NMR spectra were routinely recorded at 400 MHz using a Brüker Avance 400 MHz Ultrashield Plus spectrometer equipped with a Silicon Graphics workstation. Chemical shifts (δ_H) for all ^{1}H NMR spectra are reported in parts per million (ppm) using the centre peak of the deuterated solvent chemical shift as the reference: $CDCl_3$ (7.26) and d_6-DMSO (2.50).[46] Each resonance was assigned according to the following convention: chemical shift (δ) (multiplicity, coupling constant(s) in Hz, number of protons, and assignment). Coupling constants (J) are reported to the nearest 0.5 Hz. In reporting spectral data the following abbreviations have been used: s, singlet; d, doublet; t, triplet; q, quartet; p, pentet; m, multiplet; br, broad; app, apparent; as well as combinations of these where appropriate.

^{13}C NMR spectra were routinely recorded at 100 MHz using a Brüker Avance 400 MHz Ultrashield Plus spectrometer equipped with a Silicon Graphics workstation. Chemical shifts (δ_C) for all ^{13}C NMR spectra are reported in parts per million (ppm), using the centre peak of

the deuterated solvent chemical shift as the reference: CDCl$_3$ (77.16) and d_6-DMSO (39.52).[46]

HSQC, HMBC and COSY spectra were obtained using the standard Brüker pulse sequence to assist with structural assignment of the compounds.

Liquid Chromatography-Mass Spectrometry (LCMS) was performed on an Agilent 1200 Series coupled to the 6120 quadrupole mass spectrometer. Elution was also monitored at 254 nm. HRMS analyses were recorded in the specified ion mode using a LCT Premier XE TOF Mass Spectrometer coupled to 2795 Alliance Separations Module at cone voltages of 45 V (ESI+) and 60 V (ESI-).

Analytical reverse-phase HPLC was performed on a Waters HPLC system using a Phenomenex® Luna C8 (2) 100Å column (150 × 4.6 mm, 5 μm) and a binary solvent system; solvent A: 0.1% TFA/H$_2$O; solvent B: 0.1% TFA/80% MeOH/H$_2$O. Isocratic elution was carried out using the following protocol (time, % solvent A, % solvent B): 0 min, 100, 0; 10 min, 20, 80; 11 min, 20, 80; 12 min, 100, 0; 20 min, 100, 0; at a flow rate of 1.0 mL/min monitored at 254 nm using a Waters 996 Photodiode Array detector.

Characterization requirements for intermediate compounds were set as: mp (if solid and >90% pure), ^{1}H NMR, ^{13}C NMR, LCMS and HPLC (254 nm) or LCMS purity. Characterization requirements for final compounds were set as: mp, ^{1}H NMR, ^{13}C NMR, LRMS, HRMS, and HPLC (254 nm and 214 nm) purity >95%.

Synthesis of 3-nitro-4,5-dihydroisoxazole (20)
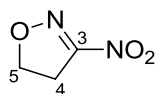
1-Bromo-3-chloropropane (**19**) (2.52 mL, 25.4 mmol) was added dropwise to a stirred mixture of isopentyl nitrite (**18**) (5.12 mL, 38.1 mmol) and sodium nitrite (3.51 g, 50.8 mmol)

in dimethylsulfoxide (45 mL). After stirring for 24 h at RT the reaction mixture was poured into ice water and extracted with dichloromethane (3 × 30 mL). The combined organic fractions were dried over MgSO$_4$, filtered and the solvent evaporated *in vacuo* to give a crude oil. Distillation (60 °C, 1.1 mmHg) yielded the target compound as a thin yellow oil. To remove residual dimethylsulfoxide, the product was redissolved in ethyl acetate (10 mL), washed with brine (2 × 20 mL) and the organic layer dried over anhydrous MgSO$_4$, filtered and the solvent evaporated *in vacuo*. 2.34 g, 79%; δ_H (CDCl$_3$) 4.83 (t, J= 11.0 Hz, 2H, H5), 3.45 (t, J= 11.0 Hz, 2H, H4); δ_C (CDCl$_3$) 75.5 (CH$_2$), 40.8 (C), 30.7 (CH$_2$); *m/z* HRMS (TOF ES$^+$) C$_3$H$_4$N$_2$O$_3$ [MH]$^+$ calcd 116.0223, found 117.0296; HPLC: t_R = 3.33 min, purity (214) = 96.1%.

Synthesis of 4-(dimethylamino)but-2-yn-1-ol (17)
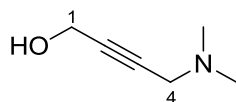
Dimethylammonium hydrochloride (**16**) (5.45 g, 66.9 mmol) was dissolved in deionized water and adjusted to pH 9 using 2 M NaOH. 40% aqueous formaldehyde solution (9.19 mL, 91 mmol), propargyl alcohol (3.16 mL, 53.5 mmol) and CuSO$_4$.5H$_2$O (414 mg, 1.66 mmol) dissolved in deionized water were added, and the reaction mixture adjusted to pH 8 using 2 M NaOH. After stirring for 1.5 h at 80 °C, the reaction mixture was poured into 25% aqueous ammonia solution (15 mL) and the solvent evaporated *in vacuo* to yield a golden brown oil with a strong hazelnut odour. This crude oil was dissolved in 2 M HCl and extracted once with ethyl acetate (20 mL). The aqueous layer was then basified to pH 9 using 2 M NaOH and extracted with ethyl acetate (5 × 20 mL). The organic fractions were dried over anhydrous MgSO$_4$, filtered and the solvent evaporated *in vacuo* to yield the target molecule

as a dark yellow oil. 1.24 g, 20%; δ_H (CDCl$_3$) 4.29 (s, 2H, H1), 4.06 (br s, 1H, OH), 3.27 (s, 2H, H4), 2.31 (s, 6H, N(CH_3)$_2$); δ_C (CDCl$_3$) 84.1 (C), 80.1 (C), 50.7 (CH$_2$), 48.0 (CH$_2$), 44.1 (N(CH$_3$)$_2$); *m/z* LCMS [MH]$^+$ 114.3.

Synthesis of 4-((4,5-dihydroisoxazol-3-yl)oxy)-*N*,*N*-dimethylbut-2-yn-1-amine (21)
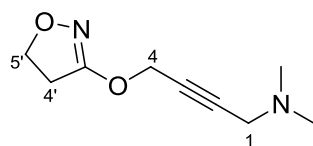
4-(Dimethylamino)but-2-yn-1-ol (**17**) (365 mg, 3.23 mmol) was stirred in dry tetrahydrofuran (5 mL) under a N$_2$ atmosphere. Sodium hydride (142 mg, 5.92 mmol) was carefully added and the mixture stirred at RT under an inert atmosphere for 1 h. 3-Nitro-4,5-dihydroisoxazole (**20**) (562 mg, 4.84 mmol), dissolved in dry tetrahydrofuran (3 mL), was syringed in dropwise and the reaction refluxed for 6 h. After cooling, the reaction mixture was poured into distilled water (20 mL), gently extracted with chloroform (5 × 20 mL) to avoid emulsion, and the organic fractions combined, dried over MgSO$_4$, filtered and the solvent evaporated *in vacuo* to yield a crude orange oil. The target molecule was isolated as a yellow oil by column chromatography (stationary phase: silica, gradient mobile phase: 100% chloroform − 90% chloroform/10% methanol). 383 mg, 72%; δ_H (CDCl$_3$) 4.74 (t, *J*= 2.0 Hz, 2H, H4), 4.35 (t, *J*= 9.5 Hz, 2H, H5′), 3.24 (t, *J*= 1.5 Hz, 2H, H1), 2.93 (t, *J*= 9.5 Hz, 2H, H4′), 2.23 (s, 6H, N(CH_3)$_2$); δ_C (CDCl$_3$) 167.0 (C), 83.4 (C), 78.6 (C), 69.8 (CH$_2$), 58.1 (CH$_2$), 48.0 (CH$_2$), 44.2 (N(CH$_3$)$_2$), 33.1 (CH$_2$); *m/z* LCMS [MH]$^+$ 183.3; HPLC: t_R = 4.19 min, purity = 96.0%.

General procedure for room temperature amine quaternisation

4-((4,5-Dihydroisoxazol-3-yl)oxy)-*N,N*-dimethylbut-2-yn-1-amine (**21**) (50 mg, 275 μmol) was stirred in chloroform (4 mL). The appropriate iodoalkane (2.5 eq.) was added dropwise and the mixture stirred at RT for 20 h. If the target molecule precipitated out, it was isolated by vacuum filtration as a white crystalline solid and washed with cold diethyl ether. If no precipitate formed, the reaction mixture was dried *in vacuo*, partitioned between chloroform (10 mL) and water (10 mL), and the organic layer extracted with water (3 × 10 mL). The combined aqueous fractions were dried *in vacuo* to yield a clear oil or waxy solid.

<u>4-((4,5-Dihydroisoxazol-3-yl)oxy)-*N,N,N*-trimethylbut-2-yn-1-aminium iodide (**7**, iperoxo)</u>
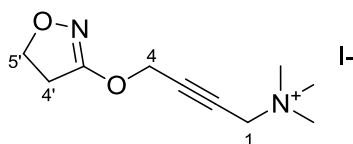
White crystalline solid; 61.8 mg, 70%; mp 217-218 °C; δ_H (d_6-DMSO) 4.95 (s, 2H, H4), 4.46 (s, 2H, H1), 4.33 (t, *J*= 9.5 Hz, 2H, H5′), 4.72 (s, 9H, N+(C*H*$_3$)$_3$), 3.03 (t, *J*= 9.5 Hz, 2H, H4′); δ_C (d_6-DMSO) 166.7 (C), 86.0 (C), 76.2 (C), 69.6 (CH$_2$), 57.2 (CH$_2$), 55.1 (CH$_2$), 51.9 (N+(*C*H$_3$)$_3$), 32.2 (CH$_2$); *m/z* LCMS [M-I]$^+$ 197.2; *m/z* HRMS (TOF ES$^+$) C$_{10}$H$_{17}$N$_2$O$_2$ [M-I]$^+$ calcd 197.1292, found 197.1286; HPLC: t_R = 4.49 min, purity (214) = >99.0%.

N-(4-((4,5-Dihydroisoxazol-3-yl)oxy)but-2-yn-1-yl)-N,N-dimethylpentan-1-aminium iodide (**14**)
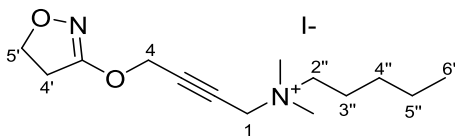
Clear, colourless oil; 48 mg, 46%; δ_H (CDCl$_3$) 4.76 (app d, 4H, H4), 4.38 (t, J= 9.5 Hz, 2H, H5′), 3.56-3.48 (m, 2H, H2″), 3.35 (s, 6H, N+(CH_3)$_2$), 2.96 (t, J= 9.5 Hz, 2H, H4′), 1.70 (app br s, 2H, H3″), 1.35 (dd, J= 9.0, 5.0 Hz, 4H, H4″, H5″), 0.88 (t, J= 7.0 Hz, 3H, H6″); δ_C (CDCl$_3$) 166.8 (C), 86.8 (C), 75.6 (C), 70.1 (CH$_2$), 64.4 (CH$_2$), 57.4 (CH$_2$), 55.1 (CH$_2$), 50.9 (N+(CH_3)$_2$), 33.0 (CH$_2$), 28.1 (CH$_2$), 22.6 (CH$_2$), 22.2 (CH$_2$), 13.9 (CH$_3$); m/z LCMS [M-I]$^+$ 253.2; m/z HRMS (TOF ES$^+$) C$_{14}$H$_{25}$N$_2$O$_2$ [M-I]$^+$ calcd 253.1925, found 253.1920; HPLC: t_R = 5.89 min, purity (214) = 98.6%.

N-(4-((4,5-dihydroisoxazol-3-yl)oxy)but-2-yn-1-yl)-N,N-dimethylnonan-1-aminium iodide (**15**)
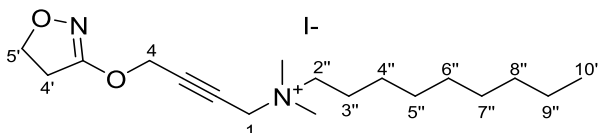
Waxy, colourless solid; 20.3 mg, 17%; mp 128-129 °C; δ_H (CDCl$_3$) 4.80 (app d, 4H, H4), 4.37 (t, J= 9.5 Hz, 2H, H5′), 3.63-3.52 (m, 2H, H2″), 3.40 (s, 6H, N+(CH_3)$_2$), 2.97 (t, J= 9.5 Hz, 2H, H4′), 1.70 (app br s, 2H, H3″), 1.41-1.12 (m, 12H, H4″-H9″), 0.81 (t, J= 7.0 Hz, 3H, H10″); δ_C (CDCl$_3$) 166.7 (C), 86.8 (C), 75.6 (C), 70.1 (CH$_2$), 64.5 (CH$_2$), 57.4 (CH$_2$), 55.1 (CH$_2$), 50.9 (CH$_3$), 33.0 (CH$_2$), 31.8 (CH$_2$), 29.3 (CH$_2$), 29.2 (CH$_2$), 29.1 (CH$_2$), 26.1 (CH$_2$), 23.0 (CH$_2$), 22.6 (CH$_2$), 14.1 (CH$_3$); m/z LCMS [M-I]$^+$ 309.3; m/z HRMS (TOF ES$^+$) C$_{18}$H$_{33}$N$_2$O$_2$ [M-I]$^+$ calcd 309.2551, found 309.2546; HPLC: t_R = 8.72 min, purity (214) = 95.4%.

Synthesis of *N*-(4-(hydroxymethyl)phenyl)acetamide (24a)
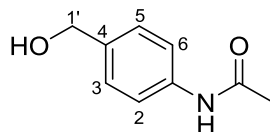
Acetic anhydride (10 mL) was cooled to 0 °C. 4-Aminobenzylalcohol (**22**) (1 g, 8.12 mmol) was added and the reaction mixture was stirred for 10 min at 0 °C. The precipitate was collected by vacuum filtration and washed with petroleum spirits to yield the target molecule as a bright yellow powder. 1.04 g, 78%; mp 120-121 °C; δ_H (d_6-CDCl$_3$) 9.94 (br s, 1H, NH), 7.59 (d, *J*= 8.5 Hz, 2H, H2, H6), 7.30 (d, *J*= 8.5 Hz, 2H, H3, H5), 5.15 (br t, *J*= 5.5 Hz, 1H, OH), 4.50 (d, *J*= 5.0 Hz, 2H, H1′), 2.10 (s, 3H, CH$_3$); δ_C (d_6-DMSO) 168.1 (C), 137.9 (C), 137.0 (C), 126.9 (CH), 118.7 (CH), 62.6 (CH$_2$), 23.9 (CH$_3$); *m/z* LRMS [MH]$^+$ 166.2; LCMS: t_R = 4.19 min, purity = >99.0%.

Synthesis of *N*-(4-(hydroxymethyl)phenyl)decanamide (24b)
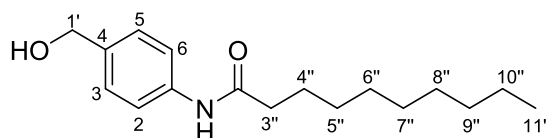
4-Aminobenzylalcohol (**22**) (300 mg, 2.44 mmol) stirred in acetonitrile (8 mL) was cooled to 0 °C. Decanoyl chloride (465 μL, 2.68 mmol) was added dropwise and the reaction mixture was stirred for 30 min at 0 °C. The precipitate was collected by vacuum filtration and washed with petroleum spirits to yield the target molecule as a bright orange powder. 373 mg, 55%; δ_H (CDCl$_3$) 7.44 (d, *J*= 8.0 Hz, 2H, H2, H6), 7.25 (d, *J*= 8.5 Hz, 2H, H3, H5), 7.06 (br s, 1H, NH), 4.58 (s, 2H, H1′), 2.28 (t, *J*= 7.5 Hz, 2H, H3″), 1.71-1.60 (m, 2H, H4″), 1.35-1.08 (m, 13H, OH, H5″-H10″), 0.81 (t, *J*= 7.0 Hz, 3H, H11″); δ_C (CDCl$_3$) 171.3 (C), 137.4 (C), 136.4

(C), 127.8 (CH), 119.9 (CH), 65.0 (CH_2), 37.9 (CH_2), 31.9 (CH_2), 29.44 (CH_2), 29.38 (CH_2), 29.27 (2 × CH_2), 25.6 (CH_2), 22.7 (CH_2), 14.1 (CH_3); *m/z* LRMS $[MH]^+$ 278.2; LCMS: t_R = 6.67 min, purity = 86.5%.

General procedure for Appel reaction

N-(4-(Hydroxymethyl)phenyl)acetamide (**24a**) or *N*-(4-(hydroxymethyl)phenyl)decanamide (**24b**) (300 or 200 mg, 1.82 mmol or 721 µmol), triphenylphosphine (1.5 eq.) and acetonitrile (12 mL) were placed in an RBF and cooled to 0 °C in an icebath. Carbon tetrabromide (1.5 eq.) was added and the reaction stirred at 0 °C for 10 min before being heated to 80 °C and stirred for 4 h. The reaction mixture was cooled, partitioned between dichloromethane (10 mL) and water (10 mL), and the aqueous layer extracted with dichloromethane (3 × 10 mL). The combined organic fractions were dried over anhydrous $MgSO_4$, filtered and the solvent evaporated *in vacuo*. The target molecule was isolated by column chromatography (stationary phase: silica, mobile phase: 2:1 petroleum spirits:ethyl acetate or 13:6:1 hexane:ethyl acetate:methanol).

N-(4-(Bromomethyl)phenyl)acetamide (**25a**)
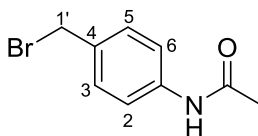
Beige solid; 347 mg, 89%; mp 157-158 °C; δ_H ($CDCl_3$) 7.41 (d, *J*= 8.5 Hz, 2H, H2, H6), 7.28 (d, *J*= 8.5 Hz, 2H, H3, H5), 7.17 (br s, 1H, NH), 4.41 (s, 2H, H1′), 2.11 (s, 3H, CH_3); δ_C ($CDCl_3$) 168.3 (C), 138.0 (C), 133.6 (C), 129.9 (CH), 119.9 (CH), 33.3 (CH_2), 24.7 (CH_3); *m/z* LCMS $[M-Br]^-$: 148.1; HPLC: t_R = 5.90 min, purity = 99.1%.

<u>N-(4-(Bromomethyl)phenyl)decanamide (**25b**)</u>
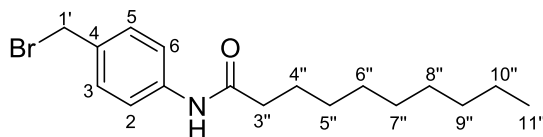
Yellow solid; 138.6 mg, 57%; mp 141-142 °C; δ_H (d_6-DMSO) 9.86 (br s, 1H, NH), 7.57 (d, J= 8.5 Hz, 2H, H2, H6), 7.25 (d, J= 8.5 Hz, 2H, H3, H5), 4.42 (s, 2H, H1′), 2.29 (t, J= 7.5 Hz, 2H, H3″), 1.64-1.53 (m, 2H, H4″), 1.34-1.20 (m, 12H, H5″-H10″), 0.86 (t, J= 7.0 Hz, 3H, H11″); δ_C (DMSO) 171.7 (C), 139.1 (C), 133.3 (C), 128.6 (CH), 119.3 (CH), 71.4 (CH$_2$), 36.9 (CH$_2$), 31.7 (CH$_2$), 29.4 (CH$_2$), 29.3 (CH$_2$), 29.1 (2 × CH$_2$), 25.6 (CH$_2$), 22.6 (CH$_2$), 14.4 (CH$_3$); m/z [M(^{81}Br)+H]$^+$: 342.3; LCMS: t_R = 6.58 min, purity = 95.8%.

Synthesis of *tert*-butyl 4-aminobenzylcarbamate (26)
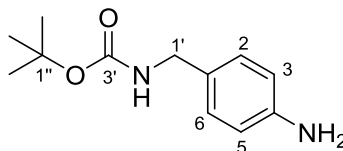
4-Aminobenzylamine (**23**) (926 μL, 8.19 mmol) and tetrahydrofuran (25 mL) were placed in an RBF and cooled to 0 °C in an icebath. Di-*tert*-butyl dicarbonate (Boc anhydride) (1.97 g, 9.00 mmol) was slowly added and the reaction allowed to return to RT. After overnight stirring (~17 h), the solvent was evaporated *in vacuo* to yield the target molecule as a yellow oil requiring no further purification. 1.82 g, quantitative; δ_H (CDCl$_3$) 7.02 (d, J= 8.0 Hz, 2H, H2, H6), 6.64 (d, J= 8.5 Hz, 2H, H3, H5), 4.70 (br s, 1H, NH), 4.12 (d, J= 5.5 Hz, 2H, H1′), 2.73 (br s, 2H, NH$_2$), 1.38 (s, 9H, C(C*H*$_3$)$_3$); δ_C (CDCl$_3$) 155.9 (C), 145.7 (C), 128.9 (CH), 115.2 (CH), 68.0 (C), 44.4 (C), 28.4 (C(*C*H$_3$)$_3$), 25.6 (CH$_2$); m/z LCMS [M-*tert*butyl]$^+$ 167.1; LCMS: t_R = 4.67 min, purity = 87.1%.

Synthesis of *tert*-butyl 4-hexanamidobenzylcarbamate (27)
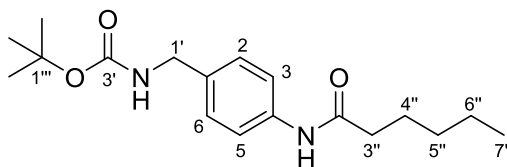
Tert-butyl 4-aminobenzylcarbamate (**26**) (1.82 g, 8.19 mmol), triethylamine (1.71 mL, 12.28 mmol) and dichloromethane (30 mL) were placed in an RBF and cooled to 0 °C in an icebath. Hexanoyl chloride (1.26 mL, 9.0 mmol) was added dropwise and the reaction allowed to return to RT. After overnight stirring (~17 h), the reaction mixture was partitioned between dichloromethane (25 mL) and deionized water (25 mL), and the aqueous layer extracted with dichloromethane (2 × 25 mL). The combined organic fractions were washed with saturated sodium bicarbonate, dried over anhydrous $MgSO_4$, filtered and the solvent evaporated *in vacuo* to yield a white solid in an orange-yellow oil. The precipitate was collected by vacuum filtration and washed with petroleum spirits to yield the target molecule as fine, needle-like white crystals. 1.89 g, 72%; mp 126-127 °C; δ_H (CDCl$_3$) 7.39 (d, *J*= 8.5 Hz, 2H, H3, H5), 7.24 (s, 1H, NH (amide)), 7.14 (d, *J*= 8.5 Hz, 2H, H2, H6), 4.77 (br s, 1H, NH (carbamate)), 4.18 (s, 2H, H1′), 2.27 (t, *J*= 7.5 Hz, 2H, H3″), 1.65 (app dt, *J*= 14.8, 7.5 Hz, 2H, H4″), 1.39 (s, 9H, C(C*H*$_3$)$_3$), 1.28 (app td, *J*= 7.0, 3.5 Hz, 4H, H5″, H6″), 0.84 (t, *J*= 7.0 Hz, 3H, H7″); δ_C (CDCl$_3$) 171.8 (C), 156.0 (C), 137.3 (C), 134.6 (C), 128.0 (CH), 120.1 (CH), 79.5 (C), 44.2 (CH$_2$), 37.6 (CH$_2$), 31.4 (CH$_2$), 28.4 (C(*C*H$_3$)$_3$), 25.3 (CH$_2$), 22.4 (CH$_2$), 14.0 (CH$_3$); *m/z* LCMS [MNa]$^+$ 343.2; LCMS: t_R = 6.56 min, purity = 97.2%.

Synthesis of *N*-(4-(aminomethyl)phenyl)hexanamide (28)
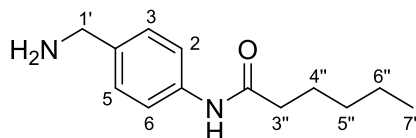
Tert-butyl 4-hexanamidobenzylcarbamate (**27**) (1 g, 3.12 mmol) and dichloromethane (5 mL) were placed in an RBF and cooled to 0 °C in an icebath. Trifluoroacetic acid (2 mL) added drop-wise and the reaction allowed to return to RT. After 2 h, the solvent was evaporated *in vacuo* and the resulting residue partitioned between ethyl acetate (20 mL) and saturated sodium bicarbonate$_{(aq)}$ (20 mL), and the aqueous layer extracted with ethyl acetate (3 × 20 mL). The combined organic fractions were dried over MgSO$_4$, filtered and the solvent evaporated *in vacuo* to yield the target molecule as a white solid. 431 mg, 63%; mp 139-140 °C; δ$_H$ (*d*$_6$-DMSO) 9.89 (s, 1H, NH), 7.59 (d, *J*= 8.5 Hz, 2H, H2, H6), 7.24 (d, *J*= 8.5 Hz, 2H, H3, H5), 4.15 (app d, *J*= 6.0 Hz, 2H, H1′), 3.73 (s, 2H, NH$_2$), 2.36 (t, *J*= 7.5 Hz, 2H, H3″), 1.66 (m, 2H, H4″), 1.38 (m, 4H, H5″, H6″), 0.96 (t, *J*= 7.0 Hz, 3H, H7″); δ$_C$ (DMSO) 171.6 (C), 138.3 (C), 135.8 (C), 127.7 (CH), 119.3 (CH), 44.0 (CH$_2$), 36.8 (CH$_2$), 31.4 (CH$_2$), 25.3 (CH$_2$), 22.4 (CH$_2$), 14.4 (CH$_3$); *m/z* LCMS [M-NH$_2$]$^+$ 204.2; LCMS: *t$_R$* = 4.62 min, purity = 99.4%.

Synthesis of ethyl-1-(4-hexanamidobenzyl)-4-oxo-1,4-di-hydroquinolone-3-carboxylate (29)
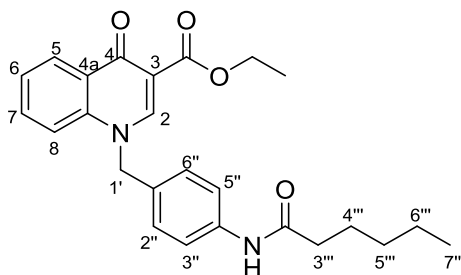
Ethyl 3-(dimethylamino)-2-(2-fluorobenzoyl)acrylate (70 mg, 264 μmol) and *N*-(4-(aminomethyl)phenyl)hexanamide (**28**) (58.13 mg, 264 μmol) were dissolved in dry *N,N*-dimethylformamide (5 mL) and stirred at 100 °C under a nitrogen atmosphere. After 2.5 h, the solvent was evaporated *in vacuo* to yield the target molecule as an off-white solid that was washed with petroleum spirits and isolated by vacuum filtration. 78 mg, 70%; mp 234-235 °C; δ_H (CDCl$_3$) 8.56 (s, 1H, H2), 8.45 (d, *J*= 8.0 Hz, 1H, NH), 7.54-7.41 (m, 4H, H5, H8, H3″, H5″), 7.33 (t, *J*= 7.5 Hz, 1H, H7), 7.26 (app d, *J*= 8.5 Hz, 1H, H6), 7.02 (d, *J*= 8.0 Hz, 2H, H2″, H6″), 5.29 (s, 2H, H1′), 4.33 (q, *J*= 7.0 Hz, 2H, OC*H*$_2$CH$_3$), 2.30 (t, *J*= 7.5 Hz, 2H, H3‴), 1.33 (t, *J*= 7.0 Hz, 3H, OCH$_2$C*H*$_3$), 1.29-1.17 (m, 6H, H4‴, H5‴, H6‴), 0.85-0.75 (m, 3H, H7‴); δ_C (CDCl$_3$) 173.9 (C), 172.0 (C), 166.5 (C), 149.8 (CH), 139.1 (C), 138.8 (C), 132.9 (CH), 129.1 (C), 127.8 (CH), 126.8 (CH), 125.4 (CH), 122.5 (C), 120.4 (CH), 116.8 (CH), 109.1 (C), 61.1 (CH$_2$), 57.3 (CH$_2$), 37.6 (CH$_2$), 31.4 (CH$_2$), 25.3 (CH$_2$), 22.4 (CH$_2$), 14.4 (CH$_3$), 13.9 (CH$_3$); *m/z* LCMS [MH]$^+$ 421.3; LCMS: t_R = 6.02 min, purity = 96.4%.

General procedure for N-benzylation

4-Oxo-1,4-dihydro-quinoline-3-carboxylic acid (45 or 22 mg) and acetonitrile (4 mL) were placed in an RBF and cooled to 0 °C in an icebath. *N*-(4-(Bromomethyl)phenyl)acetamide (**25a**) or *N*-(4-(bromomethyl)phenyl)decanamide (**25b**) (1.1 eq.) and *N,N*-

diisopropylethylamine (4 eq.) were added and the reaction stirred at 80 °C for 3 h. Upon cooling, the target molecule precipitated from the reaction mixture and was isolated by vacuum filtration and washed with diethyl ether.

1-(4-Acetamidobenzyl)-4-oxo-1,4-dihydroquinoline-3-carboxylic acid (**11**)
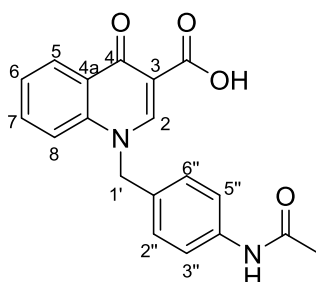
White solid; 70 mg, 87%; mp 296-297 °C; δ_H (d_6-DMSO) 15.19 (s, 1H, OH), 9.97 (s, 1H, NH), 9.26 (s, 1H, H2), 8.40 (dd, J= 7.5, 1.0 Hz, 1H, H5), 7.92-7.84 (m, 2H, H7, H8), 7.63 (ddd, J= 8.0, 6.0, 2.0 Hz, 1H, H6), 7.54 (d, J= 8.5 Hz, 2H, H3″, H5″), 7.24 (d, J= 8.5 Hz, 2H, H2″, H6″), 5.80 (s, 2H, H1′), 2.01 (s, 3H, CH$_3$); δ_C (d_6-DMSO) 178.4 (C), 168.8 (C), 166.5 (C), 150.5 (CH), 139.9 (C), 139.6 (C), 134.6 (CH), 130.0 (C), 127.8 (CH), 126.9 (CH), 126.4 (CH), 126.2 (C), 119.8 (CH), 119.2 (CH), 108.3 (C), 56.7 (CH$_2$), 24.4 (CH$_3$); m/z LCMS [MH]$^+$ 337.2; m/z HRMS (TOF ES$^+$) $C_{19}H_{16}N_2O_4$ [MH]$^+$ calcd 336.1110, found 337.1186; HPLC: t_R = 7.52 min, purity (254) = 99.3%, purity (214) = 97.0%.

1-(4-decanamidobenzyl)-4-oxo-1,4-dihydroquinoline-3-carboxylic acid (**13**)
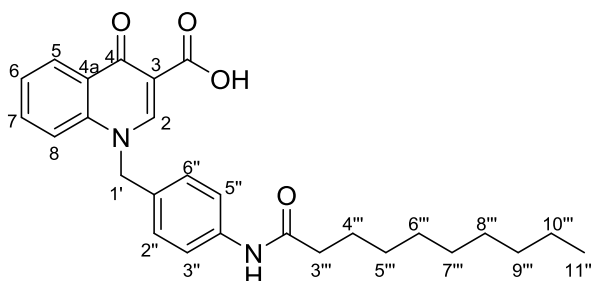
White solid; 11.6 mg, 22%; mp 224-225 °C; δ_H (d_6-DMSO) 15.19 (s, 1H, OH), 9.90 (s, 1H, NH), 9.27 (s, 1H, H2), 8.40 (dd, J= 7.5, 1.0 Hz, 1H, H5), 7.92-7.84 (m, 2H, H7, H8), 7.63

(ddd, *J*= 8.0, 6.0, 2.0 Hz, 1H, H6), 7.56 (d, *J*= 8.5 Hz, 2H, H3″, H5″), 7.24 (d, *J*= 8.5 Hz, 2H, H2″, H6″), 5.80 (s, 2H, H1′), 2.26 (t, *J*= 7.5 Hz, 2H, H3‴), 1.55 (dt, *J*= 13.5, 7.0 Hz, 2H, H4‴), 1.32-1.18 (m, 12H, H5‴-H10‴), 0.84 (t, 3H, H11‴); δ_C (d_6-DMSO) 178.4 (C), 171.8 (C), 166.5 (C), 150.5 (CH), 139.9 (C), 139.6 (C), 134.6 (CH), 130.0 (C), 127.8 (CH), 126.8 (CH), 126.4 (CH), 126.2 (C), 119.8 (CH), 119.2 (CH), 108.3 (C), 56.7 (CH_2), 36.8 (CH_2), 31.7 (CH_2), 29.3 (CH_2), 29.2 (CH_2), 29.11 (CH_2), 29.08 (CH_2), 25.5 (CH_2), 22.5 (CH_2), 14.4 (CH_3); *m/z* LCMS [MH]⁺ 449.2; *m/z* HRMS (TOF ES⁺) $C_{27}H_{32}N_2O_4$ [MH]⁺ calcd 448.2367, found 449.2444; HPLC: t_R = 11.46 min, purity (254) = 97.6%, purity (214) = 98.4%.

Synthesis of 1-(4-hexanamidobenzyl)-4-oxo-1,4-dihydroquinolone-3-carboxylic acid (12)
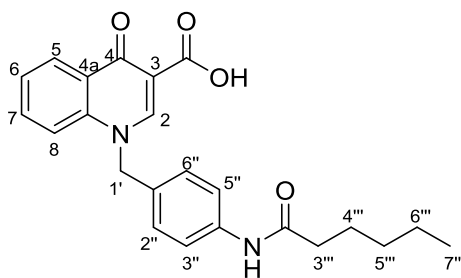
Ethyl-1-(4-hexanamidobenzyl)-4-oxo-1,4-di-hydroquinolone-3-carboxylate (**29**) (43 mg, 102.3 μmol) and tetrahydrofuran (3 mL) were brought to 0 °C in an icebath. A solution of aqueous 1 M LiOH(aq) (204.5 μL, 204.5 μmol) was added dropwise whilst stirring and then the reaction mixture was heated at 80 °C for 5 h. Following addition of excess aqueous 1 M HCl(aq), the target molecule precipitated out and was isolated as a cream-coloured solid by vacuum filtration, washed with deionized water to remove the residual acid, then dried under vacuum overnight. 15.4 mg, 38 %; mp 251-252 °C; δ_H (d_6-DMSO) 15.23 (s, 1H, OH), 9.96 (s, 1H, NH), 9.31 (s, 1H, H2), 8.45 (d, *J*= 8.0 Hz, 1H, H5), 7.93 (br app s, 2H, H7, H8), 7.72-7.64 (m, 1H, H6), 7.61 (d, *J*= 7.5 Hz, 2H, H3″, H5″), 7.29 (d, *J*= 7.5 Hz, 2H, H2″, H6″), 5.85 (s, 2H, H1′), 2.31 (t, *J*= 7.0 Hz, 2H, H3‴), 1.68-1.55 (m, 2H, H4‴), 1.31 (app s, 4H, H5‴,

H6'''), 0.91 (t, J= 6.0 Hz, 3H, H7'''); δ_C (d_6-DMSO) 183.2 (C), 176.6 (C), 171.3 (C), 155.2 (CH), 144.7 (C), 144.4 (C), 139.4 (CH), 134.7 (C), 132.5 (CH), 131.6 (CH), 131.1 (CH), 130.9 (C), 124.6 (CH), 123.9 (CH), 113.0 (C), 61.5 (CH_2), 41.5 (CH_2), 36.1 (CH_2), 30.0 (CH_2), 27.1 (CH_2), 19.1 (CH_3); m/z LCMS $[MH]^+$ 393.2; m/z HRMS (TOF ES$^+$) $C_{23}H_{24}N_2O_4$ $[M+H]^+$ calcd 392.1722, found 393.1817; HPLC: t_R = 9.33 min, purity (254) = 98.4%, purity (214) = 95.0%.

General procedure for COMU coupling reaction

N,N-Dimethylformamide (8 mL) in an RBF was brought to 0 °C in an icebath. Ethyl 1-(4-aminobenzyl)-4-oxo-1,4-dihydroquinoline-3-carboxylate (**30b**) (400 mg or 1 g), 6-bromohexanoic acid (1.1 eq.) or 6-hydroxyhexanoic acid (1.1 eq.), *N,N*-diisopropylethylamine (1.1 eq.) and (1-cyano-2-ethoxy-2-oxoethylidenaminooxy) dimethylamino-morpholino-carbenium hexafluorophosphate (COMU) (1.1 eq.) were added and the reaction mixture allowed to return to RT. After 2 h stirring at RT, the reaction mixture was poured into ethyl acetate (20 mL) and washed with 1 M HCl$_{(aq)}$ (2 × 20 mL), saturated sodium bicarbonate$_{(aq)}$ (2 × 20 mL), and saturated sodium chloride$_{(aq)}$ (2 × 20 mL). The organic layer was dried over MgSO$_4$, filtered and the solvent evaporated *in vacuo*. The target molecule was isolated as a white solid by column chromatography (stationary phase: silica, gradient mobile phase: 50% ethyl acetate:petroleum spirits → 80% ethyl acetate:petroleum spirits → 100% ethyl acetate).

Ethyl 1-(4-(6-bromohexanamido)benzyl)-4-oxo-1,4-dihydroquinoline-3-carboxylate (**31b**)
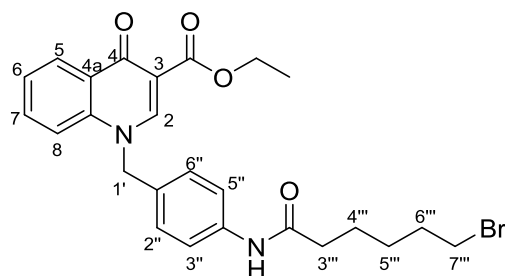
Beige solid; 212.6 mg, 34 %; mp 190-191 °C; δ_H (d_6-DMSO) 9.92 (s, 1H, NH), 8.91 (s, 1H, H2), 8.25 (dd, J= 8.0, 1.0 Hz, 1H, H5), 7.71-7.62 (m, 2H, H7, H8), 7.56 (d, J= 8.5 Hz, 2H, H3″, H5″), 7.44 (ddd, J= 8.0, 6.5, 1.5 Hz, 1H, H6), 7.20 (d, J= 8.5 Hz, 2H, H2″, H6″), 5.61 (s, 2H, H1′), 4.25 (q, J= 7.0 Hz, 2H, OCH_2CH₃), 3.52 (t, J= 6.5 Hz, 2H, H7‴), 2.28 (td, J= 7.5, 2.5 Hz, 2H, H3‴), 1.86-1.76 (m, 2H, H6‴), 1.59 (dt, J= 15.0, 7.5 Hz, 2H, H4‴), 1.44-1.35 (m, 2H, H5‴), 1.30 (t, J= 7.0 Hz, 3H, OCH₂CH_3); δ_C (d_6-DMSO) 173.4 (C), 171.6 (C), 165.1 (C), 150.5 (CH), 139.5 (C), 133.0 (CH), 130.6 (C), 128.9 (C), 127.5 (CH), 126.8 (CH), 125.4 (CH), 119.9 (CH), 118.3 (CH), 110.6 (C), 108.9 (C), 60.3 (CH₂), 55.8 (CH₂), 36.6 (CH₂), 35.5 (CH₂), 32.5 (CH₂), 27.6 (CH₂), 24.7 (CH₂), 14.8 (CH₃); m/z LCMS [MH]⁺ 500.1; LCMS: t_R = 6.18 min, purity = 93.9%.

Ethyl 1-(4-(6-hydroxyhexanamido)benzyl)-4-oxo-1,4-dihydroquinoline-3-carboxylate (**34**)
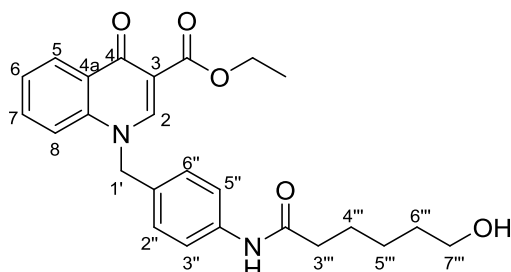
White solid; 709.5 mg, 53 %; δ_H (d_6-DMSO) 9.91 (s, 1H, NH), 8.92 (s, 1H, H2), 8.25 (dd, J= 8.0, 1.0 Hz, 1H, H5), 7.75-7.62 (m, 2H, H7, H8), 7.57 (d, J= 8.5 Hz, 2H, H3″, H5″), 7.44

(ddd, *J* = 8.0, 5.0, 1.5 Hz, 1H, H6), 7.20 (d, *J* = 8.5 Hz, 2H, H2″, H6″), 5.61 (s, 2H, H1′), 4.30-4.21 (m, 2H, OC*H*₂CH₃), 3.43-3.36 (m, 2H, H7‴), 2.31-2.21 (m, 3H, H3‴, OH), 1.62-1.51 (m, 2H, H4‴), 1.46-1.36 (m, 2H, H6‴), 1.35-1.27 (m, 5H, H5‴, OCH₂C*H*₃); δ$_C$ (*d₆*-DMSO) 173.5 (C), 171.8 (C), 165.1 (C), 150.5 (CH), 139.5 (C), 139.4 (C), 133.0 (CH), 130.6 (C), 128.9 (C), 127.5 (CH), 126.8 (CH), 125.4 (CH), 119.8 (CH), 118.3 (CH), 110.5 (C), 61.0 (CH₂), 60.3 (CH₂), 55.9 (CH₂), 36.9 (CH₂), 32.8 (CH₂), 25.7 (CH₂), 25.5 (CH₂), 14.8 (CH₃); *m/z* LCMS [MH]$^+$ 437.2; LCMS: *t*$_R$ = 5.17 min, purity = 77.7%.

Synthesis of ethyl 1-(4-(10-bromodecanamido)benzyl)-4-oxo-1,4-dihydroquinoline-3-carboxylate (31c)
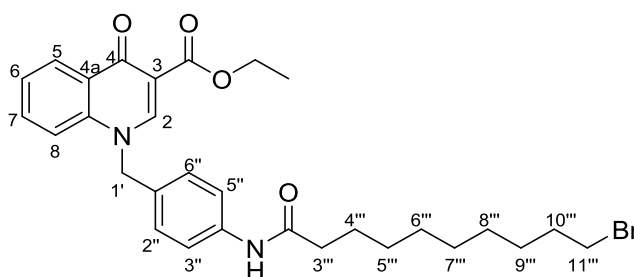
N,N-Dimethylformamide (5 mL) in an RBF was brought to 0 °C in an icebath. 10-Bromodecanoic acid (244 mg, 972.5 µmol), *N,N*-diisopropylethylamine (170 µL, 972.5 µmol) and *O*-(6-chlorobenzotriazol-1-yl)-*N,N,N′,N′*-tetramethyluronium hexafluorophosphate (HCTU) (549 mg, 1.33 mmol) added and the reaction mixture stirred for 10 min at 0 °C. Ethyl 1-(4-aminobenzyl)-4-oxo-1,4-dihydroquinoline-3-carboxylate (**30b**) (285 mg, 884.1 µmol) dissolved in *N,N*-dimethylformamide (3 mL) was added dropwise and the reaction allowed to return to RT. After 2 h stirring at RT, the reaction mixture was poured into ethyl acetate (20 mL) and washed with deionized water (2 × 20 mL), saturated sodium bicarbonate$_{(aq)}$ (1 × 20 mL), and saturated sodium chloride$_{(aq)}$ (1 × 20 mL). The organic layer,

which contained some solid, was evaporated *in vacuo* and the target molecule isolated as a white solid by column chromatography (stationary phase: silica, gradient mobile phase: 50% ethyl acetate:petroleum spirits → 80% ethyl acetate:petroleum spirits → 100% ethyl acetate). 103.5 mg, 21 %; δ_H (d_6-DMSO) 9.95 (s, 1H, NH), 8.97 (s, 1H, H2), 8.30 (d, J= 7.0 Hz, 1H, H5), 7.76-7.67 (m, 2H, H7, H8), 7.61 (d, J= 8.5 Hz, 2H, H3″, H5″), 7.49 (ddd, J= 8.0, 6.5, 1.5 Hz, 1H, H6), 7.25 (d, J= 8.5 Hz, 2H, H2″, H6″), 5.66 (s, 2H, H1′), 4.32 (q, J= 7.0 Hz, 2H, OCH_2CH$_3$), 3.59 (t, J= 6.5 Hz, 2H, H11‴), 2.31 (t, J= 7.5 Hz, 2H, H3‴), 1.87-1.70 (m, 2H, H10‴), 1.65-1.55 (m, 2H, H4‴), 1.45-1.38 (m, 2H, H9‴), 1.35 (t, J= 7.0 Hz, 3H, OCH$_2$CH_3), 1.34-1.24 (m, 8H, H5‴-H9‴); δ_C (d_6-DMSO) 173.4 (C), 171.8 (C), 165.1 (C), 150.5 (CH), 139.4 (C), 133.0 (CH), 130.6 (C), 128.9 (C), 127.5 (CH), 126.8 (CH), 125.4 (CH), 119.8 (CH), 118.3 (CH), 110.6 (C), 108.9 (C), 79.1 (CH_2), 66.4 (CH_2), 63.3 (CH_2), 60.3 (CH_2), 55.8 (CH_2), 51.8 (CH_2), 36.8 (CH_2), 35.7 (CH_2), 32.7 (CH_2), 27.9 (CH_2), 25.5 (CH_2), 14.8 (CH_3); *m/z* LCMS [M+H]$^+$ 556.2; LCMS: t_R = 6.73 min, purity = 84.2%.

General procedure for reflux amine quaternisation

Compound **31a**, **31b**, **31c**, or **43** was stirred in acetonitrile (2-4 mL). 4-((4,5-dihydroisoxazol-3-yl)oxy)-*N*,*N*-dimethylbut-2-yn-1-amine (**21**) (0.8 eq.) dissolved in acetonitrile (0.5 mL) was added and the reaction refluxed for 6-24 h. If the target molecule precipitated out, it was isolated by vacuum filtration as a beige solid and washed with cold diethyl ether. If no precipitate formed, the reaction mixture was dried *in vacuo*, partitioned between ethyl acetate (10 mL) and deionized water (10 mL), and the organic layer extracted with deionized water (3 × 10 mL). The combined aqueous fractions were dried *in vacuo* to yield a clear oil or waxy solid.

N-(2-((4-((3-carboxy-4-oxoquinolin-1(4*H*)-yl)methyl)phenyl)amino)-2-oxoethyl)-4-((4,5-

dihydroisoxazol-3-yl)oxy)-*N,N*-dimethylbut-2-yn-1-aminium bromide (**33a**)
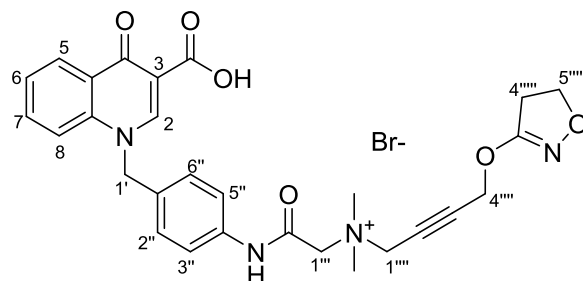
Beige solid; 56.3 mg, 78%, mp 175-176 °C; δ_H (d$_6$-DMSO) 15.19 (s, 1H, OH), 10.73 (s, 1H,

NH), 9.29 (s, 1H, H2), 8.40 (d, *J*= 8.0 Hz, 1H, H5), 7.87 (d, *J*= 3.5 Hz, 2H, H7, H8), 7.68-

7.61 (m, 1H, H6), 7.57 (d, *J*= 8.5 Hz, 2H, H2″, H6″), 7.32 (d, *J*= 8.5 Hz, 2H, H3″, H5″),

5.86 (s, 2H, H1′), 4.94 (s, 2H, H4‴′), 4.69 (s, 2H, H1‴), 4.39 (s, 2H, H1‴′), 4.29 (t, *J*= 9.5

Hz, 2H, H5‴″′), 3.32 (s, 6H, N+(C*H*$_3$)$_2$), 2.98 (t, *J*= 9.5 Hz, 2H, H4‴″′); δ_C (d$_6$-DMSO) 178.5

(C), 167.2 (C), 166.5 (C), 162.3 (C), 150.6 (CH), 139.9 (C), 137.8 (C), 134.6 (CH), 131.8

(C), 128.0 (CH), 126.9 (CH), 126.4 (CH), 126.2 (C), 120.6 (CH), 119.2 (CH), 108.3 (C), 87.2

(C), 76.3 (C), 70.1 (CH$_2$), 62.2 (CH$_2$), 57.8 (CH$_2$), 56.6 (CH$_2$), 55.5 (CH$_2$), 51.4 (CH$_3$), 32.7

(CH$_2$); *m/z*   LCMS [M-Br]$^+$ 517.3; *m/z* HRMS (TOF ES$^+$) C$_{28}$H$_{29}$N$_4$O$_6$ [M-Br]$^+$ calcd

517.2087, found 517.2081; HPLC: t_R = 7.55 min, purity (254) = 96.7%, purity (214) =

96.6%.

N-(4-((4,5-dihydroisoxazol-3-yl)oxy)but-2-yn-1-yl)-6-((4-((3-(ethoxycarbonyl)-4-oxoquinolin-1(4*H*)-yl)methyl)phenyl)amino)-*N,N*-dimethyl-6-oxohexan-1-aminium bromide (**32b**)
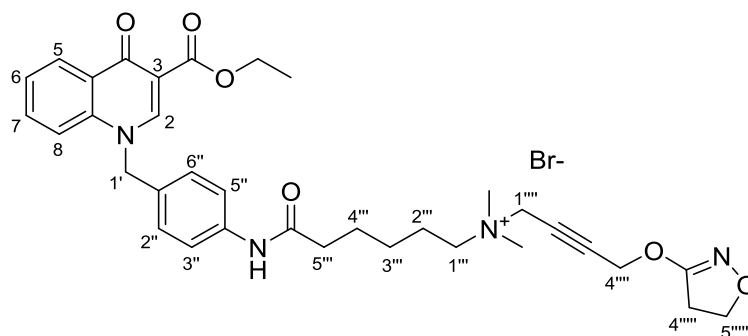
Clear pale yellow oil; 112.9 mg, 83 %; δ_H (d_6-DMSO) 9.96 (s, 1H, NH), 8.90 (s, 1H, H2), 8.25 (d, *J*= 9.0 Hz, 1H, H5), 7.72-7.62 (m, 2H, H7, H8), 7.57 (d, *J*= 8.5 Hz, 2H, H3″, H5″), 7.44 (ddd, *J*= 8.0, 6.5, 1.5 Hz, 1H, H6), 7.21 (d, *J*= 8.5 Hz, 2H, H2″, H6″), 5.61 (s, 2H, H1′), 4.92 (s, 2H, H4‴′), 4.43 (s, 2H, H1‴′), 4.27 (m, 4H, H5‴″, OC*H*$_2$CH$_3$), 3.07 (s, 6H, N+(C*H*$_3$)$_2$), 3.03-2.96 (m, 4H, H4‴″, H1‴), 2.32 (t, *J*= 7.0 Hz, 2H, H5‴), 1.76-1.56 (m, 4H, H2‴, H4‴), 1.33-1.26 (m, 5H, H3‴, OCH$_2$C*H*$_3$); δ_C (d_6-DMSO) 173.4 (C), 171.5 (C), 167.2 (C), 165.2 (C), 150.5 (CH), 139.5 (C), 139.4 (C), 133.0 (CH), 130.7 (C), 128.9 (C), 127.6 (CH), 126.9 (CH), 125.4 (CH), 119.9 (CH), 118.3 (CH), 110.6 (C), 86.5 (CH$_2$), 76.6 (CH$_2$), 69.9 (CH$_2$), 63.5 (CH$_2$), 60.3 (CH$_2$), 58.0 (CH$_2$), 55.8 (CH$_2$), 53.7 (CH$_2$), 50.3 (CH$_3$), 36.4 (CH$_2$), 32.8 (CH$_2$), 32.7 (CH$_2$), 25.0 (CH$_2$), 22.2 (CH$_2$), 14.8 (CH$_3$); *m/z* LCMS [M]$^+$ 601.3; LCMS: t_R = 4.54 min, purity = 93.6%.

<u>*N*-(4-((4,5-dihydroisoxazol-3-yl)oxy)but-2-yn-1-yl)-10-((4-((3-(ethoxycarbonyl)-4-oxoquinolin-1(4*H*)-yl)methyl)phenyl)amino)-*N*,*N*-dimethyl-10-oxodecan-1-aminium bromide (**32c**)</u>
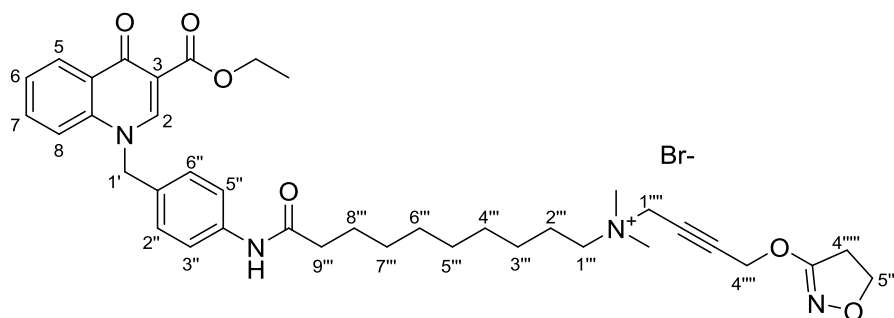
Clear colourless oil; 33.4 mg, 24 %; δ_H (d_6-DMSO) 9.97 (s, 1H, NH), 8.91 (s, 1H, H2), 8.24 (d, *J* = 7.5 Hz, 1H, H5), 7.70-7.64 (m, 2H, H7, H8), 7.58 (d, *J* = 8.5 Hz, 2H, H3″, H5″), 7.44 (ddd, *J* = 8.0, 6.0, 2.0 Hz, 1H, H6), 7.20 (d, *J* = 8.5 Hz, 2H, H2″, H6″), 5.62 (s, 2H, H1′), 4.93 (s, 2H, H4‴′), 4.48 (s, 2H, H1‴′), 4.32-4.23 (m, 4H, H5‴‴, OC*H*$_2$CH$_3$), 3.47 (m, 2H, H1‴), 3.09 (s, 6H, N+(C*H*$_3$)$_2$), 3.01 (m, 4H, H4‴‴′, H9‴), 2.29 (m, 2H, H2‴), 1.66 (br s, 2H, H8‴), 1.55 (br s, 2H, H3‴), 1.29 (m, 11H, H4‴- H7‴, OCH$_2$C*H*$_3$); δ_C (d_6-DMSO) 173.5 (C), 171.8 (C), 167.2 (C), 165.1 (C), 150.5 (CH), 139.5 (C), 133.0 (CH), 130.6 (C), 128.9 (C), 127.5 (CH), 126.8 (CH), 125.4 (CH), 119.8 (CH), 118.4 (CH), 110.5 (C), 86.4 (C), 82.4 (C), 80.7 (C), 76.7 (CH$_2$), 69.9 (CH$_2$), 63.6 (CH$_2$), 60.3 (CH$_2$), 58.0 (CH$_2$), 57.7 (CH$_2$), 55.8 (CH$_2$), 53.7 (CH$_2$), 50.2 (CH$_3$), 43.7 (CH$_2$), 36.8 (CH$_2$), 32.8 (CH$_2$), 29.1 (CH$_2$), 26.1 (CH$_2$), 25.5 (CH$_2$), 22.2 (CH$_2$), 14.8 (CH$_3$); *m/z* LCMS [M]$^+$ 657.4; LCMS: t_R = 4.80 min, purity = >99%.

N-(4-((4,5-dihydroisoxazol-3-yl)oxy)but-2-yn-1-yl)-6-((4-((3-((2-

hydroxycyclohexyl)carbamoyl)-4-oxoquinolin-1(4*H*)-yl)methyl)phenyl)amino)-*N,N*-

dimethyl-6-oxohexan-1-aminium bromide (**44**)
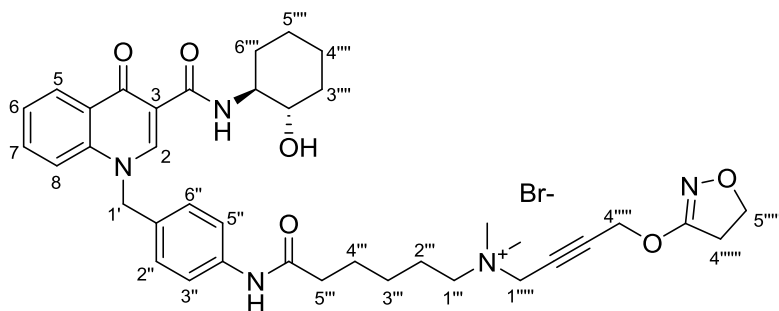
Clear colourless oil; 26.2 mg, 36 %; δ$_H$ (*d*$_6$-DMSO) 10.09 (d, *J*= 7.5 Hz, 1H, NH), 9.98 (s,

1H, NH), 9.03 (s, 1H, H2), 8.35 (d, *J*= 8.0 Hz, 1H, H5), 7.83-7.70 (m, 2H, H7, H8), 7.57 (d,

J= 8.5 Hz, 2H, H3″, H5″), 7.51 (ddd, *J*= 8.0, 6.5, 1.5 Hz, 1H, H6), 7.19 (d, *J*= 8.5 Hz, 2H,

H2″, H6″), 5.71 (s, 2H, H1′), 4.92 (s, 2H, H4″″″), 4.82 (br s, 1H, OH), 4.43 (s, 2H, H1″″″),

4.30 (app td, *J*= 9.5, 4.0 Hz, 4H, H5″″″″, H1‴), 3.39 (m, 5H, H2″″, H5‴, H2‴), 3.00 (app td,

J= 9.5, 4.5 Hz, 5H, H4″″″″, H4‴, H1″″), 2.32 (app t, *J*= 7.0 Hz, 2H, H3‴), 2.26 (s, 6H,

N+(C*H*$_3$)$_2$), 1.73-1.57 (m, 6H, H3″″, H4″″, H6″″), 1.37-1.22 (m, 2H, H5″″); δ$_C$ (*d*$_6$-DMSO)

176.1 (C), 171.5 (C), 167.2 (C), 164.3 (C), 149.0 (CH), 139.6 (C), 139.4 (C), 133.3 (CH),

130.7 (C), 127.9 (C), 127.7 (CH), 126.6 (CH), 125.5 (CH), 119.9 (CH), 118.4 (CH), 111.8

(C), 86.5 (C), 76.6 (C), 71.7 (CH), 70.1 (CH$_2$), 69.9 (CH$_2$), 63.5 (CH$_2$), 58.0 (CH$_2$), 57.7

(CH$_2$), 56.0 (CH$_2$), 53.7 (CH$_2$), 50.3 (CH), 47.4 (CH$_2$), 43.9 (CH$_3$), 36.4 (CH$_2$), 32.8 (CH$_2$),

32.7 (CH$_2$), 25.8 (CH$_2$), 25.0 (CH$_2$), 22.2 (CH$_2$); *m/z* LCMS [M]$^+$ 670.3; *m/z* HRMS (TOF

ES$^+$) C$_{38}$H$_{48}$N$_5$O$_6$ [M]$^+$ calcd 670.3603, found 670.3607; HPLC: *t*$_R$ = 7.80 min, purity (254) =

97.0%, purity (214) = 95.5%.

Synthesis of 1-(4-(6-hydroxyhexanamido)benzyl)-4-oxo-1,4-dihydroquinoline-3-carboxylic acid (35)
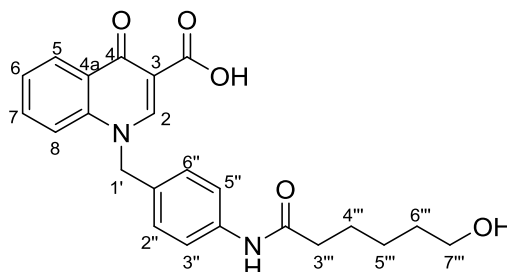
Ethyl 1-(4-(6-hydroxyhexanamido)benzyl)-4-oxo-1,4-dihydroquinoline-3-carboxylate (**34**) (98 mg, 223.6 μmol) and methanol (1.5 mL) were brought to 0 °C in an icebath. A solution of 1 M KOH$_{(aq)}$ (670.8 μL, 670.8 μmol) was added dropwise whilst stirring and then the reaction mixture was heated at 80 °C for 1 h. Reaction mixture was cooled to RT and a solution of 1 M HCl$_{(aq)}$ (670.8 μL, 670.8 μmol) was added. The target molecule precipitated out and was isolated as a cream-coloured solid by vacuum filtration, washed with deionized water to remove the residual acid, then dried under vacuum overnight. quantitative; mp 221-222 °C; δ$_H$ (d_6-DMSO) 15.12 (s, 1H, OH), 9.97 (s, 1H, NH), 9.24 (s, 1H, H2), 8.39 (d, J= 8.5 Hz, 1H, H5), 7.94-7.82 (m, 2H, H7, H8), 7.63 (ddd, J= 8.0, 6.0, 2.0 Hz, 1H, H6), 7.56 (d, J= 8.5 Hz, 2H, H3″, H5″), 7.23 (d, J= 8.5 Hz, 2H, H2″, H6″), 5.79 (s, 2H, H1′), 3.37 (t, J= 6.5 Hz, 2H, H7‴), 2.26 (t, J= 7.5 Hz, 2H, H3‴), 1.61-1.50 (m, 2H, H4‴), 1.46-1.37 (m, 2H, H6‴), 1.34-1.22 (m, 2H, H5‴); δ$_C$ (d_6-DMSO) 178.4 (C), 171.9 (C), 166.6 (C), 150.4 (CH), 139.9 (C), 139.6 (C), 134.7 (CH), 129.9 (C), 127.8 (CH), 126.9 (CH), 126.4 (CH), 126.2 (C), 119.9 (CH), 119.2 (CH), 108.2 (C), 61.0 (CH$_2$), 56.7 (CH$_2$), 36.9 (CH$_2$), 32.7 (CH$_2$), 25.6 (CH$_2$), 25.5 (CH$_2$); m/z LCMS [MH]$^+$ 409.2; LCMS: t_R = 5.27 min, purity = 96.6%.

Synthesis of 1-(4-nitrobenzyl)-4-oxo-1,4-dihydroquinoline-3-carboxylic acid (40)
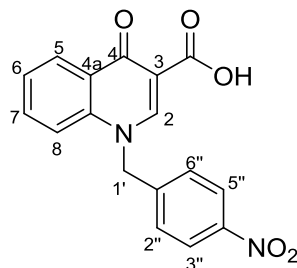
Ethyl 1-(4-nitrobenzyl)-4-oxo-1,4-dihydroquinoline-3-carboxylate (**39**) (1 g, 2.84 mmol) in 1:1 tetrahydrofuran: deionized water (18 mL total) was stirred at RT. LiOH.H$_2$O (357.3 mg, 8.51 mmol) was added and the reaction mixture was stirred at RT for 48 h. The reaction mixture was diluted with deionized water (10 mL) and washed once with diethyl ether (30 mL). The aqueous layer was then acidified to pH 2 with 1 M HCl$_{(aq)}$ before extracting with ethyl acetate (3 × 30 mL). The combined organic layers were washed with saturated sodium chloride$_{(aq)}$ then evaporated *in vacuo* to yield the target molecule as a pale yellow solid. 528 mg, 57%; mp 236-237 °C; δ_H (*d$_6$*-DMSO) 15.18 (s, 1H, OH), 9.42 (s, 1H, H2), 8.48 (dd, *J*= 8.0, 1.5 Hz, 1H, H5), 8.26 (d, *J*= 9.0 Hz, 2H, H3″, H5″), 7.98-7.88 (m, 1H, H7), 7.81 (d, *J*= 8.5 Hz, 1H, H8), 7.70 (app t, *J*= 7.5 Hz, 1H, H6), 7.59 (d, *J*= 9.0 Hz, 2H, H2″, H6″), 6.11 (s, 2H, H1′); δ_C (*d$_6$*-DMSO) 177.5 (C), 166.5 (C), 151.1 (CH), 147.4 (C), 144.8 (C), 139.5 (C), 132.9 (CH), 128.3 (C), 128.0 (CH), 127.0 (CH), 124.8 (CH), 124.5 (CH), 118.4 (C), 117.7 (CH), 55.2 (CH$_2$); *m/z* LCMS [MH]$^+$ 325.1; LCMS: t_R = 5.81 min, purity = 99.4%.

General procedure for room temperature HCTU coupling

1-(4-Nitrobenzyl)-4-oxo-1,4-dihydroquinoline-3-carboxylic acid (**40**) (158 mg, 487 µmol) or 6-bromohexanoic acid (25 mg, 128 µmol), (1*S*,2*S*)-2-Aminocyclohexanol hydrochloride or 1-(4-aminobenzyl)-*N*-(2-hydroxycyclohexyl)-4-oxo-1,4-dihydroquinoline-3-carboxamide (**42**) (1.2 eq.) and HCTU (1.2 eq.) were stirred in *N,N*-dimethylformamide (1-3 mL) at RT. *N,N*-

diisopropylethylamine (3 eq.) dissolved in dichloromethane (0.5-1 mL) was added and the reaction mixture stirred for 3-6 h at RT. The dichloromethane was removed *in vacuo*, then the reaction mixture was diluted with 1 M $HCl_{(aq)}$ (20 mL) and extracted with ethyl acetate (3 × 20 mL). The combined organic layers were washed with saturated sodium bicarbonate$_{(aq)}$ (1 × 20 mL), deionized water (1 × 20 mL) and saturated sodium chloride$_{(aq)}$ (1 × 20 mL). The organic layer was dried over Na_2CO_3, filtered and evaporated *in vacuo* to yield the target molecule.

<u>*N*-(2-hydroxycyclohexyl)-1-(4-nitrobenzyl)-4-oxo-1,4-dihydroquinoline-3-carboxamide (**41**)</u>
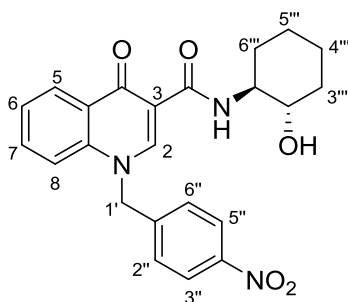
Yellow solid; 200.3 mg, 97 %; δ_H (d_6-DMSO) 10.08 (d, *J*= 7.5 Hz, 1H, NH), 9.13 (s, 1H, H2), 8.37 (d, *J*= 8.0 Hz, 1H, H5), 8.20 (d, *J*= 8.5 Hz, 2H, H3″, H5″), 7.73 (dd, *J*= 8.5, 7.0 Hz, 1H, H7), 7.64 (d, *J*= 8.5 Hz, 1H, H8), 7.57-7.41 (m, 3H, H6, H2″, H6″), 5.97 (s, 2H, H1′), 4.82 (d, *J*= 5.0 Hz, 1H, OH), 3.69 (br s, 1H, H2″), 3.40 (br s, 1H, H1″), 2.09-2.01 (m, 1H, H6‴ (1H)), 1.94-1.80 (m, 1H, H3‴ (1H)), 1.71-1.56 (m, 2H, H4‴), 1.42-1.22 (m, 4H, H3‴ (1H), H5‴, H6‴ (1H)); δ_C (d_6-DMSO) 176.3 (C), 164.2 (C), 149.5 (CH), 147.5 (C), 144.4 (C), 139.4 (C), 133.6 (CH), 128.1 (CH), 127.9 (C), 126.8 (CH), 125.7 (CH), 124.5 (CH), 118.2 (CH), 112.2 (C), 71.7 (CH), 55.6 (CH_2), 54.1 (CH), 34.2 (CH_2), 31.1 (CH_2), 24.2 (CH_2), 23.7 (CH_2); *m/z* LCMS [M+H]$^+$ 422.2; LCMS: t_R = 5.91 min, purity = 88.3%.

1-(4-(6-Bromohexanamido)benzyl)-*N*-(2-hydroxycyclohexyl)-4-oxo-1,4-dihydroquinoline-3-carboxamide (**43**)
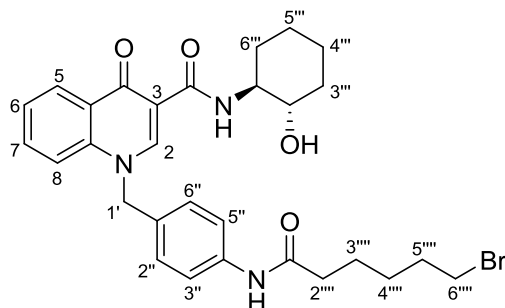
54.5 mg, 75 %; δ_H (d_6-DMSO) 10.15 (d, *J*= 7.5 Hz, 1H, NH), 9.99 (s, 1H, NH), 9.10 (s, 1H, H2), 8.41 (d, *J*= 7.5 Hz, 1H, H5), 7.91-7.74 (m, 2H, H7, H8), 7.68-7.49 (m, 3H, H6, H3″, H5″), 7.24 (d, *J*= 8.5 Hz, 2H, H2″, H6″), 5.77 (s, 2H, H1′), 4.88 (d, *J*= 5.0 Hz, 1H, OH), 3.85-3.69 (m, 1H, H2‴), 3.58 (t, *J*= 6.5 Hz, 2H, H6⁗), 2.37 (t, *J*= 7.5 Hz, 2H, H2⁗), 2.09 (d, *J*= 10.5 Hz, 1H, H1‴), 1.99-1.81 (m, 3H, H6‴ (1H), H5⁗), 1.78-1.52 (m, 5H, H3‴ (1H), H4‴, H3⁗), 1.52-1.23 (m, 6H, H3‴ (1H), H6‴ (1H), H4⁗); δ_C (d_6-DMSO) 176.1 (C), 171.6 (C), 164.4 (C), 162.5 (C), 149.1 (CH), 139.6 (C), 139.4 (C), 133.3 (CH), 127.9 (C), 127.6 (CH), 126.6 (CH), 125.5 (CH), 119.9 (CH), 118.4 (CH), 111.8 (C), 71.7 (CH), 56.0 (CH₂), 54.1 (CH), 36.6 (CH₂), 35.5 (CH₂), 34.2 (CH₂), 32.5 (CH₂), 29.3 (CH₂), 27.6 (CH₂), 24.7 (CH₂), 24.2 (CH₂), 23.7 (CH₂); *m/z* LCMS [M+H]⁺ 568.2; LCMS: t_R = 6.14 min, purity = 70.2%.

Synthesis of 1-(4-aminobenzyl)-*N*-(2-hydroxycyclohexyl)-4-oxo-1,4-dihydroquinoline-3-carboxamide (42)
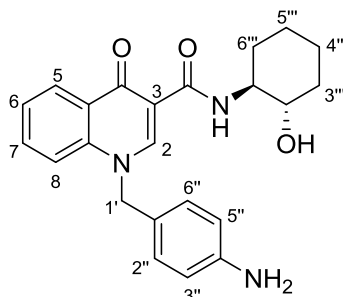
N-(2-Hydroxycyclohexyl)-1-(4-nitrobenzyl)-4-oxo-1,4-dihydroquinoline-3-carboxamide (**41**) (200 mg, 475 μmol) was dissolved in *N,N*-dimethylformamide (3 mL). 10% Pd/C (20 mg) was added under a nitrogen atmosphere then, following evacuation of nitrogen, the reaction mixture was stirred for 1 h at RT under a hydrogen atmosphere. The reaction mixture was then filtered through Celite® and washed with methanol. Upon concentration of the reaction mixture *in vacuo*, a white precipitate formed that was collected by vacuum filtration and washed with diethyl ether (64 mg, 35%). mp 185-186 °C; δ_H (d_6-DMSO) 10.09 (d, *J*= 7.5 Hz, 1H, NH), 8.97 (s, 1H, H2), 8.33 (dd, *J*= 8.0, 1.5 Hz, 1H, H5), 7.86 (d, *J*= 8.5 Hz, 1H, H8), 7.76 (ddd, *J*= 8.5, 7.0, 1.5 Hz, 1H, H7), 7.50 (app t, *J*= 7.5 Hz, 1H, H6), 6.96 (d, *J*= 8.5 Hz, 2H, H2″, H6″), 6.51 (d, *J*= 8.5 Hz, 2H, H3″, H5″), 5.52 (s, 2H, H1′), 5.14 (s, 2H, NH₂), 4.81 (d, *J*= 5.0 Hz, 1H, OH), 3.74-3.62 (m, 1H, H2‴), 3.45-3.35 (m, 1H, H1‴), 2.09-1.95 (m, 1H, H6‴ (1H)), 1.93-1.79 (m, 1H, H3‴ (1H)), 1.73-1.53 (m, 2H, H4‴), 1.38-1.11 (m, 4H, H3‴ (1H), H5‴, H6‴ (1H)); δ_C (d_6-DMSO) 176.0 (C), 164.4 (C), 149.1 (C), 148.6 (CH), 139.6 (C), 133.2 (CH), 128.5 (CH), 127.8 (C), 126.5 (CH), 125.4 (CH), 122.4 (C), 118.5 (CH), 114.4 (CH), 111.6 (C), 71.7 (CH), 56.3 (CH₂), 54.1 (CH), 34.2 (CH₂), 31.1 (CH₂), 24.2 (CH₂), 23.7 (CH₂); *m/z* LRMS (TOF ES⁺) [M+H]⁺ 392.1; LCMS: t_R = 4.91 min, purity = 94.8%.

Pharmacology

Radioligand Equilibrium Whole Cell Binding Assays

   Plate preparation. FlpIn-CHO cells stably expressing human muscarinic M_1 receptors (hM_1 mAChR FlpIn-CHO) were cultured at 37 °C in 5% CO_2 in Dulbecco's modified Eagle medium (DMEM) supplemented with 5% (v/v) foetal bovine serum (FBS) and 16 mM HEPES. Cells were seeded into white opaque Isoplates™ at 8×10^3 cells per well and then grown at 37 °C for 20-24 h. Cells were then washed twice with cold HEPES-buffered saline, 140 μL per well cold HEPES-buffered saline was added and the plates kept on ice.

   Assay protocol (one "cold" interacting ligand). Stock solutions of each ligand (10^{-2} M) were made up in cold HEPES-buffered saline. Dilutions of all ligands were made up in cold HEPES-buffered saline at ten times (10×) the required concentration and added to stock plates on ice. Cells were equilibrated at 4 °C for 4 h with 20 μL of a single interacting ligand and 20 μL of 0.1 nM [^{3}H]NMS (total volume 200 μL per well).

   Assay protocol (two "cold" interacting ligands) Stock solutions of each orthosteric ligand (10^{-2} M) were made up in cold HEPES-buffered saline. Stock solutions of the interacting allosteric ligands of choice (10^{-2} M) were made up in DMSO. Dilutions of all ligands were made up in cold HEPES-buffered saline at ten times (10×) the required concentration and added to stock plates on ice. Cells were equilibrated at 4 °C for 4 h with 20 μL of ACh, 20 μL of a single interacting allosteric ligand and 20 μL of 0.1 nM [^{3}H]NMS (total volume 200 μL per well).

   Assay termination and data collection. Assays were terminated by media removal, 2 × 100 μL per well washes with 0.9% NaCl solution and addition of 100 μL per well Microscint-20 scintillation liquid. The levels of remaining bound radioligand, and therefore

the degree of radioligand displacement, was measured in disintegrations per minute (dpm) on the Microbeta2™ LumiJET 2460 microplate counter (PerkinElmer).

AlphaScreen ERK1/2 Phosphorylation Assays

Plate preparation. FlpIn-CHO cells stably expressing human muscarinic M_1 receptors (hM$_1$ mAChR FlpIn-CHO) were cultured at 37 °C in 5% CO_2 in DMEM supplemented with 5% (v/v) FBS and 16 mM HEPES. Cells were seeded into transparent 96-well plates at 5×10^4 cells per well and grown for 6 h. Cells were then washed once with phosphate-buffered saline (PBS) and incubated in serum-free DMEM (180 µL per well) at 37 °C overnight (16-18 h) to allow FBS-stimulated phosphorylated ERK1/2 levels to subside.

Time course assays. A stock solution of ACh (10^{-2} M) was made up in MilliQ water. Stock solutions of the test ligands (10^{-2} M) were made up in DMSO. All ligands were diluted to 10^{-5} M in serum-free DMEM. Ligand additions (20 µL) were made at predetermined time points over a 30 minute period (30, 25, 20, 15, 10, 8, 6, 5, 3 and 1 min) with the cells being incubated at 37 °C following each addition. FBS, which triggers ERK1/2 phosphorylation via a tyrosine kinase receptor, was added at 6 min as a measure of the maximal levels of pERK1/2 production.

Concentration-response curves (CRCs). A stock solution of ACh (10^{-2} M) was made up in MilliQ water. Stock solutions of the test ligands (10^{-2} M) were made up in DMSO. Dilutions of all ligands were made up in FBS-free media at ten times ($10\times$) the required concentration and added to stock plates. Cells were incubated at 37 °C with 20 µL per well of each concentration of all compounds at 5 min (as determined by time course assays).

Interaction studies. A stock solution of ACh (10^{-2} M) was made up in MilliQ water. Stock solutions of the allosteric test ligands (10^{-2} M) were made up in DMSO. Dilutions of ACh

and the interacting ligand were made up in FBS-free media at twenty times (20×) the ideal concentration range (as determined by CRC assays). Equal volumes of each concentration of ACh and each concentration of the interacting ligand of choice were premixed in stock plates. Cells were incubated at 37 °C with 20 µL per well of each ligand mixture at 5 min (as determined by time course assays).

Assay termination and data collection. Agonist-stimulated ERK1/2 phosphorylation was terminated by the removal of drugs and the addition of 100 µL p/well of *SureFire*™ lysis buffer. The cell lysates were agitated for 5-10 min. Following agitation, 5 µL of cell lysates were transferred into a 384-well white opaque Optiplate™, followed by addition of 8.5 µL of a solution of Reaction buffer/Activation buffer/acceptor beads/donor beads in a ratio of 6/1/0.3/0.3 (v/v/v/v) under green light conditions. The plates were then incubated at 37 °C in the dark for 1 h and fluorescence was measured on a Fusion-α™ plate reader (PerkinElmer) using standard AlphaScreen settings.

Data analysis

All data analysis was managed using Prism 6 software (GraphPad Software, San Diego, CA). Experiments measuring radioligand equilibrium whole cell binding interactions were fitted to the allosteric ternary complex model (**1**):

$$Y = \frac{[A]}{[A] + (\dfrac{K_A K_B}{\alpha'[B] + K_B})(1 + \dfrac{[I]}{K_I} + \dfrac{[B]}{K_B} + \dfrac{\alpha[I][B]}{K_I K_B})} \quad \textbf{(1)}$$

where Y is the percentage (vehicle control) binding, [A], [B] and [I] are the concentrations of [^{3}H]NMS, the allosteric ligand, and ACh respectively, K_A and K_B are the equilibrium dissociation constants of [^{3}H]NMS and the allosteric ligand, respectively, K_I is the equilibrium dissociation constant of ACh, and α and α' are the cooperativities between the

allosteric ligand and [³H]NMS or ACh, respectively. Values of α (or α') > 1 denote positive cooperativity; values <1 (but >0) denote negative cooperativity, and values = 1 denote neutral cooperativity. Functional orthosteric and allosteric agonist concentration-response curves were fitted via nonlinear regression to the three-parameter logistic function (**2**):

$$E = Basal + \frac{(E_{max} - basal)}{1 + 10^{-pEC_{50} - Log\,[A])}} \quad \textbf{(2)}$$

where E is response, E_{max} and basal are the top and bottom asymptotes of the curve, respectively, log $[A]$ is the logarithm of the agonist concentration, and pEC_{50} is the negative logarithm of the agonist concentration that gives a response halfway between E_{max} and basal. Functional experiments measuring the interactions between ACh and each allosteric ligand were fitted to the operational model of allosterism and agonism (**3**)[47,48] to derive functional estimates of modulator affinity, cooperativity, and efficacy.

$$E = \frac{E_m(\tau_A[A](K_B + \alpha\beta[B]) + \tau_B[B]K_A)^n}{([A]K_B + K_AK_B + [B]K_A + \alpha[A][B])^n + (\tau_A[A](K_B + \alpha\beta[B]) + \tau_B[B]K_A)^n} \quad \textbf{(3)}$$

where E_m is the maximum attainable system response for the pathway under investigation; $[A]$ and $[B]$ are the concentrations of orthosteric and allosteric ligands, respectively; K_A and K_B are the equilibrium dissociation constants of the orthosteric and allosteric ligands, respectively; τ_A and τ_B are the operational measures of orthosteric and allosteric ligand efficacy (which incorporate both signal efficiency and receptor density), respectively; n is a transducer slope factor linking occupancy to response; α is the binding cooperativity parameter between the orthosteric and allosteric ligand; β denotes the magnitude of the allosteric effect of the modulator on the efficacy of the orthosteric agonist.[47,43] In all cases, the equilibrium dissociation constant of each allosteric ligand was fixed to that determined from the competition binding experiments.

References

(1) Schwyzer, R. (1977) ACTH: a short introductory review. *Ann. N.Y. Acad. Sci.*, *297*, 3-26.

(2) Portoghese, P. (1989) Bivalent ligands and the message-address concept in the design of selective opioid receptor antagonists. *Trends Pharmacol. Sci.*, *10*, 230-235.

(3) Valant, C., Lane, J. R., Sexton, P. M. and Christopoulos, A. (2012) The Best of Both Worlds? Bitopic Orthosteric/Allosteric Ligands of G Protein-Coupled Receptors. *Annu. Rev. Pharmacol. Toxicol.*, *52*, 153-178.

(4) Mohr, K., Schmitz, J., Schrage, R., Trankle, C. and Holzgrabe, U. (2013) Molecular Alliance- From Orthosteric and Allosteric Ligands to Dualsteric/Bitopic Agonists at G Protein Coupled Receptors. *Angew. Chem.*, *52*, 508-516.

(5) Valant, C., Sexton, P. M. and Christopoulos, A. (2009) Orthosteric/Allosteric Bitopic Ligands - Going Hybrid at GPCRs. *Mol. Interv.*, *9*, 125-135.

(6) Valant, C., May, L. T., Aurelio, L., Chuo, C. H., White, P. J., Baltos, J.-A., Sexton, P. M., Scammells, P. J. and Christopoulos, A. (2014) Separation of on-target efficacy from adverse effects through rational design of a bitopic adenosine receptor agonist. *Proc. Natl. Acad. Sci. USA*.

(7) Jakubik, J. and El-Fakahany, E. E. (2010) Allosteric Modulation of Muscarinic Acetylcholine Receptors. *Pharmaceuticals*, *3*, 2838-2860.

(8) Bock, A. and Mohr, K. (2013) Dualsteric GPCR targeting and functional selectivity: the paradigmatic M_2 muscarinic acetylcholine receptor. *Drug Discov. Today Technol.*

(9) Langmead, C. J., Watson, J. and Reavill, C. (2008) Muscarinic Acetylcholine Receptors as CNS Drug Targets. *Pharmacol. Ther.*, *117*, 232-243.

(10) Valant, C., Gregory, K. J., Hall, N. E., Scammells, P. J., Lew, M. J., Sexton, P. M. and Christopoulos, A. (2008) A Novel Mechanism of G Protein-coupled Receptor Functional Selectivity - Muscarinic Partial Agonist McN-A-343 As A Bitopic Orthosteric/Allosteric Ligand. *J. Biol. Chem.*, *283*, 29312-29321.

(11) Jones, C. K., Brady, A. E., Davis, A. A., Xiang, Z., Bubser, M., Noor Tantawy, M., Kane, A. S., Bridges, T. M., Kennedy, J. P., Bradley, S. R., Peterson, T. E., Ansari, M. S., Baldwin, R. M., Kessler, R. M., Deutch, A. Y., Lah, J. J., Levey, A. I., Lindsley, C. W. and Conn, P. J. (2008) Novel Selective Allosteric Activator of the M_1 Muscarinic Acetylcholine Receptor Regulates Amyloid Processing and Produces Antipsychotic-Like Activity in Rats. *J. Neurosci.*, *28*, 10422-10433.

(12) Sheffler, D. J., Sevel, C., Le, U., Lovett, K. M., Tarr, J. C., Carrington, S. J. S., Cho, H. P., Digby, G. J., Niswender, C. M., Conn, P. J., Hopkins, C. R., Wood, M. R. and Lindsley, C. W. (2013) Further exploration of M_1 allosteric agonists: Subtle structural changes abolish M_1 allosteric agonism and result in *pan*-mAChR orthosteric antagonism. *Bioorg. Med. Chem. Lett.*, *23*, 223-227.

(13) Keov, P., Valant, C., Devine, S. M., Lane, J. R., Scammells, P. J., Sexton, P. M. and Christopoulos, A. (2013) Reverse Engineering of the Selective Agonist TBPB Unveils Both Orthosteric and Allosteric Modes of Action at the M_1 Muscarinic Acetylcholine Receptor. *Mol. Pharmacol.*, *84*, 425-437.

(14) Avlani, V. A., Langmead, C. J., Guida, E., Wood, M. D., Tehan, B. G., Herdon, H. J., Watson, J. M., Sexton, P. M. and Christopoulos, A. (2010) Orthosteric and Allosteric Modes of Interaction of Novel Selective Agonists of the M_1 Muscarinic Acetylcholine Receptor. *Mol. Pharmacol.*, *78*, 94-104.

(15) Nathan, P. J., Watson, J., Lund, J., Davies, C. H., Peters, G., Dodds, C. M., Swirski, B., Lawrence, P., Bentley, G. D., O'Neill, B. V., Robertson, J., Watson, S., Jones, G. A., Maruff, P., Croft, R. J., Laruelle, M. and Bullmore, E. T. (2013) The potent M_1 receptor allosteric agonist GSK1034702 improves episodic memory in humans in the nicotine abstinence model of cognitive dysfunction. *Int. J. Neuropsychopharmacol.*, *16*, 721-731.

(16) Antony, J., Kellershohn, K., Mohr-Andra, M., Kebig, A., Prilla, S., Muth, M., Heller, E., Disingrini, T., Dallanoce, C., Bertoni, S., Schrobang, J., Trankle, C., Kostenis, E., Christopoulos, A., Holtje, H.-D., Barocelli, E., De Amici, M., Holzgrabe, U. and Mohr, K. (2009) Dualsteric GPCR targeting: a novel route to binding and signaling pathway selectivity. *FASEB J.*, *23*, 442-450.

(17) Disingrini, T., Muth, M., Dallanoce, C., Barocelli, E., Bertoni, S., Kellershohn, K., Mohr, K., De Amici, M. and Holzgrabe, U. (2006) Design, Synthesis, and Action of Oxotremorine-Related Hybrid-Type Allosteric Modulators of Muscarinic Acetylcholine Receptors. *J. Med. Chem.*, *49*, 366-372.

(18) Steinfeld, T., Mammen, M., Smith, J. A. M., Wilson, R. D. and Jasper, J. R. (2007) A Novel Multivalent Ligand That Bridges the Allosteric and Orthosteric Binding Sites of the M_2 Muscarinic Receptor. *Mol. Pharmacol.*, *72*, 291-302.

(19) Bock, A., Merten, N., Schrage, R., Dallanoce, C., Batz, J., Klockner, J., Schmitz, J., Matera, C., Simon, K., Kebig, A., Peters, L., Muller, A., Schrobang-Ley, J., Trankle, C., Hoffman, C., De Amici, M., Holzgrabe, U., Kostenis, E. and Mohr, K. (2012) The allosteric

vestibule of a seven transmembrane helical receptor controls G-protein coupling. *Nat. Commun.*

(20) Bock, A., Chirinda, B., Krebs, F., Messerer, R., Batz, J., Muth, M., Dallanoce, C., Klingenthal, D., Trankle, C., Hoffmann, C., De Amici, M., Holzgrabe, U., Kostenis, E. and Mohr, K. (2014) Dynamic ligand binding dictates partial agonism at a G protein-coupled receptor. *Nat. Chem. Biol.*, *10*, 18-22.

(21) Lane, J. R., Sexton, P. M. and Christopoulos, A. (2013) Bridging the gap: bitopic ligands of G-protein-coupled receptors. *Trends Pharmacol. Sci.*, *34*, 59-66.

(22) Dallanoce, C., Conti, P., De Amici, M., De Micheli, C., Barocelli, E., Chiavarini, M., Ballabeni, V., Bertoni, S. and Impicciatore, M. (1999) Synthesis and Functional Characterization of Novel Derivatives Related to Oxotremorine and Oxotremorine-M. *Bioorg. Med. Chem.*, *7*, 1539-1547.

(23) Ma, L., Seager, M. A., Wittman, M., Jacobson, M., Bickel, D., Burno, M., Jones, K., Graufelds, V. K., Xu, G., Pearson, M., McCampbell, A., Gaspar, R., Shughrue, P., Danziger, A., Regan, C., Flick, R., Pascarella, D., Garson, S., Doran, S., Kreatsoulas, C., Veng, L., Lindsley, C. W., Shipe, W., Kuduk, S., Sur, C., Kinney, G., Seabrook, G. R. and Ray, W. J. (2009) Selective Activation of the M_1 Muscarinic Acetylcholine Receptor Achieved by Allosteric Potentiation. *Proc. Natl. Acad. Sci. USA*, *106*, 15950-15955.

(24) Canals, M., Lane, J. R., Wen, A., Scammells, P. J., Sexton, P. M. and Christopoulos, A. (2012) A Monod-Wyman-Changeux Mechanism Can Explain G Protein-coupled Receptor (GPCR) Allosteric Modulation. *J. Biol. Chem.*, *287*, 650-659.

(25) Kruse, A. C., Ring, A. M., Manglik, A., Hu, J., Hu, K., Eitel, K., Hubner, H., Pardon, E., Valant, C., Sexton, P. M., Christopoulos, A., Felder, C. C., Gmeiner, P., Steyaert, J., Weis, W. I., Garcia, K. C., Wess, J. and Kobilka, B. K. (2013) Activation and Allosteric Modulation of a Muscarinic Acetylcholine Receptor. *Nature*, *504*, 101-106.

(26) Leach, K., Loiacono, R. E., Felder, C. C., McKinzie, D. L., Mogg, A., Shaw, D. B., Sexton, P. M. and Christopoulos, A. (2010) Molecular Mechanisms of Action and *In Vivo* Validation of an M_4 Muscarinic Acetylcholine Receptor Allosteric Modulator with Potential Antipsychotic Properties. *Neuropsychopharmacology*, *35*, 855-869.

(27) Haga, K., Kruse, A. C., Asada, H., Yurugi-Kobayashi, T., Shiroishi, M., Zhang, C., Weis, W. I., Okada, T., Kobilka, B. K., Haga, T. and Kobayashi, T. (2012) Structure of the human M2 muscarinic acetylcholine receptor bound to an antagonist. *Nature*, *482*, 547-552.

(28) Kruse, A. C., Hu, J., Pan, A. C., Arlow, D. H., Rosenbaum, D. M., Rosemond, E., Green, H. F., Liu, T., Chae, P. S., Dror, R. O., Shaw, D. E., Weis, W. I., Wess, J. and Kobilka, B. K. (2012) Structure and dynamics of the M3 muscarinic acetylcholine receptor. *Nature*, *482*, 552-559.

(29) Spalding, T. A., Birdsall, N. J. M., Curtis, C. A. M. and Hulme, E. C. (1994) Acetylcholine Mustard Labels the Binding Site Aspartate in Muscarinic Acetylcholine Receptors. *J. Biol. Chem.*, *269*, 4092-4097.

(30) Ellis, J. (1997) Allosteric Binding Sites on Muscarinic Receptors. *Drug Dev. Res.*, *40*, 193-204.

(31) Wess, J. (2005) Allosteric Binding Sites on Muscarinic Acetylcholine Receptors. *Mol. Pharmacol.*, *68*, 1506-1509.

(32) Abdul-Ridha, A., Lopez, L., Keov, P., Thal, D. M., Mistry, S. N., Sexton, P. M., Lane, J. R., Canals, M. and Christopoulos, A. (2014) Molecular Determinants of Allosteric Modulation at the M_1 Muscarinic Acetylcholine Receptor. *J. Biol. Chem.*, *289*, 6067-6079.

(33) Dror, R. O., Green, H. F., Valant, C., Borhani, D. W., Valcourt, J. R., Pan, A. C., Arlow, D. H., Canals, M., Lane, J. R., Rahmani, R., Baell, J. B., Sexton, P. M., Christopoulos, A. and Shaw, D. E. (2013) Structural basis for modulation of a G-protein-coupled receptor by allosteric drugs. *Nature*, *503*, 295-299.

(34) Wess, J., Maggio, R., Palmer, J. R. and Vogel, Z. (1992) Role of conserved threonine and tyrosine residues in acetylcholine binding and muscarinic receptor activation. A study with m3 muscarinic receptor point mutants. *J. Biol. Chem.*, *267*, 19313-19319.

(35) Gregory, K. J., Hall, N. E., Tobin, A. B., Sexton, P. M. and Christopoulos, A. (2010) Identification of orthosteric and allosteric site mutations in M_2 muscarinic acetylcholine receptors that contribute to ligand-selective signaling bias. *J. Biol. Chem.*, *285*, 7459-7474.

(36) Kuduk, S. D., Di Marco, C. N., Cofre, V., Pitts, D. R., Ray, W. J., Ma, L., Wittman, M., Seager, M., Koeplinger, K., Thompson, C. D., Hartman, G. D. and Bilodeau, M. T. (2010) Pyridine Containing M_1 Positive Allosteric Modulators with Reduced Plasma Protein Binding. *Bioorg. Med. Chem. Lett.*, *20*, 657-661.

(37) Kuduk, S. D., Di Marco, C. N., Cofre, V., Pitts, D. R., Ray, W. J., Ma, L., Wittman, M., Veng, L., Seager, M. A., Koeplinger, K., Thompson, C. D., Hartman, G. D. and Bilodeau, M. T. (2010) N-Heterocyclic Derived M_1 Positive Allosteric Modulators. *Bioorg. Med. Chem. Lett.*, *20*, 1334-1337.

(38) Kuduk, S. D., Di Marco, C. N., Cofre, V., Ray, W. J., Ma, L., Wittman, M., Seager, M. A., Koeplinger, K. A., Thompson, C. D., Hartman, G. D. and Bilodeau, M. T. (2011) Fused Heterocyclic M_1 Positive Allosteric Modulators. *Bioorg. Med. Chem. Lett.*, *21*, 2769-2772.

(39) Kuduk, S. D., Chang, R. K., Di Marco, C. N., Pitts, D. R., Greshock, T. J., Ma, L., Wittmann, M., Seager, M. A., Koeplinger, K. A., Thompson, C. D., Hartman, G. D., Bilodeau, M. T. and Ray, W. J. (2011) Discovery of a Selective Allosteric M_1 Receptor Modulator with Suitable Development Properties Based on a Quinolizidinone Carboxylic Acid Scaffold. *J. Med. Chem.*, *54*, 4773-4780.

(40) Davie, B. J., Valant, C., White, J. M., Sexton, P. M., Capuano, B., Christopoulos, A. and Scammells, P. J. (2014) Synthesis and Pharmacological Evaluation of Analogues of Benzyl Quinolone Carboxylic Acid (BQCA) Designed to Bind Irreversibly to an Allosteric Site of the M_1 Muscarinic Acetylcholine Receptor. *J. Med. Chem.*, *57*, 5405-5418.

(41) Kloeckner, J., Schmitz, J. and Holzgrabe, U. (2010) Convergent, short synthesis of the muscarinic superagonist iperoxo. *Tetrahedron Letters*, *51*, 3470-3472.

(42) Appel, R. (1975) Tertiary Phosphane/Tetrachloromethane, a Versatile Reagent for Chlorination, Dehydration, and P-N Linkage. *Angew. Chem.*, *14*, 801-811.

(43) Mistry, S. N., Valant, C., Sexton, P. M., Capuano, B., Christopoulos, A. and Scammells, P. J. (2013) Synthesis and Pharmacological Profiling of Analogues of Benzyl Quinolone Carboxylic Acid (BQCA) as Allosteric Modulators of the M_1 Muscarinic Receptor. *J. Med. Chem.*, *56*, 5151-5172.

(44) Ward, S. D. C., Curtis, C. A. M. and Hulme, E. C. (1999) Alanine-Scanning Mutagenesis of Transmembrane Domain 6 of the M_1 Muscarinic Acetylcholine Receptor Suggests that Tyr381 Plays Key Roles in Receptor Function. *Mol. Pharmacol.*, *56*, 1031-1041.

(45) Gregory, K. J., Sexton, P. M. and Christopoulos, A. (2007) Allosteric Modulation of Muscarinic Acetylcholine Receptors. *Curr. Neuropharmacol.*, *5*, 157-167.

(46) Gottlieb, H. E., Kotlyar, V. and Nudelman, A. (1997) NMR Chemical Shifts of Common Laboratory Solvents as Trace Impurities. *J. Org. Chem.*, *62*, 7512-7515.

(47) Leach, K., Sexton, P. M. and Christopoulos, A. (2007) Allosteric GPCR Modulators: Taking Advantage of Permissive Receptor Pharmacology. *Trends Pharmacol. Sci.*, *28*, 382-389.

(48) Valant, C., Aurelio, L., Urmaliya, V. B., White, P., Scammells, P. J., Sexton, P. M. and Christopoulos, A. (2010) Delineating the Mode of Action of Adenosine A_1 Receptor Allosteric Modulators. *Mol. Pharmacol.*, *78*, 444-455.

Chapter Five

Pharmacological Investigation of Analogues of Benzyl Quinolone Carboxylic Acid (BQCA) for the M$_1$ Muscarinic Acetylcholine Receptor

Introduction

Structure-activity relationship (SAR) studies are the mainstay of medicinal chemistry lead candidate optimization. Upon discovery of a novel chemical scaffold that elicits a specific biological activity via a receptor, channel or enzyme, determining the SAR between the ligand and the protein target is the next logical and crucial step; affording a better understanding of what parts of the structure are essential for activity, what parts are unnecessary, and what parts can be altered to improve activity, selectivity, or adsorption, distribution, metabolism and excretion (ADME) properties.

Typically this involves making iterative structural modifications to different regions of the molecule and observing the effects of these modifications on a single parameter in an *in vitro* pharmacological assay such as EC$_{50}$ (for agonists) or IC$_{50}$ (for antagonists). Such studies have afforded valuable information towards improving existing drug molecules or optimizing novel ligands with therapeutic potential for the treatment of a broad range of disorders including infectious disease,[1] central nervous system (CNS) disorders,[2,3] metabolic disorders,[4] cardiovascular conditions[5] and cancer[6] at a range of targets such as enzymes, DNA, ion channels and G protein-coupled receptors (GPCRs).

One barrier that SAR studies of GPCR ligands struggle to overcome is that of achieving absolute selectivity for a particular receptor subtype via the orthosteric (endogenous ligand) binding site. In the case of the aminergic GPCRs, the high degree of structural conservation across their orthosteric sites[7] renders designing a drug to target a single receptor subtype nigh on impossible. This has considerably slowed novel lead optimization efforts, prevented

otherwise clinically-useful drugs making it to market, and also resulted in millions of patients currently taking approved GPCR orthosteric drugs having to live with side effects. One example of an abandoned clinical candidate is xanomeline (**1**, **Figure 1**); an M_1/M_4-preferring muscarinic acetylcholine receptor (mAChR) ligand that made it to clinical trials for the treatment of the cognitive deficits and psychotic episodes associated with Alzheimer's disease and schizophrenia.[8] Unfortunately, despite appearing to be selective in preclinical studies, xanomeline produced severe gastrointestinal side effects likely mediated by its action at the M_2 and M_3 mAChRs.[9] One example of an approved therapeutic agent for which side effects are currently being tolerated by patients is olanzapine (**2**, **Figure 1**). Olanzapine is an atypical antipsychotic that treats both the positive and negative symptoms of schizophrenia by acting as a $D_2/5\text{-}HT_{2A}$ receptor inverse agonist.[10,11] Unfortunately, patients often experience notable weight gain from taking olanzapine due to promiscuous receptor binding at the $5\text{-}HT_{2C}$ and possibly H_1 and H_3 receptors.[12,13]
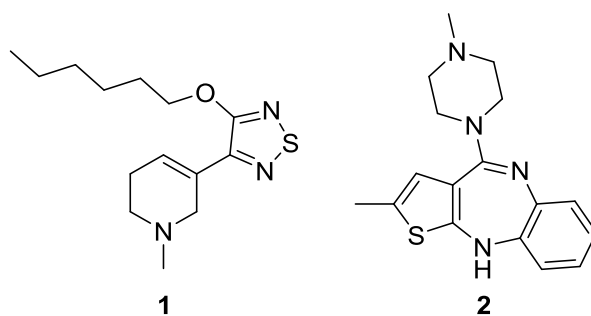
Figure 1. Structures of xanomeline (1) and olanzapine (2)

This selectivity issue has resulted in efforts being directed towards the development of ligands that target allosteric sites on GPCRs. These sites are topographically-distinct from the orthosteric site and more unique in structure across receptor subtypes, making allosteric ligands more likely to exhibit absolute subtype selectivity than their orthosteric

counterparts.[14] A plethora of studies focussing on allosteric ligand optimization have since emerged, bringing with them a veritable array of pharmacological tool compounds and exciting therapeutic lead compounds, but also an unexpected and challenging phenomenon: "flat" or "shallow" SAR. This has been noted across a broad spectrum of GPCRs, including Family A,[15] Family B,[16] and Family C.[17,18]

"Flat" SAR describes the common observation that structural modifications to allosteric ligands often have apparently minimal or confounding effects on ligand potency, whilst "shallow" SAR describes the complete abolishment of activity of allosteric ligands by small structural changes; making it difficult to elucidate trends and map the ligand's pharmacophore. This is likely an artifact of the high-throughput *in vitro* screening protocols typically chosen to assess allosteric ligands. Such testing paradigms, which involve titration of increasing concentrations of an allosteric ligand against a fixed orthosteric ligand concentration, yield estimates of a single pharmacological parameter that fail to capture the "textured" effects of allosteric ligands (see Chapter 1,[15] **Figures 9** and **10** for a more detailed explanation). Orthosteric ligands may be adequately described by a single pharmacological parameter. In the case of orthosteric agonists, their potency for stimulating a particular signalling output (EC_{50}) is routinely utilized, with some studies also reporting the maximum response elicited by the agonist in the cellular background under observation (E_{max}). In the case of orthosteric antagonists, their potency for inhibiting a particular signalling output (IC_{50}) may be measured, or (preferably) their affinity (equilibrium dissociation constant) for the receptor (K_i). In contrast, allosteric ligands require four parameters to sufficiently encompass their pharmacological capabilities;[19] their equilibrium dissociation constant or affinity for the receptor (K_B), their binding (α) and functional (β) cooperativity with the orthosteric probe of choice, and their signalling efficacy for a particular biological output

(τ_B), in the case of allosteric agonists. Hence, *in vitro* screening protocols that estimate a single pharmacological parameter are clearly more suited to orthosteric ligand optimization, whilst allosteric ligand optimization requires approaches that apply the ternary complex model[20] and the operational model of allosterism and agonism[19] to construct more "enriched" SARs that may identify interesting trends that single parameter studies would fail to uncover.

The M_1 and M_4 mAChRs are GPCRs at which allosteric interactions have been well established and characterized. BQCA (1-(4-methoxybenzyl)-4-oxo-1,4-dihydroquinoline-3-carboxylic acid)[21] and LY2033298 ([3-amino-5-chloro-6-methoxy-4-methyl-thieno[2,3-*b*]pyridine-2-carboxylic acid)[22] (**3** and **4**, **Figure 2**) are well-known positive allosteric modulators (PAMs)/allosteric agonists for the M_1 and M_4 mAChR, respectively. Whilst these ligands were originally identified employing the 'modulator titration curve' method previously described, subsequent studies utilizing more rigorous pharmacological methods have broadened our understanding of the intricacies of their pharmacological profiles.[20,23]
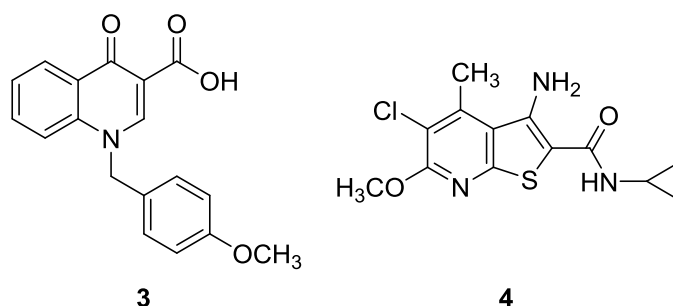
Figure 2. Structures of BQCA (3) and LY2033298 (4)

Furthermore, the SARs of these ligands have been interrogated applying both the 'traditional', single-parameter, modulator titration curve method and the more thorough, multi-parameter 'enriched' method. In the case of LY2033298, SAR studies employing the

'traditional' method determined that removal of the heterocyclic nitrogen or the primary amine was highly detrimental to activity, whilst removal of the chlorine was not. They also found that replacement of the three-membered ring with a bulkier phenyl ring with either 2,3-fluoro, 2,5-fluoro or 4-methoxy substitutions retained high nanomolar potency as did replacement of the pyridine ring methyl substituent with a methoxy or an O-linked N-containing aromatic ring.[24-26] The 'enriched' method[27] was able to identify an example of one structural modification that has opposing effects on different allosteric parameters (namely affinity vs. cooperativity); a feature of allosteric pharmacophores likely to contribute to the "flat" SAR observed in traditional studies. Furthermore, they determined that the mechanism of modulation by these M_4 mAChR PAMs may be partially accounted for by stabilization of the active state of the receptor via binding cooperativity with the orthosteric ligand.

In the case of BQCA, Kuduk and colleagues published numerous studies employing the 'traditional' method (reviewed in Chapter 1) but frequently observed "flat" or "shallow" SAR.[28-30] They were able to determine that 5- and 8-substitution of the A-ring, preservation of the methylene linker, aromaticity of the C-ring and 4-position substitution of the C-ring with halogens and lipophilic moieties were all preferred for potency (see Chapter 1, **Figure 18**).[29-33] However, it wasn't until a more recent publication by Mistry *et al.* employing an 'enriched' approach to investigating the BQCA SAR that these observations were understood in terms of individual allosteric ligand parameters.[34] Specifically, they found that 5- and 8-fluorine substitution of the A-ring appeared to be important for allosteric agonism (τ_B) whilst preserving the methylene linker and C-ring aromaticity were critical for maintaining binding cooperativity (α). They also found that 4-position substitution of the C-ring with a lipophilic moiety improved affinity without affecting cooperativity whilst, conversely, the carboxylic acid (or an isostere containing a hydrogen bond donor) is an important determinant of

cooperativity without affecting affinity. The informative conclusions obtained from these 'enriched' studies highlight the value of adopting such an approach for allosteric ligand SAR elucidation and lead optimization.

To further exemplify the importance of implementing this approach in the study of M_1 mAChR allosteric ligands, we selected two known M_1 mAChR PAMs (**5** and **6**, **Figure 3**) that have stemmed from BQCA optimization studies by Merck.[29,35,36]

5   **6**
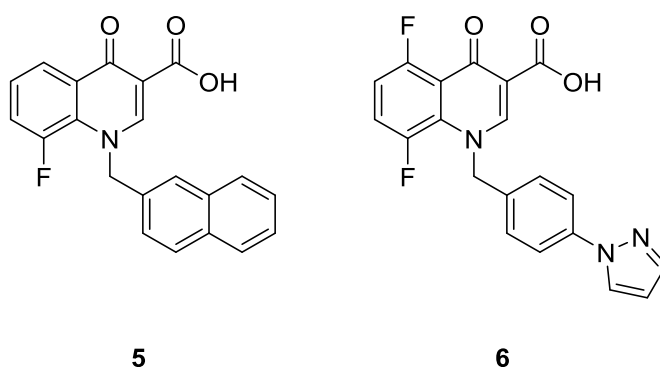
Figure 3. Structures of BQCA analogues 5 and 6

These compounds are reported to have greatly improved potency compared to BQCA in 'traditional' calcium mobilisation modulator titration curve assays (in the presence of an EC_{20} concentration of ACh). We sought to ascertain whether this improved potency was the result of improved affinity, functional efficacy, binding cooperativity, functional cooperativity, or a combination thereof. This approach also enabled us to investigate whether, despite the considerable structural variation between these compounds, the source of this improved potency could be accounted for by changes in the same allosteric parameter(s). These compounds were synthesized and pharmacologically characterized in radioligand binding and ERK1/2 phosphorylation assays in Chinese Hamster Ovary (CHO) cells stably expressing the human M_1 mAChR. Application of the ternary complex model and the operational model of

allosterism allowed us to estimate the affinity (K_B), the binding (α) and functional (β) cooperativity constants, and the functional efficacy (τ_B) of each ligand.

Results

Synthesis

The first two steps of the synthesis of **5** (**Scheme 1**) were followed as per the BQCA synthesis (see Chapter 2), starting with 2-fluoroaniline (**7a**) in place of aniline. Both **8a** and **9a** were obtained in slightly higher yields to that obtained in the BQCA synthesis (**8a:** 93%, compared to 83%; **9a:** 75%, compared to 48%). *N*-Benzylation with the commercially available 2-(bromomethyl)naphthalene was then performed to obtain **10a** in good yield, followed by ester saponification to obtain **5** in near quantitative yield. The first two steps of the synthesis of **6** (**Scheme 1**) were completed in a similar manner with similar yields, starting with 2,5-difluoroaniline (**7b**). In this case, the desired *N*-benzylating agent was not commercially available, and *N*-benzylation with 4-bromobenzylbromide followed by an Ullman coupling with pyrazole was unsuccessful due to no reaction occurring in this latter step (not shown). Hence, the desired benzyl bromide **12** was obtained by employing Appel conditions to facilitate functional group interconversion from the benzyl alcohol **11**. Subsequent *N*-benzylation and saponification steps were employed as per the synthesis of **5** to obtain **6** in reasonable yield.

Scheme 1. Synthesis of BQCA analogues 5 and 6[a]

7a R_1 = F, R_2 = H
7b R_1 = R_2 = F

8a R_1 = F, R_2 = H
8b R_1 = R_2 = F

9a R_1 = F, R_2 = H
9b R_1 = R_2 = F

11

12

5 R_1 = F, R_2 = H
R_3 =

6 R_1 = R_2 = F
R_3 =

10a R_1 = F, R_2 = H
R_3 =

10b R_1 = R_2 = F
R_3 =
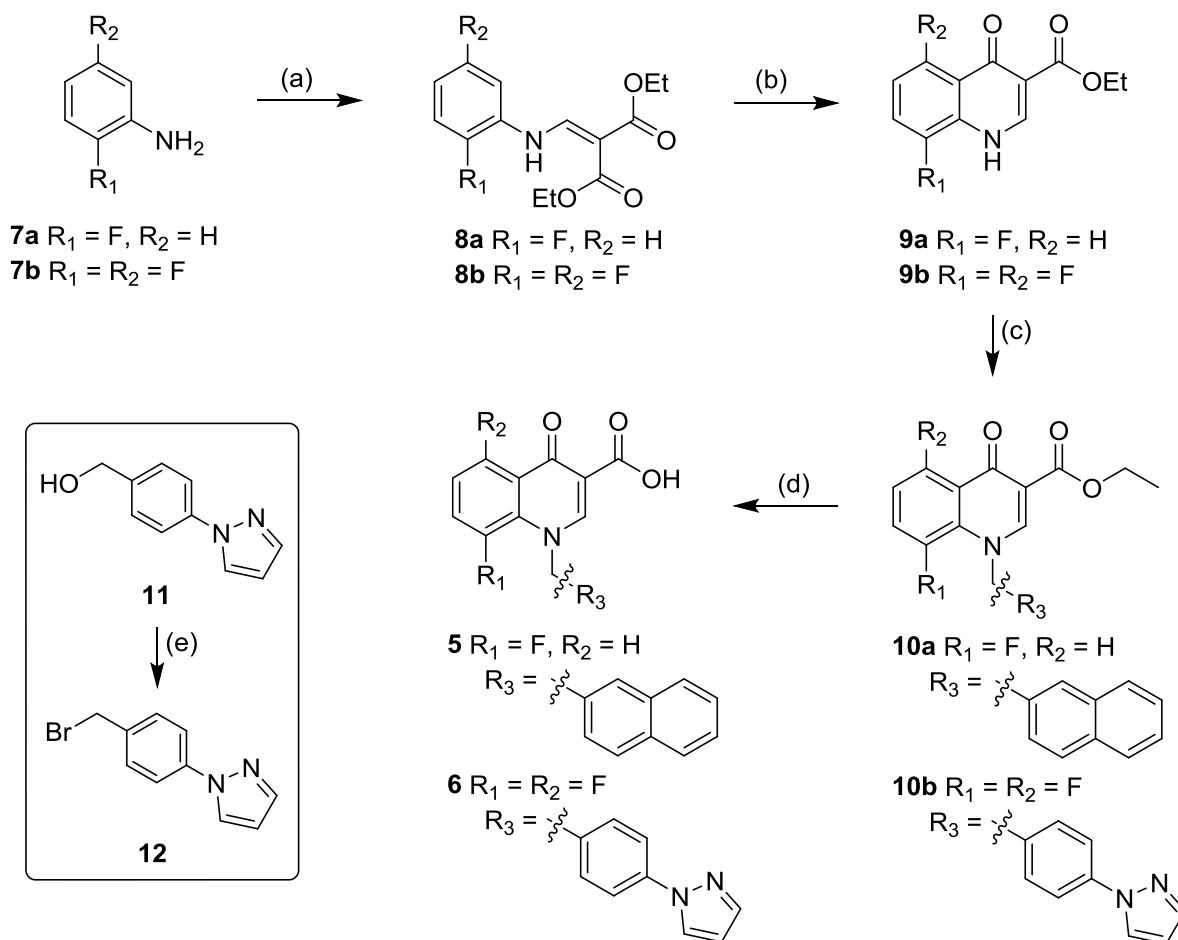
[a]**Reagents and conditions:** (a) diethylethoxymethylene malonate, 120 °C, 93% (**8a**), 73% (**8b**); (b) diphenyl ether, 220 °C, 75% (**9a**), 46% (**9b**); (c) benzyl bromide, DIPEA, ACN, 80 °C, 65% (**10a**), 74% (**10b**); (d) 1 M LiOH$_{(aq)}$, THF, 80 °C, 90% (**5**), 40% (**6**); (e) CBr$_4$, PPh$_3$, ACN, 0-80 °C, 81%.

Pharmacology

[^{3}H]NMS equilibrium whole cell binding interactions between acetylcholine and each of our test allosteric ligands (BQCA and analogues **5** and **6**) were conducted in CHO cells stably expressing the hM$_1$ mAChR (**Figure 4**). Application of the ternary complex model to these data allowed us to estimate each ligand's affinity (pK_B), binding cooperativity with [^{3}H]NMS

(log $\alpha_{[NMS]}$) and binding cooperativity with acetylcholine (log $\alpha_{[ACh]}$) (**Table 1**). All pharmacological data for BQCA are taken from Chapter 2.
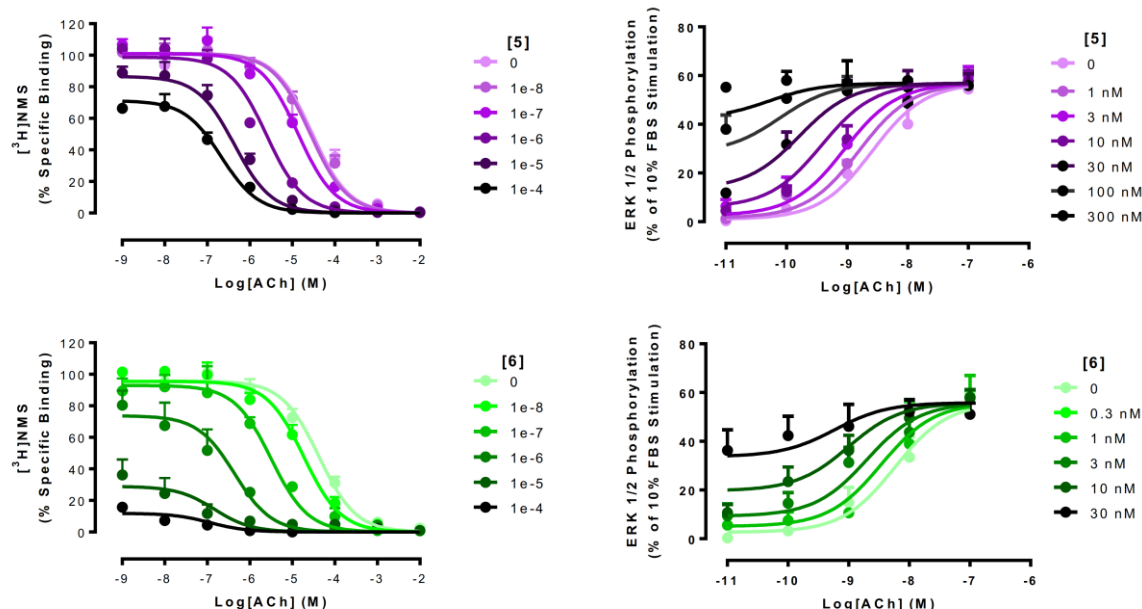
Figure 4. Equilibrium whole cell binding and ERK1/2 phosphorylation functional interaction studies between the ACh and the BQCA analogues 5 and 6 (in the presence of a K_D concentration of [3H]NMS in binding). Values represent the mean ± S.E.M. from three to four experiments performed in duplicate.

ERK1/2 phosphorylation assays were conducted in CHO cells stably expressing the hM$_1$ mAChR. Time course assays were performed to establish the length of incubation time required to measure the peak phosphorylated ERK1/2 response for each test compound (Appendix 6). Concentration-response curves applying the appropriate incubation time were subsequently completed to estimate the pEC$_{50}$ of each compound. (**Table 1**). Interaction studies, with ACh as the interacting orthosteric ligand, were conducted for each of our test allosteric ligands; BQCA, **5** and **6** (**Figure 4**). Application of the operational model of

allosterism to these data allowed us to estimate each ligand's signalling efficacy (τ_B) and the combined binding/activation cooperativity ($\alpha\beta$) (**Table 1**).

Table 1. Ternary complex model parameters for the binding interaction between [³H]NMS, ACh and each allosteric ligand, and the operational model of allosterism functional parameters for the activity of each allosteric ligand alone, and in the presence of acetylcholine (ACh).

	BQCA	5	6
$\mathbf{p}K_B{}^a$	4.44 ± 0.07	4.89 ± 0.13	5.57 ± 0.09
Log $\alpha_{[NMS]}{}^b$	-3.00*	-0.03 ± 0.03	-1.05 ± 0.16
Log $\alpha_{[ACh]}{}^c$	2.88 ± 0.11	2.17 ± 0.13	2.53 ± 0.16
$\alpha_{[ACh]}$	759	148	339
$\mathbf{pEC_{50}}{}^d$	6.77 ± 0.07	6.54 ± 0.15	7.16 ± 0.15
Log $\tau_B{}^e$	2.21 ± 0.08	2.08 ± 0.10	2.07 ± 0.14
$\tau_B{}^f$	162	120	117
Log $\alpha\beta{}^g$	3.71 ± 0.18	3.91 ± 0.19	3.28 ± 0.29
Log β (β)^h	0.83 (7)	1.74 (55)	0.75 (6)

Estimated parameter values represent the mean ± S.E.M. from at least three to four experiments performed in duplicate

[a] Negative logarithm of the equilibrium dissociation constant of the allosteric ligand

[b] Logarithm of the binding cooperativity factor between [³H]NMS and the allosteric ligand; * denotes when the parameter was constrained to an arbitrary low value consistent with very high negative cooperativity between the allosteric ligand and the radioligand

[c] Logarithm of the binding cooperativity factor between ACh and the allosteric ligand
pK_B value was fixed to that estimated for each ligand in whole cell binding experiments

[d] Negative logarithm of the ligand concentration that produces half the maximal response

[e] Logarithm of the operational efficacy parameter of the ligand

[f] Antilogarithm of the operational efficacy parameter of the ligand

[g] Logarithm of the product of the binding and activation cooperativity factors between ACh and the allosteric ligand

[h] Logarithm (and antilogarithm) of the activation cooperativity factor between ACh and the allosteric ligand (derived by fixing the binding cooperativity value to that estimated for each ligand in whole cell binding experiments – Log $\alpha_{[ACh]}$)

Discussion

The potency of the majority of BQCA analogues reported to date is taken from the concentration that yields the point of inflection of the titration curve of the ligand in the presence of an EC_{20} concentration of ACh. This method, whilst effective for identifying hit compounds, gives us limited information about the ligand binding mode and does not attempt to quantify allosteric behavior. The study performed here attempts to identify what specific pharmacological parameters may be responsible for the improvement in activity of these compounds over BQCA.

Compound **6** (pK_B = 5.57) exhibited a significant increase in affinity ($p < 0.0001$) compared to BQCA (pK_B = 4.44) (**Table 1**). The ligand's pEC_{50}, binding and functional cooperativities, and signalling efficacy were not significantly different from BQCA. This suggests that the substantial increase in potency reported by Kuduk *et al.*[35] for this analogue (from 845 nM to 171 nM) is largely dictated by the affinity of **6**, and not its modulatory ability. This improved affinity may arise from additional hydrogen bonding interactions between the receptor and the fluorine atoms of the bicyclic core, and/or the additional van der Waals interactions and H-bond acceptor of the pyrazole ring. **5** exhibited a notable gain in activation cooperativity with ACh compared to BQCA (from β = 7 to β = 55, ($p < 0.001$)) (**Table 1**). The other binding and functional parameters estimated for this compound were not significantly different from BQCA. This suggests that the enhanced potency reported by Kuduk *et al.*[29] for this analogue (from 845 nM to 80 nM) is largely driven by the activation cooperativity (with ACh) of **5**. Enhancement of this property may be the result of the lipophilic naphthalene ring system forming favourable van der Waals interactions that directly or indirectly affect amino acid residues involved in cooperativity transmission, such as F182, E397 and E401 in extracellular loop 2 and transmembrane 7.[37]

Two known BQCA analogues were synthesised and pharmacologically characterised in [^{3}H]NMS equilibrium whole cell binding and ERK1/2 phosphorylation functional assays. The data reveal that improvements in specific properties, such as affinity or activation cooperativity, drive the improved activity of these ligands compared to BQCA. Furthermore, the data also demonstrate that the source of improved potency is not the same pharmacological parameter for the two ligands. **5** and **6** may serve as useful probes for investigating the *in vivo* effect of improving properties individually.

This chapter illustrates a method by which the frequently confounding SAR observed with allosteric ligands may be deconvoluted. If changes in chemical structure can be linked specifically to changes in affinity, binding cooperativity, activation cooperativity or signalling efficacy, rather than simply "potency", a clearer, albeit more complex, picture of the ligand-receptor interaction may be elucidated. A crucial question, one that is presently unanswered, is: what properties of these M_1 mAChR allosteric ligands do we need to improve, and to what extent, to achieve a therapeutic effect in both preclinical and clinical trials? (e.g. How high does the positive cooperativity with ACh need to be to elicit a therapeutic effect without causing neurotoxicity?) Clearly, ligands for which we have more detailed binding and functional knowledge may serve as ideal tool compounds for probing the specific effects of a single parameter change such as increased affinity, increased cooperativity, or decreased signalling efficacy in an *in vivo* setting. This may yield a clearer picture of what the ideal balance of properties is, as well as an informed direction in which rational drug design may proceed.

Experimental

Chemistry

General

All materials were reagent grade and purchased commercially from Sigma-Aldrich or Matrix Scientific. Anhydrous solvents were obtained from a MBraun MB SPS-800 Solvent Purification System. Analytical thin layer chromatography (TLC) was performed on Silica Gel 60 F_{254} pre-coated plates (0.25 mm, Merck ART 5554) and visualized by ultraviolet light, iodine or ninhydrin as necessary. Silica gel 60 (Fluka) was used for silica gel flash chromatography. Microwave reactions were performed in a CEM Discover microwave reactor. Melting points (mp) were determined on a Mettler Toledo-MP50 Melting Point System.

^{1}H NMR spectra were routinely recorded at 400 MHz using a Brüker Avance 400 MHz Ultrashield Plus spectrometer equipped with a Silicon Graphics workstation. Chemical shifts (δ_H) for all ^{1}H NMR spectra are reported in parts per million (ppm) using the centre peak of the deuterated solvent chemical shift as the reference: $CDCl_3$ (7.26) and d_6-DMSO (2.50).[38] Each resonance was assigned according to the following convention: chemical shift (δ) (multiplicity, coupling constant(s) in Hz, number of protons, and assignment). Coupling constants (J) are reported to the nearest 0.5 Hz. In reporting spectral data the following abbreviations have been used: s, singlet; d, doublet; t, triplet; q, quartet; p, pentet; m, multiplet; br, broad; app, apparent; as well as combinations of these where appropriate.

^{13}C NMR spectra were routinely recorded at 100 MHz using a Brüker Avance 400 MHz Ultrashield Plus spectrometer equipped with a Silicon Graphics workstation. Chemical shifts (δ_C) for all ^{13}C NMR spectra are reported in parts per million (ppm), using the centre peak of

the deuterated solvent chemical shift as the reference: CDCl$_3$ (77.16) and d_6-DMSO (39.52).[38] Coupling to fluorine (^{19}F) is reported as $^1J_{CF}$, $^2J_{CF}$, $^3J_{CF}$ and $^4J_{CF}$ to the nearest Hz.[39]

HSQC, HMBC and COSY spectra were obtained using the standard Brüker pulse sequence to assist with structural assignment of the compounds.

Liquid Chromatography-Mass Spectrometry (LCMS) was performed on an Agilent 1200 Series coupled to the 6120 quadrupole mass spectrometer. Elution was also monitored at 254 nm. High Resolution Mass Spectrometry (HRMS) analyses were recorded in the specified ion mode using a LCT Premier XE TOF Mass Spectrometer coupled to 2795 Alliance Separations Module at cone voltages of 45 V (ESI+) and 60 V (ESI-).

Analytical reverse-phase High Performance Liquid Chromatography (HPLC) was performed on a Waters HPLC system using a Phenomenex® Luna C8 (2) 100Å column (150 × 4.6 mm, 5 μm) and a binary solvent system; solvent A: 0.1% TFA/H$_2$O; solvent B: 0.1% TFA/80% MeOH/H$_2$O. Isocratic elution was carried out using the following protocol (time, % solvent A, % solvent B): 0 min, 100, 0; 10 min, 20, 80; 11 min, 20, 80; 12 min, 100, 0; 20 min, 100, 0; at a flow rate of 1.0 mL/min monitored at 254 nm using a Waters 996 Photodiode Array detector.

Characterization requirements for intermediate compounds were set as: mp, ^{1}H NMR, ^{13}C NMR, LCMS and HPLC (254 nm) or LCMS purity. Characterization requirements for final compounds were set as: mp, ^{1}H NMR, ^{13}C NMR, LRMS, HRMS, and HPLC (254 nm and 214 nm) purity >95%.

General procedure for diethyl 2-(((R-phenyl)amino)methylene)malonate

The appropriately substituted aniline (**7a** or **7b**) (30 mmol) and diethylethoxymethylene malonate (6.06 mL, 30 mmol) were syringed into a RBF and heated at 120 °C for 3-6 h. The reaction mixture was removed from the heat, 20 mL cold petroleum spirits added and the

flask cooled on an ice bath for 30 min. The yellow crystals that formed were transferred to an Erlenmeyer flask and sonicated (in small batches) in cold petroleum spirits for 2-3 min. The target compound was obtained as pale yellow-white crystals following vacuum filtration and additional washes with petroleum spirits.

Diethyl 2-(((2-fluorophenyl)amino)methylene)malonate (**8a**)
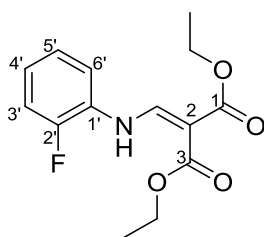
7.80 g, 93%; mp 78-79 °C; δ_H (CDCl$_3$) 10.99 (br d, J= 13.5 Hz, 1H, NH), 8.44 (d, J= 13.5 Hz, 1H, CCHNH), 7.22 (td, J= 8.0, 1.0 Hz, 1H, H5′), 7.13-7.05 (m, 2H, H3′, H6′), 7.05-6.98 (m, 1H, H4′), 4.26 (q, J= 7.0 Hz, 2H, CH_2CH$_3$), 4.19 (q, J= 7.0 Hz, 2H, CH_2CH$_3$), 1.31 (t, J= 7.0 Hz, 3H, CH$_2$CH_3), 1.26 (t, J= 7.0 Hz, 3H, CH$_2$CH_3); δ_C (CDCl$_3$) 168.6 (C), 165.6 (C), 152.8 (CF, d, $^1J_{CF}$= 245 Hz), 150.9 (CH), 127.9 (C, d, $^2J_{CF}$= 10 Hz), 125.0 (CH), 124.95 (CH, d, $^4J_{CF}$= 3 Hz), 116.3 (CH, d, $^2J_{CF}$= 12 Hz), 116.2 (CH, d, $^3J_{CF}$= 6 Hz), 95.1 (C), 60.5 (CH$_2$), 60.2 (CH$_2$), 14.4 (CH$_3$), 14.3 (CH$_3$); m/z LRMS (TOF ES$^+$) [MH]$^+$ 282.3; HPLC: t_R = 10.41 min, purity = 98.9%

<u>Diethyl 2-(((2,5-difluorophenyl)amino)methylene)malonate (**8b**)</u>
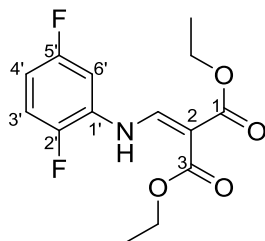
6.60 g, 73%; mp 87.8-88.5 °C; δ_H (CDCl$_3$) 10.99 (br d, J= 13.0 Hz, 1H, NH), 8.32 (d, J= 13.5 Hz, 1H, CCHNH), 7.04 (ddd, $^3J_{HF}$= 10.0, $^4J_{HF}$= 9.0, J= 5.0 Hz, 1H, H3′), 6.93 (ddd, $^3J_{HF}$= 9.0, J= 6.5, 3.0 Hz, 1H, H6′), 6.69 (dddd, $^3J_{HF}$= 9.0, J= 7.5, 3.5, 3.0 Hz, 1H, H4′), 4.26 (q, J= 7.0 Hz, 2H, CH_2CH$_3$), 4.20 (q, J= 7.0 Hz, 2H, CH_2CH$_3$), 1.31 (t, J= 7.0 Hz, 3H, CH$_2$CH_3), 1.27 (t, J= 7.0 Hz, 3H, CH$_2$CH_3); δ_C (CDCl$_3$) 168.4 (C), 165.3 (C), 159.2 (CF, dd, $^1J_{CF}$= 242, $^4J_{CF}$= 2 Hz), 149.9 (CH), 148.8 (CF, dd, $^1J_{CF}$= 241, $^4J_{CF}$= 3 Hz), 128.9 (C, dd, $^2J_{CF}$= 13, $^3J_{CF}$= 10 Hz), 117.0 (CH, dd, $^2J_{CF}$= 21, $^3J_{CF}$= 10 Hz), 110.7 (CH, dd, $^2J_{CF}$= 24, $^3J_{CF}$= 8 Hz), 103.2 (CH, d, $^2J_{CF}$= 29 Hz), 96.3 (C), 60.7 (CH$_2$), 60.4 (CH$_2$), 14.4 (CH$_3$), 14.2 (CH$_3$); m/z LRMS (TOF ES$^+$) [MH]$^+$ 300.3; HPLC: t_R = 10.89 min, purity = 97.4%

General procedure for ethyl R-4-oxo-1,4-dihydroquinolone-3-carboxylate

Diphenyl ether (8 mL) was heated to 220 °C in a small beaker directly placed on the hotplate. The appropriately substituted diethyl 2-(((R-phenyl) amino)methylene)malonate (**8a** or **8b**) (400 and 500 mg, 1.42 and 1.67 mmol, respectively) was added and the reaction mixture heated, uncovered, for 20 min. The beaker was removed from the heat and allowed to cool to RT, resulting in product formation and almost total solidification of the reaction mixture. The target compound was isolated as a grey-white powder by vacuum filtration and copious washing with cold petroleum spirits.

Ethyl 8-fluoro-4-oxo-1,4-dihydroquinoline-3-carboxylate (**9a**)
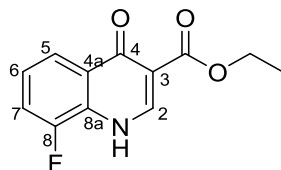
251 mg, 75%; mp 212.3-213.7 °C; δ_H (d_6-DMSO) 8.40 (s, 1H, H2), 7.97 (d, J = 8.0 Hz, 1H, H5), 7.65 (dd, $^3J_{HF}$ = 10.5, J = 8.5 Hz, 1H, H7), 7.41 (td, J = 8.0, 5.0 Hz, 1H, H6), 4.22 (q, J = 7.0 Hz, 2H, CH_2CH$_3$), 1.28 (t, J = 7.0 Hz, 3H, CH$_2$CH_3); δ_C (d_6-DMSO) 172.5 (C), 164.4 (C), 152.8 (CF, d, $^1J_{CF}$ = 248 Hz), 144.7 (CH), 129.1 (C), 128.2 (C), 124.5 (CH, $^3J_{CF}$ = 7 Hz), 121.3 (CH), 117.3 (CH, $^2J_{CF}$ = 17 Hz), 110.5 (C), 59.8 (CH$_2$), 14.2 (CH$_3$); m/z LRMS (TOF ES$^+$) [MH]$^+$ 236.3; HPLC: t_R = 6.53 min, purity = 95.6%

Ethyl 5,8-difluoro-4-oxo-1,4-dihydroquinoline-3-carboxylate (**9b**)
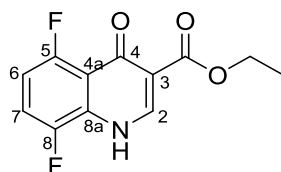
195 mg, 46%; mp 209.1-210.1 °C; δ_H (d_6-DMSO) 8.30 (s, 1H, H2), 7.64 (ddd, $^3J_{HF}$ = 10.5, 9.0, J = 4.0 Hz, 1H, H7), 7.11 (ddd, $^3J_{HF}$ = 11.5, 9.0, J = 4.0 Hz, 1H, H6), 4.21 (q, J = 7.0 Hz, 2H, CH_2CH$_3$), 1.27 (t, J = 7.0 Hz, 3H, CH$_2$CH_3); δ_C (d_6-DMSO) 171.4 (C), 164.0 (C), 156.6 (CF, dd, $^1J_{CF}$ = 256 Hz, $^4J_{CF}$ = 3 Hz), 147.6 (CF, dd, $^1J_{CF}$ = 242 Hz, $^4J_{CF}$ = 4 Hz), 144.0 (CH), 130.0 (C), 118.5 (C), 117.6 (CH, dd, $^2J_{CF}$ = 19 Hz, $^3J_{CF}$ = 10 Hz), 112.1 (C), 110.1 (CH, dd, $^2J_{CF}$ = 24 Hz, $^3J_{CF}$ = 7 Hz), 59.8 (CH$_2$), 14.2 (CH$_3$); m/z LRMS (TOF ES$^+$) [MH]$^+$ 254.3; LCMS: t_R = 4.64 min, purity = >99.0

Synthesis of 1-(4-(bromomethyl)phenyl)-1H-pyrazole (12)
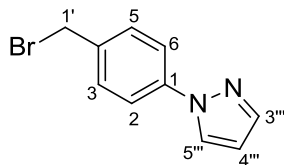
[4-(1*H*-Pyrazol-1-yl)phenyl]methanol (**11**, 200 mg, 1.15 mmol), triphenylphosphine (452 mg, 1.72 mmol, 1.5 eq.) and acetonitrile (8 mL) were placed in an RBF and cooled to 0 °C in an ice bath. Carbon tetrabromide (571 mg, 1.72 mmol, 1.5 eq.) was added and the reaction stirred at 0 °C for 10 min before being heated to 80 °C and stirred for 6 h. The reaction mixture was cooled, partitioned between dichloromethane (10 mL) and water (10 mL), and the aqueous layer extracted with dichloromethane (3 × 10 mL). The combined organic fractions were dried over MgSO$_4$, filtered and the solvent evaporated *in vacuo* to yield an orange-yellow clear oil. The target molecule was isolated as off-white crystals by column chromatography (stationary phase: silica, mobile phase: 3:1 petroleum spirits:ethyl acetate). 220 mg, 81%; mp 72-73 °C; δ_H (CDCl$_3$) 8.50 (d, *J*= 2.0 Hz, 1H, H5‴), 7.84 (d, *J*= 8.5 Hz, 2H, H2, H6), 7.76 (d, *J*= 5.5 Hz, 1H, H3‴), 7.57 (d, *J*= 8.5 Hz, 2H, H3, H5), 6.59-6.52 (m, 1H, H4‴), 4.76 (s, 2H, H1′); δ_C (CDCl$_3$) 141.4 (CH), 140.0 (C), 135.9 (C), 130.3 (CH), 126.7 (CH), 119.3 (CH), 107.9 (CH), 32.8 (CH$_2$); *m/z* LRMS (TOF ES$^+$) [MH]$^+$ 237.3; LCMS: t_R = 5.84 min, purity = >99.0%

General procedure for *N*-benzylation

The ethyl ester precursor with the appropriate substitution pattern (**9a** or **9b**) (250 and 160 mg, 1.06 mmol and 632 µmol, respectively) and acetonitrile (7 mL) were placed in a RBF and cooled to 0 °C in an ice bath. The appropriately substituted benzyl bromide (1.1 eq.) and *N,N*-diisopropylethylamine (DIPEA) (4 eq.) were added and the reaction stirred at 80 °C for

between 3-22 h. If the product was observed to precipitate from the reaction mixture, the resulting white solid was isolated by vacuum filtration and washed with diethyl ether. If no precipitate was observed, the reaction mixture was partitioned between chloroform (10 mL) and 1 M HCl$_{(aq)}$ (10 mL), and the aqueous layer extracted with chloroform (3 × 10 mL). The combined organic fractions were dried over MgSO$_4$, filtered and the solvent evaporated *in vacuo* to yield a white solid.

Ethyl 8-fluoro-1-(naphthalen-2-ylmethyl)-4-oxo-1,4-dihydroquinoline-3-carboxylate (**10a**)
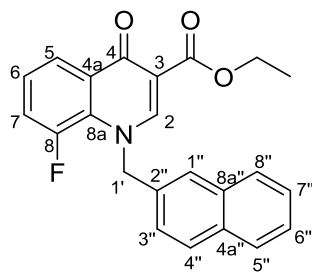
257 mg, 65%; mp 224.1-224.7 °C; δ_H (d_6-DMSO) 8.91 (s, 1H, H2), 8.14 (d, *J*= 8.0 Hz, 1H, H5), 7.97-7.81 (m, 3H, H4″, H5″, H8″), 7.59-7.49 (m, 5H, H6, H7, H1″, H6″, H7″), 7.35 (d, *J*= 8.5 Hz, 1H, H3″), 5.89 (s, 2H, H1′), 4.27 (q, *J*= 7.0 Hz, 2H, C*H*$_2$CH$_3$), 1.30 (t, *J*= 7.0 Hz, 3H, CH$_2$C*H*$_3$); δ_C (d_6-DMSO) 171.8 (C), 164.3 (C), 152.1 (CH), 151.5 (CF, d, $^1J_{CF}$= 250 Hz), 134.8 (C), 132.8 (C), 132.2 (C), 131.1 (C), 128.5 (CH), 128.4 (C), 127.6 (CH, $^2J_{CF}$= 20 Hz), 126.5 (CH), 126.1 (CH), 125.6 (CH, $^3J_{CF}$= 9 Hz), 124.0 (CH), 123.8 (CH), 122.7 (CH, $^4J_{CF}$= 3 Hz), 120.1 (CH), 119.8 (CH), 110.6 (C), 60.0 (CH$_2$), 59.8 (CH$_2$), 14.3 (CH$_3$); *m/z* LRMS (TOF ES$^+$) [MH]$^+$ 376.5; HPLC: t_R = 10.48 min, purity = 97.5%

Ethyl 1-(4-(1*H*-pyrazol-1-yl)benzyl)-5,8-difluoro-4-oxo-1,4-dihydroquinoline-3-carboxylate (**10b**)
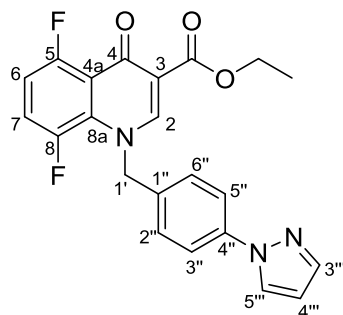
191 mg, 74%; mp 177.3-178.2 °C; δ_H (d_6-DMSO) 8.76 (s, 1H, H2), 8.45 (d, *J*= 2.5 Hz, 1H, H5‴), 7.81 (d, *J*= 8.5 Hz, 2H, H3″, H5″), 7.73 (d, *J*= 1.5 Hz, 1H, H3‴), 7.58 (ddd, $^3J_{HF}$= 13.5, 9.0, *J* = 4.5 Hz, 1H, H7), 7.28 (d, *J*= 8.5 Hz, 2H, H2″, H6″), 7.19 (ddd, $^3J_{HF}$= 11.0, 9.0, *J*= 3.5 Hz, 1H, H6), 6.53 (dd, *J*= 2.5, 2.0, 1H, H4‴), 5.71 (app d, *J*= 3.7 Hz, 2H, H1′), 4.25 (q, *J*= 7.0 Hz, 2H, C*H*₂CH₃), 1.29 (t, *J*= 7.0 Hz, 3H, CH₂C*H*₃); δ_C (d_6-DMSO) 171.0 (C), 163.9 (C), 157.3 (CF, d, $^1J_{CF}$= 258 Hz), 151.4 (CH), 147.3 (CF, d, $^1J_{CF}$= 240 Hz), 141.0 (CH), 139.0 (C), 134.7 (C), 129.9 (C), 127.7 (CH), 126.9 (CH), 120.3 (CH, dd, $^2J_{CF}$= 26 Hz, $^3J_{CF}$= 11 Hz), 119.5 (C), 118.7 (CH), 112.3 (C), 112.0 (CH, dd, $^2J_{CF}$= 24 Hz, $^3J_{CF}$= 9 Hz), 107.9 (CH), 60.1 (CH₂), 59.2 (CH₂), 14.2 (CH₃); *m/z* LRMS (TOF ES⁺) [MH]⁺ 410.5; HPLC: t_R = 9.46 min, purity = 96.5%

General procedure for ester saponification

The starting ester (**10a** or **10b**) (200 and 140 mg, 533 and 342 µmol, respectively) and tetrahydrofuran (10 mL) were brought to 0 °C in an ice bath. 1 M LiOH (2 eq.) was added dropwise whilst stirring and then the reaction mixture was heated at 80 °C for 24 h. Following addition of excess 1 M HCl₍aq₎, the target molecule precipitated out and was

isolated as an off-white powder by vacuum filtration, washed with distilled water to remove the residual acid, then dried under vacuum overnight.

8-Fluoro-1-napthalen-2ylmethyl)-4-oxo-1,4-dihydroquinolone-3-carboxylic acid (**5**)
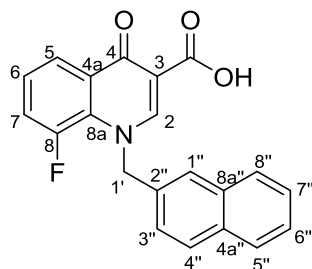
167 mg, 90%; mp 239.8-240.4 °C; δ_H (d_6-DMSO) 14.87 (br s, 1H, OH), 9.27 (s, 1H, H2), 8.28 (dd, J= 8.0, 1.5 Hz, 1H, H5), 7.97-7.81 (m, 3H, H4″, H5″, H8″), 7.71 (ddd, , $^3J_{HF}$= 14.5, J= 8.0, 1.5 Hz, 1H, H7), 7.65-7.57 (m, 2H, H6, H1″), 7.53-7.45 (m, 2H, H6″, H7″), 7.38 (dd, J= 8.5, 1.5 Hz, 1H, H3″), 6.07 (app d, J= 3.0 Hz, 2H, H1′); δ_C (d_6-DMSO) 177.1 (C), 165.6 (C), 152.4 (CH), 151.6 (CF, d, $^1J_{CF}$= 250 Hz), 134.3 (C), 132.8 (C), 132.3 (C), 129.0 (C), 128.9 (C), 128.5 (CH), 127.7 (CH), 127.5 (CH), 127.1 (CH), 126.5 (CH), 126.2 (CH), 124.1 (CH), 123.9 (CH), 122.4 (CH), 121.4 (CH), 67.0 (C), 60.7 (CH$_2$); m/z LCMS (TOF ES$^+$) [MH]$^+$ 348.0; m/z HRMS (TOF ES$^+$) $C_{21}H_{14}FNO_3$ [MH]$^+$ calcd 348.1030; found 348.1047; HPLC: t_R = 10.45 min, purity (254) = 99.7%, purity (214) = 98.5%.

1-(4-(1*H*-Pyrazol-1-yl)benzyl)-5,8-difluoro-4-oxo-1,4-dihydroquinoline-3-carboxylic acid (**6**)
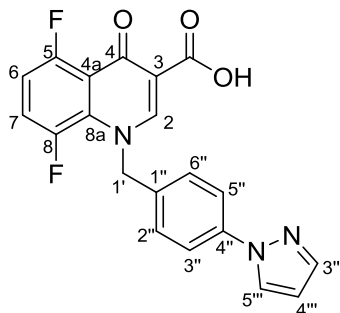
51.6 mg, 40%; mp >300 °C; δ_H (d_6-DMSO) 15.10 (s, 1H, OH), 8.95 (s, 1H, H2), 8.52 (d, $J=$ 2.5 Hz, 1H, H5‴), 7.89 (d, $J=$ 8.5 Hz, 2H, H3″, H5″), 7.81 (d, $J=$ 1.5 Hz, 1H, H3‴), 7.70-7.61 (m, 1H, H7), 7.31 (d, $J=$ 8.5 Hz, 2H, H2″, H6″), 7.24 (ddd, $^3J_{HF}=$ 12.0, 9.0, $J=$ 3.5 Hz, 1H, H6), 6.61 (dd, $J=$ 2.5, 2.0, 1H, H4‴), 5.82 (app d, $J=$ 3.7 Hz, 2H, H1′); δ_C (d_6-DMSO) 175.8 (C), 165.3 (C), 157.5 (CF, d, $^1J_{CF}=$ 260 Hz), 151.8 (CH), 147.3 (CF, d, $^1J_{CF}=$ 250 Hz), 141.0 (CH), 139.0 (C), 135.0 (C), 127.7 (CH), 127.0 (CH), 122.4 (C), 119.7 (CH, dd, $^2J_{CF}=$ 23 Hz, $^3J_{CF}=$ 12 Hz), 119.3 (C), 118.7 (CH), 112.2 (C), 110.9 (CH, dd, $^2J_{CF}=$ 24 Hz, $^3J_{CF}=$ 8 Hz), 107.9 (CH), 59.1 (CH₂); *m/z* LRMS (TOF ES⁺) [MH]⁺ 382.6; *m/z* HRMS (TOF ES⁺) $C_{20}H_{13}F_2N_3O_3$ [MH]⁺ calcd 382.0998; found 382.1013; HPLC: t_R = 9.23 min, purity (254) = 98.5%, purity (214) = 98.2%.

Pharmacology

Radioligand Equilibrium Whole Cell Binding Assays

 Plate preparation. FlpIn-CHO cells stably expressing human muscarinic M_1 receptors (hM_1 mAChR FlpIn-CHO) were cultured at 37 °C in 5% CO_2 in Dulbecco's modified Eagle medium (DMEM) supplemented with 5% (v/v) foetal bovine serum (FBS) and 16 mM HEPES. Cells were seeded into white opaque Isoplates™ at 8×10^3 cells per well and then

grown at 37 °C for 20-24 h. Cells were then washed twice with cold HEPES-buffered saline, 140 µL per well cold HEPES-buffered saline was added and the plates kept on ice.

Assay protocol. A stock solution of ACh (10^{-2} M) was made up in cold HEPES-buffered saline. Stock solutions of the interacting allosteric ligands of choice (10^{-2} M) were made up in DMSO. Dilutions of all ligands were made up in cold HEPES-buffered saline at ten times (10×) the required concentration and added to stock plates on ice. Cells were equilibrated at 4 °C for 4 h with 20 µL of ACh, 20 µL of a single interacting allosteric ligand and 20 µL of 0.1 nM [^{3}H]NMS (total volume 200 µL per well).

Assay termination and data collection. Assays were terminated by media removal, 2 × 100 µL per well washes with 0.9% NaCl solution and addition of 100 µL per well Microscint-20 scintillation liquid. The levels of remaining bound radioligand, and therefore the degree of radioligand displacement, was measured in disintegrations per minute (dpm) on the Microbeta2^{TM} LumiJET 2460 microplate counter (PerkinElmer).

AlphaScreen ERK1/2 Phosphorylation Assays

Plate preparation. FlpIn-CHO cells stably expressing human muscarinic M_1 receptors (hM$_1$ mAChR FlpIn-CHO) were cultured at 37 °C in 5% CO$_2$ in DMEM supplemented with 5% (v/v) FBS and 16 mM HEPES. Cells were seeded into transparent 96-well plates at 5 × 10^4 cells per well and grown for 6 h. Cells were then washed once with phosphate-buffered saline (PBS) and incubated in serum-free DMEM (180 µL per well) at 37 °C overnight (16-18 h) to allow FBS-stimulated phosphorylated ERK1/2 levels to subside.

Time course assays. A stock solution of ACh (10^{-2} M) was made up in MilliQ water. Stock solutions of the test ligands (10^{-2} M) were made up in DMSO. All ligands were diluted to 10^{-5} M in serum-free DMEM. 20 µL ligand additions were made at predetermined time

points over a 30 minute period (30, 25, 20, 15, 10, 8, 6, 5, 3 and 1 min) with the cells being incubated at 37 °C following each addition. FBS, which triggers ERK1/2 phosphorylation via a tyrosine kinase receptor, was added at 6 min as a measure of the maximal levels of pERK1/2 production.

Concentration-response curves (CRCs). A stock solution of ACh (10^{-2} M) was made up in MilliQ water. Stock solutions of the test ligands (10^{-2} M) were made up in DMSO. Dilutions of all ligands were made up in FBS-free media at ten times ($10\times$) the required concentration and added to stock plates. Cells were incubated at 37 °C with 20 μL per well of each concentration of all compounds at 5 min (as determined by time course assays).

Interaction studies. A stock solution of ACh (10^{-2} M) was made up in MilliQ water. Stock solutions of the allosteric test ligands (10^{-2} M) were made up in DMSO. Dilutions of ACh and the interacting ligand were made up in FBS-free media at twenty times ($20\times$) the ideal concentration range (as determined by CRC assays). Equal volumes of each concentration of ACh and each concentration of the interacting ligand of choice were premixed in stock plates. Cells were incubated at 37 °C with 20 μL per well of each ligand mixture at 5 min (as determined by time course assays).

Assay termination and data collection. Agonist-stimulated ERK1/2 phosphorylation was terminated by the removal of drugs and the addition of 100 μL p/well of *SureFire*™ lysis buffer. The cell lysates were agitated for 5-10 min. Following agitation, 5 μL of cell lysates were transferred into a 384-well white opaque Optiplate™, followed by addition of 8.5 μL of a solution of Reaction buffer/Activation buffer/acceptor beads/donor beads in a ratio of 6/1/0.3/0.3 (v/v/v/v) under green light conditions. The plates were then incubated at 37 °C in the dark for 1 h and fluorescence was measured on a Fusion-α™ plate reader (PerkinElmer) using standard AlphaScreen settings.

Data analysis

All data analysis was managed using Prism 6 software (GraphPad Software, San Diego, CA). Experiments measuring radioligand equilibrium whole cell binding interactions were fitted to the allosteric ternary complex model (**1**):

$$Y = \frac{[A]}{[A] + \left(\dfrac{K_A K_B}{\alpha'[B] + K_B}\right)\left(1 + \dfrac{[I]}{K_I} + \dfrac{[B]}{K_B} + \dfrac{\alpha[I][B]}{K_I K_B}\right)} \quad (1)$$

where Y is the percentage (vehicle control) binding, $[A]$, $[B]$ and $[I]$ are the concentrations of $[^3H]$NMS, the allosteric ligand, and ACh respectively, K_A and K_B are the equilibrium dissociation constants of $[^3H]$NMS and the allosteric ligand, respectively, K_I is the equilibrium dissociation constant of ACh, and α and α' are the cooperativities between the allosteric ligand and $[^3H]$NMS or ACh, respectively. Values of α (or α') > 1 denote positive cooperativity; values <1 (but >0) denote negative cooperativity, and values = 1 denote neutral cooperativity. Functional orthosteric and allosteric agonist concentration-response curves were fitted via nonlinear regression to the three-parameter logistic function (**2**):

$$E = Basal + \frac{(E_{max} - basal)}{1 + 10^{-pEC_{50} - Log[A])} } \quad (2)$$

where E is response, E_{max} and basal are the top and bottom asymptotes of the curve, respectively, $\log[A]$ is the logarithm of the agonist concentration, and pEC_{50} is the negative logarithm of the agonist concentration that gives a response halfway between E_{max} and basal. Functional experiments measuring the interactions between ACh and each allosteric ligand were fitted to the operational model of allosterism and agonism (**3**)[40,41] to derive functional estimates of modulator affinity, cooperativity, and efficacy.

$$E = \frac{E_m(\tau_A[A](K_B + \alpha\beta[B]) + \tau_B[B]K_A)^n}{([A]K_B + K_A K_B + [B]K_A + \alpha[A][B])^n + (\tau_A[A](K_B + \alpha\beta[B]) + \tau_B[B]K_A)^n} \quad (3)$$

where E_m is the maximum attainable system response for the pathway under investigation; [A] and [B] are the concentrations of orthosteric and allosteric ligands, respectively; K_A and K_B are the equilibrium dissociation constants of the orthosteric and allosteric ligands, respectively; τ_A and τ_B are the operational measures of orthosteric and allosteric ligand efficacy (which incorporate both signal efficiency and receptor density), respectively; n is a transducer slope factor linking occupancy to response; α is the binding cooperativity parameter between the orthosteric and allosteric ligand; β denotes the magnitude of the allosteric effect of the modulator on the efficacy of the orthosteric agonist.[40,34] In all cases, the equilibrium dissociation constant of each allosteric ligand was fixed to that determined from the competition binding experiments.

Statistical analyses were performed where appropriate using one-way analysis of variance with Dunnett's post test, and significance indicated as follows: * = $p < 0.05$, ** = $p < 0.01$, *** = $p < 0.001$ and **** = $p < 0.0001$

References

(1) Murugesan, D., Mital, A., Kaiser, M., Shackleford, D. M., Morizzi, J., Katneni, K., Campbell, M., Hudson, A., Charman, S. A., Yeates, C. and Gilbert, I. H. (2013) Discovery and Structure-Activity Relationships of Pyrrolone Antimalarials. *J. Med. Chem.*, *56*, 2975-2990.

(2) Chen, X., Sassano, M. F., Zheng, L., Setola, V., Chen, M., Bai, X., Frye, S. V., Wetsel, W. C., Roth, B. L. and Jin, J. (2012) Structure-Functional Selectivity Relationship Studies of β-Arrestin-Biased Dopamine D_2 Receptor Agonists. *J. Med. Chem.*, *55*, 7141-7153.

(3) Poulsen, M. H., Lucas, S., Bach, T. B., Barslund, A. F., Wenzler, C., Jensen, C. B., Kristensen, A. S. and Stromgaard, K. (2013) Structure-Activity Relationship Studies of Argiotoxins: Selective and Potent Inhibitors of Ionotropic Glutamate Receptors. *J. Med. Chem.*, *56*, 1171-1181.

(4) Liu, Y., Hu, Y. and Liu, T. (2012) Recent Advances in Non-Peptidomimetic Dipeptidyl Peptidase 4 Inhibitors: Medicinal Chemistry and Preclinical Aspects. *Curr. Med. Chem.*, *19*, 3982-3999.

(5) Qiao, J. X., Wang, T. C., Ruel, R., Thibeault, C., L'Heureux, A., Schumacher, W. A., Spronk, S. A., Hiebert, S., Bouthillier, G., Lloyd, J., Pi, Z., Schnur, D. M., Abell, L. M., Hua, J., Price, L. A., Liu, E., Wu, Q., Steinbacher, T. E., Bostwick, J. S., Chang, M., Zheng, J., Gao, Q., Ma, B., McDonnell, P. A., Huang, C. S., Rehfuss, R., Wexler, R. R. and Lam, P. Y. S. (2013) Conformationally Constrained *ortho*-Anilino Diaryl Ureas: Discovery of 1-(2-(1'-Neopentylspiro[indoline-3,4'-piperidine]-1-yl)phenyl)-3-(4-(trifluoromethoxy)phenyl)urea, a Potent, Selective, and Bioavailable $P2Y_1$ Antagonist. *J. Med. Chem.*, *56*, 9275-9295.

(6) Gasser, G., Ott, I. and Metzler-Nolte, N. (2011) Organometallic Anticancer Compounds. *J. Med. Chem.*, *54*, 3-25.

(7) Venkatakrishnan, A. J., Deupi, X., Lebon, G., Tate, C. G., Schertler, G. F. and Babu, M. M. (2013) Molecular signatures of G-protein-coupled receptors. *Nature*, *494*, 185-194.

(8) Bymaster, F. P., Whitesitt, C. A., Shannon, H. E., DeLapp, N., Ward, J. S., Calligaro, D. O., Shipley, L. A., Buelke-Sam, J. L., Bodick, N. C., Farde, L., Sheardown, M. J., Olesen, P. H., Hansen, K. T., Suzdak, P. D., Swedberg, M. D. B., Sauerberg, P. and Mitch, C. H. (1997) Xanomeline: A Selective Muscarinic Agonist for the Treatment of Alzheimer's Disease *Drug Dev. Res.*, *40*, 158-170.

(9) Bodick, N. C., Offen, W. W., Levey, A. I., Cutler, N. R., Gauthier, S. G., Satlin, A., Shannon, H. E., Tollefson, G. D., Rasmussen, K., Bymaster, F. P., Hurley, D. J., Potter, W. Z. and Paul, S. M. (1997) Effects of Xanomeline, a Selective Muscarinic Receptor Agonist, on Cognitive Function and Behavioral Symptoms in Alzheimer Disease. *Arch. Neurol.*, *54*, 465-473.

(10) Kapur, S., Zipursky, R. B., Remington, G., Jones, C., DaSilva, J., Wilson, A. A. and Houle, S. (1998) 5-HT$_2$ and D$_2$ Receptor Occupancy of Olanzapine in Schizophrenia: A PET Investigation. *Am. J. Psychiatry*, *155*, 921-928.

(11) Akam, E. and Strange, P. G. (2004) Inverse agonist properties of atypical antipsychotic drugs. *Biochem. Pharmacol.*, *67*, 2039-2045.

(12) Deng, C., Weston-Green, K. and Huang, X.-F. (2010) The role of histaminergic H1 and H3 receptors in food intake: A mechanism for atypical antipsychotic-induced weight gain? *Prog. Neuro-Psychopharmacol. Biol. Psychiatry*, *34*, 1-4.

(13) Kirk, S. L., Glazebrook, J., Grayson, B., Neill, J. C. and Reynolds, G. P. (2009) Olanzapine-induced weight gain in the rat: role of 5-HT2C and histamine H1 receptors. *Psychopharmacology*, *207*, 119-125.

(14) May, L. T., Leach, K., Sexton, P. M. and Christopoulos, A. (2007) Allosteric Modulation of G Protein-Coupled Receptors. *Annu. Rev. Pharmacol. Toxicol.*, *47*, 1-51.

(15) Davie, B. J., Christopoulos, A. and Scammells, P. J. (2013) Development of M$_1$ mAChR Allosteric and Bitopic Ligands: Prospective Therapeutics for the Treatment of Cognitive Deficits. *ACS Chem. Neurosci.*, *4*, 1026-1048.

(16) Willard, F. S., Bueno, A. B. and Sloop, K. W. (2012) Small Molecule Drug Discovery at the Glucagon-Like Peptide-1 Receptor. *Experimental Diabetes Research*, *2012*.

(17) Gregory, K., Nguyen, E. D., Reiff, S. D., Squire, E. F., Stauffer, S. R., Lindsley, C. W., Meiler, J. and Conn, P. J. (2013) Probing the Metabotropic Glutamate Receptor 5 (mGlu5) Positive Allosteric Modulator (PAM) Binding Pocket: Discovery of Point Mutations that Engender a "Molecular Switch" in PAM Pharmacology. *Mol. Pharmacol.*

(18) Hudson, B. D., Ulven, T. and G., M. (2013) The Therapeutic Potential of Allosteric Ligands for Free Fatty Acid Sensitive GPCRs. *Curr. Top. Med. Chem.*, *13*, 14-25.

(19) Leach, K., Sexton, P. M. and Christopoulos, A. (2007) Allosteric GPCR Modulators: Taking Advantage of Permissive Receptor Pharmacology. *Trends Pharmacol. Sci.*, *28*, 382-389.

(20) Canals, M., Lane, J. R., Wen, A., Scammells, P. J., Sexton, P. M. and Christopoulos, A. (2012) A Monod-Wyman-Changeux Mechanism Can Explain G Protein-coupled Receptor (GPCR) Allosteric Modulation. *J. Biol. Chem.*, *287*, 650-659.

(21) Ma, L., Seager, M. A., Wittman, M., Jacobson, M., Bickel, D., Burno, M., Jones, K., Graufelds, V. K., Xu, G., Pearson, M., McCampbell, A., Gaspar, R., Shughrue, P., Danziger, A., Regan, C., Flick, R., Pascarella, D., Garson, S., Doran, S., Kreatsoulas, C., Veng, L., Lindsley, C. W., Shipe, W., Kuduk, S., Sur, C., Kinney, G., Seabrook, G. R. and Ray, W. J. (2009) Selective Activation of the M_1 Muscarinic Acetylcholine Receptor Achieved by Allosteric Potentiation. *Proc. Natl. Acad. Sci. USA*, *106*, 15950-15955.

(22) Chan, W. Y., McKinzie, D. L., Bose, S., Mitchell, S. N., Witkin, J. M., Thompson, R. C., Christopoulos, A., Lazareno, S., Birdsall, N. J. M., Bymaster, F. P. and Felder, C. C. (2008) Allosteric modulation of the muscarinic M_4 receptor as an approach to treating schizophrenia. *Proc. Natl. Acad. Sci. USA*, *105*, 10978-10983.

(23) Leach, K., Loiacono, R. E., Felder, C. C., McKinzie, D. L., Mogg, A., Shaw, D. B., Sexton, P. M. and Christopoulos, A. (2010) Molecular Mechanisms of Action and *In Vivo* Validation of an M_4 Muscarinic Acetylcholine Receptor Allosteric Modulator with Potential Antipsychotic Properties. *Neuropsychopharmacology*, *35*, 855-869.

(24) Brady, A. E., Jones, C. K., Bridges, T. M., Kennedy, J. P., Thompson, A. D., Heiman, J. U., Breininger, M. L., Gentry, P. R., Yin, H., Jadhav, S. B., Shirey, J. K., Conn, P. J. and Lindsley, C. W. (2008) Centrally Active Allosteric Potentiators of the M_4 Muscarinic Acetylcholine Receptor Reverse Amphetamine-Induced Hyperlocomotor Activity in Rats. *J. Pharmacol. Exp. Ther.*, *327*, 941-953.

(25) Kennedy, J. P., Bridges, T. M., Gentry, P. R., Brogan, J. T., Kane, A. S., Jones, C. K., Brady, A. E., Shirey, J. K., Conn, P. J. and Lindsley, C. W. (2009) Synthesis and Structure-Activity Relationships of Allosteric Potentiators of the M_4 Muscarinic Acetylcholine Receptor. *ChemMedChem*, *4*, 1600-1607.

(26) Shirey, J. K., Xiang, Z., Orton, D., Brady, A. E., Johnson, K. A., Williams, R., Ayala, J. E., Rodriguez, A. L., Wess, J., Weaver, D., Niswender, C. M. and Conn, P. J. (2008) An allosteric potentiator of M_4 mAChR modulates hippocampal synaptic transmission. *Nat. Chem. Biol.*, *4*, 42-50.

(27) Huynh, T., Valant, C., Crosby, I. T., Sexton, P. M., Christopoulos, A. and Capuano, B. (2013) Probing Structural Requirements of Positive Allosteric Modulators of the M_4 Muscarinic Receptor. *J. Med. Chem.*, *56*, 8196-8200.

(28) Kuduk, S. D., Chang, R. K., Di Marco, C. N., Ray, W. J., Ma, L., Wittman, M., Seager, M. A., Koeplinger, K. A., Thompson, C. D., Hartman, G. D. and Bilodeau, M. T. (2011) Quinolizidinone Carboxylic Acid Selective M$_1$ Allosteric Modulators: SAR in the Piperidine Series. *Bioorg. Med. Chem. Lett.*, *21*, 1710-1715.

(29) Kuduk, S. D., Di Marco, C. N., Cofre, V., Ray, W. J., Ma, L., Wittman, M., Seager, M. A., Koeplinger, K. A., Thompson, C. D., Hartman, G. D. and Bilodeau, M. T. (2011) Fused Heterocyclic M$_1$ Positive Allosteric Modulators. *Bioorg. Med. Chem. Lett.*, *21*, 2769-2772.

(30) Kuduk, S. D., DiPardo, R. M., Beshore, D. C., Ray, W. J., Ma, L., Wittman, M., Seager, M. A., Koeplinger, K. A., Thompson, C. D., Hartman, G. D. and Bilodeau, M. T. (2010) Hydroxy Cycloalkyl Fused Pyridone Carboxylic Acid M$_1$ Positive Allosteric Modulators. *Bioorg. Med. Chem. Lett.*, *20*, 2538-2541.

(31) Yang, F. V., Shipe, W. D., Bunda, J. L., Nolt, M. B., Wisnoski, D. D., Zhao, Z., Barrow, J. C., Ray, W. J., Ma, L., Wittman, M., Seager, M. A., Koeplinger, K. A., Hartman, G. D. and Lindsley, C. W. (2010) Parallel Synthesis of *N*-Biaryl Quinolone Carboxylic Acids as Selective M$_1$ Positive Allosteric Modulators. *Bioorg. Med. Chem. Lett.*, *20*, 531-536.

(32) Kuduk, S. D., Di Marco, C. N., Cofre, V., Pitts, D. R., Ray, W. J., Ma, L., Wittman, M., Seager, M., Koeplinger, K., Thompson, C. D., Hartman, G. D. and Bilodeau, M. T. (2010) Pyridine Containing M$_1$ Positive Allosteric Modulators with Reduced Plasma Protein Binding. *Bioorg. Med. Chem. Lett.*, *20*, 657-661.

(33) Kuduk, S. D., Di Marco, C. N., Chang, R. K., Ray, W. J., Ma, L., Wittman, M., Seager, M. A., Koeplinger, K. A., Thompson, C. D., Hartman, G. D. and Bilodeau, M. T. (2010) Heterocyclic Fused Pyridone Carboxylic Acid M$_1$ Positive Allosteric Modulators. *Bioorg. Med. Chem. Lett.*, *20*, 2533-2537.

(34) Mistry, S. N., Valant, C., Sexton, P. M., Capuano, B., Christopoulos, A. and Scammells, P. J. (2013) Synthesis and Pharmacological Profiling of Analogues of Benzyl Quinolone Carboxylic Acid (BQCA) as Allosteric Modulators of the M$_1$ Muscarinic Receptor. *J. Med. Chem.*, *56*, 5151-5172.

(35) Kuduk, S. D., Di Marco, C. N., Cofre, V., Pitts, D. R., Ray, W. J., Ma, L., Wittman, M., Veng, L., Seager, M. A., Koeplinger, K., Thompson, C. D., Hartman, G. D. and Bilodeau, M. T. (2010) N-Heterocyclic Derived M$_1$ Positive Allosteric Modulators. *Bioorg. Med. Chem. Lett.*, *20*, 1334-1337.

(36) Kuduk, S. D. and Beshore, D. C. (2012) Novel M$_1$ Allosteric Ligands: A Patent Review. *Expert Opin. Ther. Pat.*, *22*, 1385-1398.

(37) Abdul-Ridha, A., Lopez, L., Keov, P., Thal, D. M., Mistry, S. N., Sexton, P. M., Lane, J. R., Canals, M. and Christopoulos, A. (2014) Molecular Determinants of Allosteric Modulation at the M_1 Muscarinic Acetylcholine Receptor. *J. Biol. Chem.*, *289*, 6067-6079.

(38) Gottlieb, H. E., Kotlyar, V. and Nudelman, A. (1997) NMR Chemical Shifts of Common Laboratory Solvents as Trace Impurities. *J. Org. Chem.*, *62*, 7512-7515.

(39) Furniss, B. S., Hannaford, A. J., Smith, P. W. G. and Tatchell, A. R. *Vogel's Textbook of Practical Organic Chemistry*; 5th ed.; Longman Scientific and Technical: London, 1989.

(40) Leach, K., Sexton, P. M. and Christopoulos, A. (2007) Allosteric GPCR modulators: taking advantage of permissive receptor pharmacology. *Trends Pharmacol. Sci.*, *28*, 382-389.

(41) Valant, C., Aurelio, L., Urmaliya, V. B., White, P., Scammells, P. J., Sexton, P. M. and Christopoulos, A. (2010) Delineating the Mode of Action of Adenosine A_1 Receptor Allosteric Modulators. *Mol. Pharmacol.*, *78*, 444-455.

Chapter Six

Future Directions

Chapters 2 and 3

Chapters 2 and 3 reported the development of two irreversible allosteric ligands, MIPS1262 and MIPS1455, based on the structure of the M_1 mAChR-selective allosteric ligand BQCA. Two important questions need to be answered to assess the future utility of the molecular tools developed in Chapters 2 and 3; a) Where do these ligands bind to the M_1 muscarinic acetylcholine receptor? And b) How selective are these ligands; on target, across the GPCR family and in a broader cellular context? Techniques that may be employed to address these questions are mass spectrometry, computational modeling, crystallography and screening assays.

The use of mass spectrometric techniques to probe the primary, secondary, tertiary and quaternary structures of membrane-bound proteins such as GPCRs, and the intracellular multiprotein complexes that interact with them, has advanced considerably in recent years.[1,2] One particularly accessible and well-established technique thought to have laid the foundation for the field of proteomics is peptide mass fingerprinting.[3] One of the earliest examples of the application of this technique to identify the binding site of an irreversible GPCR ligand is that of acetylcholine mustard (AChM) at mAChRs.[4] In brief, purified receptors were treated with the reactive aziridinium form of [^{3}H]AChM, digested with cyanogen bromide, and the resulting fragments subjected to SDS-PAGE and Edman degradation analysis to identify the labeled amino acid residue as the highly-conserved transmembrane domain 3 aspartic acid present in the orthosteric site of all aminergic GPCRs.[5] Based on this approach, the covalent binding site(s) of our irreversible BQCA analogues, MIPS1262 and MIPS1455, could be elucidated using a modified experimental protocol. The original AChM study did not purify individual receptor subtypes, instead using

a mixture of mAChRs isolated from the rat forebrain and striatum. Whilst this is of no consequence to their study, given the propensity for AChM to bind non-selectively to the same binding site on all five mAChR subtypes, our work necessitates the use of purified M_1 mAChR. Another important difference between the AChM study and our own prospective study is the use of a tritiated irreversible ligand. In the former study, the radioactive label aided detection of covalently modified peptides in the fragmentation mixture. However, as the speed and sensitivity of proteomics techniques has advanced considerably, the amino acid residues labeled by MIPS1262 and MIPS1455 could still be readily identified by rapid sequencing and mass spectrometric analysis of the entire protein digest in the absence of a radioactive label. Finally, it is likely that trypsin, rather than cyanogen bromide, would be applied to fragment the covalently labeled receptor as it is a more commonly used proteolytic cleavage agent.

This experiment would determine the on-target selectivity of MIPS1262 and MIPS1455. As already highlighted in Chapter 3, the inherent reactivity of the isothiocyanate functionality in MIPS1262 may result in the ligand covalently modifying multiple nucleophilic amino acid residues at the M_1 mAChR. Molecular dynamics simulations demonstrating the ability of both orthosteric and allosteric GPCR ligands to adopt metastable binding poses at distinct sites prior to reaching stable poses within their respective binding sites further support this likelihood.[6,7] Furthermore, close examination of a recent molecular model of the BQCA-M_1 mAChR interaction indicates that the nucleophilic amino acid residues present in this region of the receptor do not lie in close proximity to the benzylic pendant of BQCA, suggesting that, even if MIPS1262 interacts with the BQCA binding site, it may not be adopting the same pose. Selectivity studies across the other four mAChR subtypes (Appendix 2) provide further evidence to support this. In contrast, MIPS1455 can be pre-equilibrated with the M_1

mAChR to form a reversible ligand-receptor complex prior to photoactivation and subsequent covalent modification. This increases the likelihood that MIPS1455 will only label the allosteric binding site of interest, and in a pose that more closely resembles that which the parent molecule BQCA adopts at the M_1 mAChR. Indeed, the binding and functional data reported in Chapter 3 and the mAChR selectivity studies reported in Appendix 3 clearly support the hypothesis that, prior to photoactivation, MIPS1455 interacts with the M_1 mAChR in a similar manner to BQCA. Peptide mass fingerprinting would clearly provide more conclusive evidence to evaluate these hypotheses.

Identifying the amino acid residues that are being covalently modified by these ligands would supplement existing computational modelling of the BQCA binding site and subsequently aid the design of more soluble, pharmacokinetically viable BQCA analogues. Furthermore, if MIPS1455 was found to be selectively labelling the binding site of interest, the ligand could serve as an immensely valuable tool for co-crystallization with an orthosteric agonist-bound M_1 mAChR, which may further elucidate the structural network by which BQCA transmits its extraordinary degree of positive cooperativity and better inform rational drug design at this and potentially other GPCRs. Binding and functional screening against a panel of common GPCR targets could be employed to assess the broader selectivity of MIPS1262 and MIPS1455, though it is already clear that MIPS1262 shows off-target activity within the mAChR family. Fluorescent labelling and gel electrophoresis could be utilized to assess the selectivity of these ligands in a broader cellular context, though this necessitates further synthetic chemistry efforts that will be discussed in the next section.

Given that MIPS1455 appears to be the more promising of these two molecular tools, a second functionality or 'reporter' group could be introduced to expand the pharmacological

utility of this ligand. Fluorescent, radioactive, and biotin-based probes are examples of secondary functionalities introduced into affinity labels for enzymes and GPCRs.[8]

Biotin-based probes enable detection and purification of affinity-labeled target proteins using streptavidin-coated resin beads, facilitating target identification and monitoring of protein expression levels.[9] Incorporating a biotin tag into MIPS1455 (**1**, **Figure 1**) may yield a useful tool for monitoring changes in M_1 mAChR expression in healthy and diseased tissue, or following treatment with orthosteric agonists/antagonists or allosteric modulators in both an *in vitro* or *ex vivo* context. It may also be useful for isolating and studying M_1 mAChRs that have been functionally modified by intracellular signaling and trafficking proteins. Whilst expensive and hazardous, affinity labels containing radioactive atoms such as ^{125}I and ^3H are also commonly used in *in vitro* protein profiling studies. In contrast to biotinylation, radiolabeling offers a more subtle means to modify the structure of an affinity label and can be detected *in vivo*. An example of how radioactive iodine might be incorporated into the structure of MIPS1455 is illustrated by structure **2**, **Figure 1**.

Fluorescently-tagged affinity labels offer a broader range of capabilities than biotinylation and radiolabeling, by virtue of the extensive array of fluorophores developed in recent years and the ability to directly visualize such ligands in protein profiling, microscopy and *in vivo* imaging.[9] An analogue of MIPS1455 tagged with a fluorescent label such as tetrazine (**3**, **Figure 1**) could prove to be valuable for studying the structural dynamics of the highly-flexible extracellular vestibule of the M_1 mAChR in the presence and absence of an orthosteric agonist/antagonist, a region of the receptor shown to be crucial for determining the degree of receptor activation and G protein-coupling specificity.[10] Furthermore, such molecular tools may afford direct visualization of the trafficking and compartmentalization of the M_1 mAChR following allosteric ligand-mediated activation and internalization in live

cells, which may prove distinct from orthosteric ligand-mediated processes. An additional application may be the selective visualization of M_1 mAChRs in specific tissues following experiments involving animal models of cognition or from post-mortem human brain tissue, allowing differences in receptor expression and localization between healthy, diseased and treatment groups to be elucidated. Furthermore, a recent proof-of-concept study detailed the use of a positron emission tomography (PET) tracer as a source of light for *in vivo* photoactivation;[11] further broadening the potential applications for MIPS1455 and other photoactivatable ligands.

Whilst BQCA analogues containing each of these three types of 'reporter' groups could be separately synthesized, tandem photoaffinity-labeling-bioorthogonal conjugation is an efficient, highly advantageous method by which different probes can be synthesized *in situ* from a single affinity label depending on the needs of the individual experiment.[12] A 'clickable' handle, most commonly a terminal alkyne, is introduced into the affinity label (**4**, **Figure 1**) that allows for coupling to biotin, a fluorophore, a second reactive functionality, or an amino acid within a protein target that has been modified with the requisite alkyl azide, in a copper-catalyzed process. To date, this strategy has largely been used to study enzymatic drug targets, however examples of its application at ligand-gated ion channels and GPCRs are emerging.[13,14]
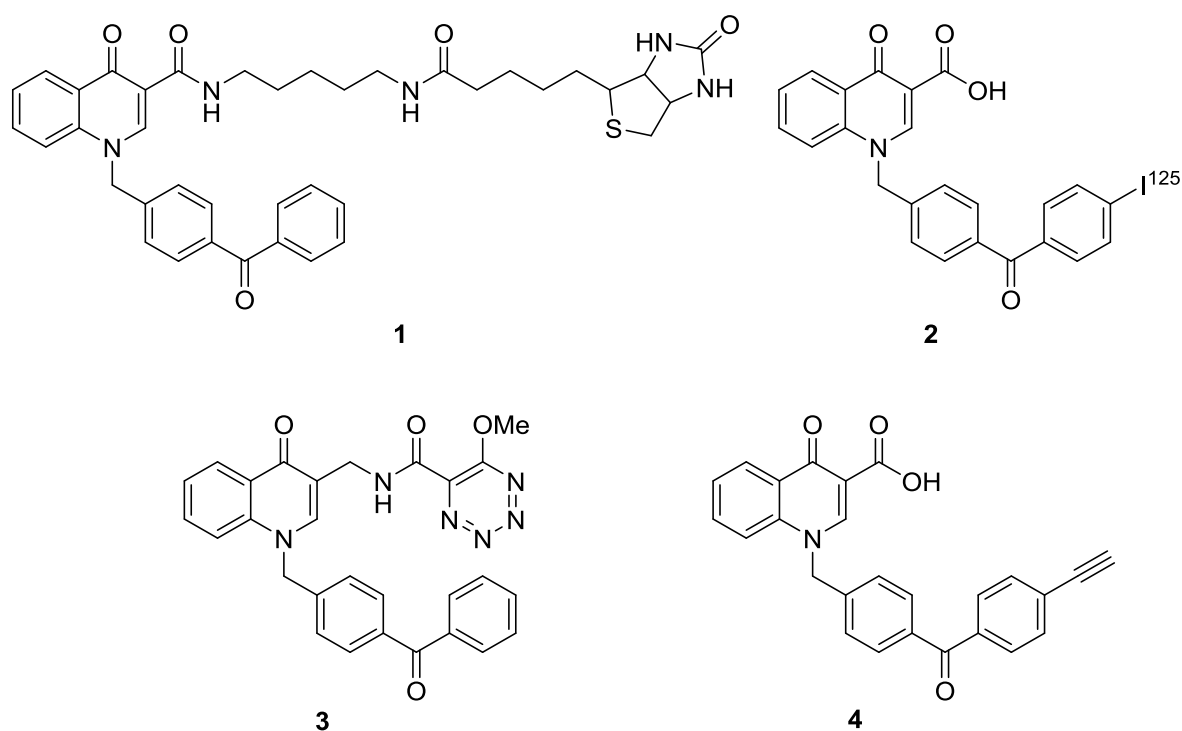
Figure 1. Prospective biotinylated (1), radiolabelled (2), fluorescently-labelled (3) and clickable (4) analogues of MIPS1455

MIPS1262 and MIPS1455 reported in Chapters 2 and 3 of this thesis may serve as templates for multifunctional molecular tools for the M_1 mAChR, though it would be worth considering applying the strategies described to one of the higher affinity BQCA-like scaffolds recently reported. This work also provides proof-of-concept for the development of such ligands for the orthosteric and allosteric sites of other GPCRs.

Chapter 4

Chapter 4 described the preliminary stages of rationally designing bitopic ligands for the M_1 mAChR. Inspired by studies undertaken at the M_2 mAChR[10,15,16] and guided by an experimental approach detailed by our own laboratory,[17] we sought to link together the high potency, non-selective orthosteric ligand iperoxo with the low affinity, highly selective

allosteric ligand BQCA. The pharmacological methods required to determine the binding mode of the putative bitopic ligands **33a** and **44**, as well as suggestions for future synthetic chemistry undertakings, have already been discussed in Chapter 4. Hence, this section will speculate on the prospective utility of these ligands should they prove to be interacting with the M_1 mAChR in a bitopic manner.

If a bitopic mechanism of action were to be confirmed, it would be necessary to assess the mAChR and broader target selectivity of these ligands in a similar manner to that described for the irreversible allosteric ligands in Chapters 2 and 3. Furthermore, to complement the mutagenesis studies that would be performed to elucidate a bitopic binding mode, molecular dynamics simulations would provide an overall picture of the poses likely being adopted by these ligands, informing further optimization and novel therapeutic design.

The level of receptor activation required to achieve a therapeutic effect (i.e. enhancement of cognition, attenuation of AD pathophysiology) without on-target side effects (i.e. neurotoxicity) remains a crucial question for the field of M_1 mAChR therapeutic development. A series of M_1 mAChR-selective bitopic ligands of different linker lengths may aid researchers in addressing this question, given the significant advances afforded by rationally-designed bitopic ligands at the M_2 mAChR (Chapter 4, **Figure 2**). Specifically, recapitulating the graded receptor activation achieved with M_2 mAChR bitopic ligands[10] in the context of the M_1 mAChR may provide suitable *in vivo* tools to ascertain the level of receptor activation required to achieve an optimal therapeutic effect and avoid toxicity in animal models of cognitive deficits. Whilst iperoxo and BQCA alone do not affect stimulus bias at the M_1 mAChR, bitopic ligands combining the two pharmacophores may adopt binding poses that give rise to distinct receptor conformations that alter the G protein-coupling preferences and signaling pathways activated by the receptor. *In vitro*

pharmacological techniques based on previous work performed in our laboratory could be undertaken to investigate whether such ligands engender stimulus bias. Examples of such techniques include the use of genetically-modified yeast strains expressing select G protein chimeras and/or the calculation of bias factors and the generation of bias plots.[18-21]

Such future undertakings, whilst purely theoretical, illustrate the potential value of advancing this project beyond the preliminary research reported in this thesis.

Chapter 5

Chapter 5 briefly demonstrated that applying more detailed pharmacological analyses may unmask the potential of known allosteric ligands to probe the effect of "dialing up" particular allosteric parameters to the exclusion of others. Future work would involve examining if selective enhancement of different allosteric parameters gives rise to divergent effects in an *in vivo* setting; i.e. does enhancing the affinity of the allosteric ligand (as in the case of **5**, Chapter 5) have a different effect than enhancing the functional efficacy of the allosteric ligand (as in the case of **6**, Chapter 5). That said, in applying such an approach to future studies, it would be more fruitful to investigate the effect of iterative structural changes on individual allosteric parameters, rather than simply comparing a parent molecule (BQCA) to two analogues containing multiple structural alterations. Furthermore, as a number of higher potency M_1 mAChR-selective allosteric ligands derived from the structure of BQCA have emerged since this project was undertaken,[22] it would be of interest to direct investigative efforts towards these ligands.

Conclusion

The overall aim of this thesis, to synthesize and pharmacologically evaluate a range of molecular tools that may be employed to advance our understanding of allosteric and bitopic interactions with the M_1 mAChR, has been successfully achieved. Future directions will involve taking these ligands beyond the preliminary development described in this thesis and into the exploration of their application in structural and functional studies of the M_1 mAChR.

References

(1) Barrera, N. P. and Robinson, C. V. (2011) Advances in the Mass Spectrometry of Membrane Proteins: From Individual Proteins to Intact Complexes. *Annu. Rev. Biochem*, *80*, 247-271.

(2) Becamel, C., Galeotti, N., Poncet, J., Jouin, P., Dumuis, A., Bockaert, J. and Marin, P. (2002) A proteomic approach based on peptide affinity chromatography, 2-dimensional electrophoresis and mass spectrometry to identify multiprotein complexes interacting ith membrane-bound receptors. *Biological Procedures Online*, *4*, 94-104.

(3) Henzel, W. J. and Watanabe, C. (2003) Protein identification: the origins of peptide mass fingerprinting. *J. Am. Soc. Mass. Spectrom.*, *14*, 931-942.

(4) Spalding, T. A., Birdsall, N. J. M., Curtis, C. A. M. and Hulme, E. C. (1994) Acetylcholine Mustard Labels the Binding Site Aspartate in Muscarinic Acetylcholine Receptors. *J. Biol. Chem.*, *269*, 4092-4097.

(5) Kruse, A. C., Kobilka, B. K., Gautam, D., Sexton, P. M., Christopoulos, A. and Wess, J. (2014) Muscarinic acetylcholine receptors: novel opportunities for drug development. *Nat. Rev. Drug Discov.*, *13*, 549-560.

(6) Dror, R. O., Pan, A. C., Arlow, D. H., Borhani, D. W., Maragakis, P., Shan, Y., Xu, H. and Shaw, D. E. (2011) Pathway and mechanism of drug binding to G-protein-coupled receptors. *Proc. Natl. Acad. Sci. USA*, *108*, 13118-13123.

(7) Dror, R. O., Green, H. F., Valant, C., Borhani, D. W., Valcourt, J. R., Pan, A. C., Arlow, D. H., Canals, M., Lane, J. R., Rahmani, R., Baell, J. B., Sexton, P. M., Christopoulos, A. and Shaw, D. E. (2013) Structural basis for modulation of a G-protein-coupled receptor by allosteric drugs. *Nature*, *503*, 295-299.

(8) Daggett, K. A. and Sakmar, T. P. (2011) Site-specific *in vitro* and *in vivo* incorporation of molecular probes to study G-protein-coupled receptors. *Curr. Opin. Chem. Biol.*, *15*, 392-398.

(9) Sadaghiani, A. M., Verhelst, S. H. L. and Bogyo, M. (2007) Tagging and detection strategies for activity-based proteomics. *Curr. Opin. Chem. Biol.*, *11*, 20-28.

(10) Bock, A., Merten, N., Schrage, R., Dallanoce, C., Batz, J., Klockner, J., Schmitz, J., Matera, C., Simon, K., Kebig, A., Peters, L., Muller, A., Schrobang-Ley, J., Trankle, C., Hoffman, C., De Amici, M., Holzgrabe, U., Kostenis, E. and Mohr, K. (2012) The allosteric

vestibule of a seven transmembrane helical receptor controls G-protein coupling. *Nat. Commun.*

(11) Ran, C., Zhang, Z., Hooker, J. and Moore, A. (2012) In vivo photoactivation without "light": use of Cherenkov radiation to overcome the penetration limit of light. *Mol. Imag. Biol.*, *14*, 156-162.

(12) Lapinsky, D. J. (2012) Tandem photoaffinity labeling-bioorthogonal conjugation in medicinal chemistry. *Biorg. Med. Chem.*, *20*, 6237-6247.

(13) Tantama, M., Lin, W. C. and Licht, S. (2008) An activity-based protein profiling probe for the nicotinic acetylcholine receptor. *J. Am. Chem. Soc.*, *130*, 15766-15767.

(14) Martin-Couce, L., Martin-Fontecha, M., Capolicchio, S., Lopez-Rodriguez, M. L. and Ortega-Gutierrez, S. (2011) Development of Endocannabinoid-Based Chemical Probes for the Study of Cannabinoid Receptors. *J. Med. Chem.*, *54*, 5265-5269.

(15) Antony, J., Kellershohn, K., Mohr-Andra, M., Kebig, A., Prilla, S., Muth, M., Heller, E., Disingrini, T., Dallanoce, C., Bertoni, S., Schrobang, J., Trankle, C., Kostenis, E., Christopoulos, A., Holtje, H.-D., Barocelli, E., De Amici, M., Holzgrabe, U. and Mohr, K. (2009) Dualsteric GPCR targeting: a novel route to binding and signaling pathway selectivity. *FASEB J.*, *23*, 442-450.

(16) Bock, A., Chirinda, B., Krebs, F., Messerer, R., Batz, J., Muth, M., Dallanoce, C., Klingenthal, D., Trankle, C., Hoffmann, C., De Amici, M., Holzgrabe, U., Kostenis, E. and Mohr, K. (2014) Dynamic ligand binding dictates partial agonism at a G protein-coupled receptor. *Nat. Chem. Biol.*, *10*, 18-22.

(17) Lane, J. R., Sexton, P. M. and Christopoulos, A. (2013) Bridging the gap: bitopic ligands of G-protein-coupled receptors. *Trends Pharmacol. Sci.*, *34*, 59-66.

(18) Canals, M., Lane, J. R., Wen, A., Scammells, P. J., Sexton, P. M. and Christopoulos, A. (2012) A Monod-Wyman-Changeux Mechanism Can Explain G Protein-coupled Receptor (GPCR) Allosteric Modulation. *J. Biol. Chem.*, *287*, 650-659.

(19) Valant, C., May, L. T., Aurelio, L., Chuo, C. H., White, P. J., Baltos, J.-A., Sexton, P. M., Scammells, P. J. and Christopoulos, A. (2014) Separation of on-target efficacy from adverse effects through rational design of a bitopic adenosine receptor agonist. *Proc. Natl. Acad. Sci. USA*.

(20) Stewart, G. D., Sexton, P. M. and Christopoulos, A. (2010) Prediction of functionally selective allosteric interactions at an M_3 muscarinic acetylcholine receptor mutant using Saccharomyces cerevisiae. *Mol. Pharmacol.*, *78*, 205-214.

(21) Shonberg, J., Klein Herenbrink, C., Lopez, L., Christopoulos, A., Scammells, P. J., Capuano, B. and Lane, J. R. (2013) A Structure-Activity Analysis of Biased Agonism at the Dopamine D2 Receptor. *J. Med. Chem.*, *56*, 9199-9221.

(22) Kuduk, S. D. and Beshore, D. C. (2012) Novel M_1 Allosteric Ligands: A Patent Review. *Expert Opin. Ther. Pat.*, *22*, 1385-1398.

Appendices

Appendix 1. Chapter 2 Published Supporting Information

SUPPORTING INFORMATION

Synthesis and Pharmacological Evaluation of Analogues of Benzyl Quinolone Carboxylic Acid (BQCA) Designed to Bind Irreversibly to an Allosteric Site of the M$_1$ Muscarinic Acetylcholine Receptor

Briana J. Davie [†,‡] Celine Valant [‡] Jonathan M. White [§] Ben Capuano,[†] Patrick M. Sexton, [‡] Arthur Christopoulos[‡,*] and Peter J. Scammells[†,*]

[†] Medicinal Chemistry and [‡]Drug Discovery Biology, Monash Institute of Pharmaceutical Sciences, Monash University, Parkville, Victoria, 3052, Australia.

[§] School of Chemistry and the Bio21 Molecular Science and Biotechnology Institute, The University of Melbourne, Parkville, Victoria, 3010, Australia.

Table of Contents

1. The 2D NMR HMBC spectrum used to confirm *N*-benzylation to form BQCA (**5**), with the key crosspeaks between position 8 and position 15 indicated by the arrows
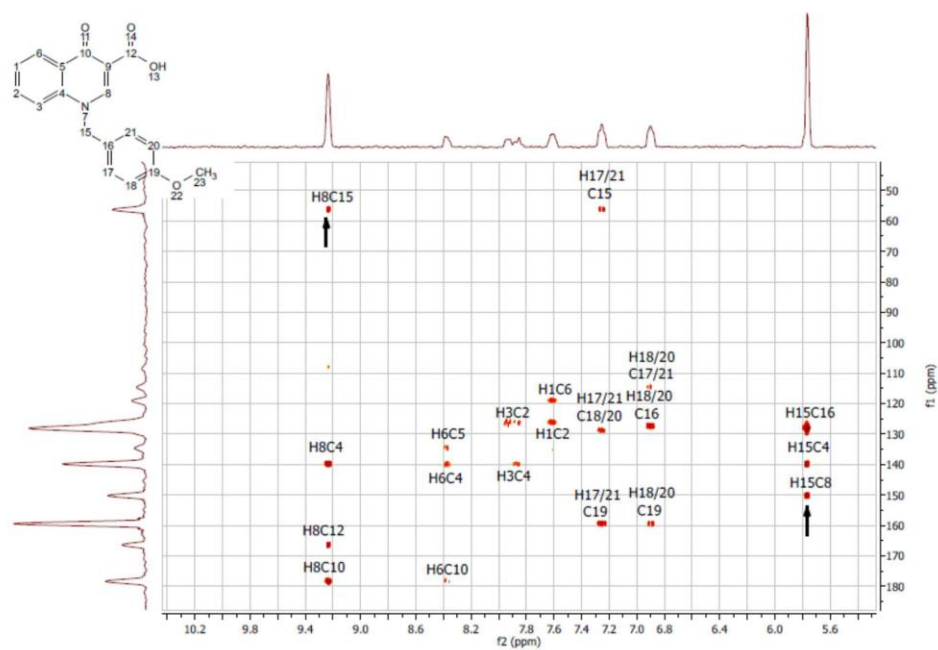
2. HPLC traces for final compound purity (254 and 214 nm)
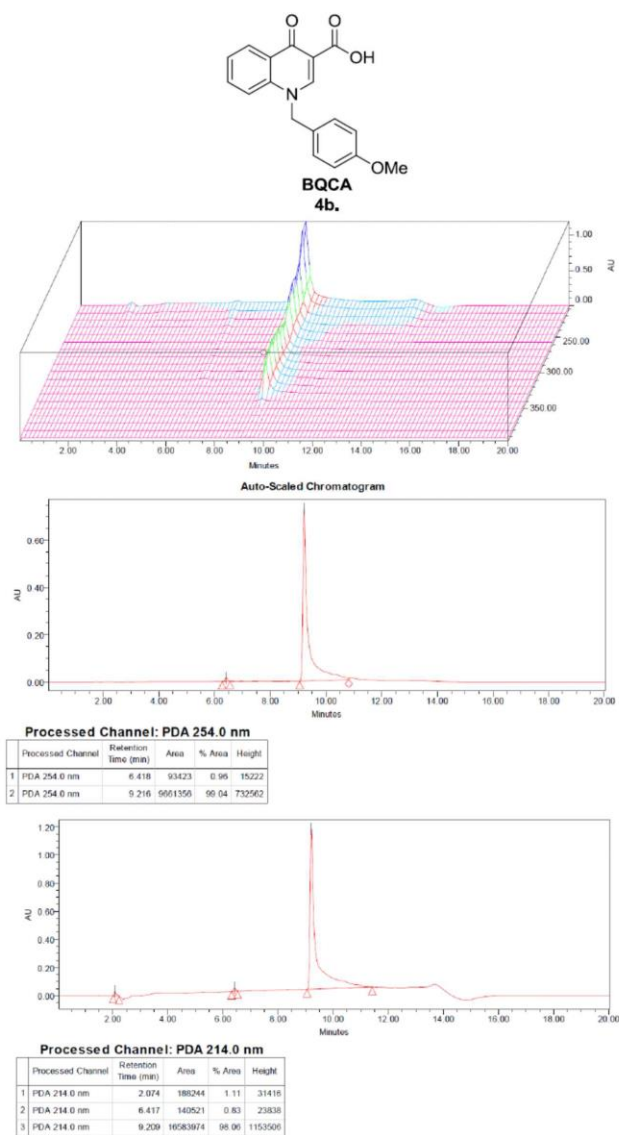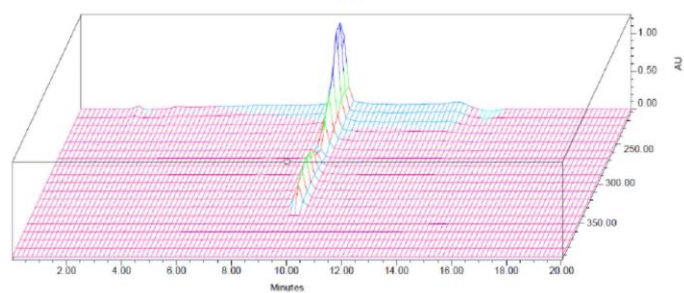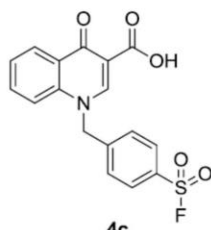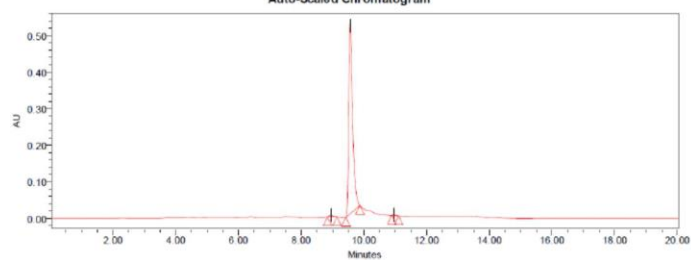
BQCA
4b.

Auto-Scaled Chromatogram

Processed Channel: PDA 254.0 nm

	Processed Channel	Retention Time (min)	Area	% Area	Height
1	PDA 254.0 nm	6.418	93423	0.96	15222
2	PDA 254.0 nm	9.216	9661356	99.04	732562

Processed Channel: PDA 214.0 nm

	Processed Channel	Retention Time (min)	Area	% Area	Height
1	PDA 214.0 nm	2.074	186244	1.11	31416
2	PDA 214.0 nm	6.417	140521	0.83	23838
3	PDA 214.0 nm	9.209	16583974	98.06	1153506

4c.

Auto-Scaled Chromatogram

Processed Channel: PDA 254.0 nm

	Processed Channel	Retention Time (min)	Area	% Area	Height
1	PDA 254.0 nm	8.946	39889	0.89	5557
2	PDA 254.0 nm	9.563	4435143	98.81	520751
3	PDA 254.0 nm	10.950	13642	0.30	2202
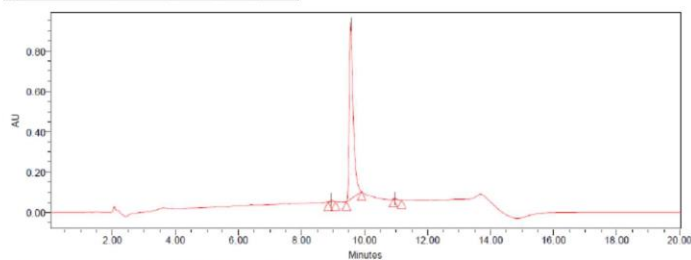
Processed Channel: PDA 214.0 nm

	Processed Channel	Retention Time (min)	Area	% Area	Height
1	PDA 214.0 nm	8.947	57608	0.75	9445
2	PDA 214.0 nm	9.563	7555547	98.94	874616
3	PDA 214.0 nm	10.953	23331	0.31	4246
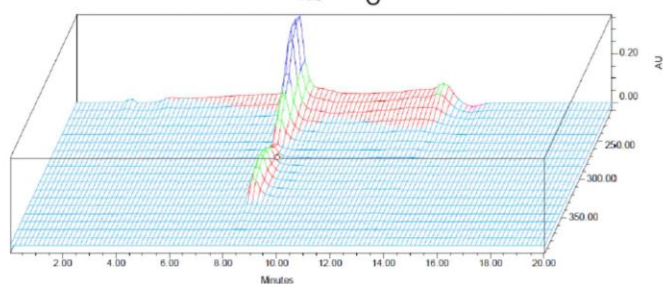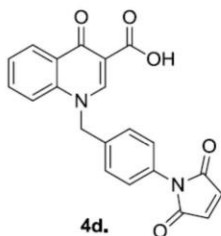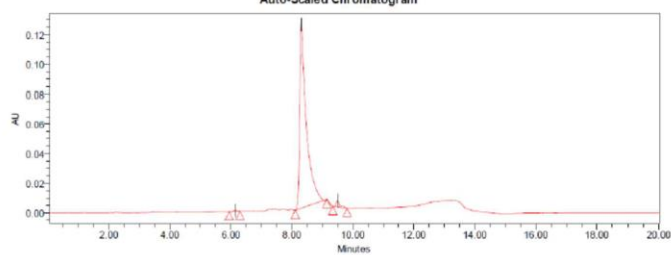
4d.

Auto-Scaled Chromatogram

Processed Channel: PDA 254.0 nm

	Processed Channel	Retention Time (min)	Area	% Area	Width (sec)	Height
1	PDA 254.0 nm	6.146	6137	0.32	21.000	828
2	PDA 254.0 nm	8.318	1855372	97.83	62.000	124546
3	PDA 254.0 nm	9.500	35067	1.85	28.000	4214
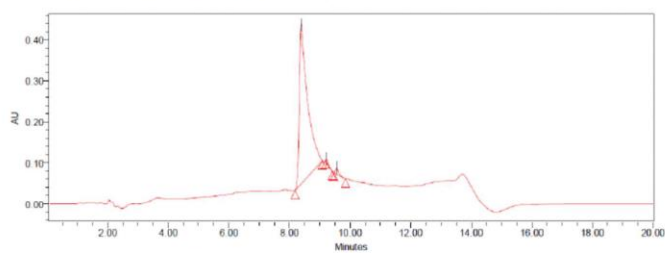
Processed Channel: PDA 214.0 nm

	Processed Channel	Retention Time (min)	Area	% Area	Width (sec)	Height
1	PDA 214.0 nm	8.389	7210809	97.94	54.000	391319
2	PDA 214.0 nm	9.210	37496	0.51	14.000	6035
3	PDA 214.0 nm	9.555	113914	1.55	23.000	15196
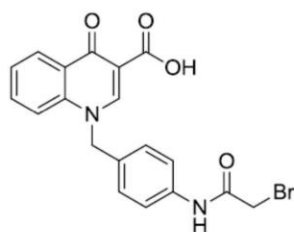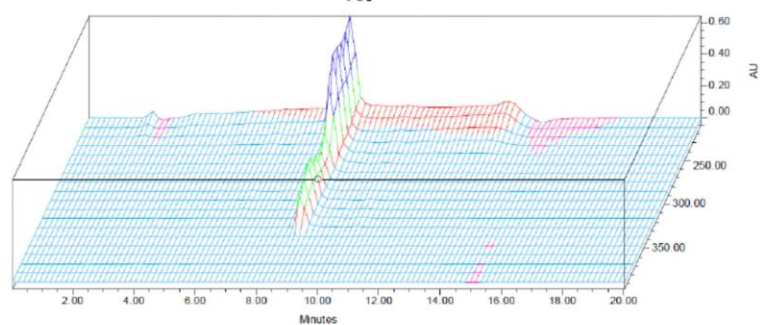
10.

Auto-Scaled Chromatogram
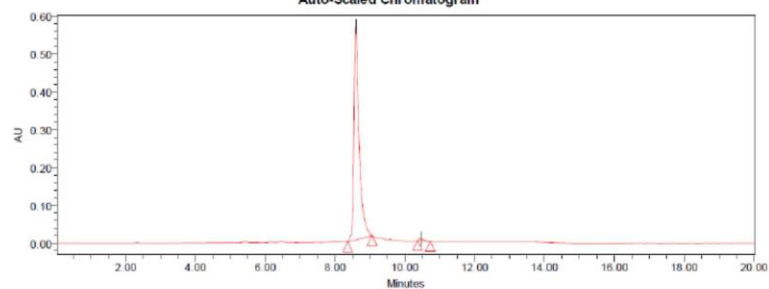
Processed Channel: PDA 254.0 nm

	Processed Channel	Retention Time (min)	Area	% Area	Height
1	PDA 254.0 nm	8.594	5759859	99.08	563840
2	PDA 254.0 nm	10.446	53315	0.92	5885
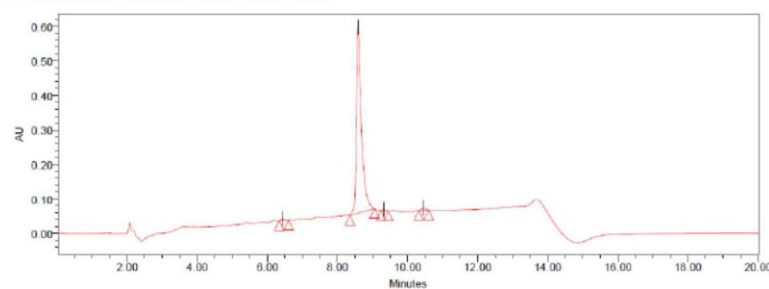
Processed Channel: PDA 214.0 nm

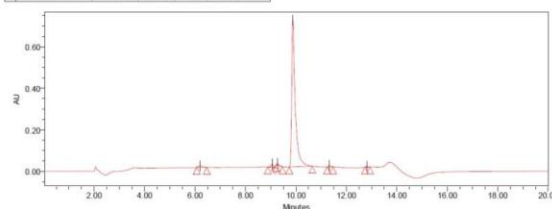|	Processed Channel	Retention Time (min)	Area	% Area	Height		Processed Channel	Retention Time (min)	Area	% Area	Height
1	PDA 214.0 nm	6.443	36868	0.67	5425	4	PDA 214.0 nm	10.444	54403	0.99	7090
2	PDA 214.0 nm	8.589	5389174	97.93	544650						
3	PDA 214.0 nm	9.312	22915	0.42	3490						
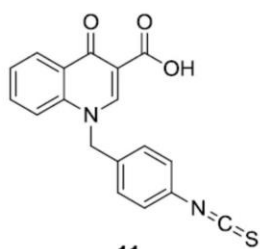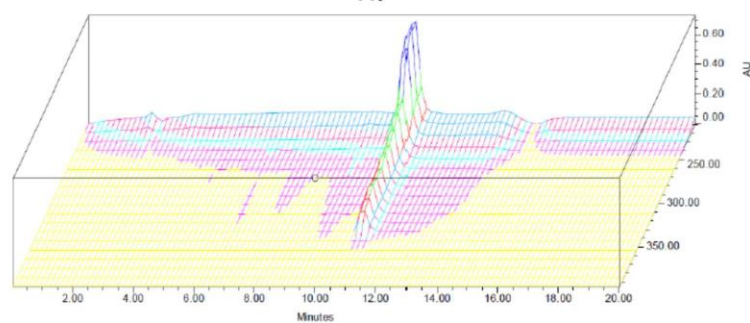
11.

Auto-Scaled Chromatogram
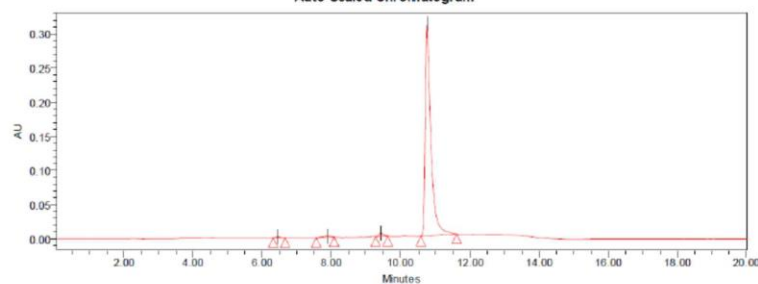
Processed Channel: PDA 254.0 nm

	Processed Channel	Retention Time (min)	Area	% Area	Width (sec)	Height
1	PDA 254.0 nm	6.453	12890	0.36	21.000	1529
2	PDA 254.0 nm	7.907	24957	0.70	31.000	1575
3	PDA 254.0 nm	9.439	46056	1.29	21.000	5003

	Processed Channel	Retention Time (min)	Area	% Area	Width (sec)	Height
4	PDA 254.0 nm	10.751	3491794	97.65	62.000	311054
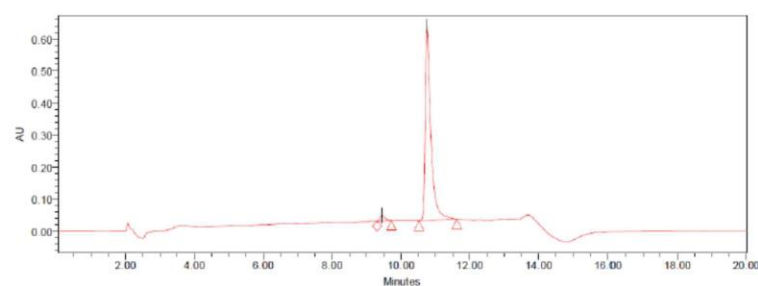
Processed Channel: PDA 214.0 nm

	Processed Channel	Retention Time (min)	Area	% Area	Width (sec)	Height
1	PDA 214.0 nm	9.444	186783	2.65	25.000	18006
2	PDA 214.0 nm	10.759	6856002	97.35	66.000	604901

194

3. Radioligand Saturation Whole Cell Binding experiments for compounds 4c, 4d and 10.
B_{max} (% vehicle) bar graphs from radioligand saturation binding experiments performed in hM_1 mAChR-expressing CHO cells in the presence of increasing concentrations of radio-labeled orthosteric antagonist [^{3}H]NMS where values significantly different from Vehicle are indicated by an * (where * = $p < 0.05$, ** = $p < 0.01$, *** = $p < 0.001$ and **** = $p < 0.0001$). **Orange.** 30 min pre-incubation with vehicle, 4c, or 4c + ACh. **Purple.** 30 min preincubation with vehicle, 4d, or 4d + ACh. **Blue.** 30 min pre-incubation with vehicle, 10, or 10 + ACh. Values represent the mean ± S.E.M from at least three to four experiments performed in duplicate.
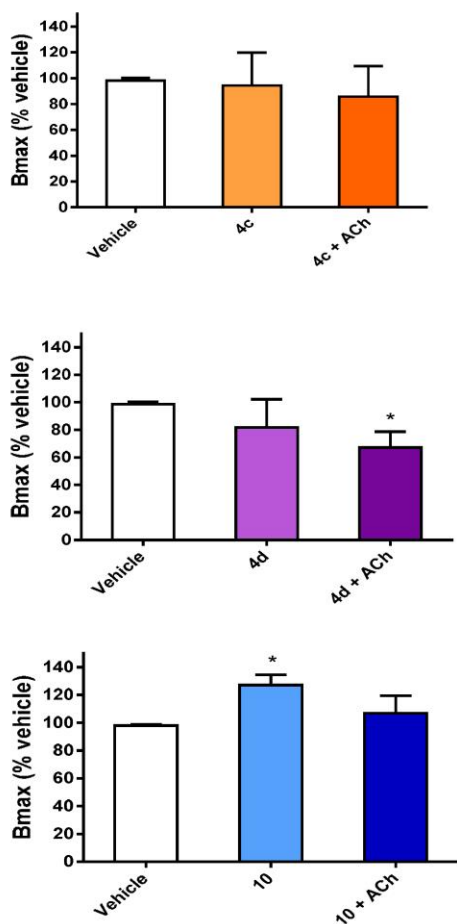
Appendix 2. Chapter 2 Unpublished Supporting Information

1. Pharmacological characterization of BQCA and putative irreversible analogues in ERK1/2 phosphorylation time course assays in FlpIn CHO cells stably expressing the hM$_1$ mAChR (top) and non-transfected FlpIn CHO cells (bottom). See *Alphascreen ERK1/2 Phosphorylation Assays – Time Course Assays* in the Experimental Section of Chapter 2 for a description of the protocol. Values represent the mean ± SEM from two to three experiments performed in duplicate.
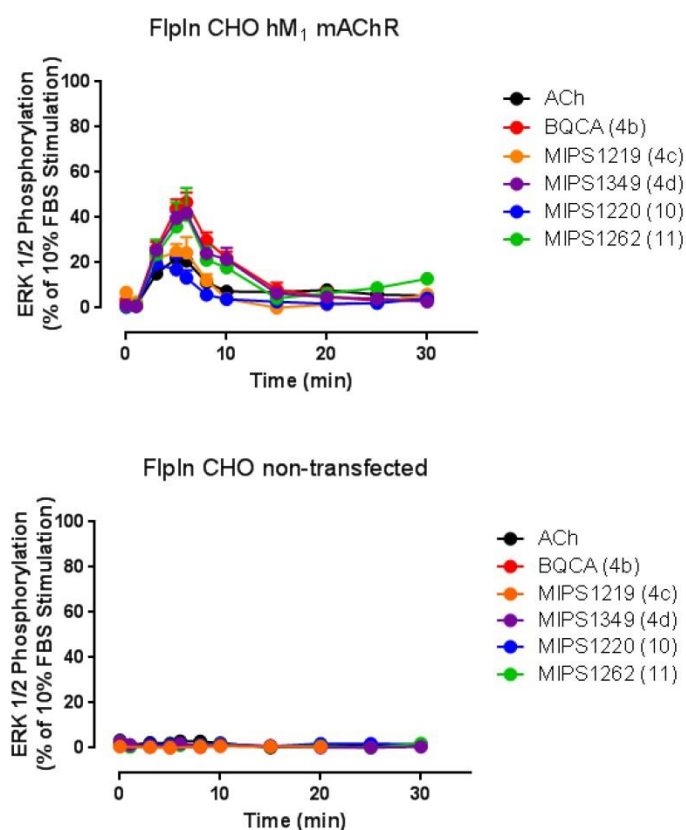
2. In situ validation of the ability of MIPS1262 to irreversibly couple to a nucleophilic amino acid residue (cysteine)
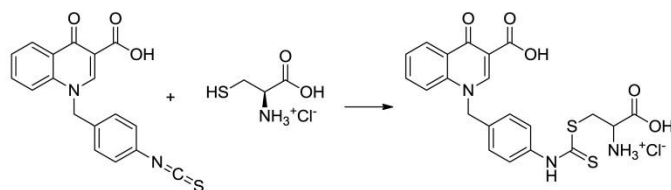
Starting material
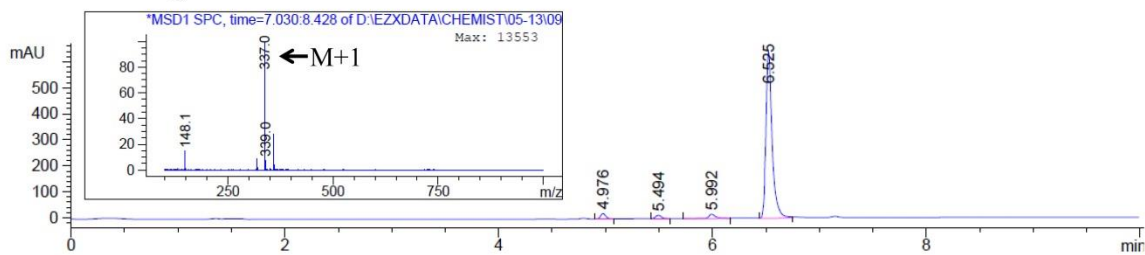
Product
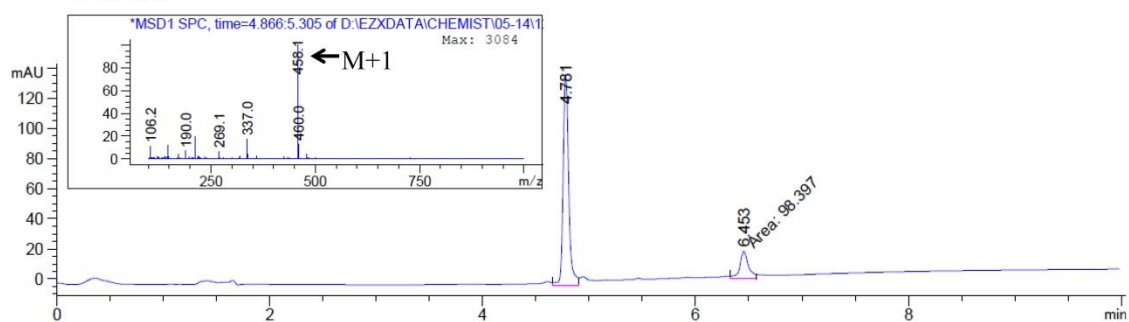
3. Pharmacological characterization of MIPS1262 (**11**) in [^{3}H]NMS competition binding assays. Experiments performed in $hM_1 - hM_5$ mAChR-expressing CHO cells in the presence of increasing concentrations of ACh with or without increasing concentrations of MIPS1262 in the presence of a K_D concentration of radiolabeled orthosteric antagonist [^{3}H]NMS. Values represent the mean ± SEM from two to three experiments performed in duplicate.
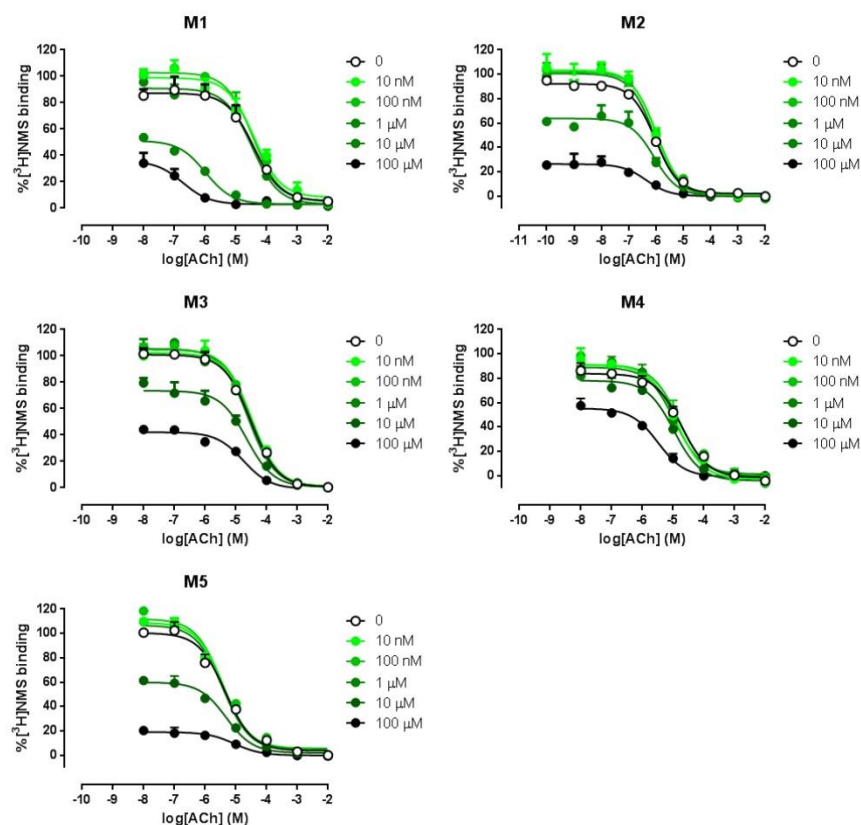
Appendix 3. Chapter 3 Published Supporting Information

SUPPORTING INFORMATION

1. [³H]NMS competition binding curves and ERK1/2 phosphorylation concentration-response curves for BQCA (**1**) and MIPS1455 (**4**) alone (in the absence of the orthosteric agonist ACh). Experiments performed in hM_1 mAChR-expressing CHO cells in the presence of increasing concentrations of BQCA or MIPS1455 in the presence of a K_D concentration of radiolabeled orthosteric antagonist [³H]NMS. Values represent the mean ± SEM from two to three experiments performed in duplicate.
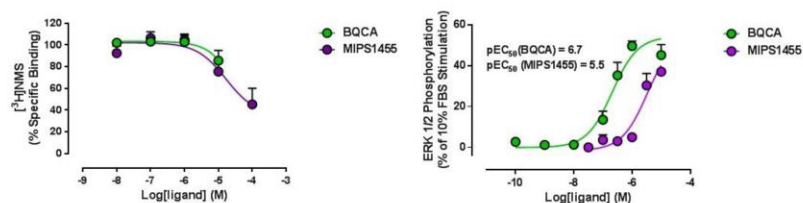
2. Pharmacological characterization of BQCA (**1**) (top) and MIPS1455 (**4**) (bottom) in [³H]NMS competition binding assays. Experiments performed in $hM_2 - hM_5$ mAChR-expressing CHO cells in the presence of increasing concentrations of ACh with or without increasing concentrations of BQCA or MIPS1455 in the presence of a K_D concentration of radiolabeled orthosteric antagonist [³H]NMS. Values represent the mean ± SEM from two to three experiments performed in duplicate.
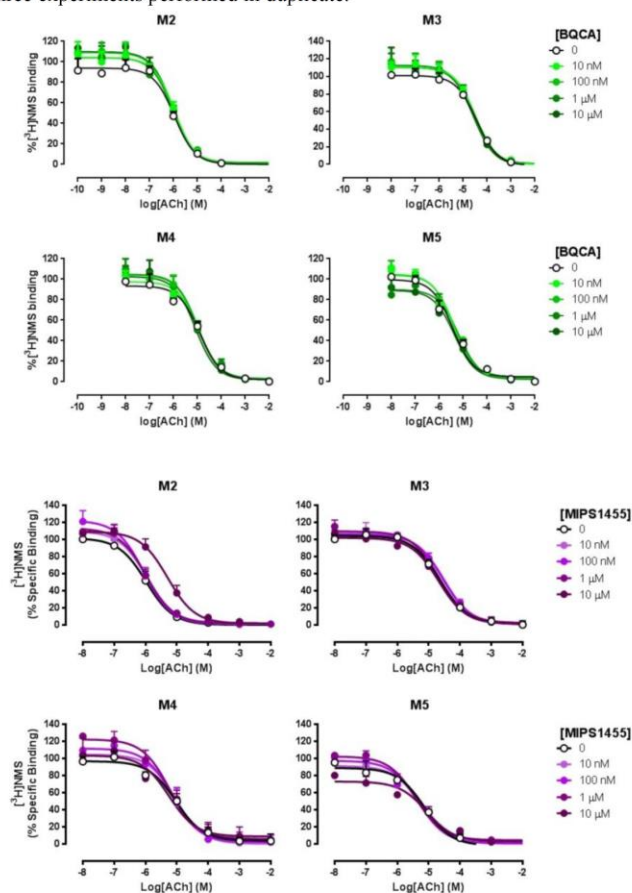
3. Structure of MIPS1262.
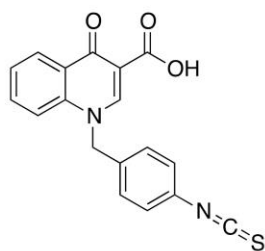
MIPS1262

4. HPLC traces for MIPS1455 (**4**) purity (254 and 214 nm).
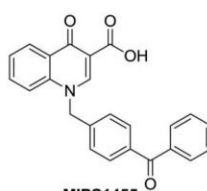
MIPS1455
4.
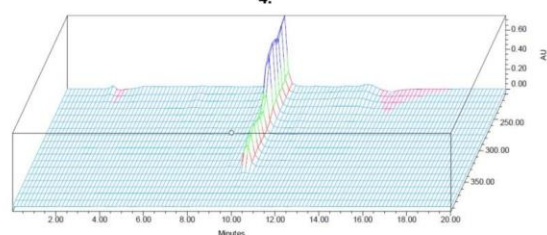
Auto-Scaled Chromatogram
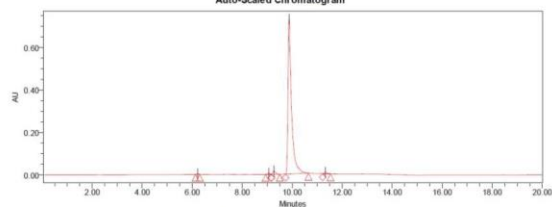
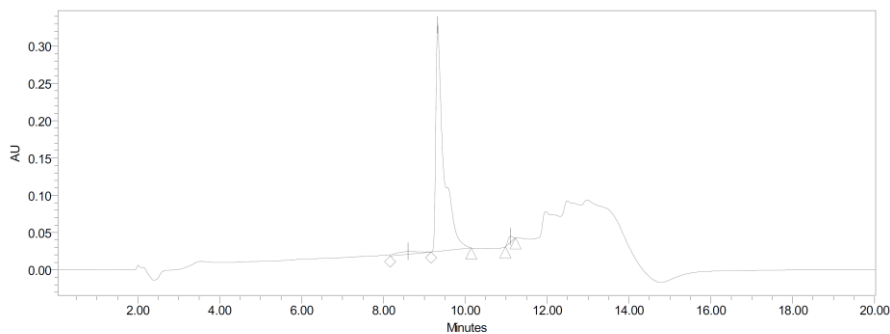**Processed Channel: PDA 254.0 nm**

	Processed Channel	Retention Time (min)	Area	% Area	Width (sec)	Height
1	PDA 254.0 nm	6.219	10242	0.14	10.000	1860
2	PDA 254.0 nm	9.053	34972	0.48	14.000	5303
3	PDA 254.0 nm	9.267	118737	1.62	20.000	15501

	Processed Channel	Retention Time (min)	Area	% Area	Width (sec)	Height
4	PDA 254.0 nm	9.880	7113736	96.96	55.000	731462
5	PDA 254.0 nm	11.327	58729	0.80	19.000	7458

Processed Channel: PDA 214.0 nm

	Processed Channel	Retention Time (min)	Area	% Area	Width (sec)	Height
1	PDA 214.0 nm	6.197	75047	1.06	24.000	6894
2	PDA 214.0 nm	9.052	101097	1.41	17.000	13956
3	PDA 214.0 nm	9.266	25803	0.36	14.000	5168

	Processed Channel	Retention Time (min)	Area	% Area	Width (sec)	Height
4	PDA 214.0 nm	9.880	6895936	96.29	55.000	708145
5	PDA 214.0 nm	11.326	40598	0.57	14.000	6235
6	PDA 214.0 nm	12.806	21913	0.31	12.000	3848

Appendix 4. Chapter 3 Unpublished Supporting Information

1. Pharmacological characterization of MIPS1455 (1) in ERK1/2 phosphorylation time course assays in FlpIn CHO cells stably expressing the hM_1 mAChR (top) and non-transfected FlpIn CHO cells (bottom). See *Alphascreen ERK1/2 Phosphorylation Assays – Time Course Assays* in the Experimental Section of Chapter 2 for a description of the protocol. Values represent the mean ± SEM from two to three experiments performed in duplicate.
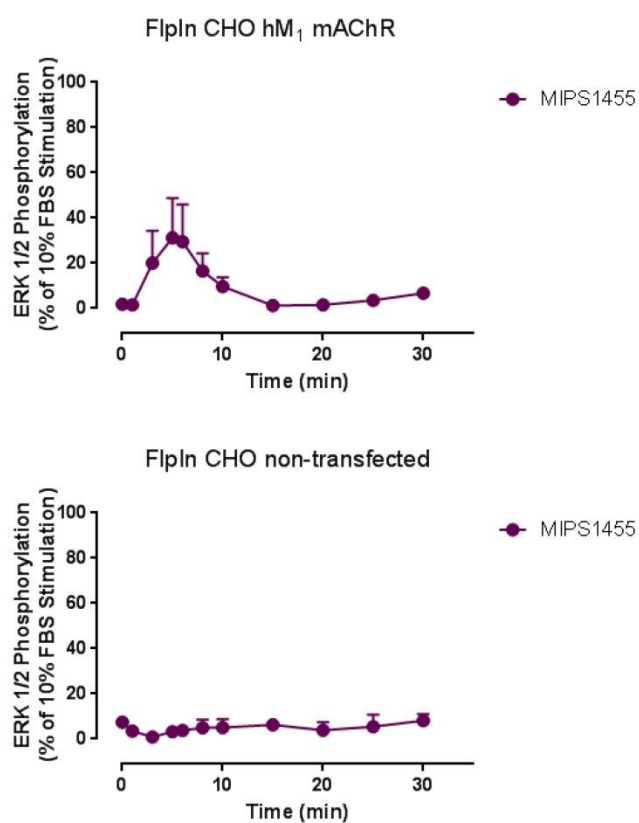
Appendix 5. Chapter 4 Supporting Information

1. HPLC traces for compound purity (254 and 214 nm) (and ^{1}H NMRs where appropriate)
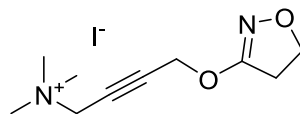
iperoxo
7.
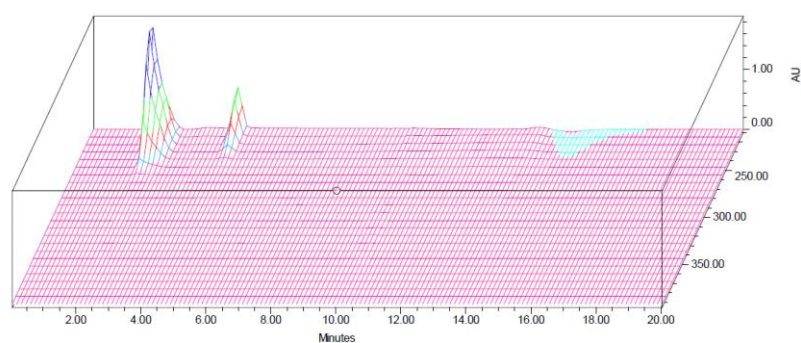
Auto-Scaled Chromatogram
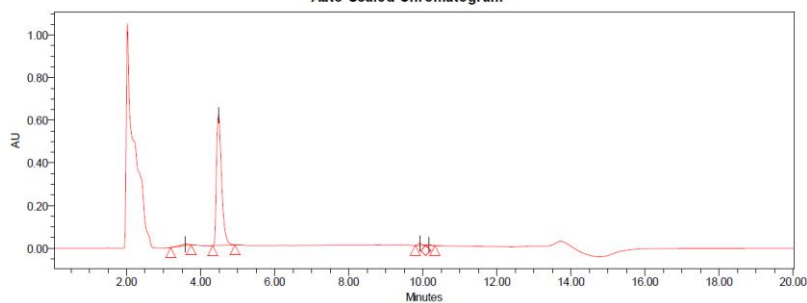
Processed Channel: PDA 214.0 nm

	Processed Channel	Retention Time (min)	Area	% Area	Width (sec)	Height
1	PDA 214.0 nm	3.582	86576	1.44	33.000	5892
2	PDA 214.0 nm	4.486	5850413	97.02	36.000	617496
3	PDA 214.0 nm	9.914	65098	1.08	17.000	8967
4	PDA 214.0 nm	10.167	28225	0.47	15.000	3521

NB: this compound did not appear in the 254 chromatogram
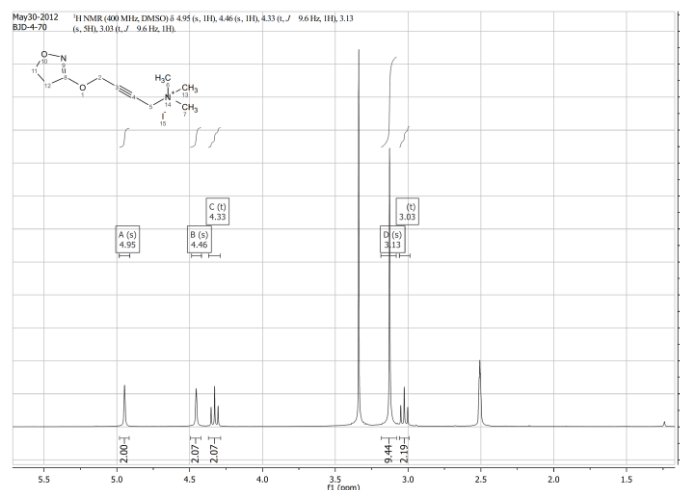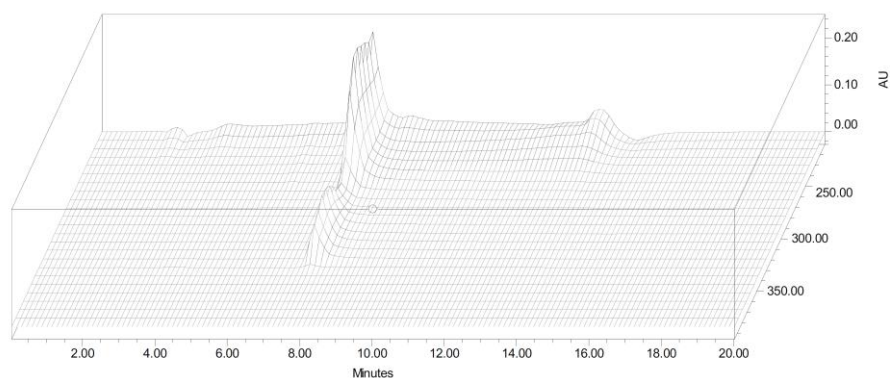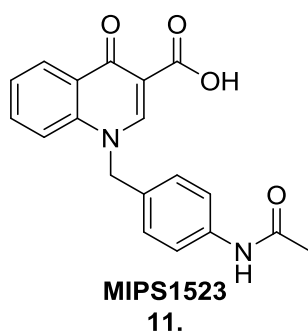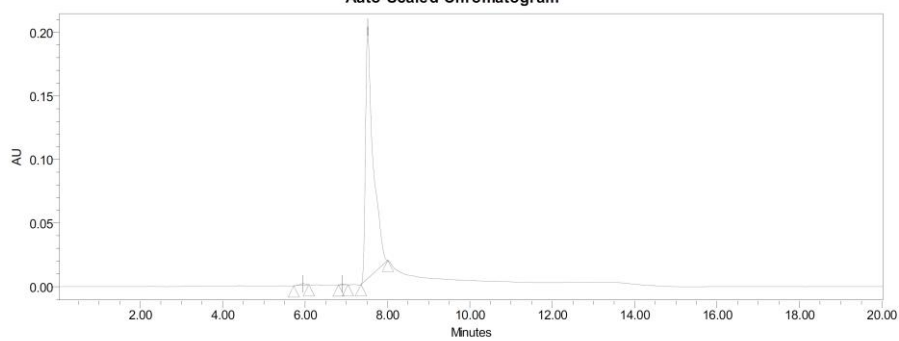
MIPS1523

11.

Auto-Scaled Chromatogram

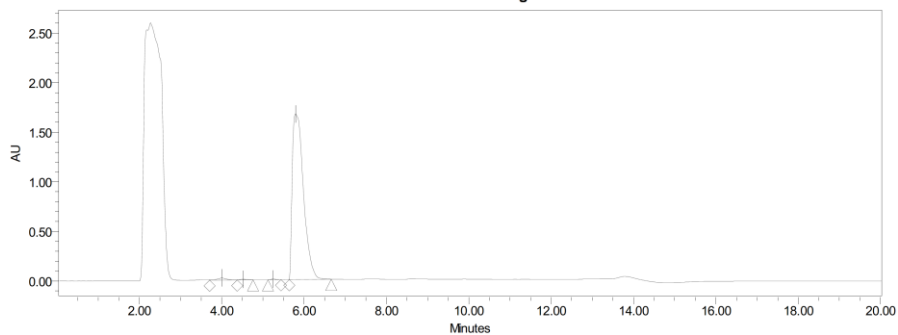**Processed Channel: PDA 254.0 nm**

	Processed Channel	Retention Time (min)	Area	% Area	Width (sec)	Height
1	PDA 254.0 nm	5.952	11251	0.44	22.000	1223
2	PDA 254.0 nm	6.899	5622	0.22	14.000	805
3	PDA 254.0 nm	7.521	2542893	99.34	39.000	198295
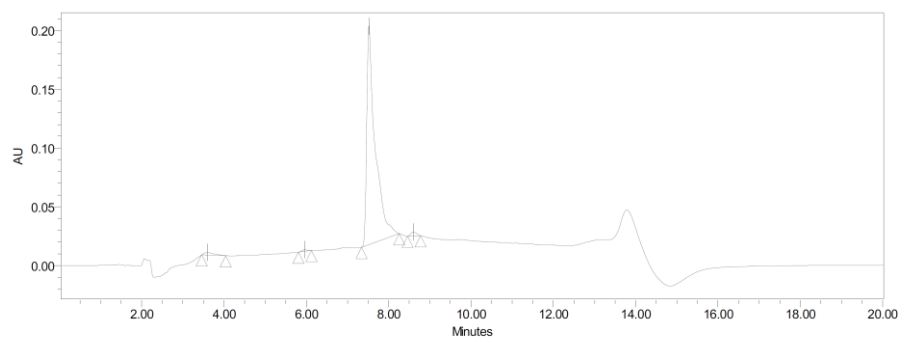
Processed Channel: PDA 214.0 nm

	Processed Channel	Retention Time (min)	Area	% Area	Width (sec)	Height
1	PDA 214.0 nm	3.592	35885	1.30	35.000	2074
2	PDA 214.0 nm	5.964	13583	0.49	19.000	1588
3	PDA 214.0 nm	7.522	2671375	97.00	55.000	186112
4	PDA 214.0 nm	8.600	33148	1.20	19.000	3358
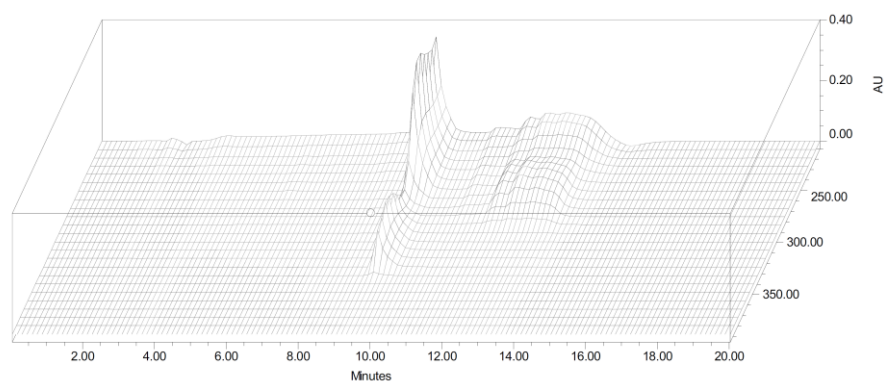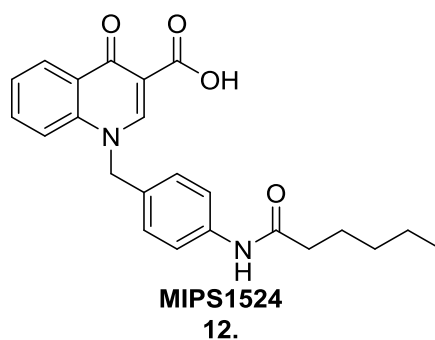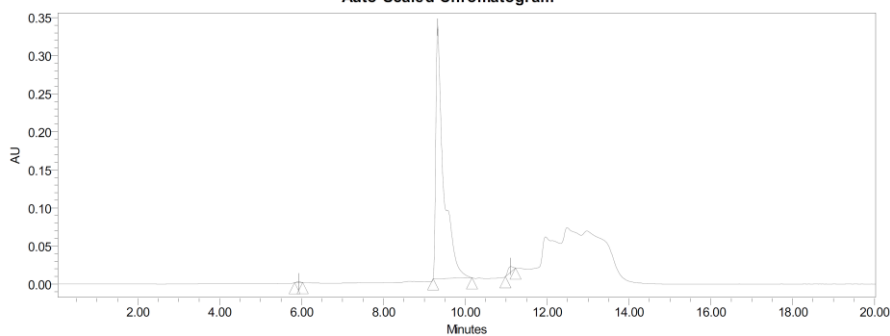
MIPS1524

12.

Auto-Scaled Chromatogram

Processed Channel: PDA 254.0 nm
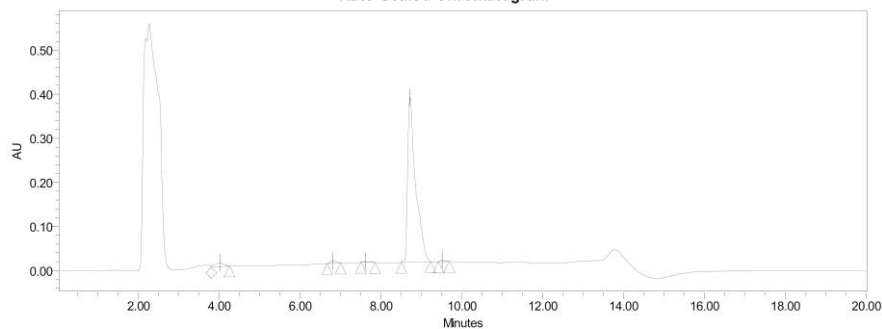
	Processed Channel	Retention Time (min)	Area	% Area	Width (sec)	Height
1	PDA 254.0 nm	5.920	8722	0.20	12.000	1441
2	PDA 254.0 nm	9.331	4384784	98.35	57.000	331553
3	PDA 254.0 nm	11.105	64771	1.45	15.000	7663

Processed Channel: PDA 214.0 nm

	Processed Channel	Retention Time (min)	Area	% Area	Width (sec)	Height
1	PDA 214.0 nm	8.602	146656	3.39	60.000	4071
2	PDA 214.0 nm	9.332	4110083	95.03	59.000	304838
3	PDA 214.0 nm	11.104	68520	1.58	15.000	8161

204

Note: The 254 and 214 nm HPLC traces of MIPS1524 on the previous page appear to be impure due to complications with the HPLC at the time of synthesis and characterization. A blank run (containing only the solvent in which MIPS1524 was dissolved, methanol) is provided below to illustrate this.
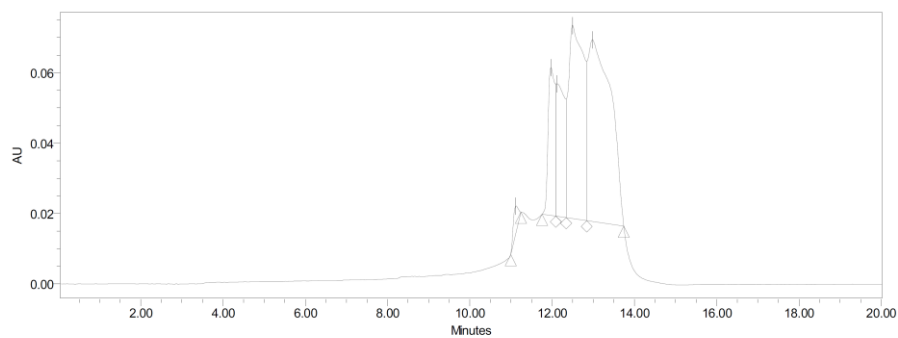
Processed Channel: PDA 254.0 nm

	Processed Channel	Retention Time (min)	Area	% Area	Width (sec)	Height
1	PDA 254.0 nm	11.117	64845	1.43	15.000	7814
2	PDA 254.0 nm	11.977	485506	10.72	20.000	42099
3	PDA 254.0 nm	12.115	539818	11.92	15.000	37674
4	PDA 254.0 nm	12.500	1429233	31.57	30.000	55039
5	PDA 254.0 nm	12.981	2008038	44.35	54.000	51671
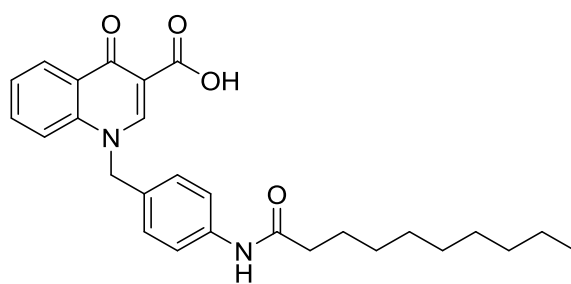
MIPS1525

13.
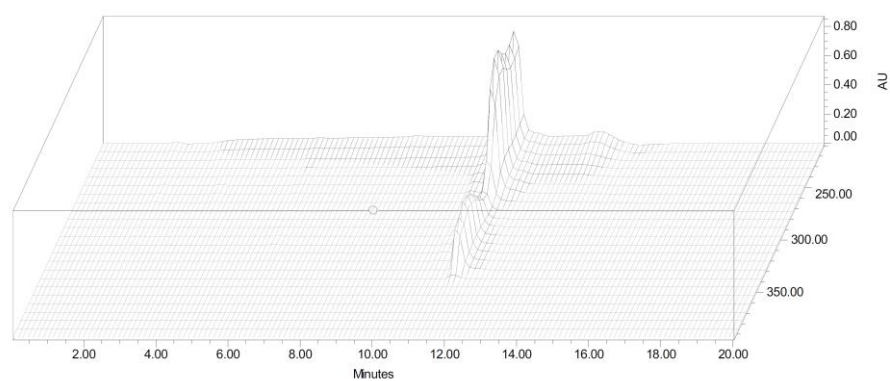
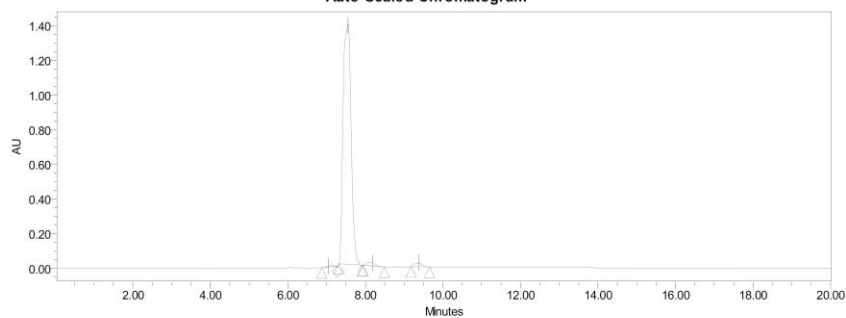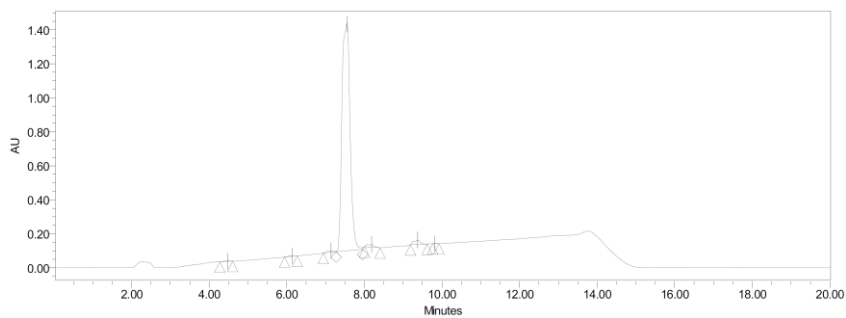**Auto-Scaled Chromatogram**
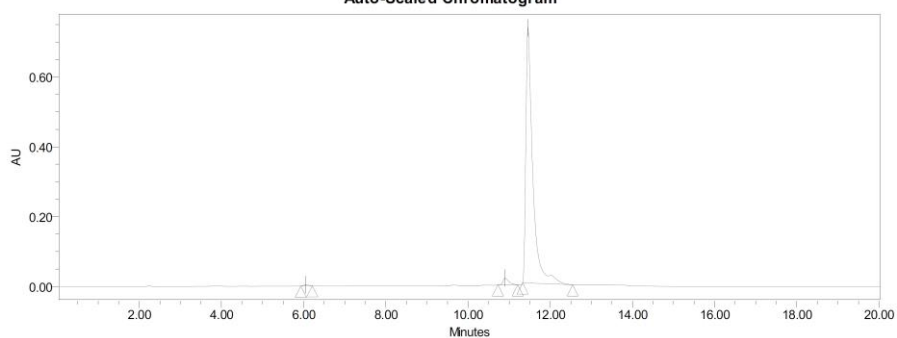
Processed Channel: PDA 254.0 nm

	Processed Channel	Retention Time (min)	Area	% Area	Width (sec)	Height
1	PDA 254.0 nm	6.055	27391	0.32	17.000	3316
2	PDA 254.0 nm	10.903	185721	2.14	29.000	19071
3	PDA 254.0 nm	11.462	8480213	97.55	73.000	730974
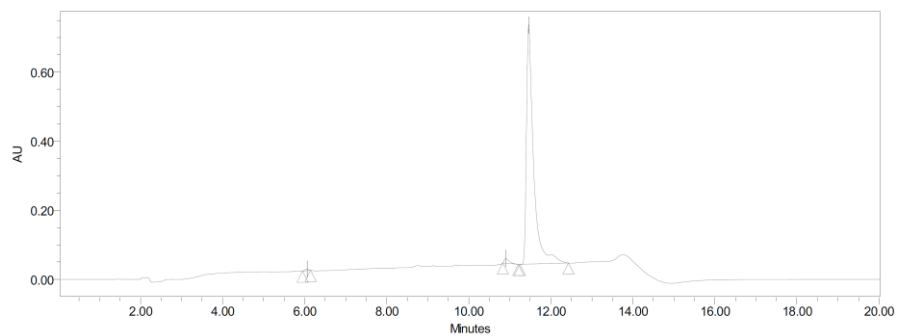
Processed Channel: PDA 214.0 nm

	Processed Channel	Retention Time (min)	Area	% Area	Width (sec)	Height
1	PDA 214.0 nm	6.056	25334	0.30	12.000	3796
2	PDA 214.0 nm	10.904	111970	1.35	23.000	13799
3	PDA 214.0 nm	11.463	8173732	98.35	71.000	692783
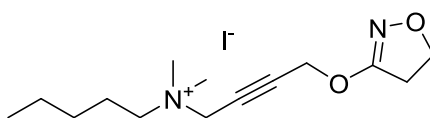
MIPS1526

14.
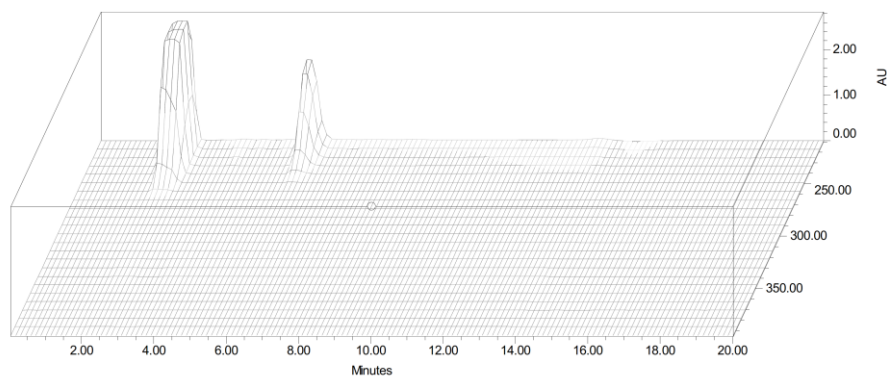
Auto-Scaled Chromatogram

Processed Channel: PDA 214.0 nm

	Processed Channel	Retention Time (min)	Area	% Area	Width (sec)	Height
1	PDA 214.0 nm	4.008	313452	0.98	40.000	21282
2	PDA 214.0 nm	4.528	79307	0.25	23.000	6840
3	PDA 214.0 nm	5.249	62193	0.19	19.000	7238
4	PDA 214.0 nm	5.798	31598427	98.58	61.000	1672853

NB: this compound did not appear in the 254 chromatogram

207
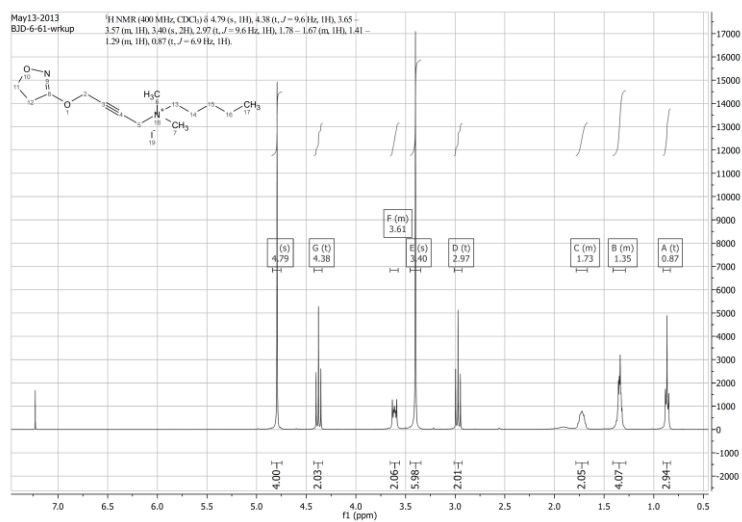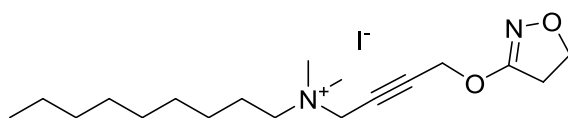
MIPS1527
15.

Auto-Scaled Chromatogram

Processed Channel: PDA 214.0 nm

	Processed Channel	Retention Time (min)	Area	% Area	Width (sec)	Height
1	PDA 214.0 nm	4.022	131656	2.44	27.000	8906
2	PDA 214.0 nm	6.810	59462	1.10	20.000	6213
3	PDA 214.0 nm	7.616	23629	0.44	21.000	1756
4	PDA 214.0 nm	8.719	5141031	95.42	43.000	374391
5	PDA 214.0 nm	9.510	32143	0.60	16.000	4215

NB: this compound did not appear in the 254 chromatogram


208
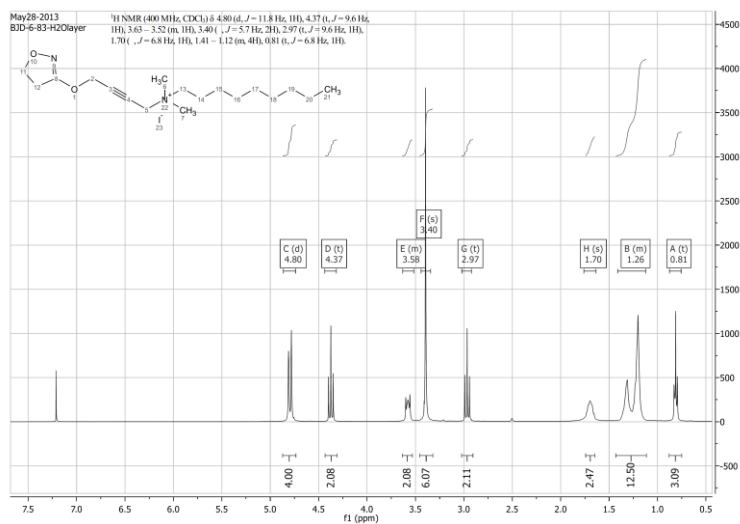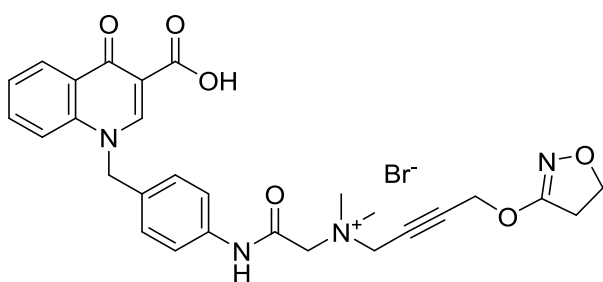
MIPS1487
33a.

Auto-Scaled Chromatogram

Processed Channel: PDA 254.0 nm

	Processed Channel	Retention Time (min)	Area	% Area	Width (sec)	Height
1	PDA 254.0 nm	7.057	90166	0.44	24.000	6860
2	PDA 254.0 nm	7.547	19851021	96.74	35.000	1391806
3	PDA 254.0 nm	8.181	274195	1.34	33.000	19038
4	PDA 254.0 nm	9.375	305138	1.49	29.000	23180

Processed Channel: PDA 214.0 nm

	Processed Channel	Retention Time (min)	Area	% Area	Width (sec)	Height
1	PDA 214.0 nm	4.470	33438	0.17	20.000	2818
2	PDA 214.0 nm	6.134	26687	0.13	20.000	2033
3	PDA 214.0 nm	7.147	122109	0.60	20.000	9246
4	PDA 214.0 nm	7.548	19549259	96.64	41.000	1345924
5	PDA 214.0 nm	8.186	184984	0.91	24.000	15190
6	PDA 214.0 nm	9.377	305733	1.51	26.000	25460
7	PDA 214.0 nm	9.817	6021	0.03	10.000	1295
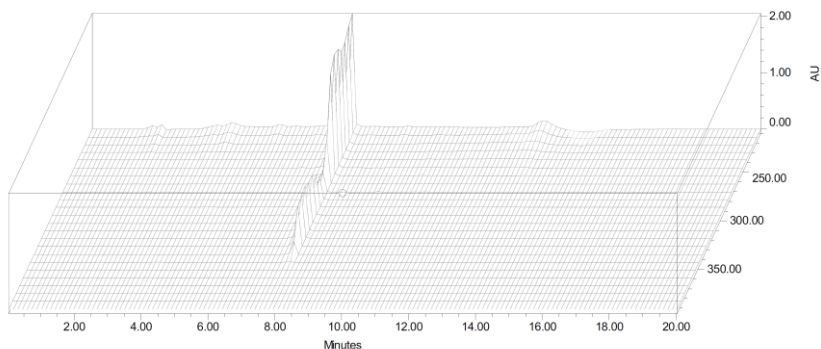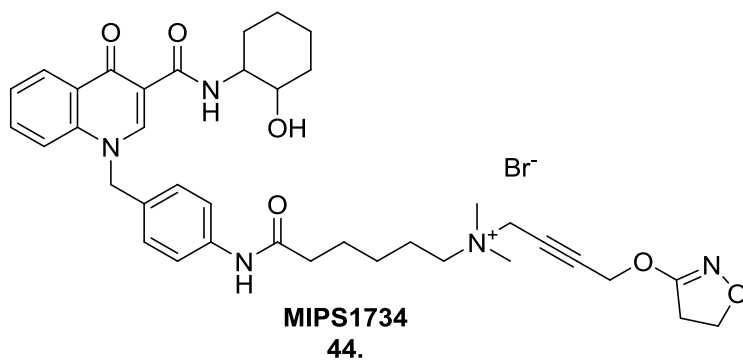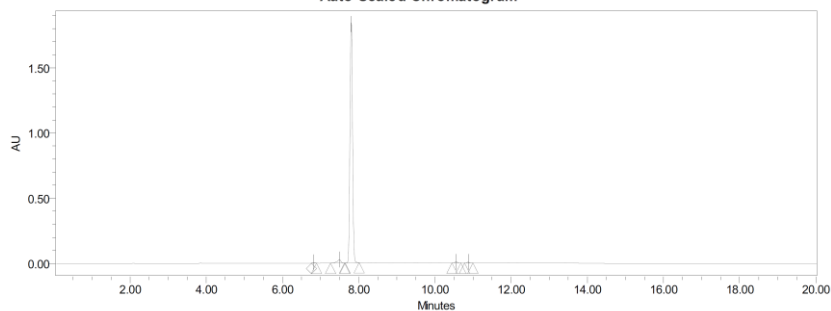
MIPS1734
44.

Auto-Scaled Chromatogram

Processed Channel: PDA 254.0 nm

	Processed Channel	Retention Time (min)	Area	% Area	Width (sec)	Height
1	PDA 254.0 nm	6.811	22169	0.25	8.000	5582
2	PDA 254.0 nm	7.492	179331	2.04	22.000	27182
3	PDA 254.0 nm	7.802	8544410	96.96	22.000	1845694
4	PDA 254.0 nm	10.557	38318	0.43	14.000	7649
5	PDA 254.0 nm	10.872	27944	0.32	13.000	5784
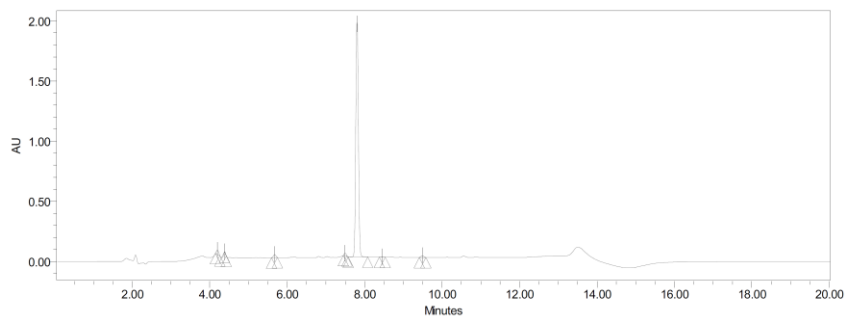
Processed Channel: PDA 214.0 nm

	Processed Channel	Retention Time (min)	Area	% Area	Width (sec)	Height
1	PDA 214.0 nm	4.195	147886	1.56	7.000	34088
2	PDA 214.0 nm	4.395	19252	0.20	3.000	12053
3	PDA 214.0 nm	5.676	112551	1.18	9.000	25630
4	PDA 214.0 nm	7.493	69660	0.73	6.000	19680
5	PDA 214.0 nm	7.802	9075492	95.48	30.000	1952085
6	PDA 214.0 nm	8.447	16396	0.17	9.000	3808
7	PDA 214.0 nm	9.488	63937	0.67	10.000	13981

2. Pharmacological characterization of monovalent and putative bitopic compounds in ERK1/2 phosphorylation time course assays in FlpIn CHO cells stably expressing the hM$_1$ mAChR (top) and non-transfected FlpIn CHO cells (bottom). See *Alphascreen ERK1/2 Phosphorylation Assays – Time Course Assays* in the Experimental Section of Chapter 4 for a description of the protocol. Values represent the mean ± SEM from two to three experiments performed in duplicate.
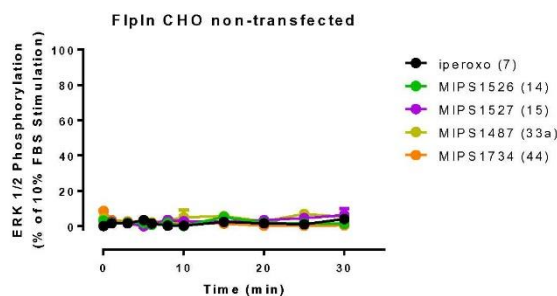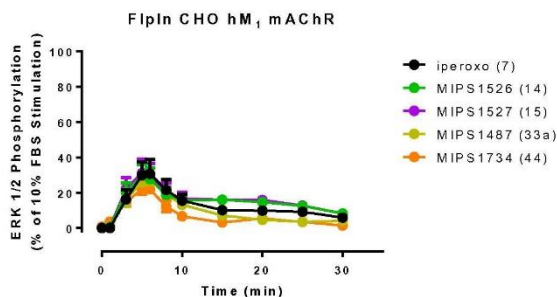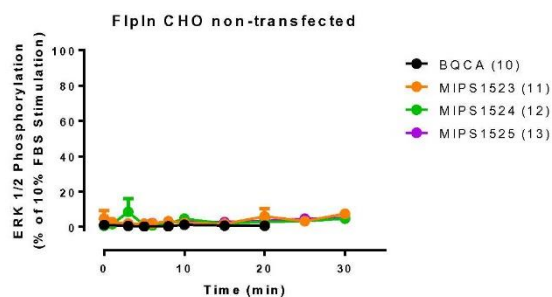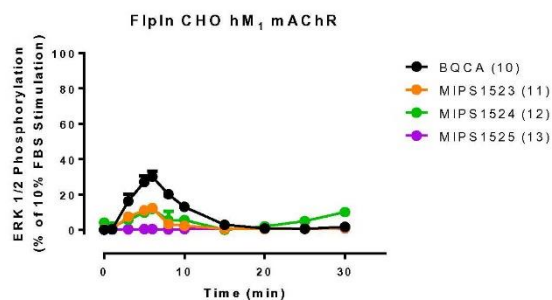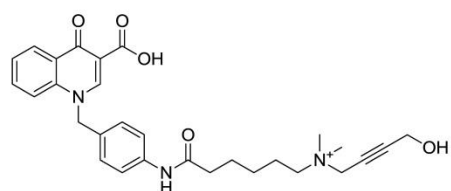
3. LCMS of base-catalyzed saponification of **32b**

VWD1 A, Wavelength=254 nm (D:\EZXDATA\CHEMIST\03-14\090314-BJD-7-41-CRUDE1-01164.D)

MSD1 TIC, MS File (D:\EZXDATA\CHEMIST\03-14\090314-BJD-7-41-CRUDE1-01164.D)   MM-ES, Pos, Scan, Frag: 130
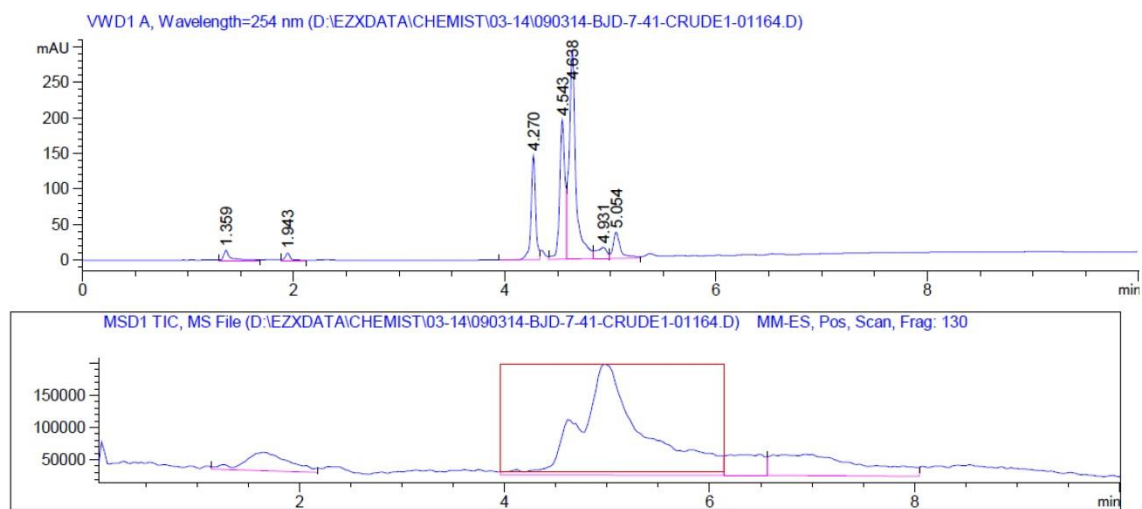
Peak at Scan 182.4. Top ions are   487 149 **(M-OH)⁺**
Peak at Scan 183.5. Top ions are   486
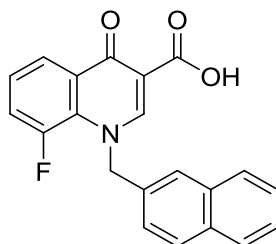Peak at Scan 184.4. Top ions are   504 **M+1**
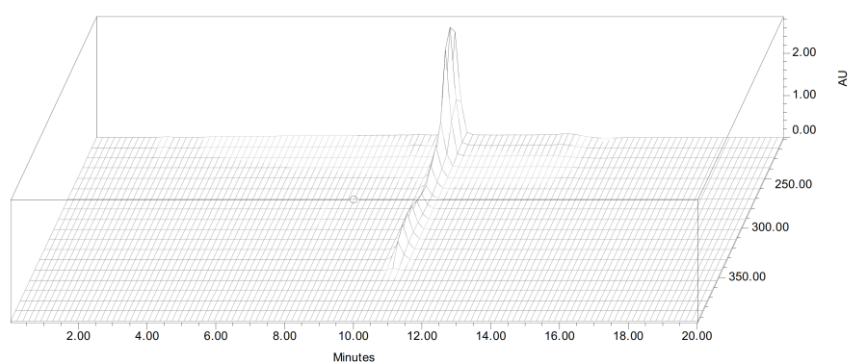
4. ¹H NMR and LCMS of acid-catalyzed hydrolysis of **32b**

VWD1 A, Wavelength=254 nm (D:\EZXDATA\CHEMIST\03-14\200314-BJD-7-51-SOLID1-01455.D)
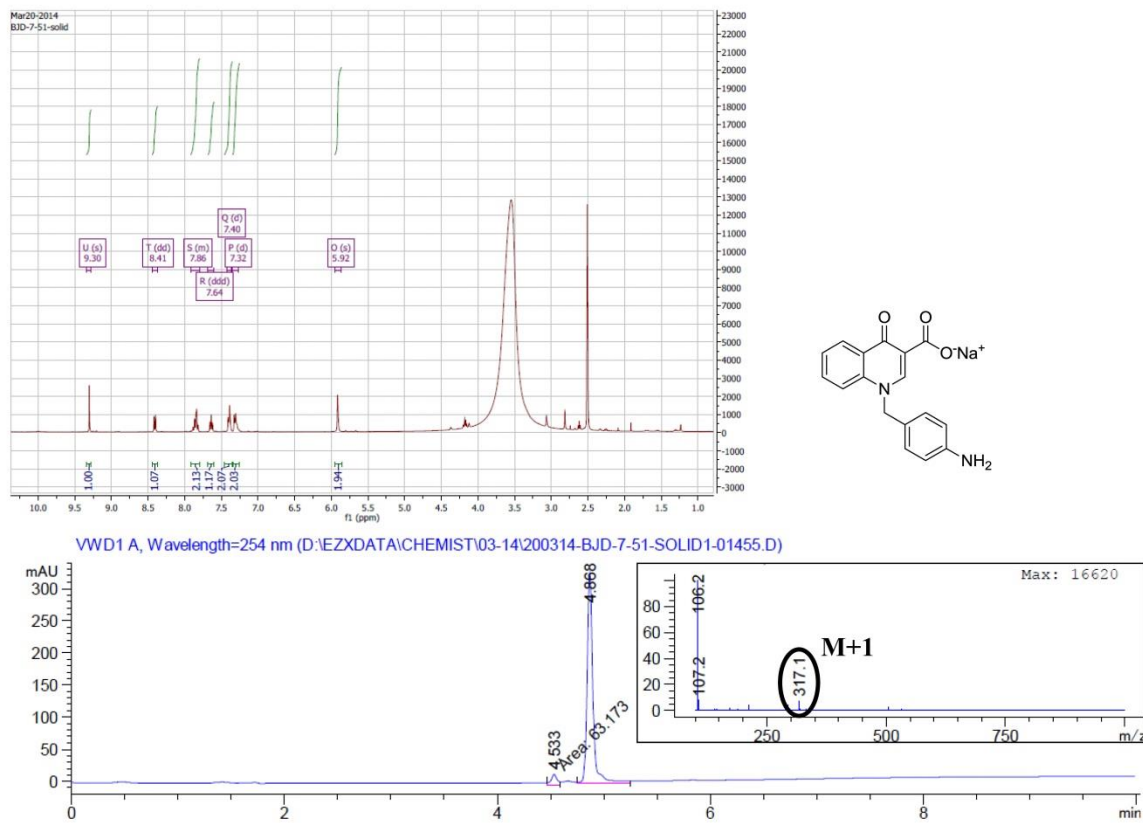
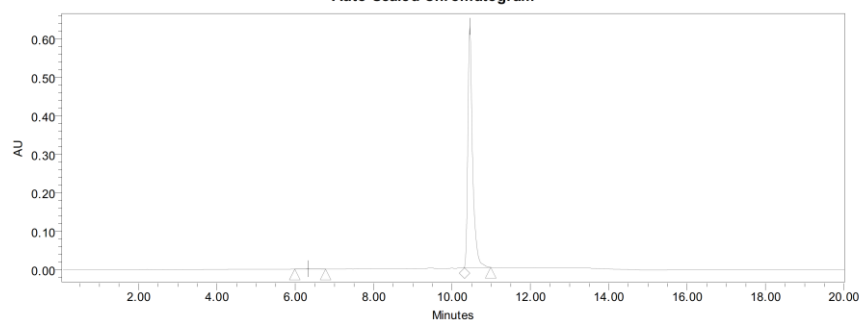# Appendix 6. Chapter 5 Supporting Information

1. HPLC traces for compound purity (254 and 214 nm)
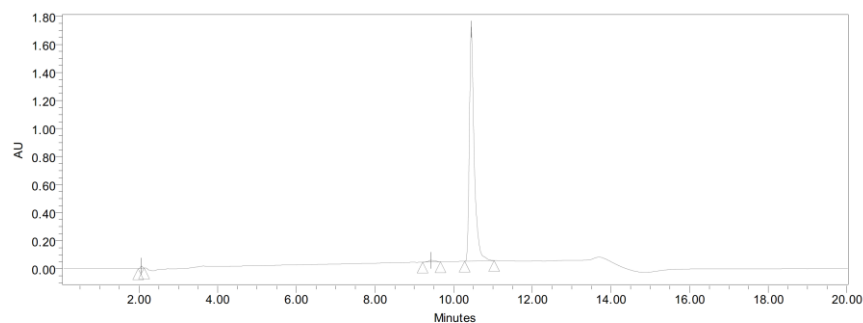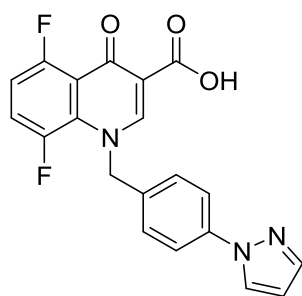

5.

Auto-Scaled Chromatogram

Processed Channel: PDA 254.0 nm

	Processed Channel	Retention Time (min)	Area	% Area	Width (sec)	Height
1	PDA 254.0 nm	6.320	15688	0.30	47.000	723
2	PDA 254.0 nm	10.454	5252967	99.70	40.000	626198

Processed Channel: PDA 214.0 nm

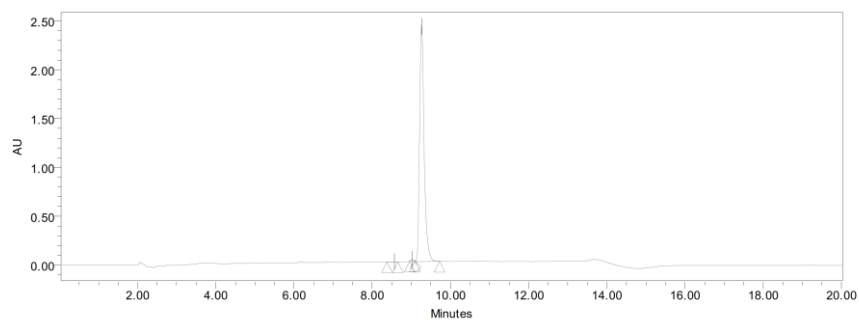|	Processed Channel	Retention Time (min)	Area	% Area	Width (sec)	Height
1	PDA 214.0 nm	2.062	59585	0.41	9.000	15768
2	PDA 214.0 nm	9.421	156160	1.09	27.000	13198
3	PDA 214.0 nm	10.449	14171440	98.50	45.000	1667018

6.
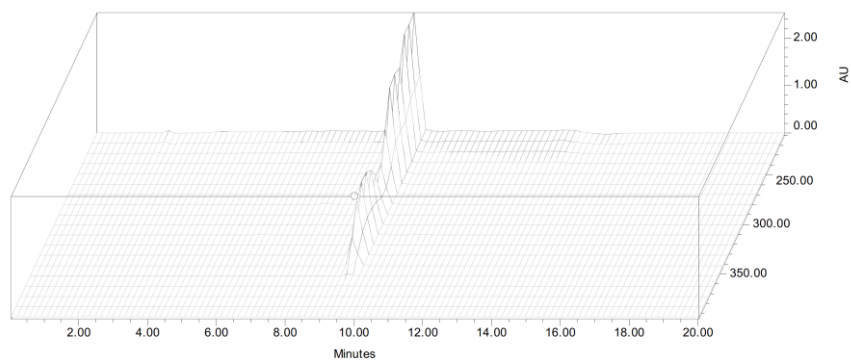
Auto-Scaled Chromatogram
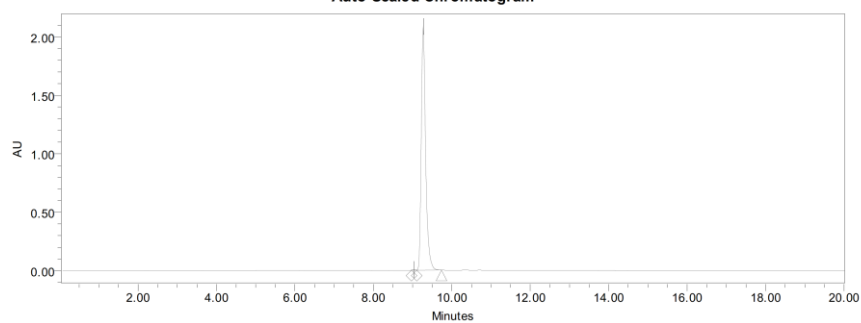
Processed Channel: PDA 254.0 nm

	Processed Channel	Retention Time (min)	Area	% Area	Width (sec)	Height
1	PDA 254.0 nm	9.033	34451	0.21	8.000	6476
2	PDA 254.0 nm	9.272	16096279	99.79	38.000	2075869

Processed Channel: PDA 214.0 nm

	Processed Channel	Retention Time (min)	Area	% Area	Width (sec)	Height
1	PDA 214.0 nm	8.568	21093	0.11	17.000	1773
2	PDA 214.0 nm	9.023	77504	0.40	8.000	16696
3	PDA 214.0 nm	9.262	19475783	99.50	37.000	2431828

215

2. Pharmacological characterization of **5** and **6** in ERK1/2 phosphorylation time course assays in FlpIn CHO cells stably expressing the hM$_1$ mAChR (top) and non-transfected FlpIn CHO cells (bottom). See *Alphascreen ERK1/2 Phosphorylation Assays – Time Course Assays* in the Experimental Section of Chapter 5 for a description of the protocol. Values represent the mean ± SEM from two to three experiments performed in duplicate.
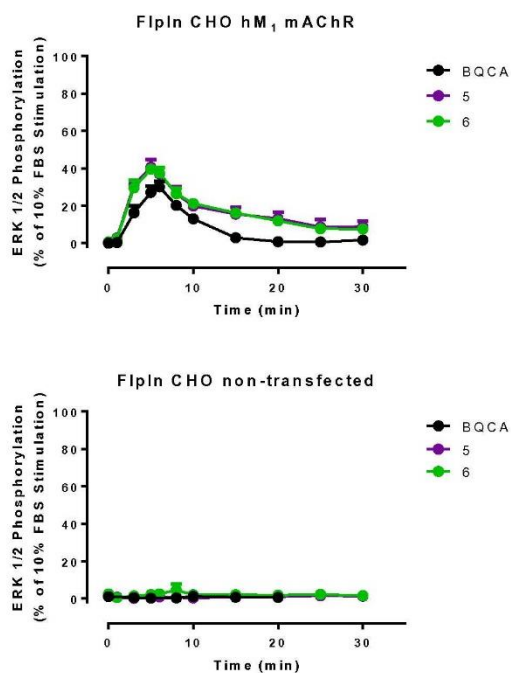
Appendix 7. List of publications

2014: Davie, B.J., Sexton, P.M., Capuano, B., Christopoulos, A., Scammells, P.J. (2014), Development of a Photoactivatable Allosteric Ligand for the M_1 Muscarinic Acetylcholine Receptor, *ACS Chemical Neuroscience*, in press, **DOI:** 10.1021/cn500173x

2014: Davie, B.J., Valant, C., Capuano, B., Sexton, P.M., Christopoulos, A. and Scammells, P.J. (2014), Synthesis and pharmacological evaluation of analogues of benzyl quinolone carboxylic acid (BQCA) designed to bind irreversibly to an allosteric site of the M_1 muscarinic acetylcholine receptor, *Journal of Medicinal Chemistry*, *57* (12), 5405-5418.

2014: Yuriev, E. and Davie, B., "Focusing on guidance in guided-inquiry learning", In *Taking inquiry-oriented learning to the teaching coalface*, Thompson, C., Rayner, G., Barratt, C., Hughes, T., and Kirkup, L. (Eds.), Office for Learning and Teaching, Sydney, 2014, pp. 37-42. ISBN 9781743617243.

2014: White, P.J., Styles, K., Yuriev, E., Evans, D.R., Rangachari, P.K., Short, J.L., Exintaris, B., Malone, D.T., **Davie, B.**, Eise, N., Mc Namara, K., Larson, I. (2014), An active learning approach to replace didactic lectures in a research intensive Faculty: changes in student attitudes and behaviours, manuscript submitted to *Higher Education Research & Development*

2013: Davie, B.J., Christopoulos, A., Scammells, P.J. (2013), Development of M_1 mAChR allosteric and bitopic ligands: prospective therapeutics for the treatment of cognitive deficits, *ACS Chemical Neuroscience*, 4 (7), 1026-1048.

Appendix 8. List of conference/symposium presentations and associated awards

2013: Davie, B.J. *et al.*, *Synthesis and pharmacological evaluation of irreversible allosteric ligands for the M_1 muscarinic acetylcholine receptor* (poster 2), The Australasian Society of Clinical and Experimental Pharmacologists and Toxicologists (ASCEPT) Annual Scientific Meeting, Melbourne, Australia (**Neville Percy Prize for Best Poster Presentation**)

2013: Davie, B.J. *et al.*, *Synthesis and pharmacological evaluation of irreversible allosteric ligands for the M_1 muscarinic acetylcholine receptor* (poster 2), Monash Parkville Postgraduate symposium, Melbourne, Australia

2013: Davie, B.J. *et al.*, *Towards the development of novel bitopic ligands for the M_1 muscarinic acetylcholine receptor* (oral), Drug Discovery Biology Student Symposium, Melbourne, Australia (**Award for Best 3rd/4th year Oral Presentation**)

2013: Davie, B.J. *et al.*, *Synthesis and pharmacological evaluation of irreversible allosteric ligands for the M_1 muscarinic acetylcholine receptor* (poster 2), European College of Neuropsychopharmacology Congress, Barcelona, Spain

2013: Davie, B.J. *et al.*, *Synthesis and pharmacological evaluation of irreversible allosteric ligands for the M_1 muscarinic acetylcholine receptor* (poster 1), Melbourne Protein Symposium, Melbourne, Australia (**Poster prize – one of top four presenters**)

2012: Davie, B.J. *et al.*, *Synthesis and pharmacological evaluation of irreversible allosteric ligands for the M_1 muscarinic acetylcholine receptor* (poster 1), Molecular Pharmacology of G Protein-Coupled Receptors conference, Melbourne, Australia

2012: Davie, B.J. *et al.*, *Synthesis and pharmacological evaluation of irreversible allosteric ligands for the M_1 muscarinic acetylcholine receptor* (poster 1), Students of Brain Research symposium, Melbourne, Australia

2012: Davie, B.J. *et al.*, *Synthesis and pharmacological investigation of irreversible allosteric ligands for the M_1 muscarinic acetylcholine receptor* (oral), Monash Parkville Postgraduate symposium, Melbourne, Australia